Cohesive properties of the *Caulobacter crescentus* holdfast adhesin are regulated by a novel c-di-GMP effector protein

Inauguraldissertation

zur

Erlangung der Würde eines Doktors der Philosophie

vorgelegt der

Philosophisch-Naturwissenschaftlichen Fakultät

der Universität Basel

von

Kathrin Sara Sprecher

aus Aesch (BL), Schweiz

Basel, 2017

Genehmigt von der Philosophisch-Naturwissenschaftlichen Fakultät

auf Antrag von:

Prof. Dr. Urs Jenal
Prof. Dr. Marek Basler

Basel, den 21.02.2017

Prof. Dr. Martin Spiess

In memory of

Jutta Nesper

a great scientist, dear colleague and much-valued mentor.

Summary

Many bacteria grow in aquatic environments such as oceans, lakes and rivers. These environments pose special challenges, as nutrient availability is poor and hard to exploit due to constant water flow. Therefore, most bacteria grow on surfaces and have developed mechanisms that anchor them on an adequate nutrient source in the moment of encounter. Yet, they need to effectively disperse when conditions become unfavorable. The switch between motile and sessile lifestyles is controlled by the global second messenger c–di–GMP, which suppresses motility and promotes sessility. Here, we use the aquatic bacterium *Caulobacter crescentus* as a model to dissect c–di–GMP mediated lifestyle changes and surface attachment. *C. crescentus* has a biphasic life cycle that comprises both a motile and a sessile phase. A motile swarmer cell can develop into a sessile surface attached stalked cell by expressing a polar exopolysaccharide-based structure called the holdfast that shows remarkably strong adhesive properties. Recent studies have shown that holdfast biogenesis requires c–di–GMP and is initiated either upon surface contact or as part of the developmental program. However, the underlying molecular mechanisms are not understood.

In an unbiased screen for c–di–GMP binding proteins in *C. crescentus* we identified a novel c–di–GMP effector of unknown function and confirmed specific binding to c–di–GMP *in vitro*. Orthologous genes of this effector were found in different phyla and showed a strong association with exopolysaccharide synthesis genes. Its importance in holdfast biogenesis could be experimentally confirmed and the protein was named HfsK following the terminology used for holdfast synthesis proteins. Cells deficient in HfsK produced holdfast but could not retain the adhesin on the cell envelope, resulting in a strong surface adhesion defect and failure in surface colonization. Furthermore, a strong deformation of the mutant holdfast was observed when it was subject to shear stress, indicating a decrease in holdfast cohesion forces. HfsK is a member of an uncharacterized subclass of Gcn5-related-N-acetyltransferases, a diverse enzyme family that could potentially acylate the holdfast exopolysaccharide. Mutations in genes encoding holdfast anchor proteins that are predicted to form membrane-anchored filaments exhibited a similar phenotype. Based on our findings we propose a model in which the anchor filaments and the

holdfast form a strong interaction network that relies on HfsK-mediated chemical modification of the holdfast exopolysaccharide.

In accordance with its proposed function in holdfast biogenesis, HfsK predominately localized to the cell membrane. The protein delocalized into the cytosol for a short period during the cell cycle, coinciding with holdfast biogenesis and with an upshift of cellular c–di–GMP levels. HfsK mutants impaired in c–di–GMP binding remained membrane associated throughout the cell cycle indicating that c–di–GMP binding controls the localization of this protein. A role in HfsK control could be attributed to a short stretch of amino acids at the C-terminus. This part of the protein is involved in c–di–GMP binding and is required for HfsK localization and activity. Functional analysis revealed a clear correlation between HfsK activity and subcellular localization. HfsK mutants that remained membrane-associated were mostly found to be active, while variants exclusively localizing to the cytosol failed to support proper holdfast formation. We propose that c–di–GMP binding to the C-terminus of HfsK leads to its delocalization and concomitant inactivation.

Finally, we show that overexpression of the glycosyltransferase HfsJ restored holdfast biogenesis in a strain lacking c–di–GMP. This exposed HfsJ as catalyst of the rate-limiting step of holdfast biogenesis when c–di–GMP levels are low. Together with recent findings that HfsJ directly binds c–di–GMP this suggested furthermore that HfsJ is the main effector through which holdfast synthesis is activated upon a cellular upshift of c–di–GMP.

This work establishes two pathways through which c–di–GMP can activate and possibly modulate the holdfast adhesin of *C. crescentus* and provides novel insight into the basis of the holdfast strong adhesive properties.

Table of Content

SUMMARY **I**

TABLE OF CONTENT **III**

ABBREVIATIONS **V**

LIST OF FIGURES AND TABLES **VI**

1 INTRODUCTION **1**

1.1 BACTERIAL BIOFILMS 2

1.1.1 From planktonic cells to three-dimensional structures *2*

1.1.2 Scaffolding and sticking of biofilms: exopolysaccharides and adhesins *5*

1.1.3 Biofilms: challenges and opportunities *8*

1.2 C–DI–GMP 11

1.2.1 C–di–GMP synthesis and degradation *11*

1.2.2 Regulation of c–di–GMP turnover *14*

1.2.3 The versatility of downstream c–di–GMP effectors *15*

1.2.4 C–di–GMP effector controlled EPS systems *17*

1.2.4.1 BcsA and BcsE control cellulose production 17

1.2.4.2 Alg44 is highly interlinked and required for alginate polymerization 18

1.2.4.3 PelD and FleQ are required for *pel* synthesis and EPS production 19

1.2.4.4 PgaCD form the PNAG synthase complex 20

1.2.4.5 BgsA is the putative synthase of mixed-linked β-glucan 23

1.2.4.6 *Listeria monocytogenes* EPS requires a degenerate GGDEF protein 23

1.3 *CAULOBACTER CRESCENTUS* 24

1.3.1 Cell cycle control *24*

1.3.1.1 A cascade of transcriptional regulators drive cell cycle progression 24

1.3.1.2 Swarmer-to-stalked cell transition is tightly controlled 26

1.3.2 C–di–GMP signaling in C. crescentus *29*

1.3.2.1 Oscillating c–di–GMP levels promote cell cycle progression and morphogenesis 29

1.3.2.2 Multiple control of flagellum function by c–di–GMP 30

1.3.3 Holdfast *32*

1.3.3.1 Holdfast structure 32

1.3.3.2 The holdfast synthesis machinery 33

1.3.3.3 Regulation of holdfast synthesis 37

1.4 GNAT PROTEINS 39

1.4.1 Function and structure of GNAT proteins *39*

1.4.2 Fem proteins have a tandem GNAT fold *41*

1.5 AIM OF THIS THESIS 45

2 RESULTS 47

2.1 COHESIVE PROPERTIES OF THE *CAULOBACTER CRESCENTUS* HOLDFAST ADHESIN ARE REGULATED BY A NOVEL C-DI-GMP EFFECTOR PROTEIN 49

2.1.1 Abstract 50

2.1.2 Introduction 51

2.1.3 Results 53

2.1.4 Discussion 65

2.1.5 Materials and Methods 68

2.1.6 Funding Information 83

2.1.7 Supplemental Material 84

2.1.8 Acknowledgments 92

2.2 ADDITIONAL WORK 93

2.2.1 Additional results 93

2.2.1.1 Cells deficient in *hfs*K can synergistically adhere with a Δ*hfaB* strain 93

2.2.1.2 HfsK overexpression affects *C. crescentus* attachment and growth 97

2.2.1.3 Interspecies complementation of HfsK orthologs is not possible 98

2.2.1.4 C–di–GMP binding determinants are partially conserved among HfsK orthologs 100

2.2.1.5 A CC1244 mutant shows strong phenotypes under very specific conditions 102

2.2.1.6 Rescue of holdfast synthesis in the cdG⁰ strain 103

2.2.2 Additional materials and methods 105

3 DISCUSSION AND PERSPECTIVES 109

3.1 DISCUSSION 110

3.1.1 Possible function of HfsK 110

3.1.2 Acylation of EPS – it can make the difference 111

3.1.3 The holdfast anchor model 113

3.1.4 Function of CC2278 and CC1244 115

3.1.5 GNAT proteins – ignored players in EPS synthesis 116

3.1.6 C–di–GMP dependent control of HfsK 117

3.1.7 Holdfast synthesis and surface adhesion control pathways - a highly connected c–di–GMP network 120

3.2 OUTLOOK 123

BIBLIOGRAPHY 126

ACKNOWLEDGEMENTS 149

Abbreviations

3D	three-dimensional
AFM	atomic force microscopy
BLUF	blue light using FAD
c-di-GMP	bis-(3',5')-cyclic-dimeric-guanosine-monophosphate
CoA	Co-enzyme A
Cori	origin of replication
DGC	diguanylate cyclase
EPS	exopolysaccharide
e.v.	empty vector
GAF	cGMP-specific phosphodiesterases, adenylyl cyclases and FhlA
GIL	GGDEF I-site like
GlcNAc	N-acetylglucosamine
GNAT	Gcn5-related N-acetyltransferase
MurNAc	N-acetyl muramic acid
IM	inner membrane
OG	Oregon Green
OM	outer membrane
PAS	Per/ARNT/Sim
PDE	phosphodiesterase
REC	phosphoreceiver
SD	standard deviation
ST	stalked cells
SW	swarmer cells
SW-to-ST	swarmer to stalked cell
TM	transmembrane
Und-P	undecaprenyl phosphate
WGA	wheat germ agglutinin

List of Figures and Tables

Figures and tables

Fig. 1: Biofilm formation 3

Fig. 2: C–di–GMP signaling 13

Fig. 3: C-di-GMP control of different EPS synthesis systems 21

Fig. 4: *C. crescentus* cell cycle and swarmer-to-stalked cell transition 28

Fig. 5: Regulation of flagellum synthesis and function by c–di–GMP 31

Fig. 6: Model of holdfast EPS synthesis and regulation 35

Fig. 7: N-acylation catalyzed by the GNAT family 40

Fig. 8: Structure core of GNAT proteins 41

Fig. 9: Synthesis of peptidoglycan peptide bridges in gram-positive bacteria 43

Fig. 10: Concept of synergistic adhesion 93

Fig. 11: Holdfast-deficient Δ*hfsK* cells can participate in synergistic adhesion 95

Fig. 12: Shed holdfasts of Δ*hfsK* cells do not support synergistic surface adhesion 96

Fig. 13: HfsK overexpression from a low copy plasmid affects surface adhesion 97

Fig. 14: HfsK overexpression from a high copy plasmid abolishes growth 98

Fig. 15: Interspecies complementation of HfsK orthologs 99

Fig. 16: The C-terminal extension contains a conserved arginine rich motive 100

Fig. 17: Growth and surface adhesion phenotypes of a *cc1244* mutant 102

Fig. 18: Overexpressing HfsJ in a cdG^0 strain rescues holdfast synthesis but not surface adhesion 104

Fig. 19: The holdfast anchor model 114

Tab. 1: Additional strains, plasmids and primers 107

Figures and tables: Publication manuscript

Figure 1: HfsK specifically binds c-di-GMP 54
Figure 2: HfsK deletion leads to an incoherent holdfast that does not support surface colonization 55
Figure 3: C-di-GMP controls HfsK localization 59
Figure 4: The C-terminus of HfsK is an important determinant for its localization and function 62
Figure 5: C-di-GMP binding is required for HfsK delocalization but not for HfsK-mediated surface colonization 64

Figure S1: Many HfsK orthologs are encoded in exopolysaccharide synthesis clusters 85
Figure S2: Attachment defect of *hfsK* mutants is caused by a less adhesive holdfast 85
Figure S3: Levels of HfsK do not change during the cell cycle 87
Figure S4: Membrane-association of HfsK depends on electrostatic interaction but not with the holdfast synthesis machinery 89
Figure S5: HfsK localization depends on its C-terminus 89
Figure S6: High c-di-GMP levels cause holdfast shedding and a severe surface colonization defect 91

Table 1: HfsK and CC1244 detection in a CCMS screen for c-di-GMP effectors 53
Table 2: Strains, plasmids and primers 77

1 Introduction

1.1 Bacterial Biofilms

Bacteria can thrive in most adverse environments and can withstand very extreme conditions such as high temperatures or salt concentrations, extreme pH or high radiation (1–6). Part of their success is due to their ability to form three-dimensional (3D) complex sessile communities that are embedded and immobilized in a protective matrix. These so called biofilms grow in various natural and man-made aquatic environments, in soil, and also populate host organisms as for example the dental plaques in humans. They usually grow slowly, which is also thought to protect them against certain stresses (6–8). The Matrix consists of exopolysaccharides (EPS), proteins and extracellular DNA. It confers stability to the structure, provides protection against predators and different types of stress, captures enzymes and nutrients, buffers against fluctuations of environmental conditions, and obstructs the immune response (6, 9, 10).

Many biofilms grow on surfaces but might also form on liquid-air interfaces to allow better access to oxygen, occur as free-floating aggregative flocs or form in turbulent flow as filamentous streamers that are only attached at one end to the surface and extend into the liquid phase as long filaments (6, 11–14). Also pathogenic bacteria form biofilms within patients, a condition mainly associated with a chronic course of disease (15).

1.1.1 From planktonic cells to three-dimensional structures

Although biofilms are the predominant life style of environmental bacteria, they can also exist in a solitary, planktonic, often motile form (13, 14). Either involuntarily pulled out from a biofilm or deliberately released by specific signaling mechanisms, those planktonic bacteria are the potential founder cells of a new biofilm. Biofilms develop in a sequence of different steps: surface contact and reversible surface adhesion, surface migration, permanent surface adhesion, formation of cell agglomerates, matrix production, development of 3D structures, and biofilm dispersion of planktonic cells (16, 17) (Fig. 1).

As soon as a surface is submerged in liquid, suspended macromolecules immediately start to adsorb, predominantly via unspecific weak interactions. This conditioning film generally renders the surface attractive for microorganisms as nutrient source and can facilitate adhesion, as the original surface properties can be

masked. Since formation of the conditioning film is a diffusion-based process it is very fast and usually happens before the first planktonic cells encounter the surface (18–20).

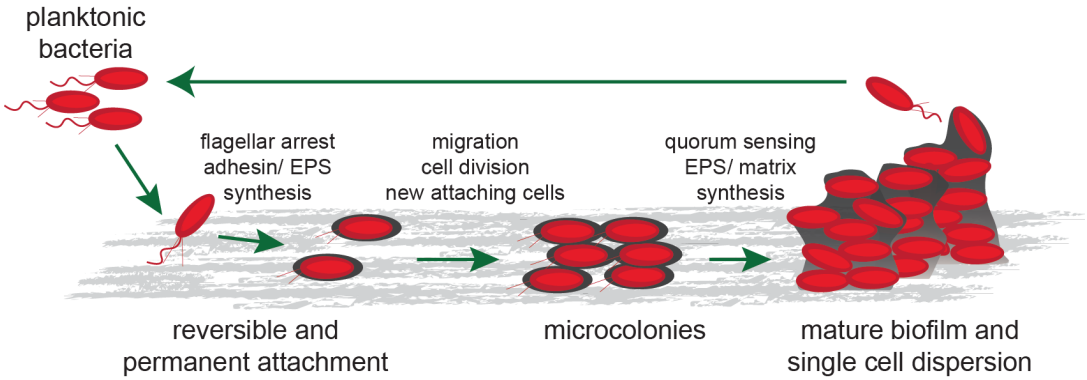

Fig. 1: Biofilm formation

When motile cells encounter a surface they can employ external appendages to move on the surface and/or synthesize EPS that helps to adhere to the surface. Migrating cells, dividing cells and new arriving planktonic cells form microcolonies. They communicate via quorum sensing and build up 3D biofilms by further EPS production and synthesis of additional matrix components. Cells that escape the biofilm can initiate biofilm formation elsewhere.

Surface contact can be either coincidental or a result of chemotaxis that directs motile cells to nutrition sources. However, depending on the surface and bacterial strains, envelope charge and hydrophobicity can impede first surface contact (21). To overcome such constrains, bacteria often use cellular appendages like pili, fimbriae or flagella (16). These not only serve as adhesins but also as sensors for surface contact. For example, type IV pili of *P. aeruginosa* seem to adhere over their entire length on various substrates and are required for surface induced alteration of gene transcription (22, 23). As the PilA pili subunits interact with a component of the Chp sensory system, it has been suggested that this sensory system might detect structural rearrangements of PilA that are generated by tension within the pilus when it adheres to a surface (24). Besides bringing cells in close contact with a surface, flagella of pathogenic bacteria are also known to facilitate adhesion to host cells via targeted receptors (25). In addition, experiments on abiotic rough and smooth surfaces have demonstrated that flagella can reach into cracks and crevices smaller than the bacterial cell and thereby serve as anchors (26). Furthermore, close to a surface, the viscous forces of a liquid are stronger compared to regions further away from the surface (27, 28). This, together with direct physical hindrance of rotation by a surface,

increases the load on flagellar rotation. It has been suggested that impeded flagellar rotation also serves a surface-sensing signal and probably leads to a change in proton motive force via the flagellum stator complex (29). However, recent findings in our group have shown that at least in *C. crescentus* only a functional flagellar stator is required for surface sensing while the filament is dispensable. This suggests that in *C. crescentus* some other physical impact, for example membrane deformation, might lead to a change in proton motive force (I. Hug, personal communication). The initial surface attachment is still reversible and allows cells to leave the surface again. Some bacteria even have means to explore the surface by swarming, twitching or gliding before finally committing to permanent attachment (30).

Surface contact triggers a multitude of processes that allow the cells to adapt to the new environment. These can be both translational and posttranslational and often include an increase of the second messenger c–di–GMP (see chapter: 1.2) and quorum sensing (cell-to-cell signaling) (16, 31–34). Production of EPS is activated in order to permanently attach to the substrate, mediate cell-cell contact and 3D growth (see chapter below). Besides EPS, other components like proteins or extracellular DNA are secreted to support the matrix of the growing biofilm. *Streptococcus mutans*, for example, produces glucan binding proteins that can be cell-bound or secreted and are necessary for biofilm structure (35). *Bacillus subtilis,* on the other hand*,* secretes a protein called Tas that forms extracellular amyloid fibers. Cells deficient in *tas* form only very weak pellicle biofilm, which can be rescued by addition of purified Tas fibers (36). In the marine bacterium *Rhodovulum* sp. and in *P. aeruginosa* extracellular DNA plays an important role in biofilm formation. Both form only very weak biofilm when treated with DNAses (37, 38). For *P. aeruginosa* it could be shown that in pellicle biofilm the extracellular DNA interacts with the Psl EPS and that DNA release is a process controlled by quorum sensing (39, 40). However, *P. aeruginosa* can also use DNA from other organisms for the same purpose (39).

Within a mature biofilm the dense matrix network limits transport to diffusion, which leads to gradients of nutrients and waste products but also potentially harmful molecules and creates different microenvironments. Therefore in nature, most biofilms home different species that occupy specific niches (6, 7). Even when a biofilm originates from one founder cell and is monoclonal, the offspring cells are phenotypically different depending on their position within the structure (7, 41).

Mature biofilms can have different forms that are largely species dependent and are also governed by external factors like nutrient availability or shear stress. When grown under flow with low nutrient availability, *P. aeruginosa* and *C. crescentus* form mushroom like structures (42, 43), which is thought to be a direct consequence of stochastic variations in nutrient availability (7). In both cases pili based motility was shown to be required for the formation of the mushroom cap (42–44). But there are also means to improve nutrient availability. When grown on agar, *E. coli* and *B. subtilis* form large round biofilms with a macroscopically wrinkled appearing surface (45, 46). Those vertical buckles form as a result of lateral compressive forces (47) and branch into a highly connected system of channels that facilitate liquid transport (46). Another possible way to facilitate transport within biofilms has been described for *Bacillus thuringiensis* by Houry and colleagues who observed swimming cells that travelled though the matrix and thereby formed transient tunnels that facilitate nutrient flow. When *B. thuringiensis* cells were equipped with a biocide, these swimming cells also helped to invade heterologous biofilms (48), illustrating that not only nutrition but also competition shape and influence biofilms.

1.1.2 Scaffolding and sticking of biofilms: exopolysaccharides and adhesins

Exopolysaccharides are a major component of the biofilm matrix. They vary in the number of different saccharide moieties present, the linkage between saccharides, the branching of the chain and the degree and type of modification of the saccharides (49). Depending on their purpose, EPS are secreted or anchored in the cell envelope.

EPS synthesis usually starts from activated UDP-coupled monosaccharides. There are three major pathways used by bacteria to assemble and export EPS polysaccharides: synthase-dependent, ABC-transporter-dependent and Wzx/Wzy-dependent pathways (50, 51). The core of the synthase-dependent pathway is the membrane spanning synthase complex, which binds the activated saccharides and directly polymerizes and transports them across the envelope (51). EPS synthesized via this pathway usually have only one single saccharide precursor (50). However, the homopolymer can be modified during export as described for alginate synthesis (see chapter: 1.2.4.2.) (52, 53). In the ABC-transporter-dependent pathway the polysaccharide is assembled on a lipid anchor at the cytosolic side of the inner membrane and transported as a whole through the cell envelope by an ABC-

transporter (54). In contrast, the Wzx/Wzy-dependent pathway first assembles lipid-linked oligosaccharide subunits. They have to be individually flipped by the Wzx protein across the membrane before being polymerized by Wzy and exported through the outer membrane. The *Caulobacter* adhesive holdfast is synthesized via this pathway and described in detail in the chapter: 1.3.3.2.

EPS are hydrated gels that show viscoelastic properties, meaning that their response to mechanical stress has both an elastic and viscous component. Besides other effects, these properties result in a time dependent response to stress (55). The reason for this behavior are the many transient entanglement interactions that occur within the polymer's network like London (dispersion)-forces, electrostatic forces or hydrogen bonds. If a mechanical stress occurs within a time window similar or below the time constant of the transient interactions the response is elastic and the stress is absorbed. If this stress persists longer, the response is viscous due to the ongoing breaking and reforming of interactions, the EPS is irreversible deformed and the strain reduced (55–57). This means, that if the interactions within the network are very strong, e.g. salt bridges or even covalent linkages, the EPS behaves more like a viscoelastic solid, their deformation upon a stress is reduced and the stress imposed onto the network does not decrease. On the other hand, if the EPS is stabilized mainly by weak and fluctuating crosslinks, it does rather behave like a viscoelastic fluid which is readily deformed upon a stress and thus the stress is reduced over time (55, 56). The nature of interactions depends not only on the core saccharides but also their decorations (57–59). Also the composition of the medium within which the EPS resides (e.g. salt) and the temperature, which reduces the time constant of non-permanent interactions, influence viscoelasticity (60, 61).

Viscoelasticity is only one characteristic of EPS and EPS modification can also serve for other purposes (59). Depending on their physical properties, EPS can have different functions within the biofilm (49). To protect biofilms form desiccation, hydrophilic EPS bind high amount of water, while neutral and charged EPS are involve in the formation of a network that confers stability and cohesion to the biofilm. Thereby, not only attractive but also repulsive forces play a role as they can confer a certain degree of stiffness to the matrix (58). Charged EPS can also be involved in the binding of organic compounds or enzymes that make the matrix an extracellular digestive system. Bacteria also secrete EPS as an extracellular storage agent for carbohydrates or energy (49). Furthermore, EPS can serve as cryo-protectants (62) or

form a protective shield against reactive oxygen species (63). In *Burkholderia cepacia* the latter is attributed to acetyl groups decorating the polymer, which are the first to be cleaved in presence of reactive oxygen species (63).

Considering the variety of applications for EPS, it is not surprising that bacteria often encode genes for several different EPS. A very common one in gram-negative bacteria is the lipopolysaccharide of which the outermost part (O-antigen) is synthesized by a Wzx/Wzy-dependent pathway (64). Besides this, *C. crescentus* produces an adhesive holdfast EPS and a surface associated capsular EPS (65, 66). *Escherichia coli* employs two different EPS: poly-N-acetyl-glucosamine (PNAG) and colanic acid. While PNAG was shown to be essential for initial permanent attachment (67), colonic acid was dispensable for this early step but crucial for the formation of complex biofilm structures (68). *P. aeruginosa* even encodes genes for three different EPS relevant for biofilm formation. Alginate gene expression is initiated early after surface contact and the polymer seems to help cells to remain attached to a surface (69). Furthermore, when overexpressed, alginate changes biofilm structure and enhances resistance against antibiotics (70). However, alginate seems not to be needed for biofilm formation (71). In the *P. aeruginosa* strain PAO1, cell surface associated Psl EPS, is needed for attachment while free extracellular Psl accumulates at the periphery of mature biofilm grown in flow chambers (72). In contrast, the cationic EPS Pel was found mainly in the core of these biofilms where it crosslinks extracellular DNA via an ion binding mechanism (73). In the *P. aeruginosa* strain PA14, on the other hand, Psl is not produced. Instead, the Pel EPS is required for the strain's biofilm maturation and can compensate for Psl in the biofilm periphery (73, 74).

An important function of some EPS is to serve as adhesins. Adhesion largely depends on non-covalent interaction forces. Thus, in very general terms, functional polar or hydrogen-bonding groups improve the adhesive (and cohesive) properties of an EPS (75). But also the molecular weight of the polymer strands has an impact on the mechanical properties of an adhesin (76). In turn, the molecular weight can depend on modifications of the polymer as recently described for alginate (53). Another important requirement for an adhesin is its resistance to moisture, as water molecules can strongly interfere with polar interactions and thereby massively reduce adhesion (75, 77). Acetylation or methylation was shown to improve moisture resistance (75).

Besides EPS, bacteria also employ proteinaceous structures for surface adhesion. Fimbrial structures like pili are one example and described in the chapter above. An example of an adhesin consisting of a single protein is the surface associated protein LapA. LapA was shown to be involved in biofilm formation for several species (78–81). It consists of an N-terminal anchoring domain, a long hydrophobic stretch of repeated amino acid sequences and a C-terminal adhesive domain. The repeated sequence region and the C-terminal domain are differentially involved in adhesion to either hydrophobic or hydrophilic surfaces (82). Cell adhesion can be regulated by a periplasmic protease that cleaves and releases LapA from the surface. This process is repressed by c–di–GMP which leads to LapA accumulation, and stronger net surface adhesion, similar to c–di–GMP induced EPS synthesis (83–85) (see chapter: 1.2.3 and 1.2.4).

1.1.3 Biofilms: challenges and opportunities

Bacterial biofilms quickly form on basically all liquid exposed surfaces of either biotic or abiotic nature. In the environment they often serve as basis for surface colonization of multicellular organisms (86, 87). Together they form biofouling communities that cause damage in navigation, drinking water supply and food industry and different industrial water systems. Schultz and colleagues estimated the yearly cost for the entire US navy incurred by biofouling to be several hundred million US$. The major part can be attributed to increased fuel consumption elicited by enhanced frictional drag (88). Also in aquaculture farms biofouling causes 5-10% of the production costs and affects both health of the cultured organisms and infrastructure of the farm (89). In water supply systems accumulation of biomass can largely affect water flow in pipes, or even obstruct them, while it also raises hygienic concerns (28, 90). Different complications arise in heat exchange systems where the microbial layer prevents heat transport by convection and dramatically reduces the system's efficiency (18). Rather recently, scientist realized that environmental biofilm in aquatic ecosystems serve as a reservoir for antibiotic resistance determinants. Yet, there is only little information to what extend such determinants can be transferred to potential pathogens (91).

Cells in the biofilm core show only slow or no growth, presumably due to limited nutritional supply and an anaerobic environment. This makes them highly tolerant against antimicrobial treatment (92, 93). The low susceptibility against antibiotics paired with the protective matrix, which can shield the cells from the immune system,

and other immune evasive mechanisms, makes it very difficult or nearly impossible to eradicate infections of biofilm forming pathogens (94). Biofilms are also the most prevalent cause for the failure of biomaterial implants, such as orthopedic implants, catheters, cardiac pacemakers or vascular prostheses. Due to limited success of antimicrobial treatment, such infections often require the surgical removal of the implant (95).

In all these fields control of biofilm formation comprises different approaches. They aim to prevent surface adhesion or reduce the organisms' viability on the surface from the beginning by selection of specific surface materials or by anti-adhesive or anti-microbial coating. Alternatively, their objective is to destroy already formed biofilms either physically or chemically (18, 87, 89, 95, 96). In the medical field recent approaches also aim to directly interfere with the signaling pathways associated with biofilm formation (96), namely quorum sensing (97–100) and c–di–GMP signaling (101, 102). Sub-MIC doses of the antibiotic azithromycin that blocks quorum sensing in *P. aeruginosa* could indeed ameliorate pulmonary functions in cystic fibrosis patients suffering from *P. aeruginosa* infection (99, 103). Yet, this type of therapy lead to a strong increase in antibiotic resistance of other pathogens found in the patient's lung making it a suboptimal treatment at best (103).

In a human point of view, microbial biofilms can form at the wrong place. Yet, they are of high ecological importance as they play a major role in nutrition cycling (104–106). This is exploited industrially in sewage water treatment systems where biofilms can be used for denitrification and reduce the load of biodegradable organic waste and phosphorous (107, 108). Recent studies have shown that, at least under laboratory conditions, such biofilm based sewage water treatment systems can be coupled with the generation of electricity (109). Furthermore, the diversity of metabolic pathways found within the bacterial world makes them an interesting tool to produce industrial chemicals in bioreactors. Biofilms of *Acetobacter* (so called "mother") are used since several thousand years to convert ethanol to acetic acid and thus produce vinegar (110). Bioreactors based on either artificially or naturally surface adherent cell cultures generally show higher production rates due to enhanced cell mass concentrations. They were already successfully applied, at least in small scale, for ethanol, butanol, lactic acid, fumaric acid and succinic acid production (111). Also, even more complex conversions could be potentially achieved by using multispecies

biofilms (112). But not only metabolites produced by biofilm have gained more and more attention. Also bacteria derived exopolysaccharides are of great interest for various industrial and medical fields, due to their remarkable and very diverse properties (see chapter above) (49, 50).

Therefore, understanding the principals of biofilm formation not only helps to prevent their formation at unfavorable places but also opens a variety of technical and ecological opportunities.

1.2 C–di–GMP

Bis-(3',5')-cyclic-dimeric-guanosine-monophosphate (c–di–GMP) is a near-ubiquitous second messenger. In many cases high levels of c–di–GMP are associated with a sessile life-style and biofilm formation including production of exopolysaccharides, matrix components and adhesins. In contrast, different types of motilities (swimming, swarming, gliding, twitching) are generally promoted when c–di–GMP levels are low (Fig. 2). But the second messenger was also shown to regulate other processes such as virulence, several resistance mechanisms, cell cycle progression, cell differentiation and antibiotic production (31).

Computational analyses of microbial genomes have shown that most bacteria encode proteins that are related to c–di–GMP, such as the enzymes involved in its homeostasis. In fact, these enzymes comprise one of the largest protein families in the bacterial kingdom, which emphasizes the importance of c–di–GMP in the microbial world (31, 113, 114). As a bacteria-specific second messenger it is not surprising that eukaryotic cells have adapted to this molecule. They can detect and elicit an immune response against intruding microorganisms by sensing c–di–nucleotides (115, 116).

Specialized enzymes called diguanylate cyclases and phosphodiesterases integrate intra and extracellular signals either directly or indirectly and synthesize or degrade c–di–GMP. C–di–GMP binds to various effector proteins that propagate the signal into downstream pathways (Fig. 2). While in some cases a global c–di–GMP pool can affect many processes in parallel (117, 118), in other cases the nucleotide produced or degraded by a specific DGC or PDE was suggested to act rather locally on a particular pathway (119–121).

1.2.1 C–di–GMP synthesis and degradation

C–di–GMP homeostasis is mediated via the c–di–GMP producing diguanylate cyclases (DGCs) and the c–di–GMP degrading phosphodiesterases (PDEs).

Diguanylate cyclase domains have a conserved and eponymous motive (GG(D/E)EF) that forms the active site. DGCs condense two GTP into one c–di–GMP molecule. As each GGDEF domain only binds one GTP, two of these domains have to symmetrically align and bring the two nucleotides into close proximity in order to allow condensation (122, 123). Many DGCs show allosteric product inhibition, which

requires an additional conserved motive (RxxD) called I-site. The I-site precedes the GGDEF motive and binds an intercalated dimer of c–di–GMP, which – in most cases – non-covalently crosslinks the GGDEF domains of two proteins in a catalytically incompetent conformation (122, 124–126). The necessity to form a correctly aligned dimer has been exploited by nature in several ways in order to control activity of DGCs. PleD, for example, is present as a monomer in its inactive form and dimerizes upon phosphorylation in order to be active (127). On the other hand, the *E. coli* DgcZ forms a constitutive dimer which can adopt a catalytically competent and an incompetent conformation in response to zinc that binds to its C-terminal zinc-binding domain (123). Moreover, the DGC of WspR from *P. aeruginosa* adopts a tetrameric conformation when activated by phosphorylation. But its full enzymatic potential was shown to be unleashed upon formation of even higher oligomers (128, 129).

Phosphodiesterases can be divided into two distinct groups namely c-di-GMP-specific phosphodiesterases harboring the consensus EAL domain or those with an HD-GYP motive. While both classes degrade c-di-GMP into linear pGpG (125, 130, 131) only HD-GYP phosphodiesterases degrade their substrate further into two molecules of GMP (132, 133). For bacteria absent of HD-GYP PDEs it was suggested that pGpG can serve as a signaling molecule itself (134) and in some cases can still be degraded into GMP by specific ribonucleases (135, 136).

EAL domain PDEs generally need to dimerize in order to be active, although from a reaction mechanisms point of view it is not entirely clear why they have to do so (137–140). The EAL motive locates to a small groove in the protein structure which is also the substrate binding and active site (141, 142). Hydrolysis of c–di–GMP was proposed to occur through a nucleophilic attack on the phosphorous atom by a deprotonated water molecule that is coordinated by two Mg^{2+} ions. Deprotonation is catalyzed by a glutamic acid which lies outside of the EAL motive and serves as a general base (138, 141, 142). Residues involved in substrate binding and Mg^{2+} ion coordination (one of which being the glutamic acid of the EAL motive) and the glutamic acid residue serving as the general base are highly conserved (138). Another highly conserved region is the dimer interface of the EAL domain (137, 143). Mutations in this region do not only affect the protein's oligomeric state but also strongly affect catalytic parameters (143). Recent studies have suggested that in some

cases the EAL domain dimer might transit from an open to a closed conformation. These quarternary changes affect its activity depending on activation stimuli transmitted though accessory domains (see below) (139, 140).

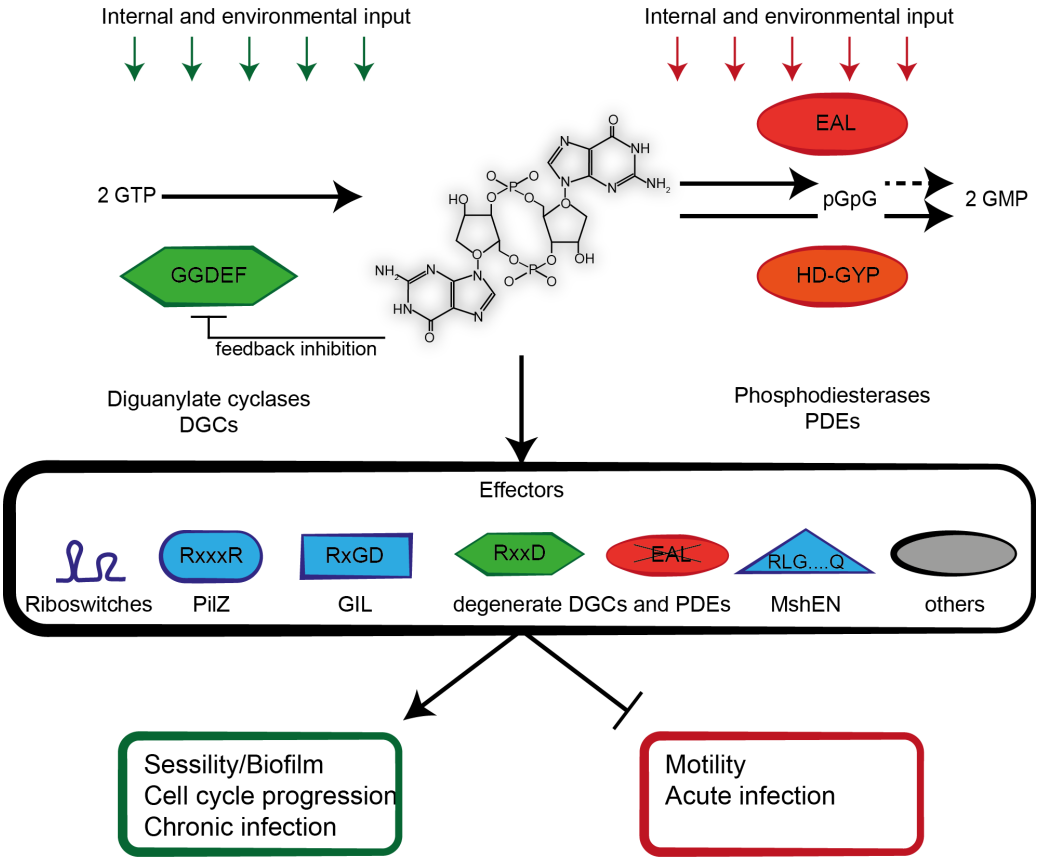

Fig. 2: C–di–GMP signaling

C–di–GMP is produced by diguanylate cyclases (DGC) that have a characteristic GGDEF domain and degraded by phosphodiesterases (PDE) that have either an EAL or HD-GYP domain. EAL and HD-GYP differ in their final degradation product. Both DGC and PDE activity can be regulated on the expression or post-transcriptional level by various inputs. C–di–GMP transmits the signal by binding to specific effector riboswitches or effector proteins that can have different binding domains some of which are not defined yet. These effectors target different processes either on the transcriptional, translational or post-translational level. Modified from (117, 144).

Finally, the HD-GYP family of phosphodiesterases is the least studied class. Up to date, only 3 structures of active enzymes have been published, which show a variable number of coordinated metal ions and different substrate bias for c–di–GMP and pGpG respectively (145–147). The structures also show a conserved loop, which has been proposed to serve as a lid and gate substrate binding to the active site (146–148).

1.2.2 Regulation of c–di–GMP turnover

About 2/3 of all sequenced bacterial genomes encode at least one GGDEF, EAL or HD-GYP domain protein. However, in some cases, for example in several *Vibrio* or *Shewanella* species, around 100 genes contain either one or both of these domains (149, 150). This suggests that c–di–GMP signaling networks allow a very precise and sophisticated response to a multitude of different signals. It is thus not surprising that *Vibrio cholerae*, which encodes 61 enzymes predicted to be involved in c–di–GMP turnover, shows an up to 20 fold variation in c–di–GMP levels depending on the growth medium tested (151).

But how is c–di–GMP turnover regulated? Some PDEs and DGCs are controlled on a transcriptional level and are only expressed under certain conditions. In *E. coli* for example, some of the GGDEF/EAL encoding genes are differentially expressed depending on growth phase and temperature (152). Furthermore, one of the *E. coli* EAL domain proteins, PdeL, activates its own transcription in response to the prevailing c–di–GMP levels (153). Also *Yersinia pestis* changes expression of its two DGCs and one PDE in response to several environmental stimuli (154) while transcription of the PDE PdeA of *C. crescentus* is cell cycle controlled (155) (see chapter: 1.3.2.1).

However, most PDEs and DGCs are also expected, and some were confirmed to be subject to posttranslational control (137, 156, 157). Their GGDEF, EAL and HD-GYP domains are linked to N-terminal accessory domains with predicted functions predominantly in protein localization, dimerization and signal sensing (150). These domains are universally used and also combined with other output domains like histidine kinases, phosphatases or DNA binding domains (113, 158–160).

The structurally similar GAF (often found in c**G**MP-specific phosphodiesterases, **a**denylyl cyclases and **F**hlA) and PAS (**P**er/**A**RNT/**S**im) domains, for example, are often associated with GGDEF, EAL and HD-GYP domains. GAF and PAS domains bind to different small molecules which are either sensed directly (e.g. cAMP/cGMP, some metabolites and ions) or serve as adaptors to sense stimuli like redox state (sensed through flavin adenine dinucleotide (FAD)), light (sensed through flavin mononucleotide or chromophores), or oxygen and nitric oxide (sensed through heme) (161–165). But GAF and PAS domains can also serve as interface for interaction with other proteins (166). Other sensory domains that control DGCs or PDEs are more specific. Globin-domains for example sense oxygen via a bound heme group (167–

170), while the BLUF (**b**lue **l**ight **u**sing **F**AD) domain responds to photons (137, 139). In *Shewanella woodyi*, the nitric oxide sensing domain H-NOX is part of a separate protein and is thought to promote PDE activity by protein-protein interaction (171).

PDEs and DGCs also often contain a REC (phospho**rec**eiver) domain and serve as two-domain response regulators in two-component systems. Upon a signal, a sensor histidine kinase phosphorylates a conserved aspartic acid in the REC domain of its cognate response regulator and thus controls the regulators output activity (172). The prevalent domain combination observed in DGCs is such a REC-GGDEF fusion (150). Examples of such phosphorylation controlled PDEs are PleD and WspR that upon phosphorylation dimer and oligomerize, respectively (127–129) (see chapter: 1.2.1).

A multitude of proteins are hybrids of GGDEF, EAL and HD-GYP domains (150). Interestingly, in most GGDEF-EAL proteins, either both domains are potentially active or only the EAL domain is active. In bi-functional proteins GGDEF-EAL domains often associate with additional regulatory domains as described above, which suggests that they employ either activity depending on external stimuli (150). In several hybrid GGDEF-EAL proteins with PDE only activity, the degenerate GGDEF domain exerts a regulatory role. It retained substrate binding and activates the EAL catalytic activity in presence of GTP (125, 173, 174).

1.2.3 The versatility of downstream c–di–GMP effectors

C–di–GMP effectors propagate the c–di–GMP signal into different downstream pathways (Fig. 2). Yet, in contrast to the well-defined motives required in DGCs and PDEs, c–di–GMP binding motives of effector proteins are very diverse. A possible reason for this diversity is that the ligand c–di–GMP can adopt various different conformations and oligomeric states (114). The binding motives commonly contain Asp and Arg residues, as these can form H-bonds with the guanine base of c–di–GMP in several ways. Furthermore Arg, Phe, Trp and Tyr can form stacks with the guanine's hydrophobic surface (114). Due to these varieties, identification and characterization of effector proteins lagged behind c–di–GMP turnover proteins. But thanks to the development of high-throughput screening methods (175–179), more and more c–di–GMP effectors are being identified.

Early detected c–di–GMP effectors were degenerate GGDEF domain proteins, which have lost enzymatic activity but retained c–di–GMP binding with their I–site (180)

(see chapter: 1.2.1). Similarly, enzymatic inactive EAL domains can also serve as c–di–GMP effector proteins (83, 181–183). A class with only one characterized member so far (BcsE, see chapter below) is the GIL (**G**GDEF **I**-site **l**ike) domain. It not only has a conserved RxGD motive required for c–di–GMP binding, which is very similar to the RxxD motive of the I-site of GGDEF domain, but also exhibits secondary structural elements around this motive which are similar to the I-site region (184).

A big class of c–di–GMP effectors binds c–di–GMP via a PilZ domain that exists as a single domain protein (185–187) but also as part of a multidomain protein (188–191). There are three types of PilZ domains (114). Type I domains bind c–di–GMP via two conserved motives (RxxxR and (D/N)xSxxG) (159). The type II PilZ domains have a degenerate binding motive and are thus incapable to bind c–di–GMP. The eponymous PilZ protein which is required for pili function belongs to this group (190, 192). Type III PilZ only has one characterized representative so far: XCC6012 from *Xanthomonas campestris*. Its domain structure is truncated by two additional helices that allow the protein to tetramerize. Also this type of PilZ does not bind c–di–GMP (114, 193).

The MshEN domain shows the so far longest conserved c–di–GMP binding motive (RLGxx(L/V/I)(L/V/I)xxG(L/V/I)(L/V/I)xxxxLxxxLxxQ) (194). It was first identified in a subset of ATPases that are involved in pili biogenesis and type II secretion but also associates with a variety of other domains such as Rec, glycosyltransferase, kinase or CheY domain (194, 195).

C–di–GMP effectors can be enzymes (195–197), transcription factors (198–200), receptors (201) adaptor proteins (202, 203) or even short stretches of non-coding RNA called riboswitches (204, 205). Together they control downstream pathways on a transcriptional, post-transcriptional and post-translational level. On a post-translational level, protein effectors pass on the signal by various ways, including adjustment of enzymatic activity, protein stability, localization, affinity to DNA or affinity to another interaction partner.

In MshE of *V. cholerae*, the eponymous representative of the MshEN biding domain, c–di–GMP activates ATPase activity and thereby promotes pilus assembly (194, 195, 206). On the other hand, c–di–GMP binding to the dimerization interface of the AAA+ ATPases FliI and HrcN of *Pseudomonas* species, which are involved in the export mechanism of the flagellum and type III secretion system, respectively, inhibits

their enzymatic activity *in vitro* (197). In *C. crescentus* the kinase CckA switches into the phosphatase mode upon c–di–GMP binding (207). On the other hand, the localization factor TipF of *C. crescentus* shows altered stability and localization in response to c–di–GMP. It is only stable and localizes to the pole when bound to c–di–GMP and is quickly degraded when c–di–GMP levels drop (182)(see chapter: 1.3.2). A well-studied example for altered protein-protein interaction is the widely conserved transmembrane protein LapD that regulates accumulation of the adhesin LapA on the cell surface (see chapter: 1.1.2). LapD binds c–di–GMP via its degenerate EAL domain. This leads to major conformational changes that are translated into the periplasmic domain of LapD and the recruitment of the periplasmic protease LapG. LapG is thereby sequestered away from LapA and thus prevented from cleaving and releasing the adhesin (83–85, 208).

1.2.4 C–di–GMP effector controlled EPS systems

C–di–GMP was shown to regulate various exopolysaccharides, either on a transcriptional level, posttranslational level or both. For the *Agrobacterium* EPS curdlan, a unipolar polysaccharide, the regulation mechanism is largely unknown. For xanthan of *Xanthomonas campestris*, *Vibrio* EPS, or Pel of *P. aeruginosa* only transcriptional control has been shown (209) which is why they are not further discussed here. Several posttranslational c–di–GMP effectors that control EPS synthesis are currently known and all but one are essential for EPS synthesis (see below). Most effectors seem to inhibit glycosyltransferase activity or export in the c–di–GMP unbound form and activate synthesis when bound to the nucleotide.

1.2.4.1 BcsA and BcsE control cellulose production

Cellulose is a widespread poly-β-(1,4)-D-glucose EPS and is important for surface colonization and virulence (149, 210–212). Cellulose synthesis in *Komagataeibacter xylinus* (former *Acetobacter xylinum*) was the first process shown to be controlled by c–di–GMP (213, 214). *In vitro*, synthesis requires only the combined action of the inner membrane protein BcsA and the periplasmic protein BcsB that couple catalysis and export (189, 215) (Fig. 3A). *In vivo,* however, additional components are necessary (216). Thanks to crystal structures of the BcsAB complex of *Rhodobacter sphaeroides* with and without c–di–GMP the underlying mechanism of cellulose synthesis control is well understood (189, 217). The synthase BcsA contains the

glycosyltransferase activity, yet its active site is blocked by a gating loop. Only binding of c–di–GMP to the BcsA's intracellular PilZ domain displaces this loop and allows substrate binding and catalysis (189, 217, 218). The PilZ domain is contained within a C-terminal β-barrel that is connected to the glycosyltransferase domain via a linker region. This linker forms a two-stranded β-sheet with part of the gating loop. In the autoinhibited state, Arg580, which is part of the PilZ RXXXR motif, tethers the gating loop in front of the active site entrance. C–di–GMP binds as an intercalated dimer. In order to accommodate the nucleotide Arg580 flips over. This leads to a slight rotation of the linker resulting in the displacement of the gating loop and enables substrate entry to the active site (189).

Recently, the protein BcsE was also shown to bind c–di–GMP specifically. BcsE is only encoded in cellulose operons type II as found in *Salmonella enterica, Pseudomonas putida*, *Burkholderia mallei* or *Chromobacterium violaceum* (149). It is required for maximal cellulose production in *S. enterica* and the authors could not rule out an alteration in cellulose fiber structure in a Δ*bcsE* mutant (184). It has no homology to any protein with known function and its mode of action remains elusive. Yet, the c–di–GMP binding site could be located within an uncharacterized domain with a conserved RxGD motive and predicted structural similarities to the I-site of GGDEF-domains. Based on this observation the domain was named **G**GDEF-**I**-site-**l**ike domain (GIL) (184) (see chapter: 1.2.1). *S. enterica* encodes 12 GGDEF-domain containing proteins. However, in a strain that was stripped of all GGDEF-domain proteins, single gene restoration revealed that only four of them could rescue the cellulose deficient phenotype. This indicates that in *S. enterica* cellulose synthesis is regulated by a partially localized pool of c–di–GMP (219).

1.2.4.2 Alg44 is highly interlinked and required for alginate polymerization

Alginate is widely used in different industrial fields and consists of variable amounts of (1,4)-linked β-mannuronic acid and its epimer α-guluronic acid. *P. aeruginosa* synthesized the EPS in a large multiprotein complex. Alg8 is the synthase and spans the inner membrane (49, 50). Before being exported by an outer membrane pore, the nascent alginate chain is O-acetylated by four acetyltransferases and epimerized by a single epimerase that converts the C6 mannuronic acid into the C5 guluronic acid. These enzymes are located in the inner membrane and the periplasm (52, 53). The alginate synthase complex furthermore contains different additional helper proteins including Alg44 (49, 50). Alg44 has a cytoplasmic PilZ domain and a periplasmic

domain similar to membrane fusion proteins that are implicated in protein-protein interaction (190, 218, 220) (Fig. 3B). C–di–GMP binding to Alg44 via the canonical PilZ c–di–GMP binding motif is required for alginate polymerization suggesting that Alg44 might act as a co-polymerase (190, 221, 222). In line with this, Alg44 interacts with Alg8 which was found to be independent of c–di–GMP or the PilZ domain (53). Due to the similarities of this synthase-PilZ heterocomplex with the cellulose synthase BcsA it was proposed that they might share a common inhibitory mechanism (189). However, there are indications that Alg44 forms a dimer and that it is involved in several c–di–GMP independent protein-protein interactions with periplasmic components of the alginate synthesis machinery conferring stability to the proteins (53, 223). Thus, the activation mechanism of alginate synthase might differ from the autoinhibitory mechanism of BcsA, and Alg44 might have additional roles during polymer synthesis (53).

It was found by Hay and colleagues (224) that membrane bound GGDEF-EAL protein MucR specifically activates alginate production. MucR shows both PDE and DGC activity *in vitro*, and was suggested to be active as a DGC in biofilms and as PDE in planktonic cells (225).

1.2.4.3 PelD and FleQ are required for *pel* synthesis and EPS production

In *P. aeruginosa*, the EPS Pel is a polysaccharide composed of partially deacetylated N-acetyl-galactosamine and N-acetyl-glucosamine (73) and is required for biofilm formation (73, 74) (see chapter: 1.1.2). Pel synthesis is controlled by c-di-GMP on both the transcriptional and post-translational level (Fig. 3C).

Expression of the *pel* operon is positively and negatively regulated by FleQ in a c–di–GMP dependent manner (199, 226). FleQ is a transcription factor with a DNA binding helix-turn-helix domain, a central AAA+ ATPase σ^{54}-interaction domain and a N-terminal REC domain which lacks the aspartic acid required for phosphorylation (227). The REC domain is required for FleQ oligomerization and function, while the central AAA+ ATPase contains the c–di–GMP binding pocket that is distinct from the ATP binding site (227, 228). The *pel* operon has two FleQ binding boxes, one (box 2) is required for transcription repression and one (box1) is required for transcription activation (226). It is thought that in the absence of c–di–GMP FleQ binds to both boxes, which leads to DNA bending and transcription inhibition. When bound to c–di–GMP, FleQ undergoes major quaternary structure rearrangements which might

reduce its affinity for box 2 and DNA bending and thus activate *pel* transcription (226, 228).

Posttranslational regulation of Pel EPS is mediated by PelD. PelD has four TM domains followed by a cytosolic GAF and degenerate GGDEF (with the sequence GGEEF) domain (229). C–di–GMP was shown to bind to the conserved I-site either as a monomer or dimer and the binding site was required for Pel synthesis (180, 229). Although the cytosolic part of PelD was always observed as a monomer *in vitro*, Whitney and colleagues (229) realized that the linker between the last TM and the GAF domain is predicted to form coiled-coils upon which they concluded that PelD might form a dimer *in vivo*. The predicted Pel glycosyltransferase is a cytosolic protein without any TM domain. This prompted the authors to suggest, that PelD might form an inner membrane transport channel and Li and colleagues proposed that the other two inner membrane proteins PelE and PelG might also contribute to the channel (229, 230). However, whether PelD really is part of a channel, how c–di–GMP controls PelD's activity and the roles of the other Pel proteins needs further investigation.

Several DGCs were shown to contribute to the c–di–GMP pool that controls Pel synthesis (Fig. 3C). Overexpression of RoeA increased Pel synthesis, which depended on an intact GGDEF motive (231). Together with another DGC called SadC, RoeA was shown to increase c–di–GMP levels and promote biofilm formation in response to increased concentrations of several amino acids (232). The YfiBNR system that activates the transmembrane DGC YfiR in response to uncharacterized periplasmic signals, strongly upregulates *pel* transcription (233). Likewise, *pel* transcription is also increased by the two-domain response regulator WspR (234). WspR activates its DGC activity upon phosphorylation via the transmembrane chemotaxis-like regulatory Wsp system that reacts to the presence of surfaces (128, 234). Last but not least, the membrane bound GGDEF-EAL protein BifA acts as a PDE and its deletion promotes Pel synthesis (235).

1.2.4.4 PgaCD form the PNAG synthase complex

Poly-β-(1,6)-N-acetyl-glucosamine (PNAG) is an important matrix component and crucial for biofilm formation in several bacteria such as *E. coli*, *Staphylococcus* and *Bordetella* (236–238). In *E. coli* it is produced by the widely conserved *pgaABCD* operon (239). Its transcription is regulated specifically by the DGC activity of DgcO (former YddV or DosC) by a yet unknown mechanism (121) (Fig. 3D). DgcO senses oxygen via a globin based domain (167). It is encoded in an operon together with

pdeO and forms a functional heterodimer with PdeO. PdeO is a PDE and has a heme binding pas domain and increases its PDE activity in presence of oxygen (240).

The Pga proteins produce PNAG in a synthase dependent mechanism. PgaA is predicted to form the outer membrane pore and is, together with the periplasmic de-N-acetylase PgaB, necessary for PNAG export (Fig. 3D). The synthase PgaC and the accessory protein PgaD are essential for PNAG synthesis (239). Biofilm formation and stability of PgaD largely depends on the c–di–GMP levels and the presence of PgaC (241, 242). Steiner and colleagues (242) could demonstrate that besides being required for *pgaABCD* transcription, c–di–GMP also allosterically activates PNAG synthesis and that for this type of control mainly the DGC DgcZ is required. C–di–GMP simultaneously bound to PgaC and PgaD and thereby stabilized PgaD. Both proteins alone were not able to interact with the nucleotide. The authors proposed that in the c–di–GMP induced stable complex, PgaD might structurally contribute to the inner membrane PNAG transport channel for which PgaC alone, with only 4 TM helices, would not be sufficient. In the absence of c–di–GMP, however, PgaC and PgaD only interact loosely and the latter is rapidly degraded which would switch off the system (242).

Fig. 3: C-di-GMP control of different EPS synthesis systems

C–di–GMP controlled synthesis steps are shown for different EPS systems. C–di–GMP effectors are colored in green, DGCs and PDEs are colored in blue, c–di–GMP is shown in yellow and the enzymes that polymerize the EPS are marked with a red star. (A) Cellulose synthesis in *S. enterica* is controlled by two effectors: the synthase BcsA with a PilZ domain and the GIL protein BcsE of unknown function. (B) The alginate synthase of *P. aeruginosa* Alg8 interacts with the PilZ domain protein Alg44 that is required for EPS synthesis. (C) The transmembrane degenerate GGDEF protein PelD of *P. aeruginosa* is required for Pel synthesis. Several DGCs and a PDE are known to contribute to the c–di–GMP pool that affects Pel synthesis. In addition, c–di–GMP binding to FleQ turns the protein from a negative into a positive transcription factor for the *pel* operon. (D) For PNAG synthesis in *E. coli,* the synthase PgaC and the accessory protein PgaD have to bind c–di–GMP together. In addition, their synthesis is controlled by c–di–GMP via an unknown mechanism. (E) The mixed-linked glucan of *S. meliloti* requires a synthase that binds c–di–GMP via its C-terminus. (F) In *L. monocytogenes* a transmembrane degenerate GGDEF protein is essential for EPS synthesis. Glc: glucose; GlcNAc: N-acetylglucosamine; Man: Mannuronic acid. Figure based on (243).
(Figure on next page →)

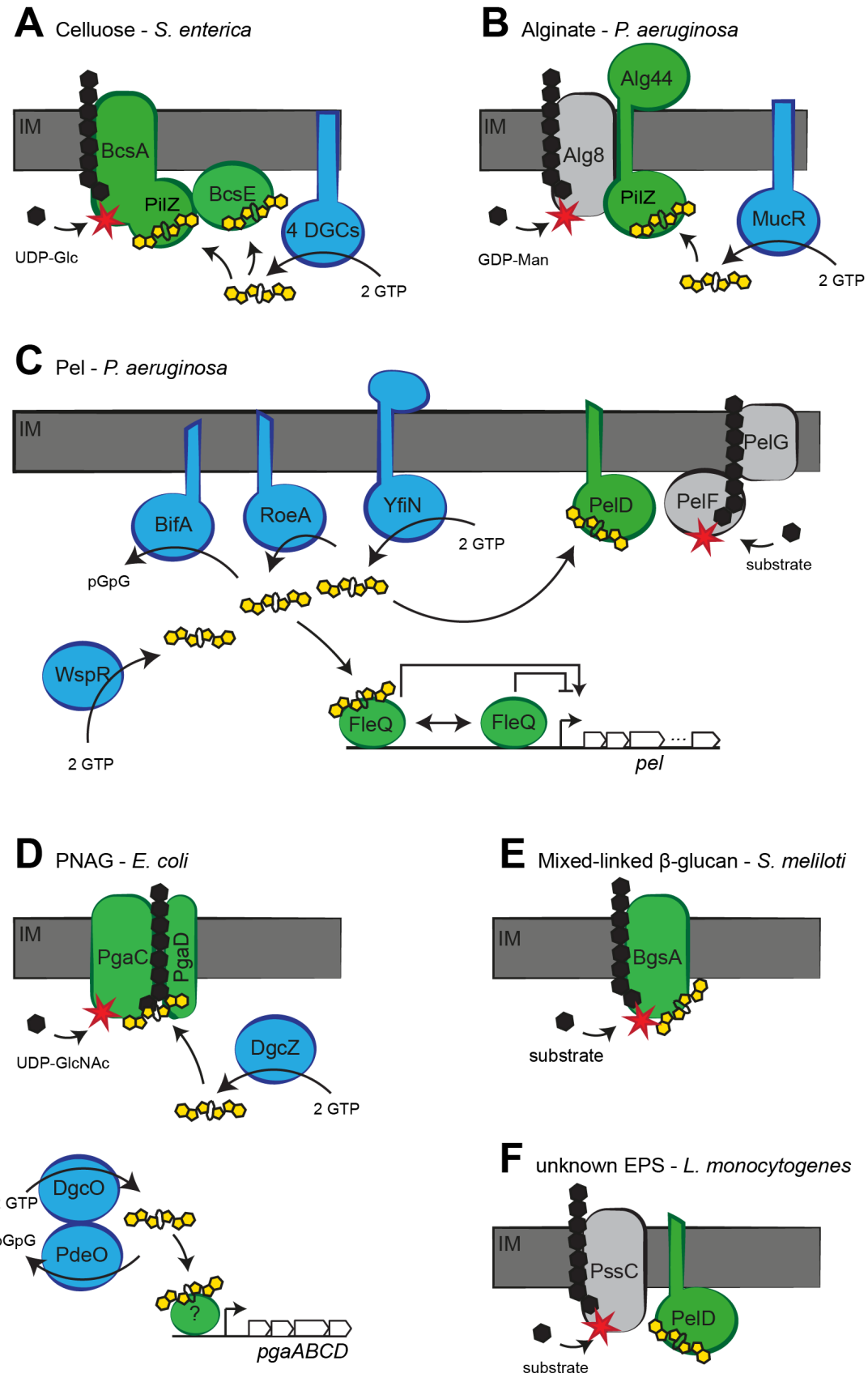
A Celluose - S. enterica
IM
BcsA
BcsE
PilZ
4 DGCs
UDP-Glc
2 GTP
B Alginate - P. aeruginosa
Alg44
IM
Alg8
PilZ
MucR
GDP-Man
2 GTP
C Pel - P. aeruginosa
IM
PelG
BifA
RoeA
YfiN
PelD
PelF
2 GTP
pGpG
substrate
WspR
2 GTP
FleQ
FleQ
pel
D PNAG - E. coli
IM
PgaC
PgaD
UDP-GlcNAc
DgcZ
2 GTP
2 GTP
DgcO
pGpG
PdeO
?
pgaABCD
E Mixed-linked β-glucan - S. meliloti
IM
BgsA
substrate
F unknown EPS - L. monocytogenes
IM
PssC
PelD
substrate

1.2.4.5 BgsA is the putative synthase of mixed-linked β-glucan

A novel EPS mixed-linked (1-3)(1-4)-β-glucan has been described by Pérez-Mendoza and colleagues in *Sinorhizobium meliloti* (209). This EPS was only produced under lab conditions when c–di–GMP levels were artificially increased. The predicted synthase BgsA was required for EPS production as well as for adhesion on plant roots and showed a wide distribution within the order of *Rhizobiales*. It shows some similarities with curdlan and cellulose synthases but does not have a PilZ domain. Yet, also BgsA binds c–di–GMP via its C-terminus, suggesting that also this protein is allosterically controlled by the second messenger (244) (Fig. 3E).

1.2.4.6 *Listeria monocytogenes* EPS requires a degenerate GGDEF protein

Synthesis of the newly described EPS of *Listeria monocytogenes* is activated by elevated c–di–GMP levels (245). This EPS is cell surface associated and required for cell aggregation but not for adhesion to abiotic surfaces. It consists of a β-(1,4)-N-acetylglucosamine chain that branches into an α-1,6-galactose every other residue (245). Encoded within the EPS synthesis gene cluster (named *pssA-E*) is the protein PssE that consists of a degenerate GGDEF domain fused to two transmembrane domains. Similar to PelD from *P. aeruginosa*, PssE binds c–di–GMP and is essential for EPS production. The polymerase of this EPS is probably PssC, which shows around 30% homology to the PNAG N-acetylglucosyltransferase IcaA of *Yersinia pestis* (245) (Fig. 3F).

1.3 *Caulobacter crescentus*

C. crescentus is an oligotrophic gram-negative bacterium belonging to the α-proteobacteria and a member of environmental biofouling communities. The cells have a crescentoid shape and grow a narrow cell envelope extension at one pole that is referred to as prostheca or stalk (246). They adhere to surfaces through the very strong holdfast adhesin, an exopolysaccharide (EPS) which is located at the tip of the stalk (247–249). Despite the physical connection of stalk and holdfast, it is assumed that the stalk rather plays a role in nutrition uptake than surface adhesion (250, 251).

C. crescentus has a biphasic cell cycle (252) (Fig. 4A). With every cell division two distinct cell types are produced: a replication competent sessile stalked cell and a replication incompetent motile swarmer cell. Swarmer cells bear pili and a flagellum and have to differentiate into stalked cells before replication can be initiated (252–254). This motile-to-sessile or swarmer-to-stalked cell (SW-to-ST) transition occurs automatically after a certain time or when the cell senses a surface which leads to immediate holdfast synthesis and attachment (255). As in *C. crescentus* the motile and sessile lifestyle are coupled to cell cycle it is not surprising that cell cycle control and c–di–GMP signaling are interwoven.

1.3.1 Cell cycle control

Newborn swarmer cells have different buoyancy than stalked cells, which allows isolation of swarmer cells and thus synchronization of cell cultures. Together with the biphasic nature of their cell cycle and the fact that cells replicate their genome only once per cell cycle (256), this makes *Caulobacter* a widely used and thoroughly studied model organism for cell cycle control.

1.3.1.1 A cascade of transcriptional regulators drive cell cycle progression

Cell cycle control of *C. crescentus* revolves around several global transcriptional regulators (DnaA, GcrA, CcrM, CtrA, SciP and the MucR paralogs MucRI/II) which target several hundred genes (65, 257, 258) and accessary proteins that are required for their regulation. These global regulators control gene expression often as antagonistic and cell-cycle specific pairs: In S-phase (stalked and early predivisional cells) activity of GcrA/CcrM dominate global transcriptional control, while in G2 phase (late predivisional cells) action of CtrA with SciP and in G1 phase (swarmer cells)

action of CtrA and MucRI/II prevail (65, 257, 258). Except for MucRI/II, the other global regulators oscillate during cell cycle (65, 259–263). They activate each other in a cascade like manner, while several positive and negative feedback loops ensure precise timing and robust progression of cell cycle events.

In swarmer cells, CtrA levels are high (260) and the protein represses DNA replication initiation in its phosphorylated form (CtrA-P) (264, 265). CtrA-P mediated replication block is alleviated only when CtrA is dephosphorylated and degraded during SW-to-ST transition (see chapter below). Release of replication block coincides with a peak of DnaA concentration (266). DnaA binding to the origin of replication (Cori) is required for DNA replication (263, 267). In *E. coli*, DnaA homo-oligomerizes upon DNA binding, which leads to the unwinding of DNA and facilitates assembly of the replisome (268). DnaA competes with CtrA for several overlapping binding sites in the *C. crescentus* Cori region (264, 267). CtrA degradation and DnaA binding to Cori thus initiate DNA replication. DnaA also activates transcription of *gcrA* (266) which in turn controls predominantly S-phase genes that harbor methylation sites including *ctrA* (257, 266, 269). Expression of *ctrA* is controlled by two promoters. The weaker promoter (P1) is only active in early predivisional cells and is negatively controlled by CtrA. Yet, P1 dependent transcription is enough to activate the stronger promoter (P2) which is positively regulated by CtrA itself and reaches maximal activity only in late predivisional cells (270). CtrA targets around 280 sites, including other regulatory genes and genes involved in polar development and cell division (65, 271). It also represses transcription of *gcrA* thus reducing GcrA levels in later stages of cell cycle and prevents its premature synthesis in swarmer cells prior G1-to-S phase transition (259) and it activates transcription of *sciP* (65). Together with MucRI/II, SciP exercises temporal control on CtrA activated genes. In G1 and G2 phase SciP represses CtrA targeted S-phase genes and in S-phase MucRI/II represses G1 and G2 phase genes. Yet both global regulators have additional, CtrA independent, regulons (65). Finally, in late predivisional cells CtrA activates transcription of *ccrM* (260). CcrM is a DNA methyltransferase that methylates adenines contained in GANTC and GATC recognition motives (262, 272). Those motives can be either hemi-methylated (after passing of DNA replication fork) or full-methylated (after remethylation by CcrM). Many promoters contain such differentially methylated motives and are thus predicted to respond either positively or negatively to their methylation state which couples their activity the progression of DNA replication (256, 273–275). The

promoter of *dnaA*, for example, is more active in its fully methylated state. Thus it only allows *dnaA* expression and thereby a new DNA replication initiation when the former replication round is completed (275). On the other hand, the P1-promoter of CtrA is repressed when fully methylated. Transcription and accumulation of this regulator can therefore only begin after the replication fork has passed (276). And finally, also the promoter of *ccrM* itself contains methylation sites and its activity is repressed in the fully methylated state. This, together with its degradation by the protease Lon (277) limits CcrM activity to the late predivisional cell which allows the resetting of the genomic cell cycle clock and prepares the cell for a new round of replication.

In recent years, researchers have used chromatin immunoprecipitation sequencing (ChIP-seq) and single-molecule, real-time (SMRT) DNA sequencing in order to draw a more complete and global picture of the *Caulobacter* cell cycle regulon (65, 257, 269, 273, 278, 279). These data, supported by growing genetic and biochemical evidence show a complex, highly interconnected and redundant regulatory network which works robustly and can support a high degree of perturbations (278, 280–284).

Yet, confronted with such a complex network, people thrived to identify the essential core components that still drive the system (278, 285). Vandecan and colleagues developed a core-oscillator model for DNA replication which comprises only three players that are essential in *C. crescentus*: CtrA, DnaA and the response regulator DivK (see chapter below). DnaA and DivK take part in two (indirect) feedback loops that project back to CtrA. The model shows that these players are sufficient to explain the oscillating behavior experimentally observed for all three proteins (285). Accordingly, besides DnaA and CtrA, the other global regulators (GcrA, CcrM, SciP, MucR/II) are not essential for *Caulobacter* viability (65, 278, 279, 286). In line with this, phylogenetic analysis revealed that within alphaproteobacteria there are several species that do not encode homologs of the antagonistic pair GcrA/CcrM. Interestingly, those species grow very slowly which indicates, that the GcrA/CcrM module brings temporal robustness to the system which is not necessary in a more relaxed cell cycle (278).

1.3.1.2 Swarmer-to-stalked cell transition is tightly controlled

In swarmer cells, DNA replication is repressed by phosphorylated CtrA that binds to the Cori region (264, 265). In order to replicate, the cells release this repression via two interconnected pathways that ultimately lead to both dephosphorylation and

degradation of CtrA (202, 207, 287). While the system can support deletion of one branch of the pathway, disruption of both branches is synthetically lethal (207).

The single domain response regulator DivK is an essential part of a signal transduction pathway that translates spatial and cell type specific information into CtrA activity by regulating both CtrA phosphorylation and degradation via the CckA-ChpT-CtrA phosphorelay (287–291) (Fig. 4B). DivK is differentially phosphorylated by the bi-functional histidine kinases/phosphatases PleC and the histidine kinase DivJ (289, 292). PleC and DivJ localization patterns change through the cell cycle (293). In swarmer cells PleC occupies the flagellated pole and dephosphorylates DivK (290). When DivK is dephosphorylated, the activity of the polarly localized CckA-ChpT-CtrA phosphorelay is promoted by DivL which leads to phosphorylation of CtrA (287, 294). CtrA-P binds Cori and thus blocks replication initiation (264, 265). During SW-to-ST transition DivJ appears at the stalked pole replacing PleC, while PleC relocalizes to the nascent pole (293). DivJ phosphorylates DivK (292, 295). DivK-P turns PleC from a phosphatase into a kinase, which - together with DivJ - can phosphorylate PleD (288, 296, 297). DivK-P interacts with DivL leading to activation of the CckA phosphatase activity, a process which is further strengthened by c-di-GMP (207, 294) (see chapter: 1.3.2.1). Together, these events lead to a reversion of the CckA-ChpT-CtrA phosphorelay and consequently to the dephosphorylation of CtrA (207, 287, 291). Furthermore, CckA phosphatase activity also promotes dephosphorylation of the CpdR adaptor protein. Unphosphorylated CpdR localizes the ClpXP protease to the stalked pole to enhance binding and degradation of certain substrates, such as CtrA and the phosphodiesterase PdeA. Degradation of PdeA supports upshift of c−di−GMP levels and provides a positive feedback loop that promotes CtrA dephosphorylation and degradation (287, 298–300). CpdR is the first of three adaptor proteins which - in a hierarchical manner - bind ClpXP. Binding of each adaptor requires the presence of the hierarchically former one and changes substrate specificity of ClpXP (300). The last adaptor protein PopA binds c−di−GMP which finally promotes degradation of CtrA by ClpXP (202).

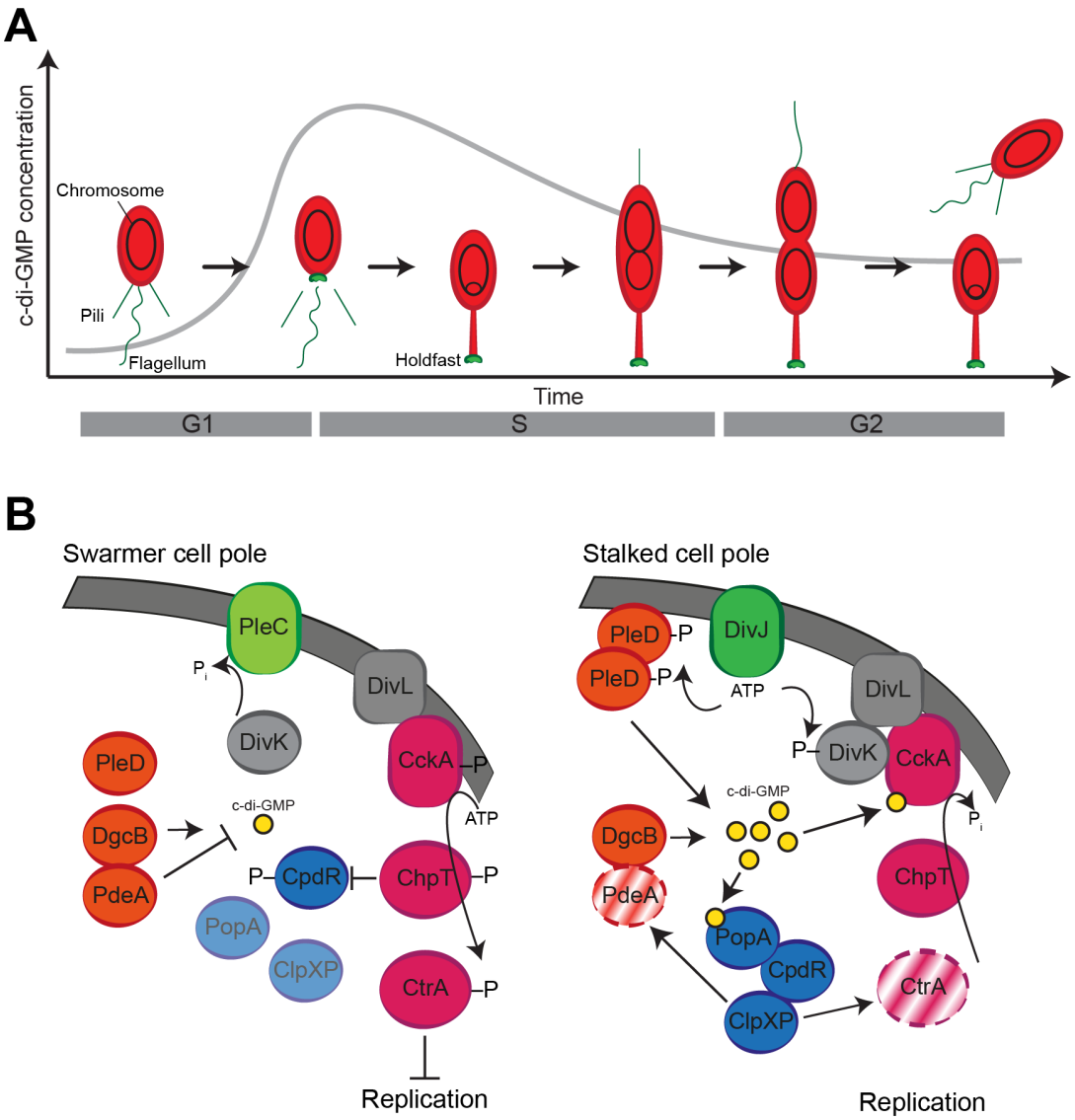

Fig. 4: *C. crescentus* cell cycle and swarmer-to-stalked cell transition

(A) *C. crescentus* has a biphasic cell cycle that follows c–di–GMP oscillations. Replication incompetent motile swarmer cells have low c–di–GMP levels. They transform into replication competent sessile stalked cells when c–di–GMP levels rise. Stalked cells replicate their chromosome and undergo cytokinesis that results in a new swarmer and stalked cell. (B) SW-to-ST transition relies on an upshift of c–di–GMP and the dephosphorylation/degradation of CtrA that is required for replication initiation. The pole determinants PleC and DivJ differentially dephosphorylate and phosphorylate the single-domain response regulator DivK that can, when phosphorylated, reverse direction of the CckA-ChpT-CtrA phosphorelay. This reversion is supported by c–di–GMP that directly binds to CckA and ultimately results in the dephosphorylation of CtrA. Additionally, these processes activate the adaptor proteins CpdR and PopA that bind the protease ClpXP and make it competent for CtrA degradation. Figure based on (207).

1.3.2 C–di–GMP signaling in *C. crescentus*

C. crescentus encodes 14 GGDEF, EAL or composite proteins (118). Two of which (PopA, TipF) were shown to be enzymatically inactive yet retained c–di–GMP binding capacity and evolved to transmit the c–di–GMP signal to downstream pathways (182, 202). In addition, there are three other c–di–GMP effector proteins described: The PilZ proteins DgrA and DgrB and the kinase CckA (185, 207). All these effectors are either involved in cell cycle progression or regulation of flagellar motility (182, 185, 202, 207). Yet, a strain completely devoid of c–di–GMP (called cdG^0 strain), due to the deletion of all GGDEF proteins encoding genes, shows a multitude of defects (no capsule, no pili, no flagellum, no holdfast and no stalk and severe defects in cytokinesis) (118). This implies that there are more effectors to uncover and indeed recent work in our research group has identified a number of additional c–di–GMP binding proteins involved in various processes (29; J. Nesper, V. Shyp, M. Kumar and C. von Arx, personal communication).

1.3.2.1 Oscillating c–di–GMP levels promote cell cycle progression and morphogenesis

In accordance with c–di–GMP supporting a sessile lifestyle, its overall levels are low in *Caulobacter* swarmer cells, rise during SW-to-ST transition and gradually decrease to intermediate levels in stalked cells (118, 301). The dominant player in swarmer cells is the phosphodiesterase PdeA. Upon its deletion cells show an increased ability to colonized surfaces and reduced motility as expected for augmented c–di–GMP levels. PdeA is supposed to counteract the c–di–GMP synthesizing DGC DgcB with which it interacts functionally and physically. Deletion of *dgcB* has the opposite effect of a Δ*pdeA* mutation and a double deletion can alleviate the single deletion phenotypes to a certain extent (155).

During SW-to-ST transition PdeA is rapidly degraded by the action of the ClpXP protease together with the adaptor protein CdpR (155, 300) (Fig. 4B). Concomitant, the DGC PleD is phosphorylated by the stalked pole determinants DivJ and PleC in its kinase mode (288, 302, 303) (see chapter: 1.3.1.2). PleD-P dimerizes, is sequestered to the pole and concurrently activates its DGC activity which leads to a sharp rise in c–di–GMP levels and pole morphogenesis, i.e. flagellum ejection and holdfast formation (296, 302, 304). A PleD mutant is delayed in holdfast synthesis, stalkless and hypermotile (254, 305, 306). Hypermotility arises from its inability to degrade the

flagellum MS-ring protein FliF and therefore fails to eject its flagellum (305). Besides morphological changes c–di–GMP also participates in cell cycle progression by changing both stability and activity of the cell cycle regulator CtrA. C–di–GMP switches its effector protein CckA from a kinase into a phosphatase, and thereby affects phosphorylation and thus activity of CtrA (207). C–di–GMP binding to PopA, on the other hand, enables recruitment of CtrA to the ClpXP protease and CtrA degradation (202) (Fig. 4B)(see Chapter: 1.3.1.2).

PleD remains localized at the stalked pole during the entire cell division process (302) where it keeps c–di–GMP levels high (301). In very late predivisional cells, the two cell compartments show distinct c–di–GMP levels: high in the stalked cell compartment and low in the swarmer cell compartment (301). PdeA levels rise in late predivisional cells and stably relocalize to the new swarmer pole, which makes the protein a good candidate to counteract the stalked pole associated PleD and establish a bipartite c–di–GMP distribution (155). Although PleD, DgcB and PdeA seem to be major players in c–di–GMP metabolism, there are indications that also some of the other GGDEF/EAL proteins contribute cumulatively to cellular c–di–GMP levels (118).

1.3.2.2 Multiple control of flagellum function by c–di–GMP

Elevated levels of c–di–GMP repress flagellum function but not assembly. On the contrary, cells with no c–di–GMP do not assemble a flagellum at all, indicating that both flagellum biogenesis and rotation are controlled by the second messenger (118, 155, 182, 185, 303). Furthermore, as mentioned above, efficient flagellum ejection requires PleD which suggest that also this process is controlled by c–di–GMP (305).

Biogenesis of the new flagellum takes place in predivisional cells at the pole opposite of the stalk (307). Proper localization is directed by the birth scar protein TipN that localizes to the division plane shortly before cytokinesis and thus marks the new pole after division (Fig. 5). TipN recruits TipF, a degenerate EAL protein (308). The EAL motive of TipF is replaced by the amino acids Glu-Ser-Phe (ESF) that still allow c–di–GMP binding but not hydrolysis. However, when substituting of the Glu to Ala TipF fails to bind c–di–GMP. TipF serves as nucleation hub for inner membrane components (class II) of the flagellum complex (182). In a Δ*tipF* mutant these proteins are delocalized and consequently no flagellum is built (182, 308). A TipF variant that fails to bind c–di–GMP does not localize and c–di–GMP depletion leads to rapid degradation of the protein, indicating that c–di–GMP is required for TipF localization

and stability. No wild-type TipF protein can be detected in swarmer cells. These observations lead to the model that, while TipF serves in predivisional cells as a localization factor at the pole for flagellum assembly, it delocalizes and is rapidly degraded by the protease ClpXP when c–di–GMP levels drop in swarmer cells. This clears the old pole from TipF and allows that the new pole can be marked by freshly synthesized TipF after G1-to-S-phase transition (182). In addition, TipF also indirectly influences expression of several flagellar genes such as the hook encoding *flgE*. However, expression of *flgE* is even more reduced in a c–di–GMP depleted strain compared to a Δ*tipF* strain. This indicates that c–di–GMP controls flagellum expression via an additional TipF independent pathway (182, 309).

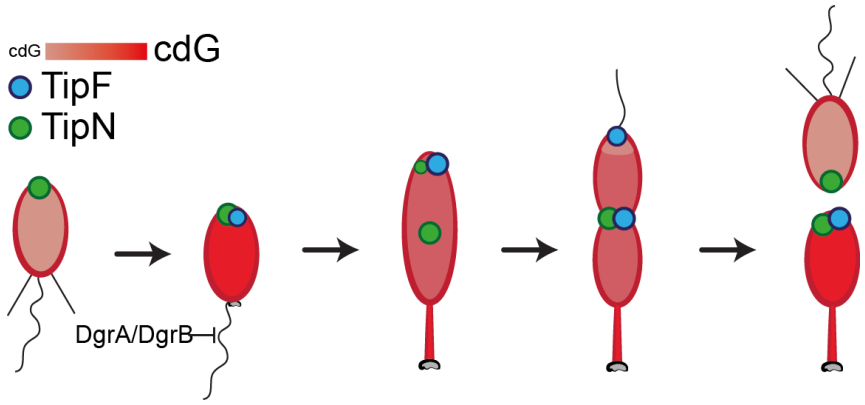

Fig. 5: Regulation of flagellum synthesis and function by c–di–GMP

In *C. crescentus* flagellum synthesis and function is both positively and negatively controlled by c–di–GMP. The flagellum is assembled in predivisional cells at the new pole opposite of the stalk where TipF is localized and probably prevails a local c–di–GMP trough. TipF is degraded in swarmer cells when c–di–GMP levels are low and the flagellum is functional. During SW-to-ST transition, c–di–GMP levels rise and the flagellum is inactivated and ejected. Flagellum inactivation requires the c–di–GMP effectors DgrA and DgrB. In predivisional cells TipN first localizes to mid cell followed by the c–di–GMP bound TipF. This marks the future new pole and new site of flagellum synthesis after cell division. Figure based on (182).

Flagellum arrest under c–di–GMP high conditions is less well understood. It requires c–di–GMP binding by the two PilZ proteins DgrA and DgrB. While deletion mutants of *dgrA* or *dgrB* maintained flagellum function even under a high c–di–GMP regime, overexpression of the two proteins leads to a non-motile phenotype independent of c–di–GMP. A DgrA overexpression strain has elevated levels of FliL, a protein required for flagellum rotation, and suppressor mutants restore wild-type FliL protein levels. But how DgrA signaling translates into FliL regulation is not clear (185).

1.3.3 Holdfast

The polar holdfast adhesin mediates surface adhesion of *C. crescentus* cells. It adheres to numerous surfaces with different chemical and physical properties and reaches adhesion forces in the micronewton range (249, 310). Its strong adhesive properties, which are even effective in an aquatic environment, makes holdfast an interesting bio-glue with properties relevant for several applications in different industrial fields (77).

1.3.3.1 Holdfast structure

Only little is known about the holdfast's underlying chemistry. It is an exopolysaccharide which binds wheat germ agglutinin (WGA) (311), a lectin that is specific for homo-oligomers of N-acetylglucosamine (N-GlcNAc) (312). Such oligomers of N-GlcNAc must be structurally important as holdfast loses its functionality upon treatment with chitinases or lysozyme, both enzymes that cleave N-GlcNAc oligomers (311). However Berne and colleagues (310) showed by probing the holdfast's adhesion force by atomic force microscopy (AFM) that polymers of pure N-acetylglucosamine do not show the same adhesive properties as the *C. crescentus* holdfast. The holdfast adhesive force increased with contact time. In addition, interaction between holdfast and surface was disrupted in multiple rupture events. Thus, the authors proposed that there must be modifications of the polysaccharide or other components embedded within the polysaccharide matrix which are responsible for the holdfast's strong adhesive force, probably by forming crosslinks within the holdfast structure but also with the surface interface in a time dependent manner (310).

The holdfast adhesin shows a certain degree of elasticity and as it shrinks upon drying it was proposed to have gel-like properties (313, 314). In line with this, Li and colleagues (315) measured holdfast size over time and described its expansion in a two-step process including a rapid but rather short spreading in diameter and a slower and prolonged thickening. Bases on this behavior the authors suggests that the holdfast behaves like a viscous fluid which can rapidly spread on a surface before it cures to a small disc which forms the basis for further deposition of holdfast material (315).

1.3.3.2 The holdfast synthesis machinery

Despite the uncertainties of the holdfast chemistry, the exopolysaccharide synthesis machinery has been identified and described in recent years. The synthesis machinery core is encodes in two neighboring operons (*hfsEFGH* and *hfsABC*) while the anchor proteins are encoded in a separate operon (*hfaABD*)(66, 316). Synthesis occurs in a Wzy-dependent manner with a cascade of glycosyltransferases that work in concert to polymerize oligosaccharide subunits onto undecaprenyl phosphate (Und-P) lipid anchors at the cytosolic side of the inner membrane. These lipid-linked subunits are then flipped into the periplasm where they are further polymerized and exported (Fig. 6)(66).

Four glycosyltransferases involved in holdfast synthesis have been described so far; HfsE, HfsJ, HfsG and CC2277; and all but HfsE were found to be essential for holdfast synthesis (66, 306, 317). The first sugar is added by HfsE, a protein belonging to the family of polyisoprenyl-phosphate hexose-1-phosphate transferases that catalyzes the formation of a phosphoanhydride bond between Und-P and a hexose-1-phosphate (318). Only when *hfsE* is deleted together with its paralogs, *pssY* and *pssZ*, *C. crescentus* loses its ability to synthesize holdfast (66). PssY lies within the capsule synthesis gene cluster (319) and has been shown by Patel and colleagues (318) to have UDP-glucose transferase activity *in vitro.* Holdfast synthesis could be restored in a Δ*hfsE* Δ*pssY* Δ*pssZ* triple mutant upon expression of WcaJ, an *E. coli* UDP-glucose transferase that initiates synthesis of colonic acid. Although the authors could not show *in vitro* transferase activity of HfsE and PssZ to any activated sugar tested, these results suggest that the initial sugar added to Und-P in holdfast synthesis is UDP-glucose (318). The recently described glycosyltransferase HfsJ is a member of the WecB/TagA-family and essential for holdfast synthesis although it is not encoded in the holdfast synthesis gene clusters (317). WecB and TagA are involved in enterobacterial common antigen and wall teichoic acid synthesis, respectively, and thought to transfer the second sugar to Und−P anchored saccharides. They are both thought to use UDP-N-acetylmannosamine as substrate suggesting that HfsJ might transfer an activated sugar with similar chemistry (320, 321).

HfsH is another protein encoded in the holdfast synthesis operon. It is a polysaccharide deacetylase and has esterase activity *in vitro* (66, 322). Surface colonization is abolished upon *hfsH* deletion (66, 322). Yet, in contrast to the holdfast-null phenotype observed for cells with mutated glycosyltransferases, Wan and

colleagues (322) could demonstrate that cells deficient in *hfsH* produce similar amounts of holdfast material, yet it is not anchored to the cell and can be deformed to filaments and washed away under shear stress. In addition, the authors observed enhanced surface colonization upon HfsH overexpression. Therefore, they proposed that the adhesive and cohesive strength of holdfast correlates with its degree of acetylation, which in turn depends on HfsH (322).

The Und-P linked oligosaccharides were proposed to be flipped across the membrane by the Wzx-like flipase HfsF and polymerized by the Wzy-like ligase HfsC. Yet, also this step shows some redundancy as only a double deletion of *hfsC* and a separately encoded flipase *hfsI* fully abrogate holdfast synthesis (66). The export is thought to be mediated by HfsA, HfsB and HfsD, which are predicted to span the cell envelope (323–325) (Fig. 6). HfsA and HfsB form together the Wzc-like polysaccharide co-polymerase (PCP), which in many other bacteria is formed by a single protein. HfsA comprises the inner membrane and periplasmic domain of PCP and HfsB is a cytoplasmic tyrosine kinase, but several important features for efficient kinase activity are not conserved (323, 325). Some members of PCP proteins are not essential for EPS synthesis and seem only to regulate polysaccharide chain length, yet for many others their exact role in EPS export and polymerization is unknown (325). In *C. crescentus* holdfast synthesis is abolished in cells lacking HfsA and strongly reduced in cells lacking HfsB. This suggests that their role extends beyond chain length determination (323, 326). Finally, the outer membrane part of the holdfast export complex is thought to be formed by HfsD, a member of the Wza-like outer membrane polysaccharide export protein family (OMX) (66, 325). Based on multiple gene deletion studies, OMX were proposed to play a role in polysaccharide translocation across the outer membrane. Consistent with this, the crystal structure of the *E. coli* Wza confirmed that the protein forms a barrel like structure that could serve as a translocoon for exopolysaccharides (325, 327).

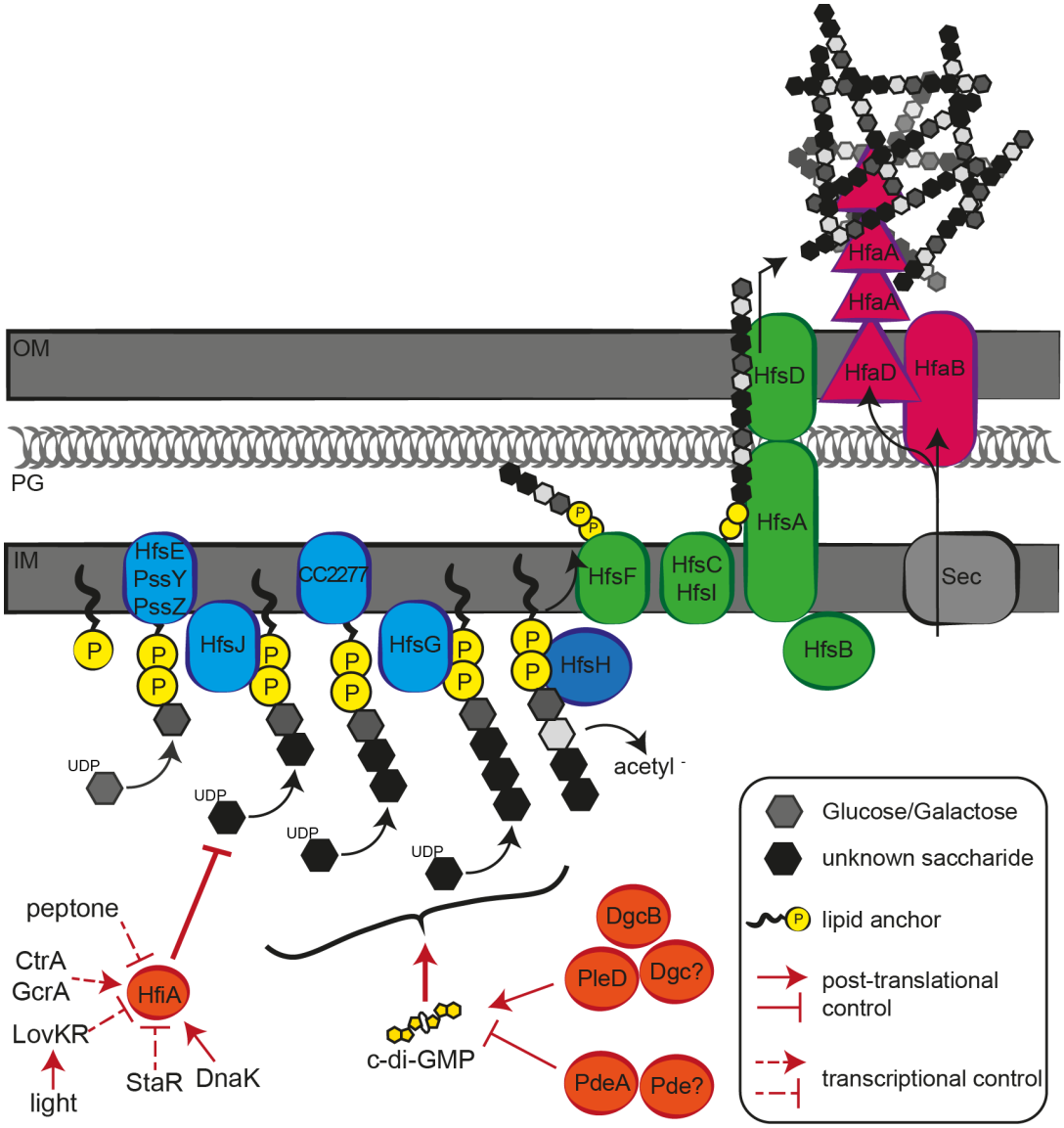

Fig. 6: Model of holdfast EPS synthesis and regulation

Holdfast EPS subunits are assembled on a lipid anchor by the combined action of different glycosyltransferases (HfsE (PssY, PssZ), HfsJ, CC2277, HfsG) from UDP-activated saccharides and modified by a deacetylase (HfsH) at the cytosolic site of the inner membrane. The subunits are flipped across the membrane (HfsF), polymerized in the periplasm (HfsC (HfsI) and exported by a membrane-spanning complex (HfsA, HfsB, HfsD). The holdfast is anchored by amyloid-like fiber forming proteins (HfaA, HfaD) that are exported across the inner membrane by the general Sec pathway and across the membrane by HfaB. Holdfast synthesis is repressed by HfiA that binds to the glycosyltransferase HfsJ. HfiA itself is controlled at the transcriptional and post-transcriptional level by various signals. Furthermore, holdfast synthesis requires c–di–GMP that is synthesized and degraded by different PDEs and DGCs. IM: Inner membrane; OM: outer membrane; PG: Peptidoglycan. Figure based on (66, 324)

Following holdfast EPS export, the polymer has to be anchored (Fig. 6). The *hfaABCD* operon responsible for this process was identified in a transposon screen (328, 329). Later studies with clean deletions showed that only cells deficient in *hfaA*, *hfaB* or *hfaD* shed their holdfast while a *hfaC* deletion revealed no phenotype under the conditions tested (330). In agreement with their proposed function in holdfast anchoring, all three proteins were shown to localize to the outer membrane of the flagellar pole in late predivisional cells, where they remain after cell division until they end up at the tip of the stalk alongside with the holdfast after SW-to-ST transition. HfaA and HfaD fail to associate with the outer membrane and are trapped in the periplasm in the absence of HfaB (331). HfaA and HfaB show some similarities with proteins of the curli system, which forms amyloid fimbrial structures that are components of the *E. coli* and *Salmonella enterica* biofilm matrix. HfaA also forms very stable high molecular weight (HMW) complexes, which is a hallmark of CsgA, the protein forming the curli amyloid fiber. HfaB shares some similarity with CsgG, which forms the outer membrane pore necessary for CsgA export (331, 332). HfaD also forms a HMW complex, which is, however, less stable as the one formed by HfaA. HfaA and HfaD are sensitive to protease K treatment even when cells are intact, indicating that they are surface exposed. Based on these finding, Hardy and colleagues (331) proposed that HfaB is involved in the export of HfaA and HfaD, while those two proteins form a filamentous structure that is the actual holdfast anchor. However, as the *hfaAD* double mutant does not phenocopy a *hfaB* mutant, HfaB likely plays a role in additional holdfast related processes (331). How this anchor actually works is not known. Cells defective in holdfast production but with intact anchor proteins are still able to form rosettes with wild-type cells and are even able to adhere via shed holdfasts to surfaces when co-cultures with holdfast shedding mutants indicating that anchoring is a process that takes place outside of the cell (333, 334).

It has been shown that holdfast production is initiated by flagellum based surface sensing in swarmer cells (255, 306, 335) which implies that the holdfast machinery has to be already assembled in these cells to ensure a rapid response. In line with this, all holdfast related genes tested so far peak in late predivisional cells and for *hfsJ* and *pssY* it could be shown that the genes are controlled by the master cell cycle regulator CtrA (317, 336). Furthermore, at least for the anchor proteins and HfsD we know that they localize to the pole as soon as they are synthesized (326, 331). Localization of

HfsD and HfaB depends on the polar localization factor PodJ and cells deficient in *podJ* produce very little and mostly delocalized holdfast (326, 331). Furthermore, localization of HfaABD depends on the presence of HfsABD (326, 331). This leads to a model in which PodJ serves as localization factor for the export proteins HfsABD, which in turn recruit the anchor proteins HfaABD. Overexpression of HfsA, HfsB or HfsD in a Δ*podJ* mutant can rescue the holdfast synthesis defect, indicating that polar localization ensures high enough protein density required to form a functional complex (326). Yet, surface colonization remains deficient when holdfast is delocalized supporting previous findings that function of holdfast, pili and flagellum have to work in concert to ensure proper surface adhesion (255, 306, 326, 335).

1.3.3.3 Regulation of holdfast synthesis

Assembly of the synthesis machinery is not sufficient to initiate holdfast synthesis. This requires c–di–GMP, as cells devoid of this second messenger are unable to produce a holdfast at all and deletion of the diguanylate cyclases *pleD* and *dgcB* or the phosphodiesterase *pdeA* lead to a delayed or premature holdfast synthesis, respectively (118, 155, 306). However, c–di–GMP levels sufficient to activate the holdfast machinery can be reached through an internal or an external signal pathway. The internal signal comes with the inherent cell cycle clock which leads to localization and activation of PleD that actively drives SW-to-ST transition (302, 303) (see chapter: 1.3.1). The external signal is initiated by the sensing of surface, which is a complex process and requires the presence of pili and a functional flagellar motor in order to be efficient (254, 305, 334; I. Hug, personal communication). But also this signal cascade ultimately converges into the production of c–di–GMP probably via activation of DgcB (I. Hug, personal communication).

Recent findings have also uncovered two other external inputs that regulate holdfast synthesis via a **h**old**f**ast synthesis **i**nhibitor called HfiA (317) (Fig. 6). Cells expressing *hfiA* are not able to produce holdfast and colonize surfaces. HfiA interacts with the glycosyltransferase HfsJ. Mutations in the C-terminus of HfsJ inhibit such an interaction and abrogate the negative effect of HfiA on holdfast production. As expected, expression of *hfiA* is minimal during SW-to-ST transition when holdfast production starts (317). One part of *hfiA* regulation goes via the cell cycle transcription factors CtrA and GcrA that act as activators and StaR that acts as repressor of *hfiA* gene expression. Interestingly, by a yet unknown mechanism, expression of *hfiA* additionally responds to nutritional input. Expression of *hfiA* is

increased in the absence of peptone which probably signals to the cell that this is not a favorable environment to adhere to and to colonize (317). Furthermore, *hfiA* expression is reduced when the light sensitive two-component sensory system LovK-LovR is activated (317). LovK is a histidine kinase fused to a LOV photosensory domain and its autophosphorylation and ATPase activity is upregulated by white light (337). HfiA protein levels also depend posttranscriptionally on the chaperone protein DnaK. Eaton and coworkers have shown that HfiA stability is reduced in presence of a truncated, less efficient DnaK chaperone mutant (338). Since DnaK is upregulated in several biofilms (339–345) the authors hypothesized that DnaK might be a measure for stress encountered in biofilms. By stabilizing HfiA, newborn cells would thus less likely form holdfast in such a stressful environment, which assist progeny dispersal (338). These examples demonstrate the ability of *C. crescentus* to perceive different parameters of its environment and translate those inputs into behavioral outputs, such as holdfast production and attachment.

1.4 GNAT proteins

Gcn5-related-N-acetyltransferase (GNAT) proteins belong to a huge and very diverse family of enzymes that catalyze N-acylation reactions on different types of substrates (Fig. 7A, B). More than 300,000 representatives of this family have been identified and they are distributed in all kingdoms of life (346).

1.4.1 Function and structure of GNAT proteins

The first GNAT proteins identified were the histone acetyltransferases, one of which is the eponymous Gcn5 of *Saccharomyces cerevisiae* (347). They transfer an acetyl group from acetyl-CoA to a lysine of the histone protein and thereby activate gene transcription (348). But also non-histone proteins can be acetylated which usually has a regulatory effect (349, 350). Activity of the Acetoacetyl-CoA synthetase of *Streptomyces lividans*, for example, is controlled via acetylation (351).

GNAT proteins can acetylate not only proteins, but also other molecules like antibiotics and metabolites. For instance, a clinically important class of GNATs is formed by the aminoglycoside N-acetyltransferases. They acetylate amino groups of aminoglycosides and thereby reduce the antibiotic's affinity for the ribosome (346, 352). But GNAT proteins can inactivate also other antibiotic classes. The tabtoxin resistance protein acetylates and confers resistance to the β-lactam tabtoxinine (353, 354), while the MccE acetyltransferase inactivates the antibacterial agent microcin (355, 356). Metabolically important are the spermidine acetyltransferases. They are required for homeostasis of the polyamine spermidine and can convert the amino acid proline to arginine (357–359). Also synthesis of the EPS precursor UDP-N-acetylglucosamine involves a GNAT protein that acetylates the saccharide glucosamine-6-phosphate (360, 361). Conversely, an already activated saccharide is used as substrate by WecD of *Salmonella enterica* which synthesizes the enterobacterial common antigen precursor TDP-N-acetylfucosamine from TDP-fucosamine (362).

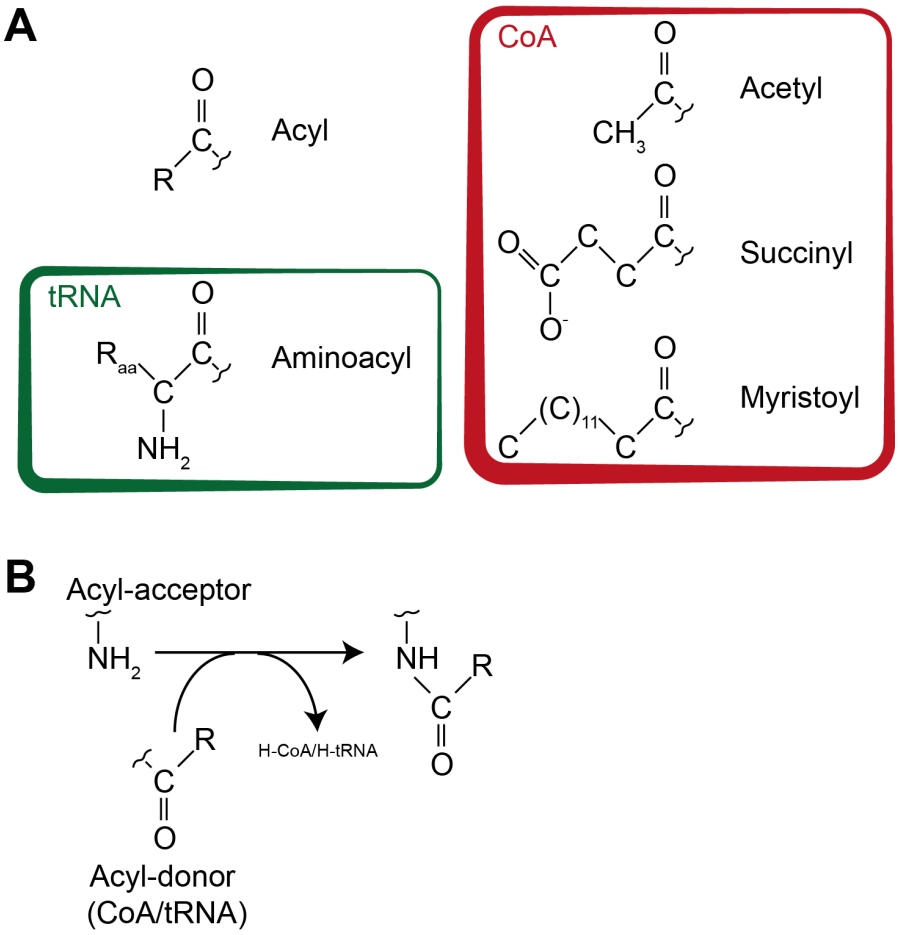

Fig. 7: N-acylation catalyzed by the GNAT family

(A) On top is a general representation of an acyl-moiety with "R" representing an organyl group. Acyl groups that are associated with CoA are depicted in the red square. tRNA is used as a donor for aminoacyl moieties, which is depicted in its general form in the green square. R_{aa} represents an amino acid side chain. (B) In general, a N-acylation reaction requires an acyl-donor, as depicted in (A) and a free amine of an acyl acceptor molecule. Corrugated lines represents connections to various types of molecules.

In all examples above, an acetyl group is transferred from Coenzyme A (CoA) to an acceptor molecule. However, GNAT proteins are not limited to the transfer of acetyl. In general terms they transfer acyl groups, the hallmark of which is a ketone group that is linked to an organyl group (Fig. 7A). A functionally uncharacterized GNAT protein of *Mycobacterium tuberculosis* was shown to bind succinyl-CoA instead of acetyl-CoA (363). Myristoylation of proteins, which has been implicated in protein-protein and protein-membrane interaction (364), is catalyzed by a GNAT protein that binds myristoyl-CoA (365, 366). Furthermore, the Fem proteins, which are involved in peptidoglycan synthesis of gram-positive bacteria, transfer an aminoacyl from a tRNA donor to the peptidoglycan pentapeptide (367–369) (see chapter below).

GNAT proteins have in general a very low sequence homology, however their core fold is highly conserved. It consists of a central β-sheet that is surrounded by several α-helixes (Fig. 8A, B). Many GNAT proteins are active as dimers and it has been suggested that dimerization is important, as the catalytic sites often locate to the dimer interface (346, 370). However, the histone acetyltransferase Hpa2 from yeast is a stable dimer that tetramerizes upon acetyl-CoA binding (371). And the very promiscuous aminoglycoside acetyltransferase Eis forms even a dimer of trimers (372).

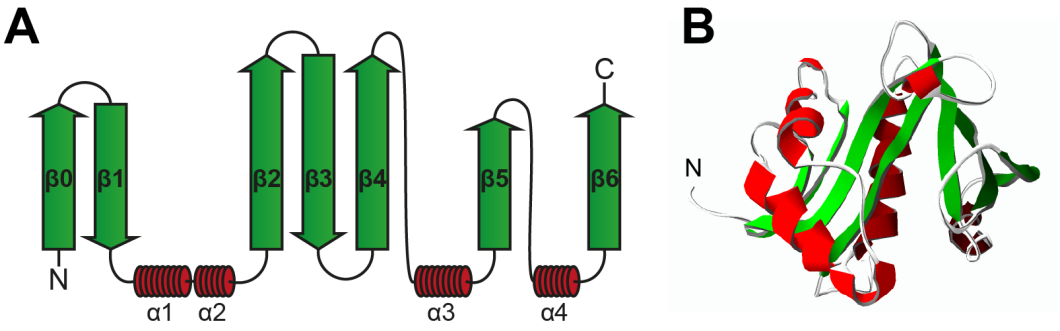

Fig. 8: Structure core of GNAT proteins

(A) Typical topology of two-dimensional structural elements found in GNAT proteins. Green arrows represent β-strands and red barrels represent α helixes. Based on (346, 361). (B) Crystal structure of sheep serotonin N-acetyltransferase (PDB: 1L0C (373)), as a representative of the generic GNAT proteins. Colors as in (A) shaded from N-terminus (bright) to the C-terminus (dark).

1.4.2 Fem proteins have a tandem GNAT fold

While many GNAT proteins form dimers or even higher oligomers (see chapter above), there are some protein classes that form an internal dimer consisting of two GNAT domains in tandem (365, 367, 370, 374–376).

One example for these tandem GNAT proteins is the Fem family. They use aminoacyl-tRNA to synthesize a peptide bridge which crosslinks the pentapeptide stems of the N-acetylglucosamine (GlucNAc)-N-acetyl muramic acid (MurNAc) subunits of the peptidoglycan in some gram-positive bacteria (Fig. 9A). Type and length of these additional peptide bridges differ between bacteria (377). But these peptide bridges are not only required for peptidoglycan crosslinking. It has been shown in different *fem* mutants of *S. aureus* that also anchoring of surface proteins depends on peptide bridges synthesized by the Fem proteins (378).

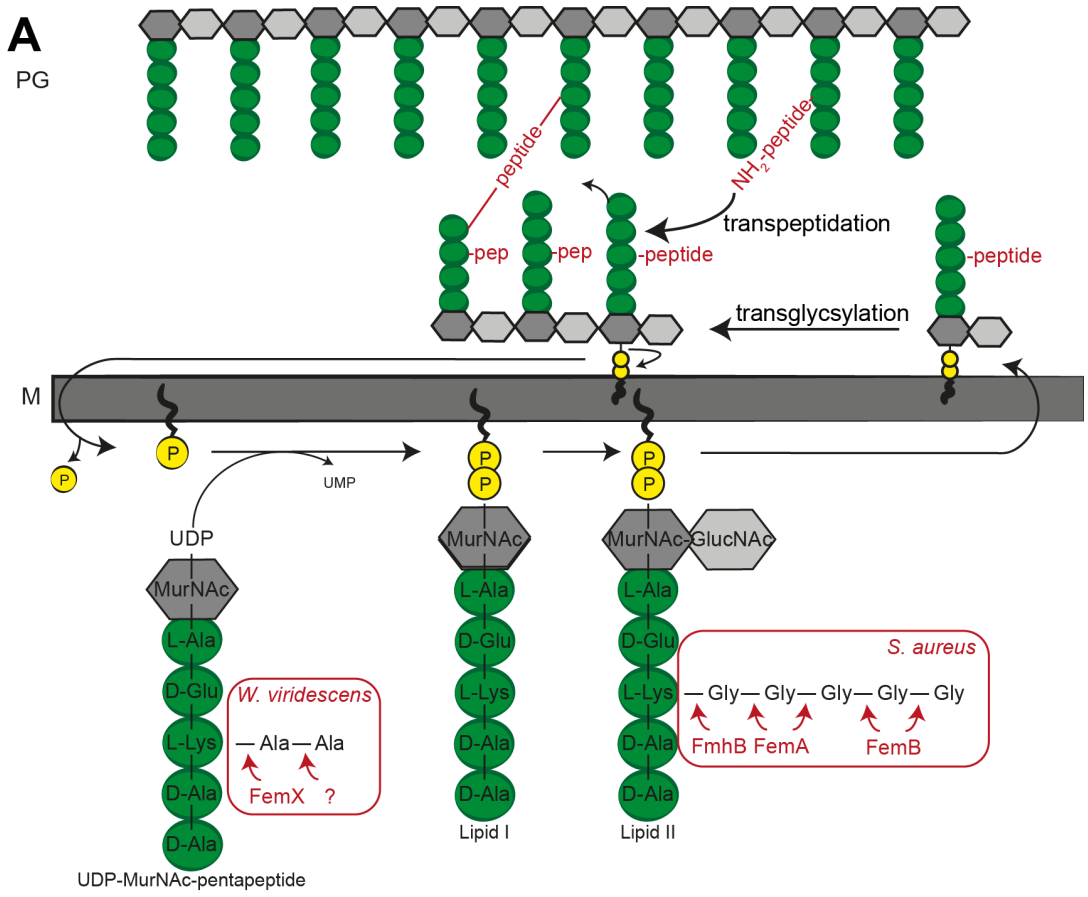
A
PG
peptide
NH2-peptide
transpeptidation
-pep
-pep
-peptide
-peptide
transglycsylation
M
P
UMP
UDP
MurNAc
L-Ala
D-Glu
L-Lys
D-Ala
D-Ala
W. viridescens
— Ala — Ala
FemX ?
UDP-MurNAc-pentapeptide
MurNAc
Lipid I
MurNAc-GlucNAc
Lipid II
S. aureus
— Gly — Gly — Gly — Gly — Gly
FmhB FemA
FemB

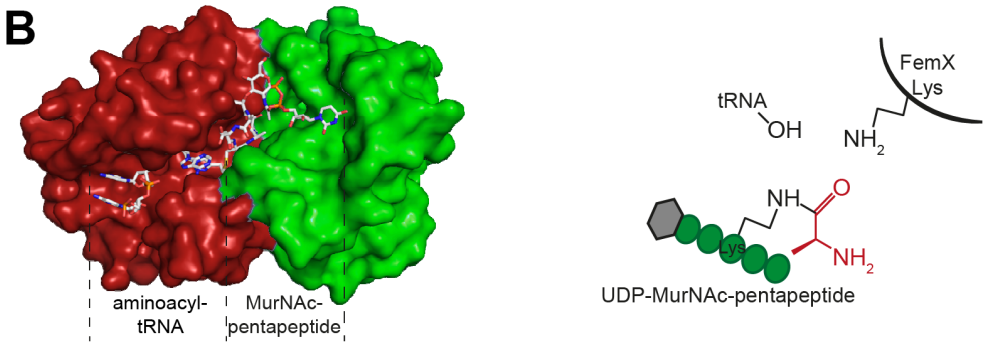
B
aminoacyl-tRNA
MurNAc-pentapeptide
FemX
Lys
tRNA
OH
NH2
NH
O
Lys
NH2
UDP-MurNAc-pentapeptide

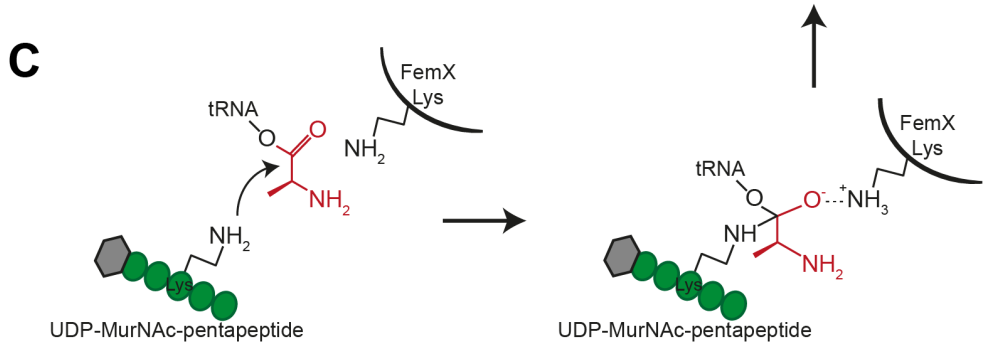
C
FemX
Lys
tRNA
O
O
NH2
NH2
NH2
Lys
UDP-MurNAc-pentapeptide
FemX
Lys
tRNA
O
O
NH3
NH
NH2
Lys
UDP-MurNAc-pentapeptide

Fig. 9: Synthesis of peptidoglycan peptide bridges in gram-positive bacteria

(A) UDP-MurNAc-pentapeptide is synthesized in the cytosol and then transferred onto the lipid anchor undecaprenyl-phosphate (Lipid I). Addition of GlucNAc completes the disaccharide-peptide subunit (Lipid II) that is flipped over the cytoplasmic membrane (M) and used for polymerization of the peptidoglycan by an enzyme complex with transglycosylation and transpeptidation activity. Insets show synthesis of the peptide chains used to form the peptidoglycan peptide bridges. In *W. viridescens* synthesis occurs already in the cytosol on UDP-MurNAc-pentapeptide, while in *S. aureus* the peptide chain is added on Lipid II. Based on (367). (B) Surface representation of FemX of *W. viridescens* adapted from (379). N- and C-terminal GNAT domain are colored in green and red, respectively. The MurNAc-pentapeptide-aminoacyl-tRNA analogue that lacks most of the tRNA moiety is shown as a stick representation. (C) Proposed reaction mechanisms for FemX that adds an alanine residue to the UDP-MurNAc-pentapeptide. A nucleophilic attack of the lysine of MurNAc-pentapeptide results in a tetrahedral intermediate. The negative charge on the oxygen in this intermediate is stabilized by a lysine of FemX. Based on (379).
(← Figure on previous page)

In *Weissella viridescens* FemX is thought to add an alanine residue to the pentapeptide stem using alanine-charged-tRNA as acyl donor. As a substrate it uses the cytosolic nucleotide-activated precursor UDP-MurNAc-pentapeptide (367). In *Staphylococcus aureus,* on the other hand, a FemX homolog FmhB adds the first glycine residue and FemA is thought to add the second and third glycine residue to the pentapeptide stem. They use LipidII (undecaprenyl-phosphate coupled MurNAc-GlucNAc-pentapeptide) as substrate (367–369, 380). In both, FemX and FemA, the peptidoglycan substrate is accommodated in a cleft between the two GNAT domains but is predominantly bound via residues of the N-terminal portion of the protein (Fig. 9B). But the two proteins have adapted this binding region according to the different natures of their substrates. FemX, which has to accommodate a UDP moiety, exhibits an additional crevice, while FemA, which binds to the lipid linked counterpart that is anchored in the membrane, is more surface accessible in this area (367, 375). In both proteins, the interdomain cleft expands into the C-terminal GNAT domain. This is the region where aminoacyl-tRNA is bound (Fig. 9B). A crystal structure solved for FemX with an analog for alanine-tRNA coupled to UDP-MurNAc-pentapeptide has shown, that the two substrates can be bound in a way that brings the alanine from tRNA and the lysine acceptor from the pentapeptide in close proximity (Fig. 9B). A reaction mechanism has been proposed, which includes a nucleophilic attack by the amine group of the pentapeptide lysine and a tetrahedral reaction intermediate that is stabilized by another lysine of FemX which is highly conserved among different Fem proteins (Fig. 9C) (379).

Interestingly, binding of tRNA is not a unique feature of the Fem proteins. Recently, a single domain GNAT protein TacT has been identified in *Salmonella* and in contrast to the Fem proteins uses tRNA as an acyl-acceptor (381). TacT transfers an acetyl from acetyl-CoA to the aminoacyl moiety of aminoacyl-tRNA and thereby blocks translation and drives cells into a non-growing persister mode that allows them to survive stress situation such as antibiotic treatment (381, 382).

1.5 Aim of this thesis

C. crescentus produces a very strong EPS adhesin in response to both environmental and cell cycle cues that are thought to converge into the c–di–GMP signaling pathway. However, the mechanistic details of how c–di–GMP controls holdfast biogenesis are not understood. This thesis describes a novel c–di–GMP effector protein HfsK that was identified in an unbiased screen for c–di–GMP binding proteins and was implicated in surface adhesion. It is the continuation of my master thesis (383) which focused on the description of the deletion mutant's phenotype. Here, I aimed to unravel the exact role of HfsK and the underlying mechanism of c–di–GMP binding and control; and tried to connect these findings with holdfast synthesis and adhesive function.

2 Results

Statement of my work

I performed all experiments shown in the manuscript with the following exceptions: Table 1, Figure 1, Figure 2C, Figure 5E, and Figure S2G-I. Furthermore, following individual experimental steps could not be performed by myself: c−di−GMP quantification after sample preparation (Figure S3B), SIM image acquisition (Figure 3C, Figure 4B, Figure 5B, Figure S5B), image acquisition in Figure S4F, and programming of the software WHSIT. All experiments shown in chapter: Additional work were performed by myself.

All plasmids and strains labeled in Table 2 and Tab. 1 were created by myself (*) or partially by myself (**).

2.1 Cohesive properties of the *Caulobacter crescentus* holdfast adhesin are regulated by a novel c-di-GMP effector protein

(This chapter is based on the publication manuscript: Sprecher KS, Hug I, Nesper J, Potthoff E, Mahi MA, Sangermani M, Kaever V, Schwede T, Vorholt J, Jenal U. 2017. *Cohesive properties of the Caulobacter crescentus holdfast adhesin are regulated by a novel c-di-GMP effector protein*. mBio 8:e00294-17)

Kathrin S. Sprecher[a], Isabelle Hug[a], Jutta Nesper[a+], Eva Potthoff[b‡], Mohamed-Ali Mahi[c], Matteo Sangermani[a], Volkhard Kaever[d], Torsten Schwede[c], Julia Vorholt[b], Urs Jenal[a]*

[a] Focal Area of Infection Biology, Biozentrum, University of Basel, Switzerland

[b] Institute of Microbiology, ETH Zurich, Zurich, Switzerland

[c] Focal Area of Computational & Systems Biology, Biozentrum, University of Basel, Switzerland

[d] Research Core Unit Metabolomics and Institute of Pharmacology, Hannover Medical School, Hannover, Germany

* for correspondence: urs.jenal@unibas.ch

+ deceased November 15, 2016

‡present address: Lonza Ltd, Visp, Switzerland

Key words:

Caulobacter crescentus; c-di-GMP; effector; dynamic localization; attachment; holdfast; exopolysaccharide synthesis; EPS; adhesin; Capture Compound mass spectrometry; CCMS; Fluidic Force Microscopy (FluidFM), single cell force spectroscopy (SCFS)

2.1.1 Abstract

When encountering surfaces, many bacteria produce adhesins to facilitate their initial attachment and to irreversibly glue them to the solid substratum. A central molecule regulating the processes of this motile-sessile transition is the second messenger c-di-GMP, which stimulates the production of a variety of exopolysaccharide adhesins in different bacterial model organisms. In Caulobacter crescentus, c-di-GMP regulates the synthesis of the polar holdfast adhesin during the cell cycle. Yet, the molecular and cellular details of this control are currently unknown. Here, we identify HfsK, a member of a versatile N-acetyltransferase family, as novel c-di-GMP effector involved in holdfast biogenesis. Cells lacking HfsK form highly malleable holdfast structures with reduced adhesive strength that cannot support surface colonization. We present indirect evidence that HfsK modifies the polysaccharide component of holdfast to buttress its cohesive properties. HfsK is a soluble protein but associates with the cell membrane during most of the cell cycle. Coincident with c-di-GMP levels reaching peak concentrations during the C. crescentus cell cycle, HfsK relocalizes to the cytosol in a c-di-GMP dependent manner. Our results indicate that the c-di-GMP mediated dynamic positioning controls HfsK activity leading to its inactivation at high c-di-GMP levels. A short C-terminal extension is essential for membrane association, c-di-GMP binding and activity of HfsK. We propose a model in which c-di-GMP binding leads to the dispersal and inactivation of HfsK as part of holdfast biogenesis progression.

Importance

Exopolysaccharides (EPS) adhesins are important determinants of bacterial surface colonization and biofilm formation. Biofilms are a major cause of chronic infections and are responsible for biofouling on water-exposed surfaces. To tackle these problems, it is essential to dissect the processes leading to surface colonization at the molecular and cellular level. Here we describe a novel c-di-GMP effector, HfsK, that contributes to the cohesive properties and stability of the holdfast adhesin in C. crescentus. We demonstrate for the first time that c-di-GMP, in addition to its role in regulating the rate of EPS production, also modulates the physico-chemical properties of bacterial adhesins. By demonstrating how c-di-GMP coordinates activity and subcellular localization of HfsK we provide a novel understanding of the cellular processes involved in adhesin biogenesis control. Homologs of HfsK are found in

representatives of different bacterial phyla suggesting that they play important roles in various EPS synthesis systems.

2.1.2 Introduction

Microorganisms are predominantly surface associated and often grow in complex multicellular structures called biofilm (13, 14). At the same time, they are able to disperse as motile single cells and explore their environment (384, 385). To effectively switch between these fundamentally different lifestyles, many bacteria have evolved regulatory mechanisms that robustly promote cellular processes associated with motility and sessility, respectively. The ubiquitous second messenger c-di-GMP plays a central role in this transition (386). While c-di-GMP interferes with flagellar and pili based motility (173, 387), it stimulates the synthesis of adhesion factors and extracellular matrix components like curli fibers or exopolysaccharides (EPS) (152, 209, 388). A prime example for c-di-GMP mediated control is the production of cellulose, a secreted glucose polymer mediating surface attachment and biofilm stability in many bacteria (149). Cellulose is synthesized and translocated through the cell envelope by the membrane-integral BcsAB complex (389). The synthase BcsA is held in an autoinhibitory state by a gating loop that blocks the access of glucose monomers to the catalytic site and that is released upon c-di-GMP binding (189, 217). Similarly, the synthesis of poly-β-1,6-N-acetyl-glucosamine (PGA) in *E. coli* requires the simultaneous binding of c-di-GMP to the synthase PgaC and to its co-synthase PgaD to stabilize their interaction and boost their activity (242).

We use *Caulobacter crescentus* as a model to study the regulatory mechanisms of the motile-to-sessile transition of bacteria. This gram-negative freshwater bacterium has a biphasic cell cycle with an asymmetric division producing a motile, replication inert swarmer (SW) and a sessile, replication competent stalked (ST) cell (247). SW cells are equipped with a flagellar motor and adhesive pili and remain motile for an extended period before differentiating into ST cells. During this process they replace their flagellum and pili with an exopolysaccharide adhesin, the holdfast, which is located at the tip of a cell extension, the stalk. The holdfast, which consists of EPS (311, 313) and additional, undefined components (310, 313, 322), mediates strong and permanent attachment of ST cells to surfaces (66, 334, 335). The holdfast EPS is composed of oligomers of N-acetylglucosamine and is synthesized and anchored by the **h**old**f**ast **s**ynthesis (Hfs) and **h**old**f**ast **a**nchoring (Hfa) proteins, most of which are

encoded in two separate operons on the *C. crescentus* genome (66, 323, 330). Based on homology models and deletion studies, several glycosyltransferases were predicted to participate in the assembly of a glycosyl-oligomer onto a lipid anchor (66, 306, 317). The sugar moieties were proposed to be chemically modified. For example, HfsH is thought to deacetylate glycosyl subunit(s) of the growing polymer (322). The lipid-linked oligomers are then flipped through the cytoplasmic membrane into the periplasm, further polymerized, and exported to the cell surface (66). Mutants that lack the anchor proteins HfaA, B, or D shed their holdfast. How these proteins contribute to EPS anchoring is not understood (330, 331).

C. crescentus cell morphogenesis and behavior is regulated by c-di-GMP, the levels of which oscillate through the cell cycle (118, 207). The c-di-GMP concentration is low in SW cells, rises to peak levels during the SW-to-ST cell transition, and later reaches intermediate levels in dividing cells (118, 301). Changes in c-di-GMP concentration are mediated by cell type-specific diguanylate cyclases (DGC) and phosphodiesterases (PDE). While c-di-GMP levels are kept low in SW cells by the PDE PdeA, the c-di-GMP upshift during cell differentiation is mediated by the specific degradation of PdeA (155) and the consecutive activation of PleD, a DGC that is active only in the sessile cell type (127, 302). The upshift of c-di-GMP during cell differentiation leads to the ejection of the flagellum (305), stimulates the assembly of the stalk and prompts the biogenesis of the holdfast adhesin (118). However, how c-di-GMP stimulates these processes has remained unclear.

Here we identify the acetyltransferase HfsK as a novel c-di-GMP effector protein that is required for the formation of a cohesive and stably anchored holdfast. Cells harboring an *hfsK* deletion shed abnormal holdfasts that formed elastic filamentous structures when subject to shear stress. We show that HfsK activity depends on its association with the cytoplasmic membrane. HfsK remains membrane-associated throughout most of the cell cycle but is released into the cytoplasm in a c-di-GMP dependent manner during the SW-to-ST transition coinciding with c-di-GMP reaching peak concentrations and with holdfast assembly. We identify a short 25 amino acid stretch at the C-terminus of HfsK as critical determinant for c-di-GMP binding, membrane association and protein function. Based on our data we propose that c-di-GMP controls HfsK by coupling its activity to its membrane compartmentalization.

2.1.3 Results

CC3689 is a novel c-di-GMP binding protein

We have recently described capture compound coupled mass spectrometry technology (CCMS), a biochemical method to isolate c-di-GMP binding proteins (176). Using CCMS we isolated an uncharacterized protein (CC3689) directly from *C. crescentus* cell extracts (Table 1). Structure-based homology searches with HHpred (390) revealed that CC3689 belongs to the Gcn5-related-N-acetyltransferase (GNAT) family, a ubiquitous group of N-acyltransferases that acylates a variety of different substrates, ranging from proteins to polyamines and amino-glycosides (346).

Table 1: HfsK and CC1244 detection in a CCMS screen for c-di-GMP effectors

No. spectral counts of identified peptides (CCMS experiment/ CCMS competition[a])			
	Experiment[b]	**Soluble fraction**	**Membrane fraction**
HfsK (CC3689)	1	9/0	14/5
	2	8/0	13/4
	3	10/0	14/4
CC1244	1	4/0	1/0
	2	0/0	2/1
	3	0/0	8/3

[a] Competition experiments were performed in the presence of 1 mM c-di-GMP

[b] 3 independent experiments are indicated using 10 µM (soluble fraction) or 8 µM (membrane fraction) c-di-GMP-CC

To confirm binding of c-di-GMP to CC3689, we affinity purified a His-CC3689 fusion protein and used it for isothermal titration calorimetry (ITC). His-CC3689 bound c-di-GMP in a concentration dependent manner with an equilibrium disassociation constant (K_d) of 724 nM and a binding stoichiometry of 2:1 (c-di-GMP:CC3689) (Figure 1A). To test binding specificity, we performed UV-crosslinking assays (5). His-CC3689 binding to ^{33}P-labelled c-di-GMP was effectively outcompeted by the addition of unlabeled c-di-GMP, but not by other nucleotides (Figure 1B). From this we concluded that CC3689 is a *bona fide* c-di-GMP binding protein.

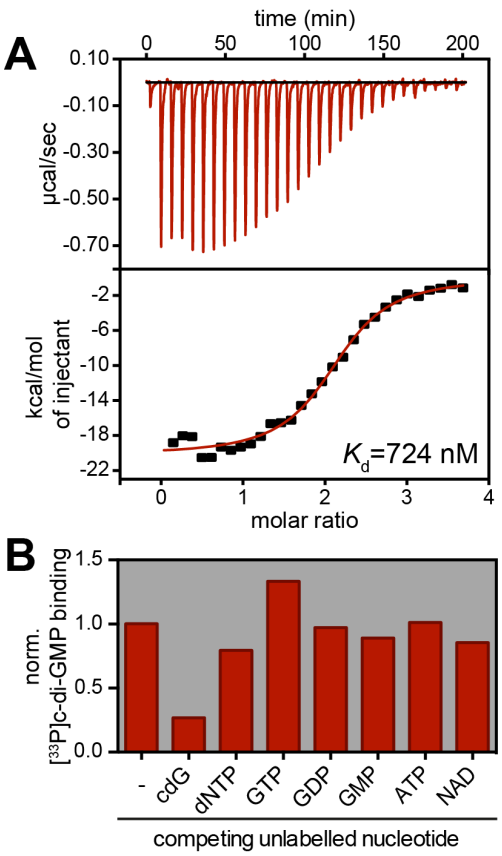

Figure 1: HfsK specifically binds c-di-GMP

(A) ITC measuring interaction of His-HfsK with c-di-GMP. Heat release upon ligand injection (upper panel), integrated heat plotted against the molar ratio of ligand and protein (lower panel), and the resulting disassociation constant (K_d) are shown. (B) Quantified autoradiographs of 1 µM purified His-HfsK that has been UV-crosslinked to 10 µM [^{33}P]c-di-GMP in presence or absence of a 10-fold excess of non-labeled nucleotides to test competition.

HfsK and its paralogs contribute to *C. crescentus* surface attachment by modifying the holdfast adhesin

C. crescentus encodes two additional paralogs of *cc3689* (*cc2278* and *cc1244*) with sequence identities of around 30%. (Figure S1A, B). While the neighboring genes gave no hints about a possible function of *cc3689*, *cc2278* lies in an operon containing a gene for a predicted glycosyltransferase that is required for holdfast synthesis (306). In addition, when analyzing the genomic context of *cc3689* orthologs, we found that many of them cluster with genes predicted to function in EPS biogenesis (Figure S1C). Strains encoding such orthologs belong to different phyla, indicating that the connection of this protein class with EPS synthesis is of ancient evolutionary origin. Interestingly, in three closely related marine species, namely *Maricaulis maris*, *Oceanicaulis alexandrii*, and *Woodsholea maritima* (391), orthologs of *cc3689* cluster with homologs of *C. crescentus* holdfast synthesis genes (324) (Figure S1D). Based on these observations and on the results presented below we renamed CC3689 **h**old**f**ast **s**ynthesis protein K (HfsK).

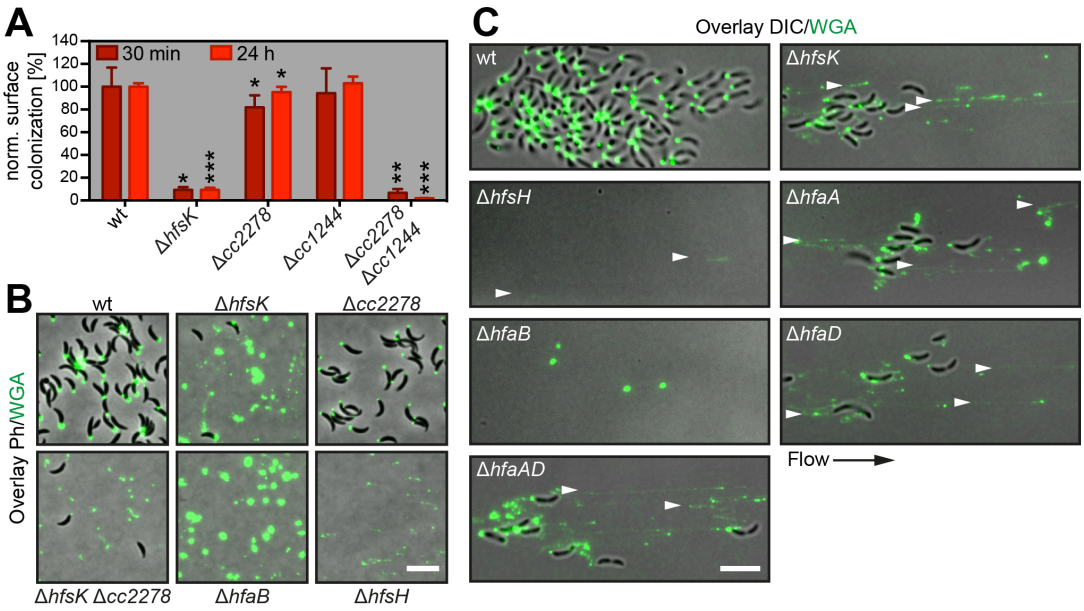

Figure 2: HfsK deletion leads to an incoherent holdfast that does not support surface colonization

(A) Surface colonization of wild type (WT) and mutants lacking the *hfsK* paralog family determined by crystal violet staining of adherent cells after 30 min (dark red bars) and 24 h (light red bars) growth in microtiter plates. Normalized per condition. Error bars = standard deviation (SD) of 3 independent experiments, */**/*** represent P-value <0.1/0.01/0.001. (B) Analysis of holdfast shedding in *hfsK* and *cc2278* mutants as well as in strains that shed (Δ*hfaB*) or form incoherent (Δ*hfsH*) holdfast. Shown are overlays of phase contrast and fluorescence images of adhered WGA stained holdfast on glass coverslips after 2 h cells adsorption. (C) Holdfasts analyzed under shear stress after 15 h growth in microfluidics channels with constant flow of fresh medium containing OG-WGA. Shown is an overlay of fluorescence and inverted DIC images. Arrowheads point out holdfast filaments. Scale bars in panel B and C = 5 µm.

To test whether *hfsK* or its paralogs *cc2278* and *cc1244* are involved in holdfast biogenesis, we engineered deletions of all three genes in the chromosome of *C. crescentus* wild-type strain CB15 and investigated surface colonization of the resulting mutant strains as a proxy for their ability to form a functional holdfast. The Δ*hfsK* mutant showed a 90% reduction in surface colonization after 30 min and after 24 hours of growth as compared to wild type. In contrast, the Δ*cc2278* mutant showed only minor defects in surface colonization during the initial phase of growth (Figure 2A, Figure S2A). Surface colonization was fully restored when the *hfsK* and *cc2278* mutants were complemented with a wild-type copy of the respective gene *in trans*, but the two proteins failed to cross-complement each other (Figure S2B). A Δ*hfsK* Δ*cc2278* double mutant showed lower surface colonization than the *hfsK* single mutant

indicating additive contributions of both proteins to surface attachment (Figure 2A). Finally, deletion of the third paralog, *cc1244,* revealed no obvious phenotype alone or in combination with deletions of *hfsK* or *cc2278*. However, the Δ*hfsK* Δ*cc2278* Δ*cc1244* triple mutant failed to adhere completely (Figure 2A, Figure S2A).

In line with the strong surface colonization defect, the Δ*hfsK* mutant showed a severe reduction in holdfast biogenesis. Upon staining of holdfast with the Oregon-green labeled lectin wheat germ agglutinin (OG-WGA), 63% of wild-type ST cells carried a holdfast, whilst only 4% of the Δ*hfsK* cells were holdfast-positive (Figure S2C). Whereas strains carrying deletions of *cc2278* or *cc1244* showed normal holdfast formation, holdfast formation was completely abolished in the triple mutant lacking HfsK and its paralogs.

The observed reduction of Δ*hfsK* cells bearing an adhesive holdfast could be explained by either a diminished production of holdfast or by defective anchoring and increased shedding of holdfast material (331). To distinguish between these possibilities, wild-type and mutant strains were adsorbed to glass surfaces for two hours before the glass was washed, stained with OG-WGA, and analyzed by fluorescence microscopy. Glass surfaces incubated with the wild-type strain were covered with cells adhering via their holdfasts. In contrast, only few cells of the Δ*hfsK* mutant remained attached after washing, yet the amount of holdfast material observed was comparable to that of wild type (Figure 2B, Figure S2C). Of note, this is similar to the shedding phenotype observed for a strain lacking the holdfast anchor protein HfaB (330, 331). Cells lacking CC2278 did not shed their holdfast, but produced smaller, less intensely stained adhesins. A Δ*hfsK* Δ*cc2278* double mutant shed small holdfasts, again indicating that the two proteins affect holdfast properties independently. Intriguingly, the Δ*cc2278* Δ*cc1244* double and the triple mutant completely failed to adhere to glass (Figure S2C, D). This, and the observation that surface colonization of the Δ*cc2278* Δ*cc1244* double mutant was barely affected in polystyrene microtiter plates (Figure S2A) indicated that distinct members of this family of proteins might optimize the attachment to different surface chemistry.

Mutations in *hfsK* or its paralogs retained normal surface adherent pili and active flagellar motors (Figure S2E, F), two c-di-GMP dependent cellular appendages that are required for optimal surface attachment (42, 118, 306, 335). Based on these data, we propose that the reduction in surface colonization observed for *hfsK*, *cc2278,* and

cc1244 mutants can be attributed to defective holdfast biogenesis or, in case of *hfsK*, possibly holdfast anchoring.

HfsK contributes to holdfast cohesion and adhesion strength

Recently, Wan and colleagues showed that a mutant lacking the polysaccharide deacetylase HfsH sheds holdfast material that is less cohesive and forms fiber-like structures when exposed to shear forces (322). The authors suggested that the degree of acetylation might be critical for the physical properties of holdfast. Similarly, the N-acyltransferase HfsK might influence the acetylation state of holdfast. To analyze holdfast performance under shear stress, wild type and mutants were grown in a microfluidic device under permanent flow of fresh medium. After overnight growth, individual wild-type cells formed micro-colonies with discrete foci of WGA stained holdfast material at the adherent cell poles (Figure 2C). Mutants lacking HfaB or HfsH were unable to attach but shed compact holdfast structures and faint holdfast fibers, respectively. In contrast, the *hfsK* mutant formed micro-colonies smaller than wild type with fluorescent trails of abraded, filamentous holdfast structures. Holdfast trails were generated by mutant cells that secreted holdfast material onto the surface while slowly drifting with the medium flow. Some holdfast structures elongated into extended filaments from which cells were dangling for some time before the connection ruptured. Upon rupturing several holdfast filaments bounced backwards like a released rubber band, indicating that the cohesive and elastic properties of the holdfast are severely altered in the Δ*hfsK* mutant.

To analyze the adhesive forces of wild-type and mutant holdfast more precisely we used a single cell force spectroscopy (SCFS) approach and Fluidic Force Microscopy (FluidFM) technology. This setup enables single-cell manipulation by combining the precise force control of an Atomic force microscope with a microfluidic device (392, 393) (Figure S2G). Comparison of detachment forces revealed that on average wild-type cells showed approximately 5 times stronger adherence than Δ*hfsK* cells (Figure S2H). Of note, in several cases cells could not be detached at all and were not included in the analysis. During holdfast biogenesis, dimensions of the secreted structures increase over time (315). Thus, we next compared the adherence of Δ*hfsK* cells with weaker (young holdfast) and more intense holdfast staining (mature holdfast). Larger holdfasts were indeed more likely to remain surface-bound with ruptures often occurring between the adhesin and the cell body (Figure S2I). These results indicated that holdfast from the Δ*hfsK* mutant, although more fragile and less

cohesive, can still gain adhesion strength over time as observed for holdfasts of wild-type cells (310).

The above experiments argued that holdfasts of Δ*hfsK* cells, similar to a Δ*hfsH* mutant, show altered cohesive or adhesive properties. However, it is unclear if the observed changes influence the overall properties of the holdfast material or its anchoring in the cell envelope. In line with the latter, microfluidic experiments exposed similar phenotypes for Δ*hfsK* cells and for mutants lacking the holdfast anchor proteins HfaA or HfaD. When growing Δ*hfaA*, Δ*hfaD,* or double mutants in microfluidic devices, trails of WGA-stained material were observed, similar to the structures formed by Δ*hfsK* mutants (Figure 2C). Thus, we asked whether the holdfast anchoring process is still functional in Δ*hfsK* cells. For this we took advantage of the observation that *hfs,* but not *hfa* mutants, are able adhere to holdfasts shed by anchor mutants (334). We combined the Δ*hfsK* with a Δ*hfsJ* deletion, which completely abolishes holdfast EPS formation (317), and tested co-attachment of these cells with a Δ*hfaB* strain. Deletion of *hfsK* did not change the co-attachment capacity of the holdfast deficient strain (Figure S2J, Chapter 2.2.1.1), suggesting that this strain produces an intact holdfast anchor.

Together these results demonstrate that HfsK contributes to the effective surface adherence of *C. crescentus* by modulating the cohesive properties of the holdfast material and/or by facilitating the efficient anchoring of the adhesin in the cell envelope that is necessary to withstand strong shear forces.

C-di-GMP controls HfsK compartmentalization

Holdfast production is controlled by c-di-GMP and coincides with an upshift of c-di-GMP levels during the SW-to-ST cell transition (118, 306). From this and from the observation that HfsK binds c-di-GMP, we anticipated that the activity of this protein might be controlled by c-di-GMP during the cell cycle, akin to other c-di-GMP effector proteins (182, 207, 394). Similar to other *hfs* genes (317), *hfsK* expression is specific to the late predivisional stage of the cell cycle (395). However, this does not result in significant changes of HfsK protein levels during the cell cycle (Figure S3A). Accordingly, HfsK levels showed only minor changes in engineered strains with different c-di-GMP levels (Figure S3B, C). Thus, c-di-GMP affects HfsK abundance only marginally, making it unlikely that holdfast maturation is controlled by c-di-GMP at the level of HfsK expression or stability.

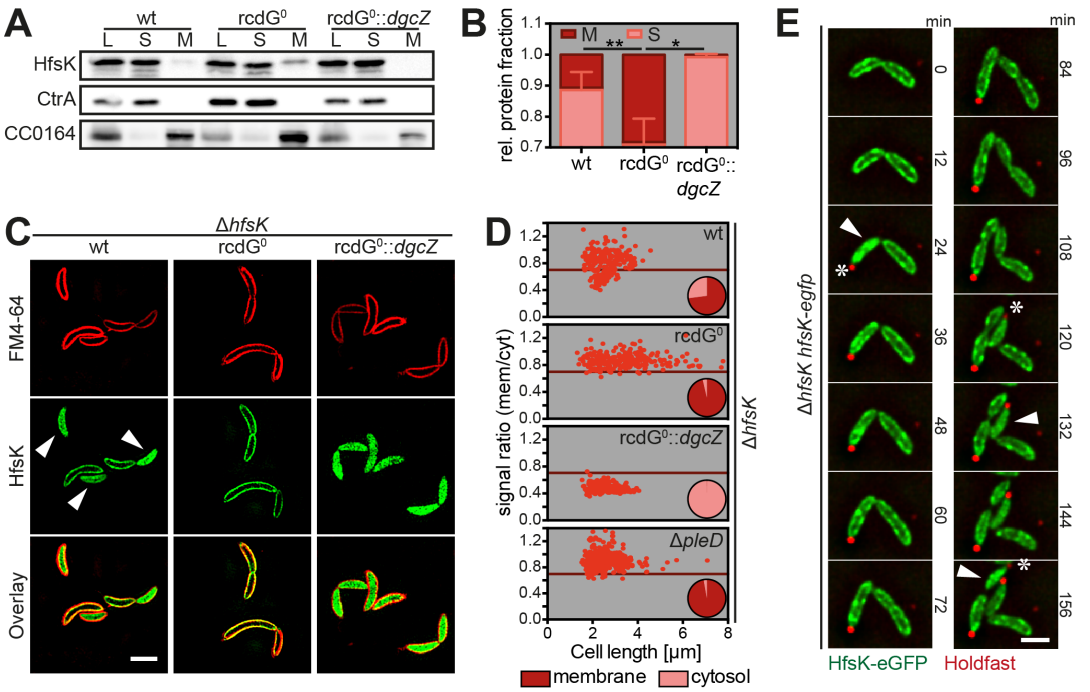

Figure 3: C-di-GMP controls HfsK localization

(A-B) HfsK localization in wild-type, rcdG⁰ (c-di-GMP low), and rcdG⁰::*dgcZ* (c-di-GMP high) cells analyzed by cell fractionation followed by immunoblotting. CtrA (cytosolic) and CC0164 (inner membrane) are shown as controls. Cell lysates (L); soluble fraction (S); membrane fraction (M) (A). Quantification of 3 independent cell fractionations showing the fraction of soluble (light red) and membrane-associated (dark red) HfsK. Error bars = SD, */** represent P-value <0.1/0.01 (B). (C) 3D-SIM images of HfsK-eGFP in cells with different c-di-GMP levels. Stained with the membrane dye FM4-64. Arrowhead indicates cells with cytosolic HfsK-eGFP. Scale bar = 2 µm. (D) Quantification of HfsK-eGFP localization on standard fluorescence microscopy images. The ratio of average signal intensity in the membrane and cytosolic compartments is correlated with cell length. Pie chart inset shows the fraction of cells with membrane-associated ($ratio_{membrane\text{-}cytosol}$>0.7, dark red) or cytosolic (ratio≤0.7, light red) GFP signal. n = 250 cells per strain from 2 independent experiments. (E) Time lapse of Δ*hfsK* P_{van}-*hfsK-egfp* grown on PYE agarose pads supplemented with rhodamine-WGA and vanillic acid (Van) at 30°C. Cells with dispersed HfsK-eGFP (arrowhead) and the first appearance of holdfast in each cell (asterisk) are indicated. Scale bar = 1 µm. In all panels expression of *egfp* constructs and *dgcZ* was induced with 0.55 mM Van and 0.5 mM IPTG, respectively.

Although assembly and maturation of EPS generally occurs in or at the cytoplasmic membrane (50), HfsK is predicted to be a cytosolic protein (396). We used cell fractionation experiments to determine HfsK localization. After ultracentrifugation of cell lysates about 90% of HfsK remained in the soluble fraction, while 10% was retained in the pellet (Figure 3A, B). This indicated that HfsK is at least partially membrane-associated, possibly by binding to an interaction partner in the membrane. In agreement with this idea, HfsK was lost from the membrane fraction when lysates

were treated with increasing salt concentrations that are known to disturb such interactions (397)(Figure S4A). Importantly, none of the known inner-membrane components of the holdfast synthesis machinery was required for sequestration of HfsK to the membrane (Figure S4B).

To test if membrane-association of HfsK is c-di-GMP controlled, cell fractionation was carried out with a newly constructed strain that lacks all genes encoding diguanylate cyclases and phosphodiesterases (rcdG^0) and with the same strain harboring a P_{lac}-driven copy of *dgcZ* from *E. coli* (rcdG^0::*dgcZ*), which allows tuning of intracellular c-di-GMP levels. Expression of the DgcZ diguanylate cyclase (241) in this background produced six-fold higher c-di-GMP levels as compared to wild type (Figure S3B). In the rcdG^0 strain the fraction of membrane-associated HfsK increased to about 30%, while the rcdG^0::*dgcZ* strain had lost the HfsK protein from the membrane fraction almost entirely (Figure 3A, B). Likewise, when c-di-GMP was added to cell extracts of the rcdG^0 strain before fractionation, HfsK primarily localized to the cytosol (Figure S4C). These results indicated that c-di-GMP modulates HfsK membrane interaction with high levels of c-di-GMP promoting its cytosolic state and low levels of c-di-GMP stimulating its association with the membrane.

HfsK dynamically repositions to the cytoplasm during the cell cycle

To more carefully analyze HfsK localization and its association with the cytoplasmic membrane, we expressed a P_{van} driven chromosomal copy of *hfsK-eGFP* in the Δ*hfsK* strain (Figure S4D). Localization of HfsK-eGFP relative to the membrane was visualized by super–resolution 3D structured illumination microscopy (3D-SIM) after cells were stained with the membrane specific dye FM4-64. While the majority of cells showed peripheral HfsK-eGFP co-localizing with the membrane stain, HfsK-eGFP was dispersed in the cytosol in a subfraction of the population (Figure 3C,D). Of note, with the exception of HfsH, which was reported to be cytosolic (322), all functional mCherry fusions of proteins catalyzing early steps of holdfast biogenesis (Figure S4E) localized to the membrane but lacked the cytosolic subfraction characteristic for HfsK (Figure S4F).

To investigate if these changes are driven by c-di-GMP, HfsK-eGFP localization was analyzed in cells harboring different c-di-GMP levels. Strikingly, in the rcdG0 strain HfsK-eGFP showed strong membrane localization in a large majority of the cells, while HfsK-eGFP was entirely cytosolic in the rcdG^0::*dgcZ* strain (Figure 3C, D). Note that the rcdG^0 strain constructed in this study shows a similar filamentous

morphology like the cdG0 strain lacking all diguanylate cyclases (118). To carefully quantify HfsK-eGFP localization at the single cell level, averages of the fluorescent signal at the cell periphery and in the cytosol were determined and ratios calibrated with soluble eGFP and the membrane dye FM4-64 (Figure S4G). The fraction of cells with membrane-associated HfsK-eGFP ranged from 0% in the rcdG^0::*dgcZ* strain, to roughly 70% in wild-type, and 96% in the rcdG^0 background (Figure 3D). Importantly, wild-type cells with membrane-associated HfsK-eGFP included the entire spectrum of measured cell length, while cells with a cytosolic signal were all short. This suggested that HfsK distribution changes during the cell cycle. To test this, time lapse experiments were carried out with a Δ*hfsK* strain expressing HfsK-eGFP. HfsK-eGFP was membrane-associated in newborn SW cells but became cytosolic about 24 min after division and shortly after the appearance of holdfast (Figure 3E, Figure S4H). About 12 min after its dispersal, HfsK-eGFP gradually re-localized to the membrane coincident with cells starting to elongate and divide. These observations indicated that HfsK transiently delocalizes in newly differentiated ST cells coincident with c-di-GMP reaching peak levels during the cell cycle. In line with this idea, HfsK-eGFP failed to discharge from the membrane fraction in a strain lacking PleD, the main DGC responsible for the upshift of c-di-GMP during the SW-to-ST transition (118, 398) (Figure 3D).

Together these results demonstrated that HfsK localization is dynamic and indicated that its repositioning to the cytoplasm during SW-to-ST transition is driven by peak levels of c-di-GMP.

The C-terminus is required for activity and membrane localization of HfsK

Despite low sequence homology, GNAT proteins have a remarkably conserved core-fold (346). The closest homolog of HfsK with a solved 3D structure is FemX, an enzyme involved in peptidoglycan synthesis in gram-positive bacteria (367, 399). Both proteins have two GNAT domains in tandem. Sequence comparisons revealed that HfsK has a short C-terminal extension of 25 amino acids that is absent in FemX (Figure S5A). Surprisingly, an eGFP fusion protein with truncated HfsK ($HfsK_{trnc}$) that lacks this extension, although being stable, lost its characteristic membrane-association and, in contrast to full length HfsK-eGFP, failed to complement the Δ*hfsK* phenotype (Figure 4A-C, Figure S4C). HfsK and $HfsK_{trnc}$ exclusively localized to the membrane when fused to the transmembrane helix of *C. crescentus* SecE (TM), which is sufficient to restrict reporter proteins to the membrane (400) (Figure 4A, B).

However, these proteins harboring the TM from SecE failed to respond to changes in c-di-GMP (Figure S5B). Whereas the TM-tagged wild-type HfsK was fully functional, cells expressing $HfsK_{trnc}$ did not support surface colonization even if shuttled to the cytoplasmic membrane by the exogenous TM segment (Figure 4C). Thus, the C-terminus of HfsK is required for its membrane localization and for its function. These experiments also indicated that membrane-associated HfsK represents the active species of the protein and that release of HfsK from the membrane at high levels of c-di-GMP might lead to its inactivation.

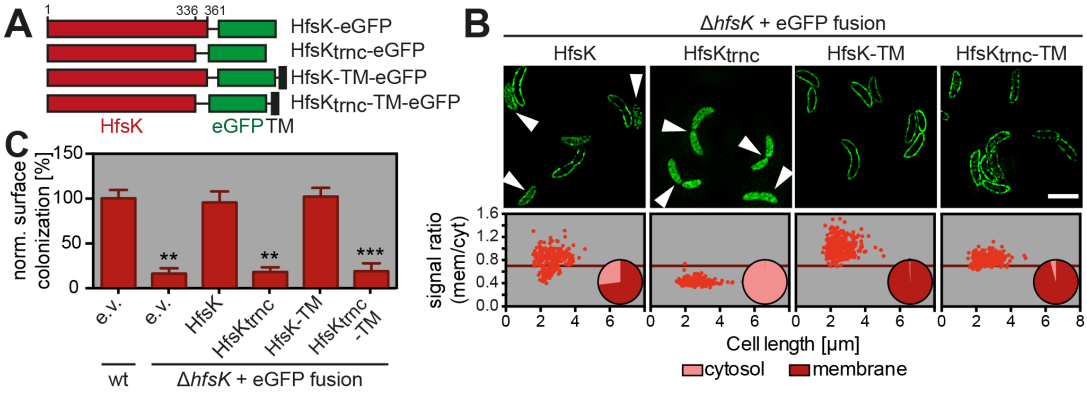

Figure 4: The C-terminus of HfsK is an important determinant for its localization and function

(A) Schematic representation of the HfsK-eGFP mutants used in this figure. Amino acid positions are indicated on top. Not drawn to scale. TM = trans membrane domain of SecE. (B) Localization quantification of different HfsK-eGFP mutants expressed by addition of 0.55 mM Van as described in Figure 3D. n = 260 cells per strain from 2 independent experiments. Representative 3D-SIM images for visualization are shown above. Arrowhead indicates cells with dispersed HfsK-eGFP. Note: due to a weak signal intensity of $HfsK_{trnc}$-TM the 3D-SIM image recreation resulted in images with high background signal. Scale Bar = 3 µm. (C) Functionality of HfsK-eGFP mutants compared to a wild-type strain harboring the empty vector control (e.v.) in surface colonization after 24 h growth in microtiter plates in presence of 0.1 mM Van. Error bars = SD of 3 independent experiments, **/*** represent P-value <0.01/0.001.

C-di-GMP drives HfsK to the cytosol but is dispensable for its activity

We have shown above that both c-di-GMP and the C-terminus of HfsK are important for the localization of the protein during the cell cycle. This indicated that the C-terminus of HfsK itself could be targeted by c-di-GMP and could contribute to c-di-GMP binding. In agreement with this we found that a StrepII-HfsK fusion lacking the 25 C-terminal amino acids ($HfsK_{trnc}$) showed reduced binding of c-di-GMP as compared to wild-type HfsK (Figure 5A). Structural examination of c-di-GMP binding

proteins had revealed important roles for arginine residues in ligand binding (114). We thus generated the mutant HfsK(RR352AA) that had two central arginine residues of the C-terminus (Figure S1A) changed to alanine. Similar to the shortened $HfsK_{trnc}$, this mutation reduced affinity for c-di-GMP (Figure 5A). To identify residues located in the core region of HfsK that are involved in c-di-GMP binding we compared the sequences of HfsK and its two *C. crescentus* paralogs. Because HfsK and CC1244, but not CC2278, were identified by CCMS, we searched for arginine residues that are conserved in HfsK and CC1244 but not in CC2278 (Figure S1A). Several of these residues of HfsK (R102, R112, R151, R240 and R267) were substituted with alanine and the resulting mutant proteins were expressed as StrepII-tagged fusions in *E. coli*. Binding studies with radiolabeled c-di-GMP identified $HfsK_{R112A}$ as the only mutant variant with reduced binding affinity for c-di-GMP (Figure 5A). These results suggested that R112 as well as arginine residues located in the HfsK C-terminus may contribute to c-di-GMP binding.

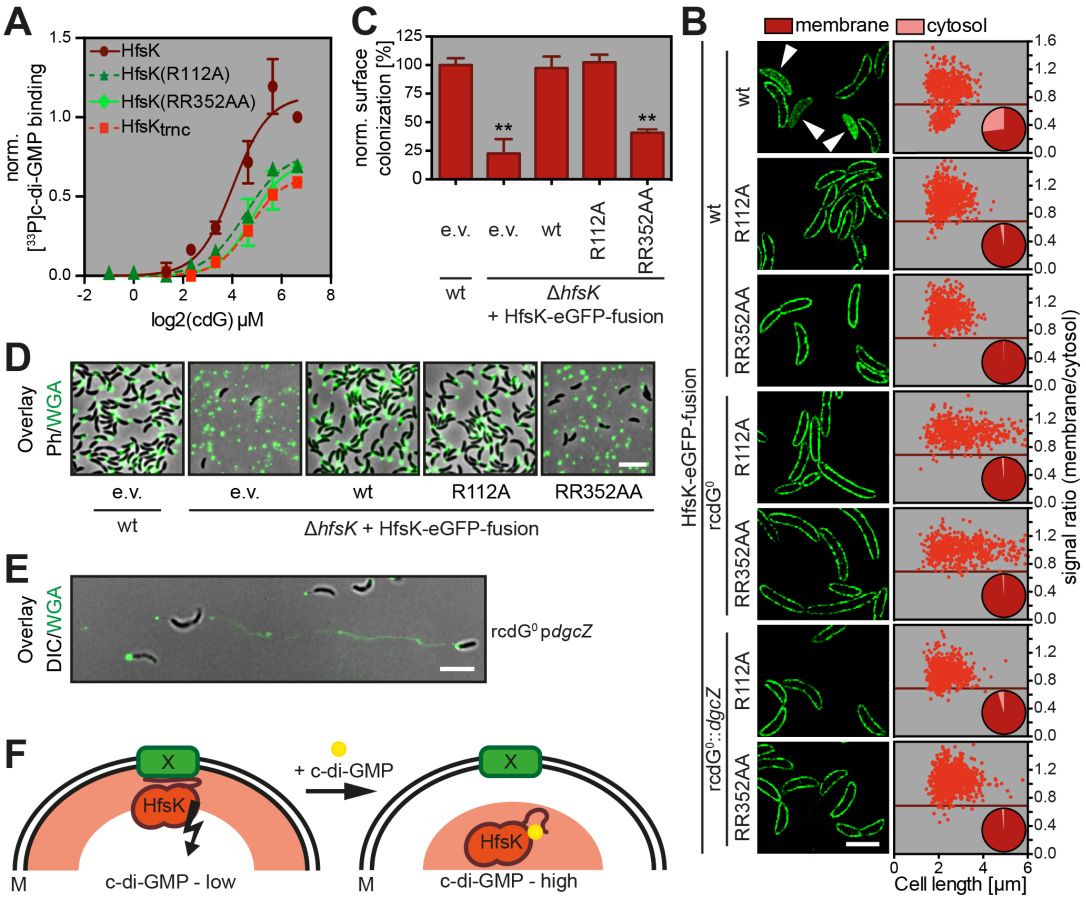

Figure 5: C-di-GMP binding is required for HfsK delocalization but not for HfsK-mediated surface colonization

(A) Quantified autoradiographs of 1 µM purified StrepII-HfsK mutants that were UV-crosslinked to increasing concentrations of [^{33}P]c–di–GMP. (B) Localization analysis of different arginine mutants fused to GFP expressed by addition of 0.55 mM Van. Representative 3D-SIM images for visualization (left panel) and localization quantification as described in Figure 3D are shown. n = 575 cells per strain from 2 independent experiments. Expression of *dgcZ* was induced with 0.5 mM IPTG. Scale bar = 3 µm. (C) Functionality of HfsK arginine mutants compared to a wild-type strain harboring the empty vector control (e.v.) in surface colonization after 24 h growth in microtiter plates in presence of 0.1 mM Van. (D) Analysis of adhered OG-WGA stained holdfast on coverslips after 2 h adsorption of cells. Representative overlays of fluorescence and phase contrast images are shown. Scale bar = 5 µm. (E) Holdfasts of a strain with high c-di-GMP levels analyzed under shear stress after 15 h growth in microfluidics channels with constant flow of fresh medium containing OG-WGA. Shown is an overlay of fluorescence and inverted DIC images. Scale bar = 5 µm. (F) Model of HfsK regulation. General protein localization is represented by red shades. Active HfsK binds to membrane component X in absence of c-di-GMP via its C-terminus. Upon c-di-GMP binding the C-terminus rearranges to accommodate the nucleotide, the protein is inactivated, and disperses in the cytosol. Error bars in panel A and B = SD of 3 independent experiments, ** represent P-value <0.01. (← Figure on previous page)

Importantly, HfsK-eGFP fusions containing point mutations R112A or RR352AA remained membrane-associated even in strains harboring high levels of c-di-GMP, arguing that they no longer respond to the second messenger *in vivo* (Figure 5B). Functional analysis revealed that the $HfsK_{RR352AA}$ -eGFP fusion protein failed to restore the Δ*hfsK* phenotype, underlining the importance of the C-terminus for protein function. In contrast, expression of the $HfsK_{R112A}$-eGFP fusion was able to substitute for HfsK in surface colonization and holdfast biogenesis (Figure 5C, D, Figure S5C). Together, these data support a model in which c-di-GMP binding determines HfsK subcellular localization and possibly HfsK activity. Our data are in line with the view that binding of c-di-GMP inactivates HfsK by sequestering the protein away from a membrane associated active conformation. In agreement with this view, we found that unphysiologically high levels of c-di-GMP not only severely reduced surface colonization but, akin to the Δ*hfsK* mutant, changed the cohesive properties of holdfast structures (Figure 5E, Figure S6A-C). The finding that the C-terminus of HfsK is essential for its function and for its subcellular localization and contributes to c-di-GMP binding implies that this part of the protein is the central regulatory hub controlling HfsK dynamics and activity in response to the second messenger.

2.1.4 Discussion

The second messenger c-di-GMP controls EPS production in a wide range of bacteria by stimulating the activity of glycosyltransferases directly or via adaptor proteins (51, 190, 242, 244). By this means c-di-GMP directly affects the polymerization and secretion rate of EPS across the inner membrane. Here we describe the first c-di-GMP effector, which is not required to adjust the amount of EPS produced, but rather controls EPS adhesin modification and thus changes its physical properties and strength. However, HfsK activity does not seem to depend on c-di-GMP. Rather, our data argue that c-di-GMP affects HfsK negatively, possibly to adjust or coordinate its activity with other processes of holdfast biogenesis. Because cells that lack c-di-GMP are unable to produce holdfast (118), additional c-di-GMP controlled catalytic components must contribute to this process. This example nicely illustrates that c-di-GMP can influence EPS production both quantitatively and qualitatively.

Cells lacking HfsK produce normal amounts of holdfast material. However, mutant holdfasts form elastic and abrasive filaments that are unable to withstand strong shear forces, suggesting that they are reduced in cohesiveness and stability. A similar change of the physical properties of the holdfast adhesin was described for mutants deficient in HfsH. HfsH was proposed to deacetylate holdfast EPS precursors and by that unmask amine groups that might serve as holdfast anchoring sites (322). This is consistent with our findings that cells lacking holdfast anchoring proteins HfaA or HfaD display comparable holdfast behavior under shear stress. In contrast to the *ΔhfaA ΔhfaD* double mutant, shed holdfasts of Δ*hfaB* cells did not deform under shear stress and retained a globular shape. Because HfaA and HfaD are thought to be exported and inserted in the outer membrane by the action of HfaB, these factors should, in principle, behave epistatically. However, similar observations were made by Hardy and colleagues indicating that HfaB likely adopts additional roles (331). For instance, it is possible that HfaB directly contributes to EPS anchoring and that in its absence shedding of the holdfast is unrestrained. Altogether, the similarity of the mutant phenotypes suggested that the putative acyltransferase HfsK, the deacetylase HfsH, and the holdfast anchor proteins HfaD and HfaA, may be part of the same pathway that is required for holdfast anchoring and proper holdfast cohesion – two aspects that seem to be interdependent.

The exact role of HfsK in this pathway remains unclear. The closest homologs with known structure are the Fem proteins of gram-positive bacteria that transfer

aminoacyl moieties to peptidoglycan sugar precursors (367, 399). Given the low overall sequence similarity, the functional versatility of GNAT proteins, and their diversity in terms of acyl-donors and acceptors (346), it is difficult to make predictions about the catalytic role of HfsK. It might transfer an acyl group to amines exposed by the action of HfsH (322). Depending on the nature of this acyl group, it could be involved in the covalent linkage of polysaccharide moieties to anchor proteins (378) or participate in electrostatic interactions required for adhesion, cohesion or anchoring. This is in line with the observation that isolated holdfasts from a Δ*hfsH* mutant showed reduced electrostatic interactions with the substrate (310). While we cannot fully exclude that HfsK acylates an anchor protein to provide crosslinking sites, several observations indicated that HfsK chemically modifies holdfast EPS precursors directly. (1) HfsK homologs are genetically coupled to various EPS synthesis systems. (2) Deletion of the paralogs *cc2278* and *cc1244* affect the adhesin without observable shedding phenotype. (3) Cells lacking HfsK are able to adhere to shed holdfasts of a Δ*hfaB* mutant, indicating an intact anchor mechanism. (4) HfsK co-localizes with other holdfast components involved in EPS precursor biogenesis. This is in contrast to holdfast export and anchoring proteins that localize to the cell pole where holdfast is assembled (326, 330, 331). Based on these arguments, we propose that HfsK acylates the exopolysaccharide component of the holdfast and that this modification is necessary for proper holdfast cohesion and anchoring.

HfsK was originally isolated using a c-di-GMP specific capture and was shown to specifically bind c-di-GMP *in vitro*. The binding affinity of HfsK lies in the sub-micromolar range, which correlates well with the peak concentrations of c-di-GMP during the *C. crescentus* SW-to-ST differentiation (118, 301). These values are in line with our findings that the protein delocalizes in a c-di-GMP dependent manner coincident with holdfast formation during the cell cycle. HfsK may thus be retained at the cytosolic membrane when c-di-GMP levels are low or intermediate and be transiently released from the membrane during a short period of the cell cycle, when c-di-GMP reaches a high concentration. Our data also suggest that the membrane-associated form of HfsK is catalytically active, while membrane release results in its inactivation. In line with this we found that the c-di-GMP binding mutant R112A permanently localized to the membrane while retaining its activity for holdfast formation. Several observations point to the C-terminus as a central determinant for

HfsK localization and catalytic activity. Mutants lacking the C-terminus failed to localize to the membrane and were inactive even when forced to bind to the membrane artificially. Moreover, the C-terminus is also involved in c-di-GMP binding. A mutant lacking two central arginine residues within this region failed to efficiently bind c-di-GMP and remained membrane-associated throughout the cell cycle irrespective of the c-di-GMP concentration. Unlike the R112A mutant, the RR352AA variant was inactive, indicating that this site may be the core of HfsK control. We propose a model, in which the C-terminus of HfsK serves as interaction site for a putative membrane partner (Figure 5F). In this model, membrane tethering is necessary for HfsK activity, while c-di-GMP binding interferes with the tether and leads to delocalization and inactivation of HfsK. Based on our data we envisage that the arginine residues in the C-terminus are involved in c-di-GMP binding and activity of HfsK, offering a simple switch through which c-di-GMP can control conformation, membrane association, and catalytic activity. A FemX-derived structure model of HfsK could provide a molecular frame for this c-di-GMP mediated switch (Figure S6D). Residue R112, which is localized on the surface of one of the GNAT domains, and R352 and/or R353 in the C-terminus might jointly contribute to c-di-GMP binding. Accordingly, ligand binding would provoke the C-terminus to swing back and interact with the GNAT core. To clarify such mechanistic details additional biochemical and structural studies with HfsK and c-di-GMP are needed.

This study represents one of few examples for a c-di-GMP effector protein that is inactivated by ligand binding (197, 207). It remains unclear why HfsK activity would need to be turned off during the cell cycle and why this process is linked to peak levels of c-di-GMP. Given the timing of HfsK delocalization it is possible that it is involved in some early step of holdfast biogenesis, catalyzing a reaction that is detrimental for later steps of holdfast export or maturation. If so, *C. crescentus* may elegantly use c-di-GMP for a dual control of holdfast biogenesis. During the SW-to-ST transition, when c-di-GMP levels begin to increase, one or several key enzyme(s) may be turned on to initiate holdfast biogenesis. But when c-di-GMP ascents to peak levels, the cell might turn off enzyme(s) that are no longer needed or damaging. Alternatively, HfsK may engage in additional processes. For several holdfast synthesis steps, redundant functional equivalents exist with one copy being encoded in the *hfs*-operons and its paralog(s) being encoded elsewhere. It was proposed that paralogs may act in other pathways but can contribute to holdfast synthesis due to substrate similarities (66). It

is plausible that HfsK interferes with related cellular pathways required for the synthesis of capsule, LPS, O-antigen, or possibly even peptidoglycan. In this case, proper timing of enzyme activity during the cell cycle could help prevent substrate depletion or leakage, thereby providing a rationale for c-di-GMP mediated control.

2.1.5 Materials and Methods

Bacterial strains and growth conditions

All bacterial strains and plasmids used in this study are listed in Table 2. *E. coli* strains were grown at 37°C or 30°C under aeration in Luria Broth (LB) medium supplemented with the appropriate antibiotic (solid/liquid in µg/ml: kanamycin 50/30; chloramphenicol 30/20) and the inducer Isopropyl β-D-1-thiogalacto-pyranoside (IPTG 0.3 or 0.75 mM) if required. *C. crescentus* strains were grown at 30°C under aeration in peptone yeast extract (PYE) or M2 minimal medium supplemented with 0.1% glucose (M2G). Media were supplemented with the appropriate antibiotic (solid/liquid in µg/ml: kanamycin 20/5; nalidixic acid 20/n.a.) or inducer (IPTG 0.2 or 0.5 mM, xylose 0.1%, vanillic acid 0.1 mM or 0.55 mM) if required. Media were solidified by addition of 1.5%, 0.75% or 0.3% agar for regular growth plates, top-agar and, motility plates, respectively. Optical density of cultures was measured at 600 nm (*E. coli*) or 660 nm (*C. crescentus*) with a photo spectrometer (Ultrospec 2100 pro, Amersham Biosciences, USA). If required cell cultures were synchronized using density gradient centrifugation as previously described (401).

Attachment assay

For 24-hour attachment assay 5 µl overnight culture were added to 155 µl appropriate medium in a 96 well polystyrene microtiter plate and grown for 24 h under aeration at 30°C. After absorbance was measured at 660 nm to confirm equal growth, the plates were rinsed thoroughly with water and, incubated for 30 min with 180 µl 0.1% (m/V) crystal violet/ 1% Methanol/ Isopropanol. The plates were rinsed again, dried, and the adherent crystal violet was dissolved in 200 µl 20% acetic acid for 15 min shaking at 30°C before absorption at 600 nm was measured.

For a 30-min attachment assay, overnight cultures were diluted to an OD_{660} of 0.06 in fresh medium, grown to an OD_{660} of 0.3-0.5. Cell numbers were adjusted to an OD_{660} of 0.3 before 160 µl culture was incubated into 96 well polystyrene microtiter

plates and grown for 30 min under aeration at 30°C. Crystal violet staining was done as described above.

Fluorescence microscopy

Cells were harvested in mid-log phase (OD_{660} 0.3 - 0.5) and mounted on 1% agarose pads (Sigma, USA) in water for snap shots or in PYE containing appropriate supplements for time-lapse experiments. For 3D-SIM and time lapse microscopy samples were sealed with highly viscous silicone grease (Sigma Aldrich) to avoid agar shrinking.

Fluorescence, phase contrast (PH), and differential interference contrast (DIC) images were taken with a wide-field DeltaVision Core Olympus IX71 microscope (Applied Precision, USA) with SoftWoRx software and environmental chamber, equipped either with UPlanSApo 100x/ 1.40 oil objective (Olympus, Japan) and a coolSNAP HQ-2 CCD camera (Photometrics, USA) or UPlan FL 100x/ 1.3 and UPlanSApo 100x/1.40 oil objectives (Olympus, Japan) and a pco.Edge sCMOS camera (PCO, Germany). Images with mCherry fusion proteins were taken with a Nikon Ti-E inverted motorized microscope with Perfect Focus System and PlanApo 100x/1.4 Oil Ph3 DM objective lens, SPECTRA × light engine (Lumencore), camera pco.Edge 4.2 (PCO, Germany), and VisiView software (Visitron Systems, Germany). Images showing protein localization were deconvolved using SoftWoRx and Huygens software.

3D-SIM imaging was performed on a microscope system (DeltaVision OMX-Blaze version 4; Applied Precision, USA) equipped with 405, 445, 488, 514, 568, and 642 nm solid-state lasers. Images were acquired using a PlanApoN 60x/1.42 oil objective lens (Olympus) and 4 liquid-cooled sCMOS cameras (pco.Edge, full frame 2560 x 2160; Photometrics). Exciting light was directed through a movable optical grating to generate a fine-striped interference pattern on the sample plane. The pattern was shifted laterally through five phases and three angular rotations of 60° for each z section. Optical z-sections were separated by 0.125 µm. The laser line 488 nm was used for 3D-SIM acquisitions. Multichannel imaging was achieved through sequential acquisition of wavelengths by separate cameras.

Raw 3D-SIM images were processed and reconstructed using the DeltaVision OMX SoftWoRx software package (Applied Precision (402, 403)). The resulting size of the reconstructed images was of 512 x 512 px from an initial set of 256 x 256 raw images. The channels were aligned in the image plane and around the optical axis using predetermined shifts as measured using a target lens and the SoftWoRx alignment

tool. The channels were then carefully aligned using alignment parameter from control measurements with 0.5 µm diameter multi-spectral fluorescent beads (Invitrogen, Molecular Probes).

Holdfast and membrane stain

To visualize membrane, mid log phase cultures were mounted on 1% agarose in PYE pads supplemented with 0.66 µg/ml FM4-64 dye (Molecular probes, USA). To visualize holdfast, mid log phase cultures were mixed with a final concentration of 1 µg/ml wheat germ agglutinin (WGA) coupled to Oregon green (Invitrogen, USA), incubated for 10 min, and visualized by fluorescence microscopy. For time-lapse microscopy experiments 2.66 µg/ml tetramethylrhodamine-WGA was added into the agarose pads.

Adherence to glass

To visualize adherent holdfast on glass a protocol was adapted from (330). 500µl/well overnight culture were diluted to an OD_{660} of 0.15 and incubated with round 12 mm borosilicate coverslips (Thermo Scientific, USA) in 24 well polystyrene plates for 2 h at 30°C under aeration. If plasmid induction was required, overnight grown cultures were diluted first 1:10 in medium containing the inducing agent and grown to mid-log phase, before cell numbers were adjusted to an OD_{660} of 0.15 and added to the coverslips. After incubation, the coverslip side facing upwards was stained for 15 min with 2.5 µg/ml WGA coupled to Oregon green, tetramethylrhodamine, or AlexaFluor®350, rinsed with water, and mounted on 1% agarose pads. Co-attachment experiments were performed on glass coverslips as described above, yet the co-cultured strains were mixed 1:1 to a final OD_{660} of 0.15 before incubation. For quantification 10 images were taken in random areas and the mean gray value was measured for each using the FIJI software (404). The mean gray value measured on glass slides prepared with the holdfast-minus NA1000 strains was subtracted to correct for background fluorescence.

Quantification of protein localization

Quantitative fluorescent signal measurements of individual cells were performed using a MATLAB based program developed in our group (WHISIT). WHISIT calculated average pixel fluorescent signal intensity for the membrane and cytoplasmic compartments. The membrane compartment was defined to enclose the first four intracellular pixel flanking the cell outline which was computed by Oufti (405) on

phase contrast images, whilst the remaining intracellular pixels were defined as cytoplasmic compartment. The WHISIT program is available online at http://ch.mathworks.com/matlabcentral/fileexchange/61676-whisit.

Microfluidics

For the observation of bacteria under flow conditions they were grown in polydimethylsiloxane (PDMS) based microfluidics devices produced as previously described (406), consisting of a single channel of 10 mm length, 40 µm width, and 25 µm height connecting an in- and outlet. Mid-log phase cells were carefully filled into the channel before a constant flow (0.002 µl/s) of PYE medium supplemented with 1 µg/ml Oregon green-WGA was installed to allow growth. If necessary movies were corrected for bleaching using ImageJ Plugin CorrectBleach (V2.0.2, Kota Miura; Curtis Rueden; Mark Hiner; Johannes Schindelin; Jens Rietdorf, Centre for Molecular and Cellular Imaging (CMCI), EMBL Heidelberg, [http://wiki.cmci.info/downloads/bleach_corrector])

Immunoblots

Cells were harvested and normalized in 1x SDS-SB (0.1 M Tris pH 6.8/ 5% Glycerol/ 0.2% sodium dodecyl sulfate (SDS)/ 1% β-Mercaptoethanol/ 0.025% Bromophenol blue) to the same OD_{660}. Samples were boiled for 5 min at 95°C, separated on 12% SDS-acrylamide gel electrophoreses (PAGE), and transferred onto PVDF-membranes (Immobilon-P, Millipore, USA). Proteins were detected using specific primary polyclonal antibodies (anti-CtrA 1:10,00, anti-CC0164 1:20,000, anti-ClpX 1:10,000, anti-GFP 1:800 (Invitrogen, USA)) and anti-rabbit secondary antibodies coupled to horseradish peroxidase (1:10,000, Dako, Denmark). After incubation with LumiGLO or LumiGLO reserve chemiluminescent substrate (KPL, USA) luminescence was detected using LAS-4000 luminescent image analyzer (Fujifilm, Japan). Immunoblot bands were quantified by measuring mean gray values with FIJI (404, 407).

StrepII-HfsK was purified as described below and injected into rabbits to raise polyclonal antibodies, (Josman LLC, USA). The serum was used in a 1:20,000 dilution.

Cell fractionation

150 ml mid log phase cultures were harvested by centrifugation (8000 xg, 20 min, 4°C) and washed in 50 ml PBS. The pellet was resuspended in 7 ml per gram wet weight CellFrac-Buffer (PBS/ 1x cOmplete mini EDTA-free Protease Inhibitor (Roche)/ 2.5 µg/ml DNAseI (Roche)), lysed using a French- pressure cell press at

1 bar (Thermo Electron corporation, USA), and spun to remove cell debris (10 min, 18,000 xg, 4°C). To separate soluble from insoluble proteins, 1 ml of this cleared cell lysate was centrifuged at high speed (1 h, 100,000 xg, 4°C). The supernatant was removed and kept as soluble fraction whereas the pellet was washed in CellFrac-Buffer. The washed pellet was resuspended in 1 ml CellFrac-Buffer and kept as the pellet fraction. Cleared lysate, soluble and pellet fraction were diluted in 5x SDS-SB, boiled for 5 min at 95°C, and further analyzed using immunoblot.

Protein purification

pET28aStrepII plasmids expressing wild-type HfsK and mutant derivatives were transformed into *E. coli* Rosetta (DE3). Cells were grown at 30°C to an OD_{600} of 0.6, before the plasmid was induced with 0.75 mM IPTG for 4 h. Cells were harvested and resuspended in 50 mM NAH_2PO_4 / 300 mM NaCl supplemented with 1 µM Pepstatin / 1 mM DTT / 1x cOmplete mini (Roche) / 2.5 µg/ml DNAseI (Roche) and lysed using a French- pressure cell press at 1 bar. The StrepII-tagged proteins were purified from cleared lysates with Strep-Tactin Superflow plus resins (Qiagen) according to the manufacturer's protocol and used in the elution buffer or in 20 mM Tris pH 8.5/200 mM NaCl for further experiments.

The pET28aHis-HfsK plasmid was transformed into NiCo21(DE3) cells and grown at 37°C to an OD_{600} of 0.6. Protein expression was induced with 0.3 mM IPTG and incubation was continued at 22°C overnight. Cells were resuspended in 20 mM Tris pH 8.5/ 0.75 M NaCl/ 3 mM beta-mercaptoethanol/ 0.1%Tween-20 / 20 mM/ 1mM PMSF/ 1 µm pepstatin supplemented with protease inhibitor tablet (Roche) and disrupted using a microfluidizer (M-110L pneumatic, Microfluidics). Cleared lysate was applied to a 5 ml HisTrap HP column (GE Healthcare) and the His-tagged protein was eluted with a gradient of elution buffer containing 20 mM Tris pH 8.5/ 0.5 M NaCl/ 3 mM beta-mercaptoethanol/ 0.1%Tween-20/ 500 mM imidazole. The eluted fractions containing HfsK protein were concentrated and injected on a Superdex 200 10/300 GL increase gel filtration column (GE Healthcare) equilibrated with 30 mM HEPES pH 7.4/ 0.3 M NaCl/ 3 mM beta-mercaptoethanol/ 5 mM MgCl2. The peak fractions corresponding to HfsK were collected and the concentration adjusted for ITC experiment.

Isothermal titration calorimetry

The interaction of HfsK with c-di-GMP was measured with a VP-ITC isothermal titration calorimeter from MicroCal with 13 µM HfsK in the cell and 211 µM c-di-GMP in the syringe (buffer: 30 mM HEPES pH 7.4, 0.3 M NaCl, 5 mM MgCl2, and 3 mM beta-mercaptoethanol). All solutions were thoroughly degassed and equilibrated to 22°C before filling into the calorimeter. The first injection of 3 µl was followed by 29 injections of 10 µl and the temperature of the calorimetric cell was maintained at 22°C. The delay between the injections was set to 6-7 min to ensure complete re-equilibration between subsequent injections. The observed data were analyzed using the MicroCal version of ORIGIN and fitted with the "One binding site model" of ORIGIN.

UV crosslinking with [^{33}P]c-di-GMP

[^{33}P]c-di-GMP was synthesized using [^{33}P]GTP (Hartmann Analytic, Germany) and the diguanylate cyclase DgcZ from *E. coli*. DgcZ purification and c-di-GMP productions was performed as previously described (123, 241). Crosslinking experiments were performed as described in (125). In short, 1 µM purified protein, an appropriate concentration of [^{33}P] c-di-GMP, and reaction buffer (50 mM NaH2PO4 pH 6.5/ 200 mM NaCl/ 1 mM DTT or 20 mM Tris pH 8.5/200 mM NaCl/ 1 mM DTT) were mixed and incubated for 10 min at RT. In competition experiments the protein was pre-incubated with unlabeled competitor before [^{33}P]c-di-GMP was added. Samples were irradiated at 254 nm for 3 min at 4°C, mixed with 5x SDS-Sample Buffer, and boiled for 5 min. The samples were separated on 12% acrylamide gels using SDS-PAGE. The gels were dried and exposed to a phosphor screen that was scanned on a Typhoon FLA 7000 imaging system (GE Healthcare). Autoradiogram bands were quantified using FIJI (404, 407) by measuring the mean gray value and binding curves were fitted with GraphPad Prism 6.0.

SCFS measurements with FluidFM

In order to obtain clean substrates for the SCFS experiments, glass dishes (WillCo Wells B.V., The Netherlands) were sonicated in 2-propanol (Scharlau, Spain) and subsequently in ultra-pure water for 10 min at room temperature in a Branson 2210 Ultrasound bath and dried under nitrogen gas stream right before use. Cultures grown overnight in PYE were diluted to an OD_{600} of 0.001 and together with a final concentration of 0.1 µg/ml Oregon green-WGA were added to the clean glass dishes.

SCFS measurements were started right away and could last several hours. Thus, measurements comprise this range of surface contact times for all strains.

Preparation and calibration of the cantilever was performed as described earlier (392). Briefly, rectangular, hollow silicon nitride cantilevers containing a hollow pyramid at the free-end (Cytosurge AG, Switzerland) were 36 µm wide, 150 µm long, and had a channel height of 1 µm, resulting in a stiffness of about 2.5 N/m. Circular 300 – 700 nm diameter openings at the pyramidal apex were drilled by focused ion beam after sloping the pyramid's tip to compensate for the 10° tilt angle of the AFM probe holder (408). Prior to the experiments the probes were plasma-cleaned for 30 s (Plasma Cleaner PDG-32G, Harrick Plasma, USA) and covered with an antifouling coating of 0.5 mg/ml poly-L-lysine (PLL) (20 kDa) that was grafted with poly-ethylene glycol (PEG) (2 kDa) (PLL-*g*-PEG) (Surface Solution SuSoS AG, Switzerland) in filtered ultra-pure water (409). FluidFM probes were coated from the in- and outside with PLL-*g*- PEG for 1 h and subsequently washed in filtered PBS for 5 min (410). Cantilever sensitivity was calibrated using software-implemented scripts based on the formalism described by Sader and colleagues (411).

A FluidFM connected via tubing to a pressure controller (Cytosurge AG, Zürich and Nanosurf AG, Liestal, Switzerland) was mounted on an Axio Observer D1 inverted microscope (Carl Zeiss, Jena, Germany). For previously developed FluidFM applications, the probe was directly approached onto adherent cells prior to underpressure based cell immobilization to the cantilever and subsequent cell detachment of the substrate (392, 409). However, a direct approach onto the cell is not possible for *C. crescentus*, as the flexible parts of the cells are pushed away during the downward movement of the probe. In order to achieve a defined distance above the substrate, the pyramidal tip was approached next to a *Caulobacter* cell and retracted until the desired separation was achieved. Subsequently, to immobilize the cell to the cantilever, the probe was moved in x-y directions above the target cell and 0.8 atm underpressure was applied for reversible cell immobilization at the pyramidal tip opening. Subsequently the probe, together with the attached cell was retracted at a piezo velocity of 1 µm/s, while forces were recorded. Underpressure was maintained during this process until the bacterium was completely detached from the substrate. Subsequently the bacterium was released from the cantilever by an overpressure pulse of 1 atm. SCFS data were analyzed with SPIP software (Image Metrology A/S, Hørsholm, Denmark).

Statistics

For statistical comparison, paired t-tests were used if not stated otherwise. Calculations were performed with GraphPad Prism.

C-di-GMP quantification

C-di-GMP was extracted from 20 ml liquid culture of strains harboring a deletion in *hfsA* (holdfast$^-$) and *cc00471* (capsule$^-$) to prevent EPS based clogging of the HPLC column. Extraction and quantification was performed as previously described (387, 412).

Alignments, phylogenetic analysis and structural model

Sequence homologs of HfsK were obtained using Blast search (413) (database accessed July 2015) and the phylogenetic tree was computed with Geneious 7.1.7 using global alignment with free end gaps and neighbor joining methodology.

The structural model of HfsK was created with the MPI bioinformatics Toolkit (414) using structural homology search with HHpred (390), followed by structure prediction with the build-in modeller function (415). Structure based alignment was adapted from the HHpred structural homology search output and multiple sequence alignments were created using MUSCLE (416).

Phage and motility assay

Phage lysates were prepared based on (417). In short, mid-log phase bacterial culture was mixed with phage lysate, incubated for 10 min at room temperature, mixed with prewarmed PYE top-agar (0.75%) and poured onto a PYE plate. After overnight growth at 30 °C, 5 ml CPB buffer (10 mM Tris pH 7.5/ 1 mM $MgSO_4$/ 1 mM $CaCl_2$) were added and incubated again overnight at 4 °C. The next day, lysed cells were scraped from the plate, mixed with 150 µl chloroform and incubated for 1 h. After centrifugation (5,000 xg, 10 min), another 150 µl chloroform were added to the cleared supernatant to get the phage lysate stock.

To assess phage susceptibility, 200 µl stationary phase culture was mixed with 2.5 ml PYE top-agar (45°C) and poured on top of PYE plates. Onto the solidified agar 5 µl of serial dilutions of phage lysate were spotted. Phage lysates were made in CPB buffer. The plates were incubated for 1 day at 30°C and scanned (ScanMaker i800, Microtek International). To score motility, semi-solid PYE 0.3% agar plates were inoculated with a single colony and incubated for 3 days in a humidified chamber at 30°C. The plates were scanned and colony size was measured using FIJI (404, 407).

Construction of plasmids

For pNPTS138-based deletion plasmids roughly 500 bp up-and downstream of the target gene were amplified from genomic CB15 DNA with PCR, cut with restriction enzymes as indicated in Table 2, and ligated at the same time into EcoRI/ HindIII (or in case of pNPTS-Δ*2278*: SpeI/ EcoRI) cut pNPTS138 vector. In case of pNPTS138-Δ*hfsK* and the inner primers (3585/35876) have extensions that are complementary to each other, thus the two fragments were fused using SOE-PCR and primers 8584/3587. The fused products were cut with EcoRI/HindIII and ligated in the likewise cut pNPTS138 vector.

StrepII-fusions were generated using the subcloning vector pET28A-StrepII-MCS which was generated by annealing of two complementary oligonucleotides encoding the *strepII* tag (primer 3287/3288), followed by restriction enzyme digest with NcoI/ BamHI and ligation into the likewise cut pET28a vector. pKaS105 was generated by amplification of $hfsK_{R352A,R353A}$ from pKaS95 with PCR followed by restriction enzyme digest using primers and enzymes as indicated in Table 2 and ligation into the likewise cut pET28A-StrepII-MCS subcloning vector. pET28strepII-hfsK and pKaS93 were generated by amplification of *hfsK* and $hfsK_{trnc}$ from genomic CB15 DNA with PCR followed by restriction enzyme digest using primers and enzymes as indicated in Table 2 and ligation into the likewise cut pET28A-StrepII-MCS subcloning vector. pKaS84 was generated similarly except that in addition SOE-PCR was used to introduce mutation R112A with the mutagenic primers 8890/8891.

pKaS2, pKaS1, pKaS9, pKaS22, pKaS67, pKaS95, pKaS106, pKaS111, pKaS12, pMT687-*hfsK*, pKaS113, and pKaS114 were generated by amplification of the gene of interest from genomic CB15 DNA with PCR followed by restriction enzyme digest using primers and enzymes as indicated in Table 2 and ligation into the likewise cut pMT552, pMT590, or pMT697 vector. pKaS77 was generated by using primers 8828/8830 as well as template pMT552 to amplify *egfp* and primers 8829/8831 as well as the template pNPTS138-*hfsK-tm* (see below) to amplify *secE-tm* with a linker region. As Primer 8829 and 8830 have extensions that are complementary to each other, the two fragments were fused using SOE-PCR generating *egfp-tm* with primers 8828/8831. This was cut with EcoRI and NheI and ligated into the cut pKaS22 vector. pNPTS138-*hfsK-tm* was generated by amplifying with PCR from genomic DNA the last

500 bp of *hfsK* with primer 4033/8396, *tm* region of *secE* with primer 8395/8398 and 500 bp downstream region of *hfsK* with primer 8397/4036. As the primer pairs 8395/ 8396 and 8397/8398 have extensions that are complementary to each other, SOE-PCR was used to first fuse the *hfsK* fragment with *secE-tm* using primers 4033/8398 and then the resulting *hfsK-tm* fragment with the downstream fragment of *hfsK* using primers 4033/4036. The resulting product was cut with HindIII and EcoRI and ligated into the likewise cut pNPTS138 vector.

pKaS90 was generated by extracting $hfsK_{trnc}$ from pKaS67 by restriction enzyme digest with NdeI/ KpnI followed by ligation into the linearized vector pKaS77.

Table 2: Strains, plasmids and primers

Plasmids

Plasmid	Description	Source/ Reference
pET28a	Kan^R, pBR322 based high copy vector with promoter from T7 bacteriophage	Novagen
pNPTS138	Kan^R, suicide vector with *sacB* and *oriT*, for generation of genomic mutations by allelic exchange	D. Alley
pMT552	Kan^R, pVGFPC-2, *vanA*-P_{van}-MCS-*egfp*; for generating C-terminal egfp fusions inserted in the *vanA* locus expressed from P_{van} or for expression of *egfp* alone	(418)
pMT585	Kan^R, pXGFPC-2, *xylX*-P_{xyl}-MCS-*egfp*; for generating C-terminal egfp fusions inserted in the *xylX* locus expressed from P_{xyl} or for expression of *egfp* alone	(418)
pMT590	Kan^R, pXCHYC-2, *xylX*-P_{xyl}-MCS-*chy*; for generating C-terminal *mcherry* fusions inserted in the *xylX* locus expressed from P_{xyl} or for expression of *mcherry* alone	(418)
pMT697	Kan^R, pXCHYN-2, *xylX*-P_{xyl}-*chy*-MCS; for generating N-terminal *mcherry* fusions inserted in the *xylX* locus expressed from P_{xyl} or for expression of *mcherry* alone	(418)
pMT687	Kan^R, RK2 based low-copy vector with P_{xyl}	(418)
pSRK	Kan^R, pBBR1MCS-2 based high copy vector with P_{lac}	(419)
pET28strepII-*hfsK*	pET28a plasmid encoding *strepII-hfsK*	this study
pKaS93	pET28a plasmid encoding *strepII-*$hfsK_{trnc}$	this study*
pKaS84	pET28a plasmid encoding *strepII-*$hfsK_{R112A}$	this study*
pKaS105	pET28a plasmid encoding *strepII-*$hfsK_{R352A, R353A}$	this study**
pET28his-*hfsK*	pET28a plasmid encoding 6x*his-hfsK*	M. Meier
pNPTS138-Δ*hfsK*	pNPTS138 derivative for generation of Δ*hfsK* mutation	Y. Cohen
pNPTS138-Δ*2278*	pNPTS138 derivative for generation of Δ*cc2278* mutation	Y. Cohen
pKaS110	pNPTS138 derivative for generation of Δ*1244* mutation	this study*
pSA223	pNPTS138 derivative to integrate a P_{lac} driven *dgcZ-3xflag* into the intergenic region of *cc3065* and *cc3066*	(118)
pSA81	pNPTS138 derivative for generation of Δ*pdeA* mutation	(155)
pSA156	pNPTS138 derivative for generation of Δ*cc0091* mutation	(118)

Plasmid	Description	Source/ Reference
pNPTS138-Δ*00471*	pNPTS138 derivative for generation of Δ*ccna00471* mutation	this study
pSA79	pNPTS138 derivative for generation of Δ*cc1086* mutation	(118)
pSA90	pNPTS138 derivative for generation of Δ*cc3148* mutation	(118)
pNPTS138Δ*hfaA*	pNPTS138 derivative for generation of Δ*hfaA* mutation	(331)
pNPTS138-Δ*hfaB*	pNPTS138 derivative for generation of Δ*hfaB* mutation	this study
pNPTS138Δ*hfaD*	pNPTS138 derivative for generation of Δ*hfaD* mutation	(331)
pKaS59	pNPTS138 derivative for generation of Δ*hfsA* mutation	this study*
pKaS25	pNPTS138 derivative for generation of Δ*hfsE* mutation	this study*
pKaS26	pNPTS138 derivative for generation of Δ*hfsF* mutation	this study*
pNPTS138Δ*hfsG*	pNPTS138 derivative for generation of Δ*hfsG* mutation	(66)
pNPTS138Δ*hfsH*	pNPTS138 derivative for generation of Δ*hfsH* mutation	(66)
pNPTS138Δ*hfsI*	pNPTS138 derivative for generation of Δ*hfsI* mutation	(66)
pDM25	pNPTS138 derivative for generation of Δ*hfsJ* mutation	D. Meyer
pKaS52	pNPTS138 derivative for generation of Δ*hfsABCDEFGH* mutation	this study*
pNPTS138Δpss*Y*	pNPTS138 derivative for generation of Δ*pssY* mutation	(66)
pNPTS138Δ*pssZ*	pNPTS138 derivative for generation of Δ*pssZ* mutation	(66)
pKaS22	pVGFPC-2 derivative for expression of *hfsK-egfp* from P_{van}	this study*
pKaS67	pVGFPC-2 derivative for expression of $hfsK_{trnc}$-*egfp* from P_{van}	this study**
pKaS77	pVGFPC-2 derivative for expression of *hfsK-egfp-tm* from P_{van}	this study**
pKaS90	pVGFPC-2 derivative for expression of $hfsK_{trnc}$-*egfp-tm* from P_{van}	this study*
pKaS95	pVGFPC-2 derivative for expression of $hfsK_{R352A,R353A}$-*egfp* from P_{van}	this study**
pKaS106	pVGFPC-2 derivative for expression of $hfsK_{R112A}$-*egfp* from P_{van}	this study*
pKaS111	pXCHYC-2 derivative for expression of *mcherry-hfsE* from P_{xyl}	this study*
pKaS112	pXCHYC-2 derivative for expression of *mcherry-hfsF* from P_{xyl}	this study*
pKaS2	pXCHYN-2 derivative for expression of *hfsG-mcherry* from P_{xyl}	this study*
pKaS1	pXCHYN-2 derivative for expression of *hfsH-mcherry* from P_{xyl}	this study*
pKaS9	pXCHYN-2 derivative for expression *of hfsK-mcherry* from P_{xyl}	this study*
pMT687-*hfsK*	pMT687 derivative for expression of *hfsK* from P_{xyl}	this study
pKaS113	pMT687 derivative for expression of *cc2278* from P_{xyl}	this study*
pKaS114	pMT687 derivative for expression of *cc1244* from P_{xyl}	this study*
pTB4	pSRK derivative for expression of *dgcZ* from P_{lac}	(118)

Strains

Strain	Genotype	Description	Source/ Reference
E. coli			
DH5alpha	F- *endA1* hsdR17 ($r_K^- m_K^+$) *glnV44 thi-1 recA1 gyrA96 relA1* Δ(*lacZYA-argF*)U169 *deoR* Φ80*dlacZ*ΔM15)	High efficiency transformation strain	(420)
DH10B	F- *mcrA* Δ(mrr-hsdRMS-mcrBC) Φ80d*lacZ*ΔM15 *lacX74 endA1 recA1* Δ(*ara, leu*)7697 *araD139 galU galK nupG λ*-	Used in conjugations transferring plasmids to *C. crescentus* with help of MT607 as plasmid donor	Invitrogen
S17-1	RP4-2, Tc::Mu, KM-Tn7	Used in conjugations transferring plasmids to *C. crescentus* as plasmid donor	(421)
MT607	pRK600 (cam^R)	Conjugation helper strain with F- plasmid	
Rosetta (DE3)	F- *ompT hsdS*$_B$(r_B^- m_B^-) *gal dcm* (DE3) pLysSRARE2 (Cam^R)	BL21 derivative; compatible with T7 expression vectors	Novagen
NiCo21 (DE3) pLys	*can::CBD fhuA2 [lon] ompT gal* (*λ DE3*) *[dcm] arnA::CBD slyD::CBD glmS6Ala ΔhsdS λ DE3 = λ sBamHIo* Δ*EcoRI-B int::*(*lacI::PlacUV5::T7 gene1*) *i21* Δ*nin5*	BL21 derivative; compatible with T7 expression vector; minimizes *E. coli* protein contamination in immobilized metal affinity chromatography	New England Biolabs
C. crescentus			
NA1000	CB15N	*C. crescentus* laboratory strain derived from CB15	(422)
CB15	CB15	*C. crescentus* Wild-type ATCC19089	(248)
UJ5990	Δ*hfsK*	Markerless deletion of *hfsK* in CB15 using pNPTS138-Δ*hfsK*	this study
UJ6136	Δ*cc2278*	Markerless deletion of *cc2278* in CB15 using pNPTS138-Δ*2278*	Y. Cohen
UJ6237	Δ*cc1244*	Markerless deletion of *cc1244* in CB15 using pKaS110	this study*
UJ6155	ΔhfsK Δ*cc2278*	Markerless deletion of *cc2278* in CB15 Δ*hfsK* using pNPTS138-Δ*2278*	this study*
UJ6238	ΔhfsK Δ*cc1244*	Markerless deletion of *cc1244* in CB15 Δ*hfsK* using pKaS110	this study*
UJ6239	Δcc2278 Δ*cc1244*	Markerless deletion of *cc1244* in CB15 Δ*cc2278* using pKaS110	this study*
UJ6241	Δ*hfsK* Δ*cc2278* Δ*1244*	Markerless deletion of *cc1244* in CB15 Δ*hfsK* Δ*2278* using pKaS110	this study*
UJ7113	Δ*hfsK* Δ*hfsH*	Markerless deletion of *hfsH* in CB15 Δ*hfsK* using pNPTS138Δ*hfsH*	this study*
UJ9545	Δ*hfaA*	Markerless deletion of *hfaA* in	this study*

Strain	Genotype	Description	Source/ Reference
		CB15 using pNPTS138Δ*hfaA*	
UJ6951	Δ*hfaB*	Markerless deletion of *hfaB* in CB15 using pNPTS138-ΔhfaB	this study*
UJ9547	Δ*hfaD*	Markerless deletion of *hfaD* in CB15 using pNPTS138Δ*hfaD*	this study*
UJ9583	Δ*hfaA* Δ*hfaD*	Markerless deletion of *hfaA* in CB15 Δ*hfaD* using pNPTS138Δ*hfaA*	this study*
UJ7112	Δ*hfsH*	Markerless deletion of *hfaH* in CB15 using pNPTS138Δ*hfsH*	this study*
UJ8820	Δ*hfsE* Δ*pssY* Δ*pssZ*	Markerless deletion of *hfsE*, *pssY* and *pssZ* in CB15 using pKaS25, pNPTS138Δ*pssY* and pNPTS138Δ*pssZ*	this study*
UJ8162	Δ*hfsF*	Markerless deletion of *hfsF* in CB15 using pKaS26	this study*
UJ7847	Δ*hfsG*	Markerless deletion of *hfsG* in CB15 using pNPTS138Δ*hfsG*	this study*
UJ9470	Δ*hfsABCDEFGH* Δ*hfsI* Δ*hfsJ* Δ*hfsK*	Markerless deletion of *hfsABCDEFGH* operons, *hfsI*, *hfsJ*, and, *hfsK* in CB15 using pKaS52, pNPTS138Δ*hfsI*, pDM25 and, pNPTS138-Δ*hfsK*	this study*
UJ5100	cdG^0; Δ*cc0655* Δ*cc0740* Δ*cc0857* Δ*cc0896* Δ*dgcB* Δ*pleD* Δ*cc3094* Δ*dgcA*	Markerless deletion of *cc0655 cc0740 cc0857 cc0896 dgcB pleD cc3094 dgcA* in CB15	(118)
UJ8732	rcdG^0; (Δ*cc0091* Δ*cc0655* Δ*cc0740* Δ*cc0857* Δ*cc0896* Δ*cc1086* Δ*dgcB* Δ*pleD* Δ*cc3094* Δ*cc3148* Δ*dgcA* Δ*pdeA*)	Markerless deletion of *cc0091*, *cc1086*, *cc3148*, *pdeA* in CB15 cdG^0 using pSA156, pSA79, pSA81, and pSA90	this study**
UJ8781	rcdG^0+*dgcZ*; (Δ*cc0091* Δ*cc0655* Δ*cc0740* Δ*cc0857* Δ*cc0896* Δ*cc1086* Δ*dgcB* Δ*pleD* Δ*cc3094* Δ*cc3148* Δ*dgcA* Δ*pdeA* P_{lac}-*dgcZ-3xflag*)	Chromosomal integration of P_{lac} driven *dgcZ* into CB15 rcdG^0 using pSA223	this study**
UJ8877	rcdG^0 Δ*hfsK*	Markerless deletion of *hfsK* in CB15 rcdG^0 using pNPTS138-ΔhfsK	this study*
UJ8878	rcdG^0+*dgcZ* Δ*hfsK*	Markerless deletion of *hfsK* in CB15 rcdG^0+*dgcZ* using pNPTS138-Δ*hfsK*	this study*
UJ4463	Δ*pleD*	Markerless deletion of *pleD* in CB15	(155)
UJ9078	Δ*pleD* Δ*hfsK*	Markerless deletion of *hfsK* in Δ*pleD* using pNPTS138-ΔhfsK	this study*
UJ9633	Δ*hfsA* Δ*ccna00471*	Markerless deletion of *hfsA* and *ccna0471* in CB15 using pKaS59 and pNPTS138-Δ*00471*	this study*
UJ9634	rcdG^0 Δ*hfsA* Δ*ccna00471*	Markerless deletion of *hfsA* and *ccna0471* in CB15 rcdG^0 using pKaS59 and pNPTS138-Δ*00471*	this study*
UJ9635	rcdG^0+*dgcZ* Δ*hfsA*	Markerless deletion of *hfsA* and	this study*

Strain	Genotype	Description	Source/ Reference
	Δ*ccna00471*	*ccna00471* in CB15 rcdG^0+*dgcZ* using pKaS59 and pNPTS138-Δ*00471*	
UJ7870	Δ*hfsJ*	Markerless deletion of *hfsJ* in CB15 using pDM25	this study*
UJ7871	Δ*hfsJ* Δ*hfsK*	Markerless deletion of *hfsJ* in CB15 Δ*hfsK* using pDM25	this study*
Phages			
ΦCbK		Bacteriophage that uses pili of *C. crescentus* for infection	(423)
ΦCR30		Bacteriophage that uses the paracrystalline surface- layer proteins of *C. crescentus* as a receptor	(424)

Primers

Primer	Sequence	Restriction site	Used for plasmid
1380	GAATTCTTCGACCGTTCCCAGCCC	EcoRI	pDM25
1381	GGATCCCGCTGTCCAGACGCTCTA	BamHI	pDM25
1382	GGATCCTGAGGAACGAACATCTCCGCAG	BamHI	pDM25
1383	AAGCTTCGACAAGGACGGCCAGAAGGA	HindIII	pDM25
3287	ATATACCATGGGATGGAGCCACCCGCAGTTCGAAAAAGGATCCAAGCTT	n/a	pET28strepII-*hfsK*/ pKaS93/ pKaS84/ pKaS105
3288	AAGCTTGGATCCTTTTTCGAACTGCGGGTGGCTCCATCCCATGGTATAT	n/a	pET28strepII-*hfsK*/ pKaS93/ pKaS84/ pKaS105
3300	AAGGATCCCCCATCGAAATCGTCAAAGC	BamHI	pET28strepII-*hfsK*/ pKaS93/ pKaS84/ pKaS105
3301	AAGCAAGCTTTCAGTGCAGTCCGCGCAGCA	HindIII	pET28strepII-*hfsK*/ pKaS84/ pKaS105
3584	AGAGAAGCTTGCAAGATCACCTCGCCGCGT	HindIII	pNPTS-Δ*hfsK*
3585	TTGCCCATCGAAATCGTCAAACTGCTGCGCGGACTGCACTGA	n/a	pNPTS-Δ*hfsK*
3586	TCAGTGCAGTCCGCGCAGCAGTTTGACGATTTCGATGGGCAA	n/a	pNPTS-Δ*hfsK*
3587	CTCTGAATTCCGCTGTTCGAGCGCATGGCC	EcoRI	pNPTS-Δ*hfsK*
3942	AGACGACCATATGCCCATCGAAATCGTCAAAGC	NdeI	pKaS22/ pKaS67/ pKaS95/ pKaS106/ pKaS9
3943	GTGGTACCTCAGTGCAGTCCGCGCAGCA	KpnI	pMT687-hfsK
3984	ATATACTAGTATCGTGGTGATAGAGGCTCAC	SpeI	pNPTS-Δ*2278*
3985	ATATAAGCTTCTGCAATCGACAGGCCATTCC	HindIII	pNPTS-Δ*2278*
3986	ATATAAGCTTGCCTGATGGCGCGCGTCACGG	HindIII	pNPTS-Δ*2278*
3987	ATATGAATTCCGGCGACGAGACCGAAGACTG	EcoRI	pNPTS-Δ*2278*
4033	GACAAAGCTTTGCTGACCCACCAGACCGAC	HindIII	pKaS77

4036	TAGAATTCTTCGAGCGCATGGCCGAGGC	EcoRI	pKaS77
4088	GTCCAAGCTTCGACCCCCTGATCGACTG	HindIII	pKaS110
4089	ATGGTACCCGCATTAGGCCTTAAGCATC	KpnI	pKaS110
4090	GAGGTACCGGTCTGGCGATGATGGTG	KpnI	pKaS110
4091	TGAATTCCCTGAGCGATTTCCAGCTT	EcoRI	pKaS110
4164	CTTAAGGTCATATGCAGCCGGCGATCCATCTTT	NdeI	pKaS113
4165	ACTGGTACCATCAGGCCTCCGTGTGCTCT	KpnI	pKaS113
4587	AGACGACCATATGCAGGCCGACCGTATCAAGGT	NdeI	pKaS114
4596	TCAGGTACCTGAGGAGAGGCTACCGAGG	KpnI	pKaS114
4726	TAGAATTCGCCTGGAAAAGAAGACCAAG	EcoRI	pNPTS-Δ*00471*
4727	ATGGTACCGATCACGTCATTCGGCATTG	KpnI	pNPTS-Δ*00471*
4728	CAGGTACCCACTTCCTCTCGGCCCAATA	KpnI	pNPTS-Δ*00471*
4729	CATTGAAGCTTGACTGCGAACGATCGCTAGA	HindIII	pNPTS-Δ*00471*
5181	GGAATTCGACTTCTATCTAGGGGCTCG	EcoRI	pNPTS138-Δ*hfaB*
5182	GAGGTACCTGTGCGCTTGACCATCATTT	KpnI	pNPTS138-Δ*hfaB*
5183	GAGGTACCGATATCCGTGATGCTAAGCG	KpnI	pNPTS138-Δ*hfaB*
5184	GCTAGAAGCTTTCACGTTGATGTTGTTGCCC	HindIII	pNPTS138-Δ*hfaB*
5592	GTGGTACCAGCAGTACTTCCGCGACCT	KpnI	pKaS52
5593	GGAATTCCAGAGTCCTGTTCGGTCAGC	EcoRI	pKaS52
5684	GAGATTACCATATGAACGCGCCCGTCAACGA	NdeI	pKaS2
5685	CCGGTACCGACGGCCTCGCTGTAGAGCG	KpnI	pKaS2
5686	GAGATTATCATATGCCGATGGAATTCGAGAA	NdeI	pKaS1
5687	CCGGTACCGAGCCCGATCCGCCGCG	KpnI	pKaS1
5692	TAGGTACCGTTTTCCCAACGACGAGCAT	KpnI	pKaS111
5693	TAGAATTCCTAGCGCACGGCGGACCGAT	EcoRI	pKaS111
5694	TAGGTACCTTCTGGCGCGGCGTCCTCGG	KpnI	pKaS112
5695	TAGAATTCTCATGCGGCTTGCGCCTTTC	EcoRI	pKaS112
6119	AGCAGGTACCGTGCAGTCCGCGCAGCAGGT	KpnI	pKaS22/ pKaS106/ pKaS9
6874	TTAACGGTACCCGCCGGATCCAGCACGCGCG	KpnI	pKaS26
6875	TTAACAAGCTTCTTCAACAACGAGGCGATTC	HindIII	pKaS26
6876	CGTTATAGAATTCAAAAGCCCTCGTCGAAGC	EcoRI	pKaS26
6877	TTAGTGGTACCCGTCGAAAGGCGCAAGCCGC	KpnI	pKaS26
6878	TTAACGGTACCGCTGGCCCCGATCCCCATCA	KpnI	pKaS25/ pKaS52
6879	TTAACAAGCTTCGAACCCTCGATACCCTTT	HindIII	pKaS25/ pKaS52
6880	TTAAAGGAATTCGCCGGTCATGAACTTCAACT	EcoRI	pKaS25
6881	TTAAAGGTACCGGGGATCGGTCCGCCGTGCG	KpnI	pKaS25
8373	TGAGGTACCGGTGAGCGCTTTGGTCGCCT	KpnI	pKaS59
8374	ATTGAAGCTTGACGGTCTGGTCCATGTGC	HindIII	pKaS59
8375	TGTAAGAATTCCCTTCACCGAAATCTGCAC	EcoRI	pKaS59
8376	ATCGGTACCGGCACGCTGATCCAGGCGCT	KpnI	pKaS59
8395	ACGGSTCTAGAGGAAGATCTTGGATCACCTCGG TGATGGT	n/a	pKaS77
8396	CAAGATCTTCCTCTAGACCCGTGCAGTCCGCGC AGCAGGT	n/a	pKaS77

8397	TCAAGCTGGCGACCGCGGGATAGCGTCTAGAGC ATTTTCC	n/a	pKaS77
8398	GGAAAATGCTCTAGACGCTATCCCGCGGTCGCC AGCTTGA	n/a	pKaS77
8425	GTGGTACCCTCGGCCACACTGCGGACCC	KpnI	pKaS67
8828	GAATTCGAACGTTACGCGTC	EcoRI	pKaS77
8829	GCATGGACGAGCTGTACAAGGGGTCTAGAGGAA GATCT	n/a	pKaS77
8830	AGATCTTCCTCTAGACCCCTTGTACAGCTCGTCC ATGC	n/a	pKaS77
8831	AGTGGCTAGCCTATCCCGCGGTCGC	NheI	pKaS77
8890	TGGGTGCGATCGACTTTTGCCACATGATG	n/a	pKaS84
8891	CAAAAGTCGATCGCACCCACGCCGAGCACGT	n/a	pKaS84
9216	AGTGAAGCTTTCACTCGGCCACACTGCGGACCC	HindIII	pKaS93
9432	GTAGGTACCGTGCAGTCCGCGCAGCAGGTCGAT GGCGGCCATCGCCTTG	KpnI	pKaS95

* Plasmid/strain generated by myself

**Partial contribution to plasmid/strain construction

2.1.6 Funding Information

This work was supported by an ERC Advanced Research Grant to U.J.; by a Biozentrum PhD program Fellowship for Excellence to K.S.S; and by a grant of the Swiss innovation promotion agency KTI-CTI (11722.1 PFNMNM) to JAV.

2.1.7 Supplemental Material

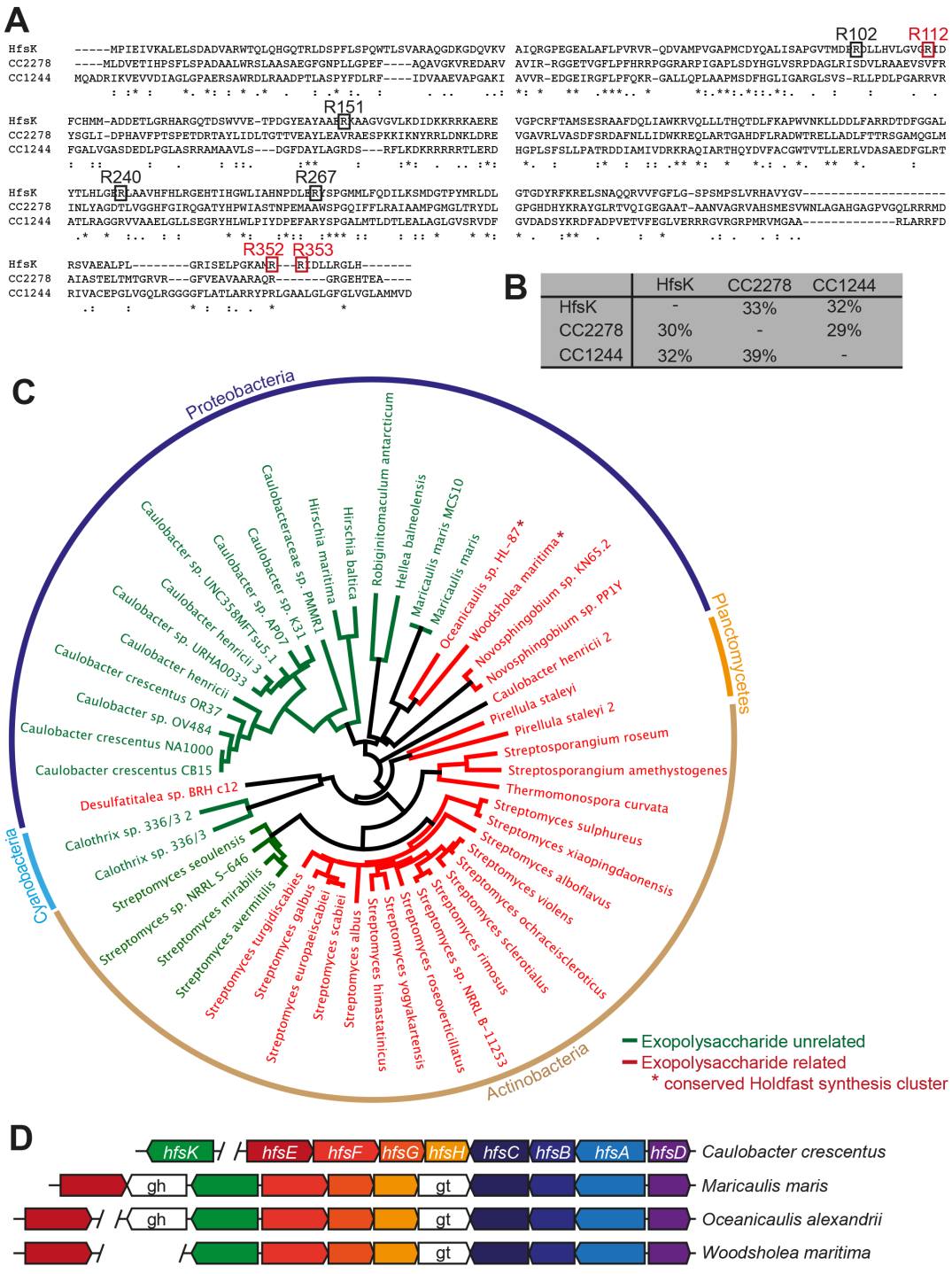

	HfsK	CC2278	CC1244
HfsK	-	33%	32%
CC2278	30%	-	29%
CC1244	32%	39%	-

Figure S1: Many HfsK orthologs are encoded in exopolysaccharide synthesis clusters

(A) Multiple sequence alignment of HfsK with its paralogs. Arginines mutated in this study are indicated with a square and those shown to be involved in c-di-GMP binding are highlighted in red. Fully conserved residues are indicated by a star, strong and weak conservation are indicated by two and one dot, respectively. (B) Sequence identities between the different HfsK paralogs (C) Phylogenetic tree composed of the TOP58 hits of HfsK orthologs search with Blast (413). Colors indicate species that have orthologous genes in a conserved holdfast synthesis cluster (red) or in clusters with genes that do not show a connection with polysaccharide synthesis (green). The different corresponding phyla are indicated. (D) Schematic representation of conserved holdfast synthesis clusters that contain an *hfsK* orthologous gene in comparison to the holdfast synthesis cluster of *C. crescentus*. Note: Holdfast synthesis associated HfsK ortholog in *M. maris* is not under TOP58 Blast hits. gh: glycosylhydrolase, gt: glycosyltransferase. (← Figure on previous page)

Figure S2: Attachment defect of *hfsK* mutants is caused by a less adhesive holdfast

(A-B) Surface colonization determined by crystal violet staining after 30 min (dark red bars) and 24 h (light red bars) growth in microtiter plates. Normalized per condition. Comparison of the *hfsK* paralog family with strains that shed (Δ*hfaB*) and form incoherent (Δ*hfsH*) holdfast, and the non-adherent *C. crescentus* NA1000 strain (A). Complementation and cross-complementation of the surface colonization defect of Δ*hfsK* and Δ*cc2278* cells harboring a plasmid borne xylose promoter (P_{xyl}) driven copy of *hfsK* or *cc2278*, or the empty vector (e.v.) alone (B). (C) Analysis of holdfast shedding. Fraction of ST cells from liquid culture with visible OG-WGA stained holdfast was counted (dark red bars). As comparison, fluorescence intensity of adhered WGA stained holdfast on glass coverslips after 2 h adsorption of cells (as shown in Figure 2B and Figure S2D) was quantified (light red bars). (D) Representative images of adhered OG-WGA stained holdfast on glass coverslips after 2 h adsorption of cells. Shown are overlays of phase contrast and fluorescence images. Scale bar = 5 µm. (E-F) Assessing the involvement of HfsK and its paralogs in other c-di-GMP controlled pathways. Quantification of colony size indicative for swimming after 3 days grows on semi-solid agar plates (E). Phage susceptibility was tested by adding serial dilutions of ΦCBK (pili specific) and ΦCR30 (S-layer specific) phage lysate onto a lawn of cells (F). (G) Schematic view of a SCFS using FluidFM. The course of pressure (p) and force (f) is shown over time. Illustrations indicate the SCFS procedure and characteristic cantilever bending. (H) Relative adhesion forces of wild-type and Δ*hfsK* cells grown in PYE medium. 3-5 cells were measured per culture as described in Text S1 and different glass substrates were investigated. For all conditions substrate contact times range from 0.5-6 h. Error bars = SD of 3 independent cultures. (I) Comparison of the detachment breaking point of Δ*hfsK* cells treated and measured as in panel H. Cells were categorized according to their holdfast intensity: reversibly attached on glass without a visible OG-WGA stained holdfast (no), or attached via a weak or strong fluorescently labeled holdfast indicative for short (minutes) and long (hours) contact time. (J) Co-attachment of holdfast-null Δ*hfsJ* strains with and without an intact *hfsK* and the holdfast shedding anchor mutant Δ*hfaB*. Holdfast-null and the shedding strains harbor a plasmid expressing *egfp* or *mcherry* from P_{xyl}. respectively. The strains were mixed 1:1 in PYE supplemented with 0.1% xylose and adsorbed for 2 h on glass slides that were then stained with AlexaFluor350-WGA and washed prior microscopy. Scale bar = 5 µm.

In panel A-D Error bars represent SD of at least 3 independent experiments, */**/***/ns represent P-value <0. 1/0.01/0.001/not significant. (Figure on next page →)

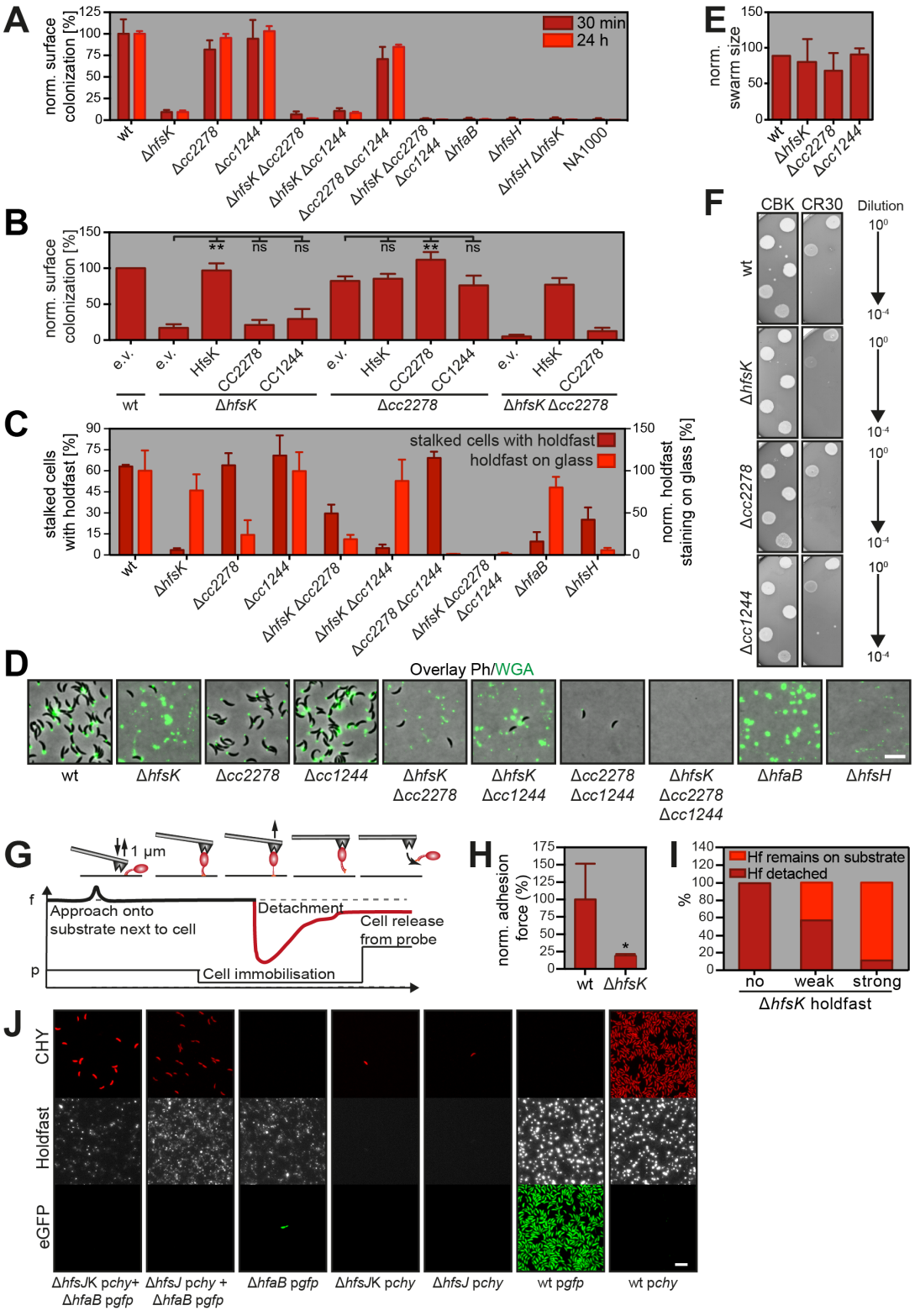
A
norm. surface colonization [%]
30 min
24 h
wt
ΔhfsK
Δcc2278
Δcc1244
ΔhfsK Δcc2278
ΔhfsK Δcc1244
Δcc2278 Δcc1244
ΔhfsK Δcc2278 Δcc1244
ΔhfaB
ΔhfsH
ΔhfsH ΔhfsK
NA1000
E
norm. swarm size
B
norm. surface colonization [%]
e.v.
HfsK
CC2278
CC1244
wt
ΔhfsK
Δcc2278
ΔhfsK Δcc2278
C
stalked cells with holdfast [%]
norm. holdfast staining on glass [%]
stalked cells with holdfast
holdfast on glass
F
CBK
CR30
Dilution
D
Overlay Ph/WGA
ΔhfaB
ΔhfsH
G
1 µm
f
p
Approach onto substrate next to cell
Detachment
Cell release from probe
Cell immobilisation
H
norm. adhesion force (%)
I
Hf remains on substrate
Hf detached
no
weak
strong
ΔhfsK holdfast
J
CHY
Holdfast
eGFP
ΔhfsJK pchy+ ΔhfaB pgfp
ΔhfsJ pchy + ΔhfaB pgfp
ΔhfaB pgfp
ΔhfsJK pchy
ΔhfsJ pchy
wt pgfp
wt pchy

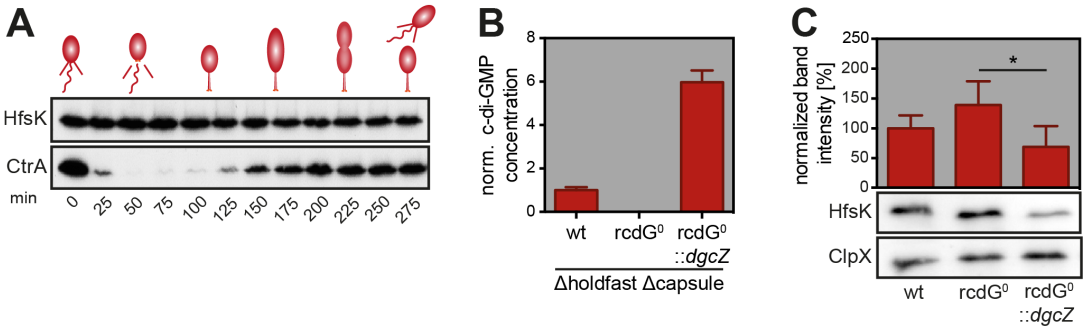

Figure S3: Levels of HfsK do not change during the cell cycle

(A) HfsK protein levels of synchronized wild-type cells grown in M2G through one cell cycle analyzed with immunoblot probed with anti-HfsK antibodies. The cell cycle regulated protein CtrA is shown as a control. (B) Measurement of c-di-GMP concentrations of wild-type cells, cells that have no c-di-GMP metabolism (rcdG⁰), and cells with elevated c-di-GMP levels (rcdG⁰::*dgcZ*). Expression of *dgcZ* was induced by addition of 0.5 mM IPTG. Error bars = SD of 3 technical replicas. (C) Impact of c-di-GMP on HfsK homeostasis. HfsK protein levels analyzed with immunoblot in wild-type, rcdG⁰, and rcdG⁰::*dgcZ* (induced with 0.5 mM IPTG) cells. ClpX is shown as loading control. Quantification of immunoblots of 4 independent experiments is shown below. Error bars = SD, */** represents P-value <0.1/0.01.

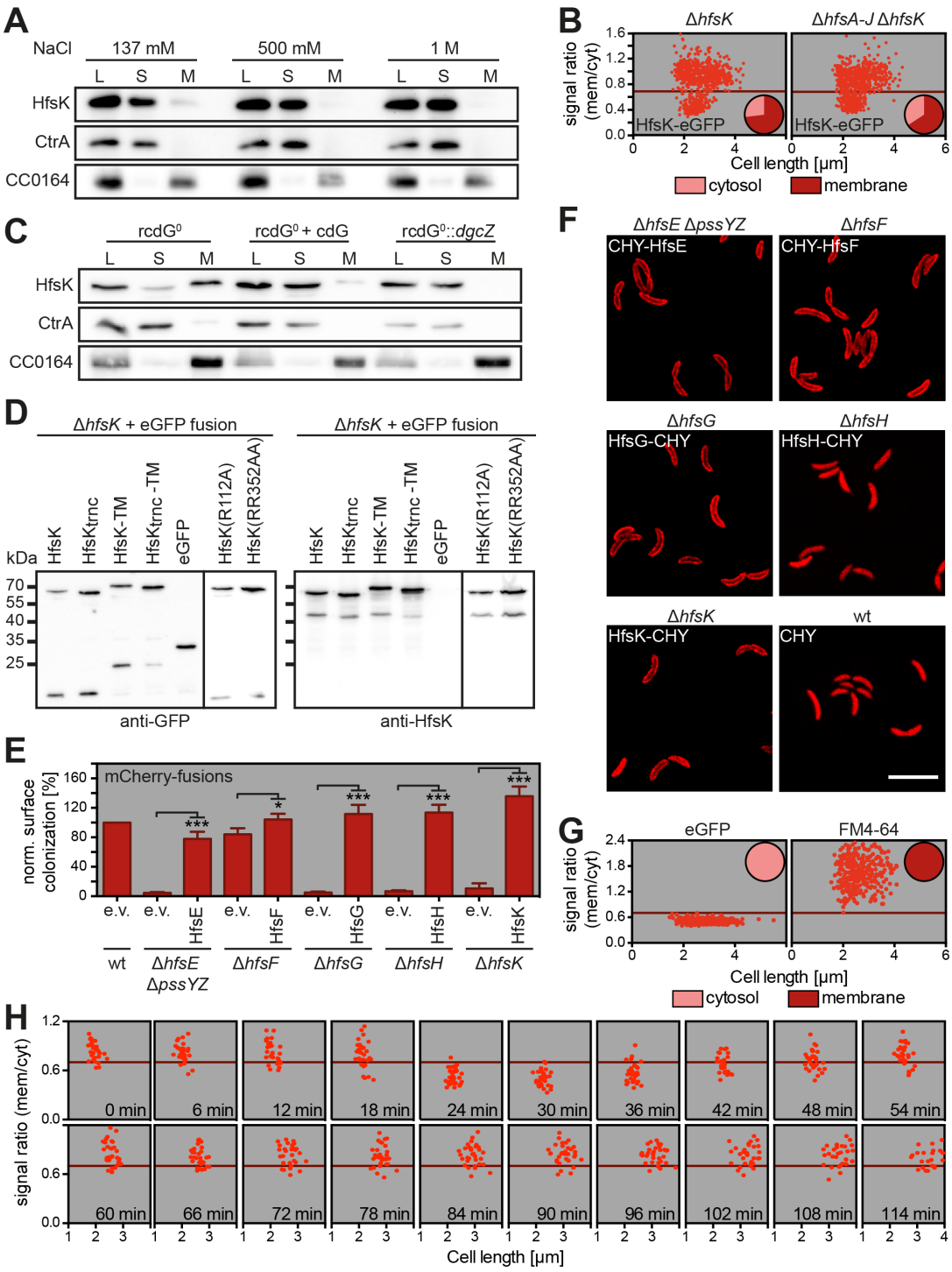
A
NaCl
137 mM
500 mM
1 M
L S M L S M L S M
HfsK
CtrA
CC0164
B
ΔhfsK
ΔhfsA-J ΔhfsK
signal ratio (mem/cyt)
HfsK-eGFP
Cell length [µm]
cytosol
membrane
C
rcdG⁰
rcdG⁰ + cdG
rcdG⁰::dgcZ
D
ΔhfsK + eGFP fusion
HfsK
HfsKtrnc
HfsK-TM
HfsKtrnc -TM
eGFP
HfsK(R112A)
HfsK(RR352AA)
kDa
70
55
40
35
25
anti-GFP
anti-HfsK
E
mCherry-fusions
norm. surface colonization [%]
e.v.
HfsE
HfsF
HfsG
HfsH
HfsK
wt
ΔhfsE ΔpssYZ
ΔhfsF
ΔhfsG
ΔhfsH
ΔhfsK
F
ΔhfsE ΔpssYZ
CHY-HfsE
ΔhfsF
CHY-HfsF
ΔhfsG
HfsG-CHY
ΔhfsH
HfsH-CHY
ΔhfsK
HfsK-CHY
wt
CHY
G
eGFP
FM4-64
H
signal ratio (mem/cyt)
0 min
6 min
12 min
18 min
24 min
30 min
36 min
42 min
48 min
54 min
60 min
66 min
72 min
78 min
84 min
90 min
96 min
102 min
108 min
114 min
Cell length [µm]

Figure S4: Membrane-association of HfsK depends on electrostatic interaction but not with the holdfast synthesis machinery

(A) HfsK localization analyzed by cell fractionation followed by immunoblotting. The cytosolic protein CtrA and the inner membrane protein CC0164 are shown as controls. Cell lysates (L); soluble fraction (S); membrane fraction (M). Wild type cell lysates were supplemented with increasing concentrations of NaCl to disrupt potential electrostatic interactions. (B) Comparison of HfsK-eGFP localization in Δ*hfsK* cells and Δ*hfsK* cells lacking the entire holdfast synthesis machinery (Δ*hfsABCDEFGHIJ*) grown in presence of 0.55 mM Van. Localization quantification was done as described in Figure 3D. A minimum of 720 cells from two independent experiments was analyzed per strain. (C) HfsK localization analyzed by cell fractionation followed by immunoblotting using the same controls as in panel A. C-di-GMP concentrations were enhanced in the rcdG^0 strain by supplementing all buffers with 10 µM c-di-GMP or by additionally expressing *dgcZ* form P_{lac} by addition of 0.5 mM IPTG in addition to c-di-GMP supplementation in buffers. (D) Immunoblot of all HfsK-eGFP fusion constructs used in this study probed with anti-GFP and anti-HfsK antibodies. Degradation bands correspond to a truncation within the eGFP protein that leads to a complete loss of fluorescent signal (425) and thus does not impact microscopy analysis. (E) Functionality of mCherry fusions compared to a wild-type strain harboring the empty vector control (e.v.) in a surface colonization assay scored after 24 h growth in microtiter plates in presence of 0.1% xylose. Error bars represent SD of 3 independent experiments, */*** represent P-value <0. 1/0.001 calculated with an unpaired t-test. (F) Localization of early holdfast synthesis proteins compared to HfsK, all fused to mCherry and expressed from P_{xyl} by addition of 0.1% xylose in the respective deletion background. Representative fluorescence microscopy images are shown. Scale bar = 10 µm. (G) Ratio of average membrane and cytosol signal. EGFP expressed from P_{xyl} in wild-type cells with 0.1% xylose is used as cytosolic marker and the membrane dye FM4-64 is used as membrane marker. Pie charts show that with the arbitrary set threshold of 0.7, 100% of all GFP and FM4-64 signals are categorized as cytosolic and membrane associated, respectively. (H) Localization of HfsK-eGFP in Δ*hfsK* P_{van}-*hfsK-egfp* grown on PYE agarose pads containing 0.55 mM Van. New born swarmer cells (cell division = 0 min) were followed through one cell cycle. Localization was quantified as described in Figure 3D for 32 cell originating from 2 independent experiments were analyzed. (← Figure on previous page)

Figure S5: HfsK localization depends on its C-terminus

(A) Alignment of HfsK with FemX of *Weissella viridescens* based on structure prediction. Quality of conservation is indicated (very low = ; low - ; neutral . ; high + ; very high |). The C-terminal amino acids that were deleted in the $HfsK_{trnc}$ mutant are highlighted with a red line. (B) Localization of P_{van}-HfsK-eGFP mutants expressed as sole copy of HfsK in the wild-type, rcdG^0, and rcdG^0+*dgcZ* (+ 0.5 mM IPTG) background by addition of 0.55 mM Van. Representative 3D-SIM images are shown in the upper panel. The lower panel shows localization quantification as described in Figure 3D. A minimum of 255 cells from two independent experiments was analyzed per strain. Scale bar = 3 µm. (C) Quantification of fluorescence intensity of adhered rhodamine-WGA stained holdfast of R-mutant strains on glass coverslips after 2 h adsorption. Error bars = SD of 3 independent experiments.
(Figure on next page →)

A

```
HfsK   14 ADVARWTQLQHGQTRLDSPFLSPQWTLSVARAQGDKGDQVKVAIQRGPEGEALAFLPV-RVRQDVAMPVGAPMCDYQALI   92 (361)
          ...++|++|+.++ +.+++|||+++|++++.    +.    .+.++++++++|+++|++|+ .+....   .+.....++||+
FemX   10 QAVERYEEFMRQS-PYGQVTQDLGWAKVKN---NW---EPVDVYLEDDQGAIIAAMSMLLGDTPT---DKKFAYASKGPV   79 (336)

HfsK   93 SAPGVTMDPRDL------LHVLGVGRIDFCHMMADD---------ETLGRHA-----------RGQTDSWVVETPD--GY  144 (361)
          +.+.....+.++       ++..++..+.+.+.....          ..+....           .....+++++++.  ++
FemX   80 MDVTDVDLLDRLVDEAVKALDGRAYVLRFDPEVAYSDEFNTTLQDHGYVTRNRNVADAGMHATIQPRLNMVLDLTKFPDA  159 (336)

HfsK  145 EAYAAERKAAGVGVLKDIDKKRRKAEREVGPCRFTAMSESRAAFDQLIAWKRVQLLLTHQTDLFKAPWVNKLLDDLFARR  224 (361)
           |++++   +++++.|+++||+.|+       |++++...+ .+.++.|++++..++++++.     .....+|++++.+.+
FemX   160 KTTLD---LYPSKTKSKIKRPFRD------GVEVHSGNS-ATELDEFFKTYTTMAERHGI-----THRPIEYFQRMQAAF  224 (336)

HfsK  225 DTDFGGALYTLHLGERLAAVHFHLRGEHTIHGWLIAHNPDLERYSPGMMLFQDILKSMDGTPYMRLDLGTGDY-------  297 (361)
          .. +.+.+++++.||++||+.+++.++++++++.+|+|+++ +++||.+|+|++|++++++|++.+|||++..
FemX   225 DA-DTMRIFVAEREGKLLSTGIALKYGRKIWYMYAGSMDGN-TYYAPYAVQSEMIQWALDTNTDLYDLGGIESESTDDSL  302 (336)

HfsK  298 -RFKRELSNA-QQRVV-FGFLGSPSMPSLVRHAVYGVRSVAEALPLGRISELPGKAMRRIDLLRGLH  361
           +||.+||++ .++++ .+....++.....
FemX   303 YVFKHVFVKDAPREYIGEIDKVLDPEVYAELVKD                                  336
```

B

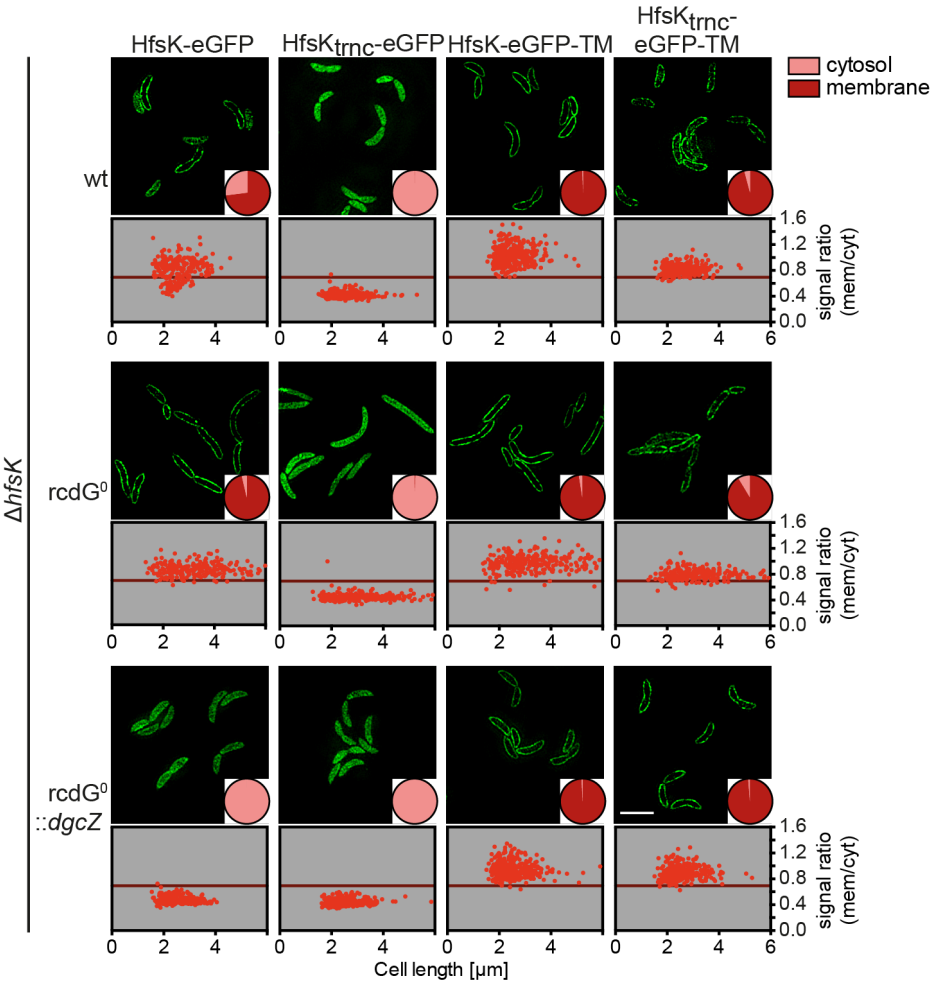

C

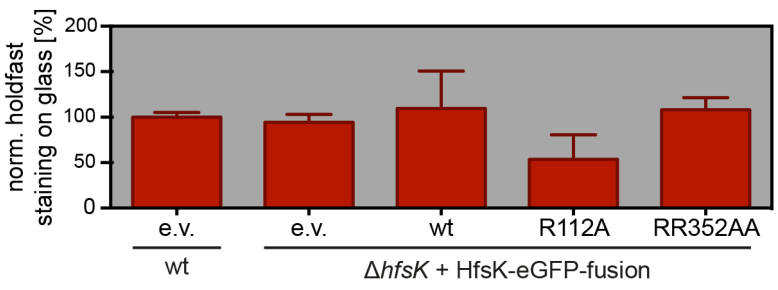

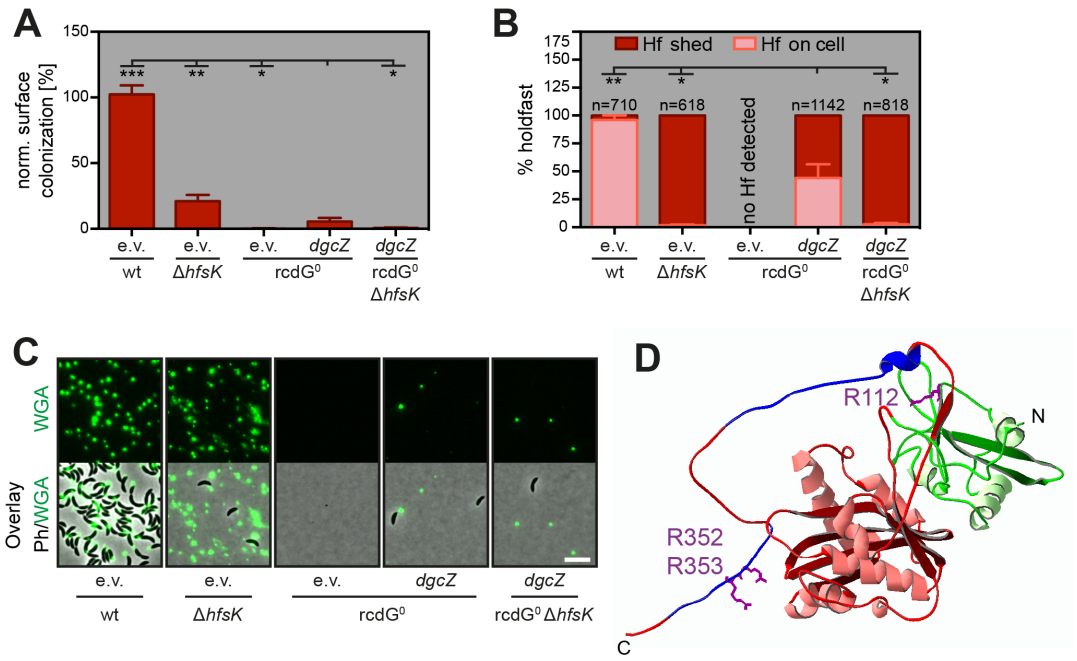

Figure S6: High c-di-GMP levels cause holdfast shedding and a severe surface colonization defect

(A) Surface colonization of a strain expressing *dgcZ* from a high copy number plasmid or harboring the empty vector (e.v.) control determined by crystal violet staining after 24 h growth in the presence of 200 µm IPTG in microtiter plates. (B) Amount of shed holdfast quantified on fluorescence microscopy images taken of mid-log phase cultures that were stained with OG-WGA and directly spotted on agarose pads. The number of the total number of assigned holdfasts is indicated (n). (C) Analysis of adhered OG-WGA stained holdfast on coverslips after 2 h adsorption of cells. Representative fluorescence and phase contrast images are shown. Scale bar = 5 µm. (D) Structural model of HfsK based on FemX (PDB ID 3gkr). Colors show N-terminal GNAT-domain (red) and C-terminal GNAT-domain (green). As the HfsK protein is longer than FemX the C-terminus appears unstructured in the model. C-terminal helical stretches predicted separately by Jpred (426) are colored in blue. Arginines involved in c-di-GMP binding are highlighted in purple. Error bars in panel A and B represents SD of 3 independent experiments, */**/*** represent P-value <0.1/0.01/0.001.

2.1.8 Acknowledgments

We would like to acknowledge Alexia Loynton-Ferrand and Kai Schleicher of the Imaging Core Facility (IMCF) of the Biozentrum (University of Basel) for technical assistance with superresolution microscopy; Timothy Sharpe of the Biophysics Facility (BF) of the Biozentrum (University of Basel) for technical assistance with ITC; Fabienne Hamburger for plasmid construction; Annette Garbe for assistance with c-di-GMP quantification; Shogo Ozaki, Chee Seng Hee, Benoît-Joseph Laventie, and Orane Guillaume-Gentil for fruitful discussions and critical comments on the manuscript. We thank Patrick Viollier for providing antibodies against CC0164 and Gail Hardy, Yves Brun, Yaniv Cohen, Markus Meier, and Dominique Meyer for providing plasmids.

2.2 Additional work

This chapter comprises additional data concerning HfsK, its homologs and the control of holdfast synthesis by c–di–GMP that are beyond the scope of the publication manuscript.

2.2.1 Additional results

2.2.1.1 Cells deficient in *hfs*K can synergistically adhere with a Δ*hfaB* strain

Deletion mutants of the holdfast anchor genes *hfaA* and *hfaD* have a very similar phenotype as an *hfsK* mutant (Manuscript Figure 2). This lead to the hypothesis, that not the holdfast EPS but the anchor structure might be affected by an *hfsK* deletion. Ong and colleagues (334) could show in *C. crescentus* CB2 that a holdfast deficient strain with an intact anchor can adhere to shed holdfast when co-cultured with a holdfast shedding mutant (Fig. 10).

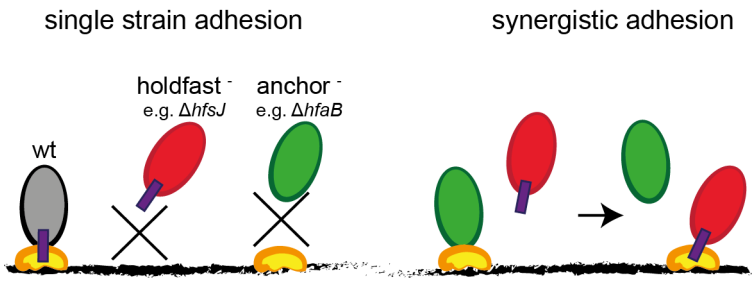

Fig. 10: Concept of synergistic adhesion

Wild type cells have a holdfast anchor and produce the holdfast adhesin. Both, holdfast mutants (red) and anchor mutants (green) cannot adhere, yet anchor mutants deposit shed holdfast on the surface. When grown together, holdfast mutants can adhere via their intact anchor to shed holdfasts of the anchor mutant.

This experiment was repeated in *C. crescentus* CB15 with strains harboring a single copy plasmid either expressing *mcherry* (holdfast mutants) or e*gfp* (anchor mutants). As proof of principle, a strain lacking the glycosyltransferase HfsJ was used as a holdfast mutant and a strain lacking HfaB as an anchor mutant. When grown alone on glass slides, both strains failed to adhere to the glass after washing. In comparison, wild type cells expressing either fluorophore nearly covered the entire glass (Fig. 11). However, when Δ*hfsJ* and Δ*hfaB* cells were grown together, there was a number of mCherry expressing Δ*hfsJ* cells found adhered to the glass, indicating that they can

synergistically adhere (Fig. 11, green box). Of note, as already reported by Ong and colleagues (334), synergistically adhering cells did not reach the adhesion level of wild type cells, indicating that these events are rather rare.

To test whether in Δ*hfsK* cells the holdfast anchor is defective we combined this deletion with a Δ*hfsJ* mutation in order to assure that the strain does not produce holdfast itself. If this double mutant can synergistically adhere together with a Δ*hfaB* strain, this would indicate that the anchor is still intact. In line with this, we could readily detect mCherry positive Δ*hfsJ* Δ*hfsK* cells, when they were grown together with a Δ*hfaB* strain expressing *gfp* (Fig. 11, green box). The Δ*hfsJ* Δ*hfsK* strain grown alone failed to adhere (Fig. 11).

Vice versa, if a Δ*hfsK* mutation solely affects the holdfast anchor, one would expect that holdfast deficient Δ*hfsJ* cells could adhere not only to the shed holdfasts of a Δ*hfaB* strain but also to shed holdfasts of a Δ*hfsK* strain. However, when mixing an *egfp* expressing Δ*hfsK* strain with a *mcherry* expressing Δ*hfsJ* strain, we could not detect any adherent mCherry positive Δ*hfsJ* but only some eGFP positive Δ*hfsK* cells that were also visible when growing the Δ*hfsK* strain alone (Fig. 12, green box). This shows that holdfasts shed by Δ*hfsK* cells do not support surface adhesion even for cells with an intact anchor complex.

Together, these results suggest that Δ*hfsK* cells have an intact holdfast anchor and that the holdfast structure itself is altered.

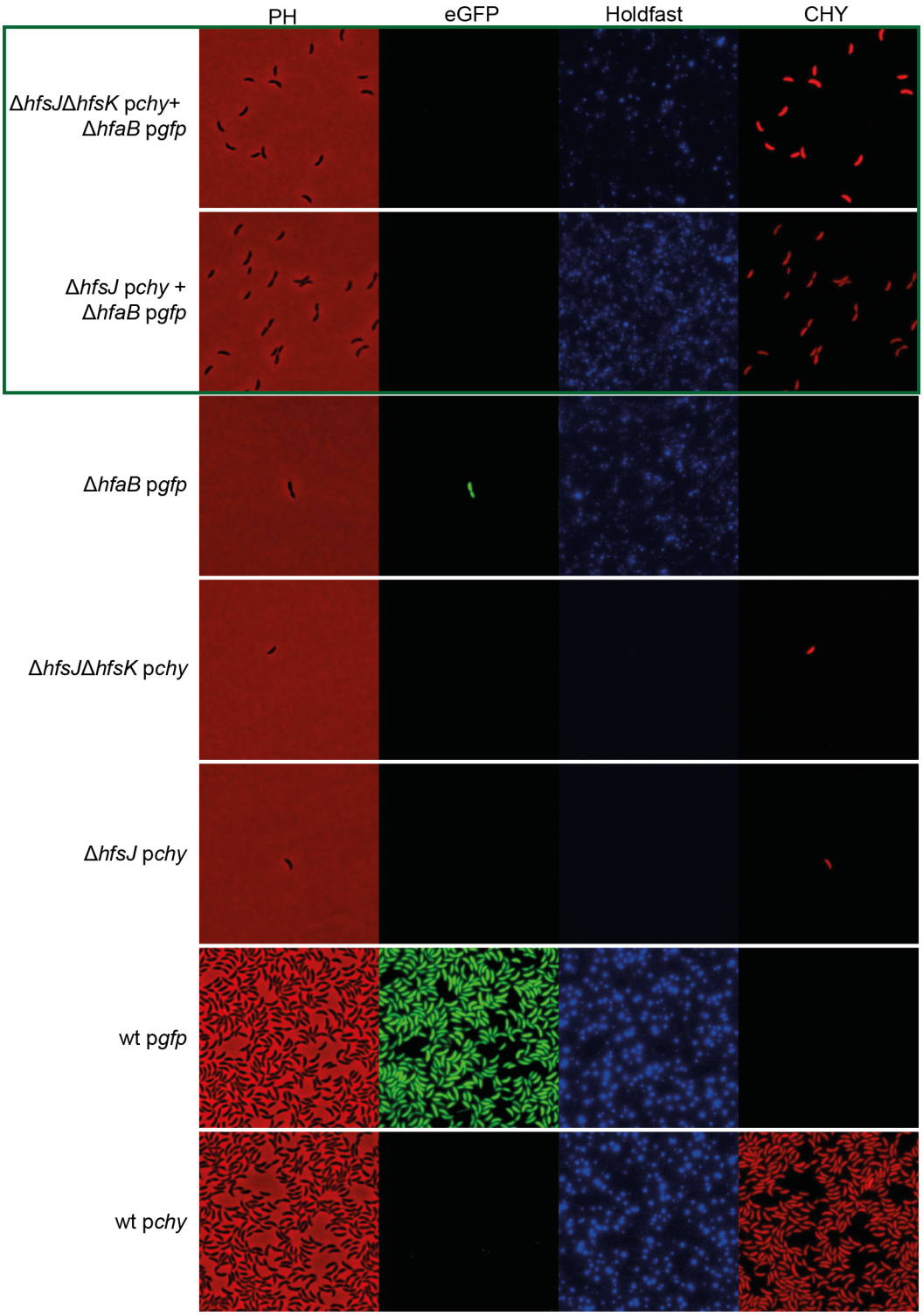

Fig. 11: Holdfast-deficient Δ*hfsK* cells can participate in synergistic adhesion

Synergistic adhesion shown with phase contrast (PH) and fluorescence microscopy images of washed glass slides after 3.5 h adsorption of *mcherry* expressing holdfast$^-$ anchor$^+$ Δ*hfsJ* strain or holdfast$^-$ anchor$^?$ strain Δ*hfsJ*Δ*hfsK* together with the *egfp* expressing holdfast shedding anchor$^-$ strain Δ*hfaB* (green box). All strains alone and wild-type cells expressing *eGFP* or *mcherry* (CHY) are shown as controls below. Fluorophore expression was induced with 0.1 % xylose. Holdfast was stained with WGA-Alexa Fluor ®350.

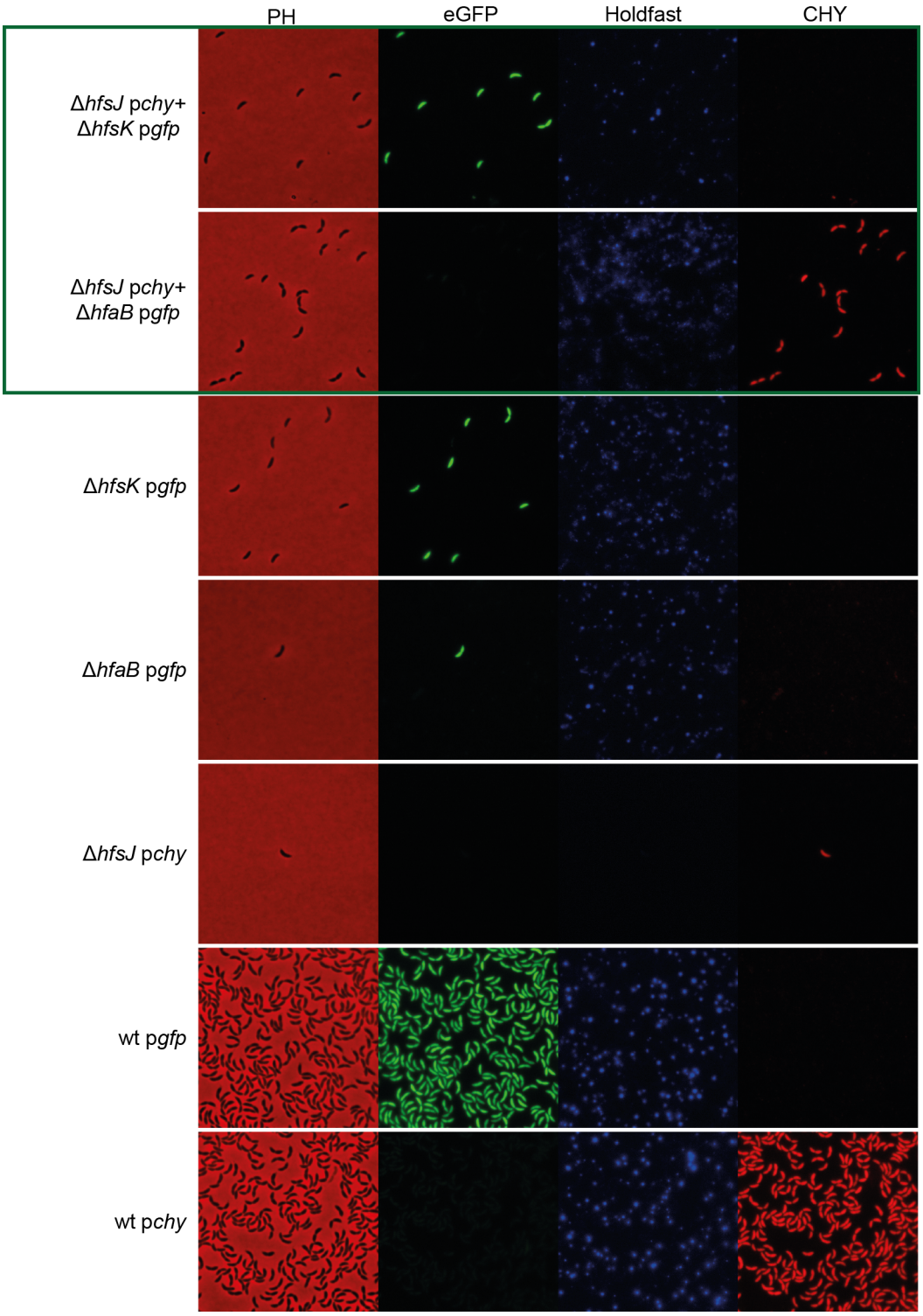

Fig. 12: Shed holdfasts of Δ*hfsK* cells do not support synergistic surface adhesion

Synergistic adhesion shwon with phase contrast (PH) and fluorescence microscopy images of washed glass slides after 3.5 h adsorption of the *mcherry* expressing holdfast$^-$ anchor$^+$ Δ*hfsJ* strain together with the *egfp* expressing holdfast shedding strains Δ*hfaB* (anchor$^-$) or Δ*hfsK* (green box). All strains alone and wild-type cells expressing *egfp* or *mcherry* (CHY) are shown as controls below. Fluorophore expression was induced with 0.1 % xylose. Holdfast was stained with WGA-Alexa Fluor ®350.

2.2.1.2 HfsK overexpression affects *C. crescentus* attachment and growth

Deletion of *hfsK* results in shedding of less cohesive holdfast structures and reduced attachment (Manuscript Figure 2, Figure S2). Next, it was tested whether overexpression of *hfsK* would have an adverse effect. Expression of *hfsK* from P_{xyl} on a low copy vector had no effect on surface colonization after 24 h growth. However, surface colonization after 30 minutes incubation was reduced to 80 % compared to wild-type cells harboring the empty vector (Fig. 13A, B).

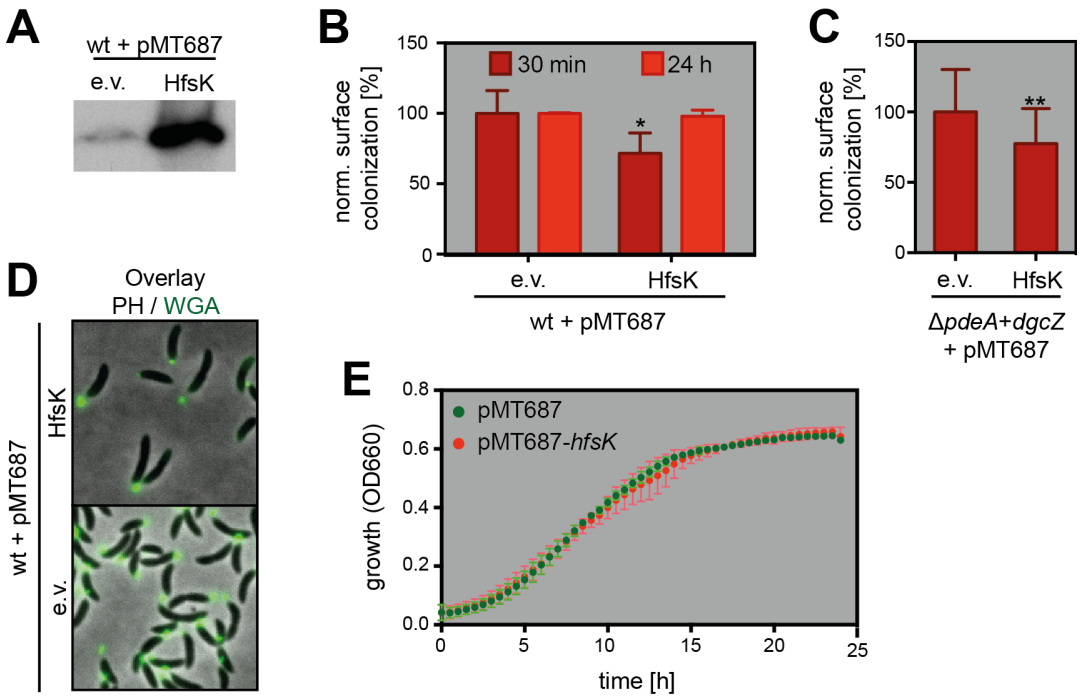

Fig. 13: HfsK overexpression from a low copy plasmid affects surface adhesion

(A) Immunoblot probed with anti-HfsK antibodies showing HfsK protein levels of wild-type cells harboring a low copy plasmid (pMT687) expressing *hfsK* from P_{xyl} or the empty vector control (e.v). (B, C) Surface colonization determined by crystal violet staining after 30 min (dark red bars) and 24 h (light red bars) growth in microtiter plates for cells expressing *hfsK* from pMT687 in a wild-type background (B) or a strain with elevated c–di–GMP levels due to P_{lac}::dgcZ expression induced with 1 mM IPTG (C). Normalized per condition. (D) Analysis of holdfast shedding in a strain expressing *hfsK* from pMT687. Shown are overlays of phase contrast and fluorescence images of adherent WGA-OG stained holdfast on glass coverslips after 4 h cell adsorption. (E) Growth of wild-type cells expressing *hfsK* from pMT687 and e.v. control in microtiter plates determined by measuring optical density. In all panels expression of *hfsK* was induced with 0.1 % xylose. Error bars represent SD of 2 (B, 24h), 3 (B, 30min) and 4 (C) independent experiments, */** represent P-value <0.1/0.01

A possible explanation for this slight surface colonization defect could be that there is not enough c–di–GMP to sequester HfsK away from the membrane during SW-to-ST transition when HfsK levels are elevated. To test this hypothesis, surface colonization was assessed in a strain lacking *pdeA* and in addition expressing *dgcZ* to reach elevated c–di–GMP levels (118). But also when HfsK was overexpressed in this background, surface colonization decreased to 80 % of the empty vector control (Fig. 13C). In contrast to the *hfsK* deletion phenotype, reduced surface colonization in the overexpression strain was not due to holdfast shedding as there were no shed holdfasts detectable after cell were adsorbed to glass nor were the adhered holdfast different in size compared to the empty vector control (Fig. 13D). Reduced surface colonization could also not be attributed to a growth defect as a strain expressing HfsK from the low-copy vector did show similar growth kinetics as the empty vector control (Fig. 13E). It has to be mentioned, however, that when HfsK was overexpressed from a high copy vector growth on agarose plates was nearly abolished (Fig. 14).

These results show that elevated HfsK levels negatively affect cells in a manner that goes beyond a pure holdfast defect.

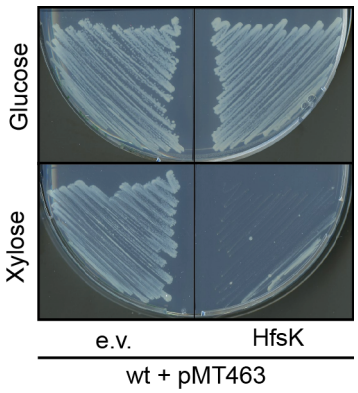

Fig. 14: HfsK overexpression from a high copy plasmid abolishes growth

Growth on PYE agarose plates supplemented with 5 µg/ml gentamycin of wild-type cells expressing *hfsK* form P_{xyl} on a high copy vector (pMT463) or harboring the empty vector control (e.v.) under inducing (0.26 % xylose) or repressing (0.26 % glucose) conditions.

2.2.1.3 Interspecies complementation of HfsK orthologs is not possible

Orthologs of HfsK are encoded in conserved holdfast synthesis gene clusters of *M. maris*, *O. alexandrii* and *W. maritima* (Manuscript Figure S1D). This observation lead to the question of how similar these proteins are in function and thus whether they are able to rescue a Δ*hfsK* phenotype. While the orthologous *hfsK* gene of *M. maris* could not be successfully cloned, the corresponding genes of *O. alexandrii* and *W. maritima* were fused to a C-terminal *3xflag* tag and successfully expressed from a low copy plasmid in *C. crescentus* Δ*hfsK* cells (Fig. 15A). However, surface colonization

was indistinguishable from a Δ*hfsK* mutant harboring an empty vector control (Fig. 15B). The C-terminal 3xFlag-tag could disturb the functionality of the proteins, but at least in case of HfsK this is not the case (Fig. 15C). Thus, these results indicate that HfsK of *C. crescentus* and its orthologs are functionally different and not interchangeable.

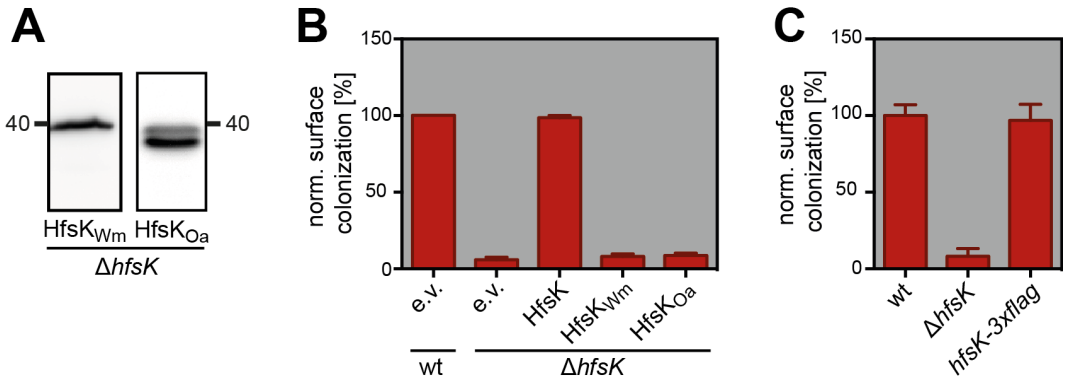

Fig. 15: Interspecies complementation of HfsK orthologs

(A) Immunoblots probed with anti-Flag antibodies to verify expression of 3xflag-tagged HfsK orthologs from *W. maritima* ($HfsK_{Wm}$) and *O. alexandrii* ($HfsK_{Oa}$). (B) Interspecies complementation of a Δ*hfsK* mutation in surface colonization determined by crystal violet staining after 24 h growth in microtiter plates for cells expressing *hfsK* and its orthologs in comparison with the empty vector controls (e.v.). Error bars represent SD of 2 independent experiments. (C) Functionality of a C-terminally Flag-tagged HfsK tested in a 24 h surface colonization assay. Error bars represent SD of 6 colonies tested in one assay. In panels (A) and (B) gene expression was induced by addition of 0.1 % xylose.

2.2.1.4 C–di–GMP binding determinants are partially conserved among HfsK orthologs

HfsK was clearly shown to bind c–di–GMP, yet preliminary data suggest that at least its paralog CC2278 does not bind c–di–GMP. This raises the question whether the HfsK orthologs encoded in other organisms are also potentially able to bind the nucleotide or whether this trait evolved in *C. crescentus* only.

All strains that encode an HfsK ortholog listed by Chou and Galperin (114) encode several c–di–GMP related genes and in all but one of the non-listed strains the presence of at least one GGDEF domain protein with conserved GGDEF motive was manually confirmed using Blast (413) (data not shown). This suggests that all organisms that encode HfsK orthologs rely on c–di–GMP signaling.

The arginines R112 and R352/R353 were identified to be important for c–di–GMP binding of HfsK (Manuscript Figure 5A). To assess their conservation among the HfsK orthologs a structure based alignment was computed using the PROMALS3D multiple sequence and structure alignment server (427) (Fig. 16). R112 is only conserved in a subgroup of strains all of which belong to the proteobacteria. In contrast, the C-terminal extension contains several quite conserved arginines, including R352/R353, that add up to a (R/K)xx(R/K)R*xxxxR* motive (R* being less conserved). Besides this motive, the C-terminal extension varies quite strongly in length and sequence especially between the different phyla. However, apart from the HfsK ortholog of *Desulfatitalea* and the second of two orthologs in *Pirelulla staleyi* all others do have a C-terminal extension underlining the importance of this region for this class of GNAT proteins.

Fig. 16: The C-terminal extension contains a conserved arginine rich motive

Structure based alignment of HfsK and its orthologs showing the sequence region around R112 and R352/R353 (red dashed square), separated by black angled brackets. The numbers in brackets before and after a sequence line indicate the number of the succeeding or preceding amino acid, the number after the dash indicates the total number of amino acids present in this protein. The black arrow shows the beginning of the C-terminal extension. The corresponding phylum and the genomic surrounding of the corresponding gene are indicated in colored lines next to the species name using the same color code as in Manuscript Figure S1C: Proteobacteria (violet), Planctomycetes (orange), Actinobacteria (ocher), Cyanobacteria (cyan); gene in an EPS unrelated cluster (green), gene in an EPS operon (red). (Figure on next page →)

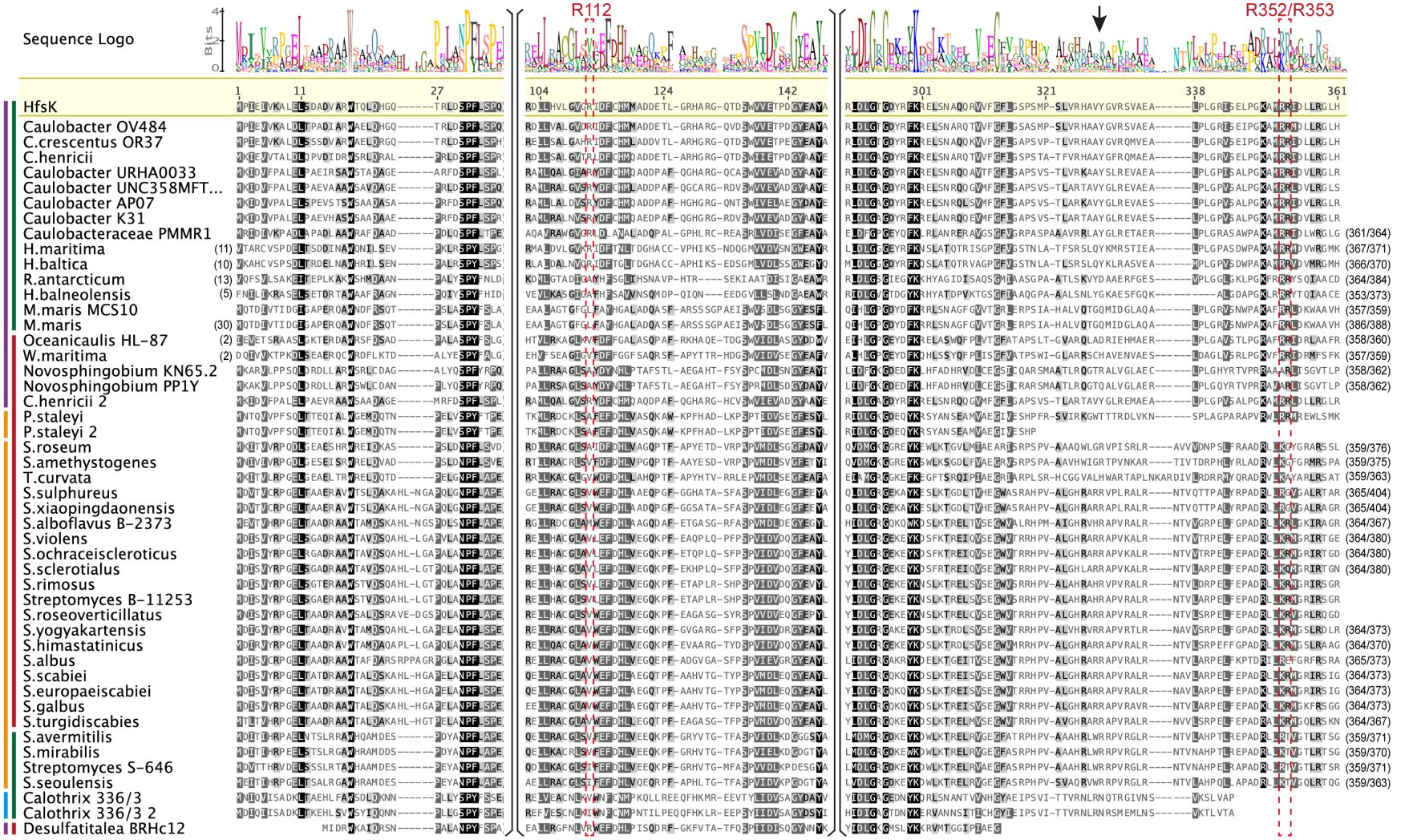
Sequence Logo
Bits
R112
R352/R353
HfsK
Caulobacter OV484
C.crescentus OR37
C.henricii
Caulobacter URHA0033
Caulobacter UNC358MFT...
Caulobacter AP07
Caulobacter K31
Caulobacteraceae PMMR1
H.maritima (11)
H.baltica (10)
R.antarcticum (13)
H.balneolensis (5)
M.maris MCS10
M.maris (30)
Oceanicaulis HL-87 (2)
W.maritima (2)
Novosphingobium KN65.2
Novosphingobium PP1Y
C.henricii 2
P.staleyi
P.staleyi 2
S.roseum
S.amethystogenes
T.curvata
S.sulphureus
S.xiaopingdaonensis
S.alboflavus B-2373
S.violens
S.ochraceiscleroticus
S.sclerotialus
S.rimosus
Streptomyces B-11253
S.roseoverticillatus
S.yogyakartensis
S.himastatinicus
S.albus
S.scabiei
S.europaeiscabiei
S.galbus
S.turgidiscabies
S.avermitilis
S.mirabilis
Streptomyces S-646
S.seoulensis
Calothrix 336/3
Calothrix 336/3 2
Desulfatitalea BRHc12

2.2.1.5 A CC1244 mutant shows strong phenotypes under very specific conditions

In this work surface colonization was only assessed in PYE complex medium so far. When testing deletion strains of *hfsK* and its paralogs in the minimal medium M2G, a similar but aggravated pattern as already observed in PYE arises (Fig. 17A). In M2G medium, an *hfsK* mutant fails to colonize the surface similar to the holdfast deficient NA1000 strain. In addition, while deletion of *cc2278* showed a slight defect after 30 min and nearly no phenotype after 24 h growth in PYE (Manuscript Figure 2, Figure S2), it shows a 50% reduction in surface colonization when grown for 24 h in M2G medium (Fig. 17A). Furthermore, only little surface colonization could be observed for the Δ*cc1244* mutant in M2G medium. However, this is most probably a result of nearly abolished growth in M2G medium as determined by the optical density measured after 24 h growth in microtiter plates (Fig. 17A). Interestingly, this growth defect was only observed for the single Δ*cc1244* mutation and not when this mutation was combined with deletion of the other paralogs (Fig. 17A).

On the other hand, when probing attachment in PYE medium on glass, a Δ*cc2278* Δ*cc1244* double mutant failed to adhere completely (Fig. 17B) while the Δ*cc1244* single mutant adhered like Wild-type and the Δ*cc2278* single mutant adhered normally but produced smaller holdfast as already described above (Fig. 17B, Manuscript Figure 2B). This was unexpected, as on polystyrene the Δ*cc2278* Δ*cc1244* mutant behaves like a Δ*cc2278* single mutant (Manuscript Figure S2A). This implicates CC1244 in (holdfast) adhesion as already shown for HfsK and CC2278.

Fig. 17: Growth and surface adhesion phenotypes of a *cc1244* mutant

(A) Surface colonization determined by crystal violet staining after 24 h growth in M2G medium in microtiter plates for deletion mutants of *hfsK* and its paralogs. End point measurements of the optical densities relative to Wild-type are shown to demonstrate culture growth. Error bars represent SD of 3 independent experiments. (B) Surface colonization and holdfast staining on glass was performed as described in additional material and methods. Shown are fluorescence images and overlays of phase contrast and fluorescence images of adhered WGA stained holdfast on glass coverslips after 4 h cell adsorption. Scale bar = 5 µm
(Figure on next page →)

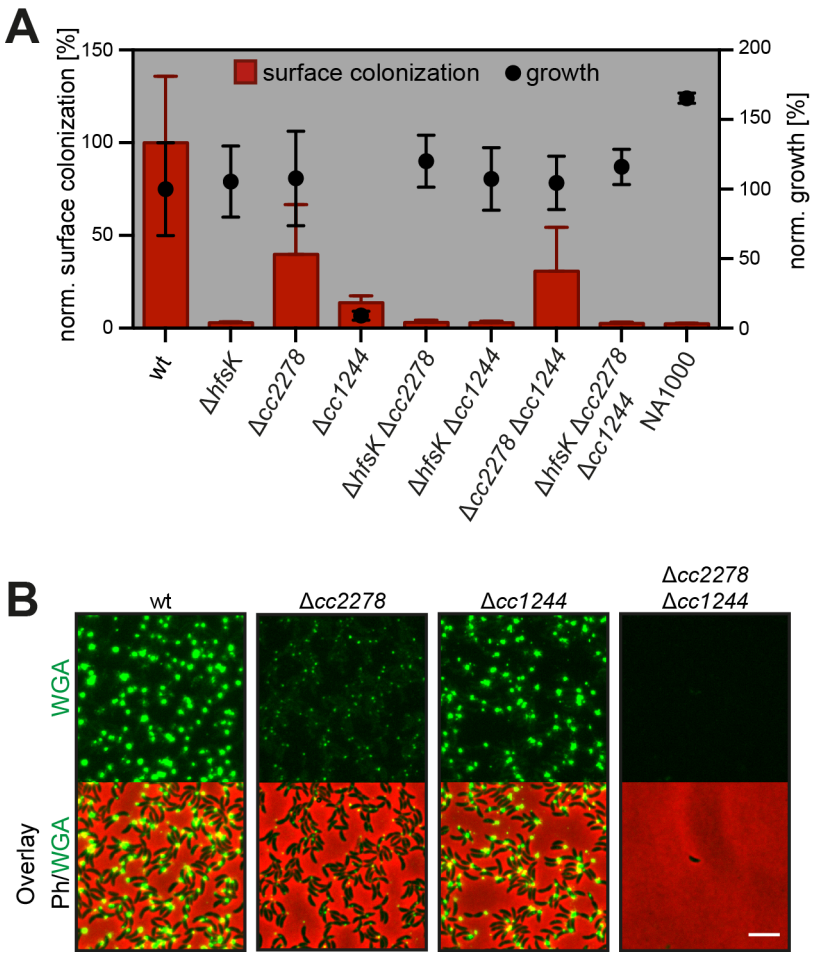

2.2.1.6 Rescue of holdfast synthesis in the cdG⁰ strain

Abel and colleagues (118) could show that a strain without c–di–GMP does not produce a holdfast, yet, based on our data, the c–di–GMP effector HfsK has only a modulatory effect on holdfast production. Conclusively, there must exist another effector that initiates holdfast synthesis upon a c–di–GMP signal. In recent CCMS experiments the glycosyltransferase HfsJ (see chapter: 1.3.3.2) was enriched from *C. crescentus* lysates when using a c–di–GMP specific Capture Compound (J. Nesper, personal communication). In subsequent *in vitro* experiments, HfsJ was shown to bind c–di–GMP specifically (I. Hug, personal communication). HfsJ is essential for holdfast synthesis and seems to be inactivated by binding of the small protein HfiA when cells are starved (317) (see chapter: 1.3.3.3). This raised the question whether HfsJ is also rate limiting for holdfast synthesis when c–di–GMP level are low. I expressed *hfsJ* from a high-copy plasmid in the cdG⁰ strain and a cdG⁰ strain that in addition lacks the inhibitor HfiA and compared holdfast formation with the wild-type strain. In wild-type cells many polar holdfasts could be readily detected and upon HfsJ

overexpression holdfast signal intensity strongly increased, as previously shown (428). In contrast, neither the cdG^0 nor the cdG^0 Δ*hfiA* cells produced any detectable holdfast material (Fig. 18A). However, when HfsJ was overexpressed in those cells, holdfasts appeared which were in general a bit smaller compared to the Wild-type empty vector control. Thereby, additional deletion of *hfiA* did not have a remarkable effect, which was not surprising as the experiment was performed in a nutrient rich medium where HfiA levels are low (317) (Fig. 18A).

Previous results in this work suggested that HfsK is inactivated when c–di–GMP levels are high and active when c–di–GMP levels are low. Thus, the holdfast rescue strain was used to verify those results. I tested the cohesive properties of these rescued holdfasts by quantifying the number of shed holdfasts. For both, Wild-type and cdG^0 Δ*hfiA* that expressed HfsJ, less than 10 % shed holdfasts were counted. In comparison, deletion of *hfsK* in either background led to more than 75% holdfast shedding (Fig. 18B). These results confirm that under a low c–di–GMP level regime HfsK is active while the novel c–di–GMP effector HfsJ is indeed rate limiting.

However, although the holdfasts produced by the HfsJ overexpressing cdG^0 Δ*hfiA* strain were not shed and seemed to be normally anchored in the cell, they were still not able to support surface colonization (Fig. 18C). This is in line with previous findings that in addition to holdfast, also pili and flagellum, which are both not produced in the cdG^0 strain, are required for this process (118, 255, 306, 326, 335).

Fig. 18: Overexpressing HfsJ in a cdG^0 strain rescues holdfast synthesis but not surface adhesion

(A) Holdfast formation visualized with WGA-OG staining of wild-type or cdG^0 strains harboring a plasmid for HfsJ overexpression or the empty vector control (e.v.). Scale bar = 5 µm. (B) Amount of shed holdfast quantified on fluorescence microscopy images for the wild-type and holdfast rescue strain, each in comparison with an *hfsK* mutation in the same background. Mid-log phase cultures were stained with WGA-OG and directly spotted on agarose pads before images were taken. The total number of assigned holdfasts (n) is indicated (C) Attachment assay with the cdG^0 holdfast rescue strains in comparison with the wild-type strain. In all assays *hfsJ* was induced with 0.5 mM IPTG. (Figure on next page →)

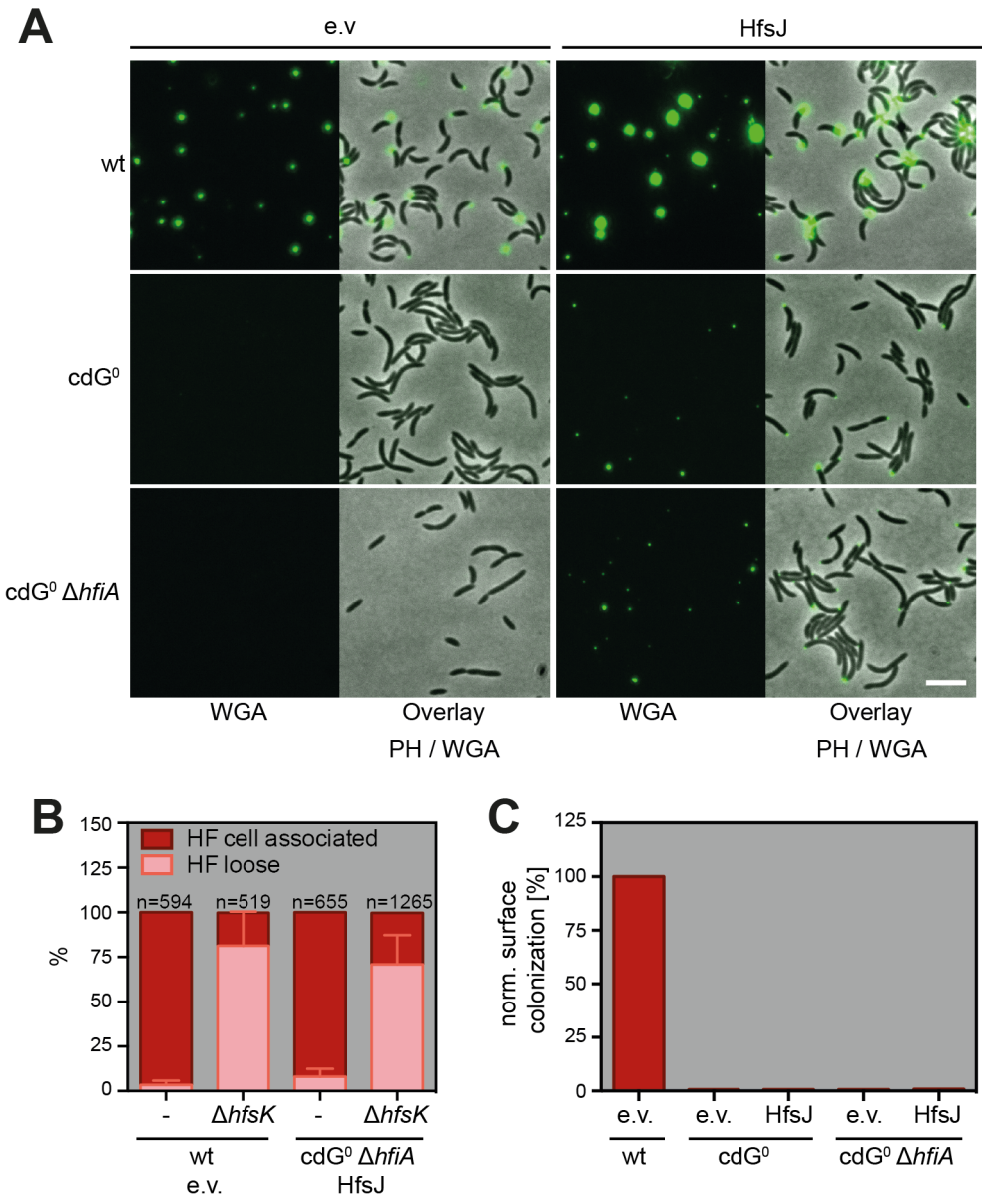

2.2.2 Additional materials and methods

All additional experiments were performed as described in the materials and methods section of the publication manuscript with the following exceptions.

Growth conditions

Marine strains were grown at 30°C under aeration in in Marine Broth 2216 (Difico). To solidify the medium 1.5 % agar were added and 0.03 M MgCl2 were supplemented.

Holdfast staining on glass

To visualize adherent holdfast of a HfsK overexpression strain on glass a protocol was adapted from (330). For plasmid induction, overnight grown cultures were diluted first 1:10 in medium containing the inducing agent and grown to mid log phase, before cell numbers were adjusted to an OD_{660} of 0.11. 2000µl/well diluted culture were co-incubated with round 18 mm borosilicate coverslips (Thermo Scientific, USA) in 6-well polystyrene plates for 4 h at 30°C under aeration. After incubation, the coverslip was washed with $PO4^{3-}$buffer (12.3 mM Na_2HPO_4 / KH_2PO_4), stained for 10 min with 1 µg/ml WGA-Oregon green and washed again before mounting on 1 % agarose pads.

For the synergistic adhesion experiment the protocol in the publication manuscript for holdfast staining on glass was applied as described. However, overnight grown cultures were directly diluted into medium containing the inducing agent. When two strains were co-incubated the final cell density of each strain was adjusted to 0.075. Holdfast was stained with 2.5 ug/ml WGA-Alexa Fluor ®350

Structure based alignment of HfsK orthologs

Structure based alignments of HfsK orthologs were performed with PROMALS3D multiple sequence and structure alignment server (427). The final graph was created using Geneious 7.1.7 software.

Construction of plasmids

pKaS56 and pKaS72 were generated by amplification of *hfsK* or its ortholog from genomic *C. crescentus* CB15 or *W. maritima* DNA (BCCM, Belgium) with PCR followed by restriction enzyme digest using primers and enzymes as indicated in Tab. 1 and ligation into the likewise cut plasmid pMT463 and pMT687, respectively.

pKaS70 was generated by amplification of the *hfsK* ortholog from genomic *O. alexandrii* DNA with PCR followed by restriction enzyme digest using primers and enzymes as indicated in Tab. 1. The plasmid pMT687 was digested with NdeI, treated with Klenow-fragment and subsequently digested with SacI before being ligated with the PCR fragment.

For the pNPTS138-Δ*hfiA* plasmid roughly 500 bp up-and downstream of the target gene were amplified from genomic CB15 DNA with PCR and fused using overlap

extension polymerization, cut with restriction enzymes as indicated in Tab. 1, and ligated at the same time into the likewise digested pNPTS138 vector.

pKaS28 was generated by amplification of the *dgcZ* gene from plasmid pSA223 with PCR followed by restriction enzyme digest using primers and enzymes as indicated in Tab. 1 and ligation into the likewise cut plasmid pSA223.

Tab. 1: Additional strains, plasmids and primers

Plasmids

Plasmid	Description	Source/ Reference
pBBR1MCS2	Kan^R, broad host range high-copy vector with IPTG inducible P_{lac}	(429)
pMT463	pBBR1 based high-copy vector with P_{xyl}, $Gent^R$	(418)
pKaS70	pMT687 derivative for expression of the *hfsK*$_{Oa}$*-3xflag* from P_{xyl}	this study*
pKaS72	pMT687 derivative for expression of the *hfsK*$_{Wm}$*-3xflag* from P_{xyl}	this study*
pNPTS-Δ*hfiA*	pNPTS138 derivative for generation of Δ*hfiA* mutation	this study**
pNPTS138-CC3689Flag	pNPTS1138 derivative for generation of the *hfsK-3xflag* fusion in the *hfsK* locus	J. Nesper
pKaS28	pNPTS138 derivative to integrate a P_{lac} driven *dgcZ-10xhis* into the intergenic region of *cc3065* and *cc3066*	this study*
pDM13	pBBR1MCS2 derivative for overexpression of *hfsJ* from P_{lac}	D. Meyer
pKaS56	pMT463 derivative for overexpression of hfsK from P_{xyl}	this study*
	pNPTS138 derivative for generating the deletion mutation of HfsK	

Strains

Strain	Genotype	Description	Source/ Reference
C. crescentus			
UJ8254	Δ*pdeA* + *dgcZ-10xhis*	Markerless deletion of *pdeA* and chromosomal integration of P_{lac} driven *dgcZ-10xhis* in CB15 using plasmids pSA81 and pKaS28	this study*
UJ6157	*hfsK-3xflag*	Chromosomal integration of *hfsK-3xflag* in CB15 using plasmid pNPTS138-CC3689Flag	this study*
UJ7776	cdG^0 Δ*hfiA*	Markerless deletion of *hfiA* in the CB15 cdG^0 strain using pNPTS-Δ*hfiA*	this study*
UJ7882	cdG^0 Δ*hfiA* Δ*hfsK*	Markerless deletion of *hfsK* in the CB15 cdG^0 Δ*hfiA* strain using pNPTS138- Δ*hfsK*	this study*
O. alexandrii			
UJ9005	Wild type		Y. Brun

Primers

Primer	Sequence	Restriction site	Used for plasmid
3029	CCATGAGCTCGGATCCGCGTTACTATTTATCGTCGTC ATC	BamHI	pKaS70/ pKaS72

3942	AGACGACCATATGCCCATCGAAATCGTCAAAGC	NdeI	pKaS56/
4579	TTCGAATTCTCAGTGCAGTCCGCGCAGCA	EcoRI	pKaS56
6531	TAGTCAGAATTCGGCCATCATCACCGGCC	EcoRI	pNPTS-Δ*hfiA*
6532	CATTTATTGAGCGCGGACAGGTGAGACCTTGGCGCGCC	n/a	pNPTS-Δ*hfiA*
6533	GGCGCGCCAAGGTCTCACCTGTCCGCGCTCAATAAATG	n/a	pNPTS-Δ*hfiA*
6534	TGACTAACTAGTCGGCGGCGAGGTAAAGC	SpeI	pNPTS-Δ*hfiA*
7154	TGCTGAGCTCATGATCAAGAAGACAACGGA	SacI	pKaS28
7155	TGGGTACCTTACTAATGATGGTGATGGTGGTGATGGTGATGATGGAAAACTCGGTTAATCACAT	KpnI	pKaS28
8590	TGTTGTCGGTGGAGCTGAAGTC	n/a	pKaS70
8591	GCCGCGCTTTACGGCGTCGACTACAAAGACCATGAC	n/a	pKaS70
8592	GTCATGGTCTTTGTAGTCGACGCCGTAAAGCGCGGC	n/a	pKaS70
8596	GAGATTACCATATGGATCAGATTGTCGTTAA	NdeI	pKaS72
8597	TTCAGCTTTAAAGGGTCAGACTACAAAGACCATGAC	n/a	pKaS72
8598	GTCATGGTCTTTGTAGTCTGACCCTTTAAAGCTGAA	n/a	pKaS72

* Plasmid/strain generated by myself
**Partial contribution to plasmid/strain construction

3 Discussion and Perspectives

3.1 Discussion

Several aspects of HfsK function and regulation were already discussed as part of the publication manuscript above. Some important considerations are reviewed here again in more detail while also several additional aspects are covered.

3.1.1 Possible function of HfsK

Computational analysis showed that HfsK belongs to the GNAT protein family that catalyzes an acylation reaction using acyl donors bound to an acetyl, aminoacyl or acyls with other organic substituents (Fig. 7). But not only the acyl-donor but also the acyl-acceptor molecule can vary substantially (see chapter: 1.4.1). This makes a functional assignment for HfsK and other homologs not straightforward. Shearing of the holdfast structure in an *hfsK* mutant proposes that the holdfast itself is changed. But given the observation that strains lacking the holdfast anchor proteins HfaA and HfaD showed similar phenotypes as a Δ*hfsK* strain could also indicate that the holdfast anchor is altered in these strains. Yet, the latter scenario seems less likely for the following reasons. First, the strong association of *hfsK* orthologs with genes involved in EPS synthesis indicates that HfsK participates directly in the synthesis of the holdfast EPS and not the anchor proteins, which are encoded elsewhere. Second, the synergistic adhesion experiments showed, that an *hfsJ* mutant, which has an intact anchor but no holdfast can adhere to surface-deposited shed holdfasts of a Δ*hfaB* strain. This was also possible when in addition to *hfsJ* also *hfsK* was deleted (Fig. 11), which indicates that also in this double mutant the anchor is intact. Because of the considerations above, a scenario where HfsK acylates the holdfast EPS is discussed below.

Many EPS components are acetylated (59, 430–434) or carry other acyl decorations like succinyl and pyruvyl residues (435). However, the knowledge about their synthesis is limited. Most information available is about O-acetylation of EPS, which usually requires different enzymes as compared to N-acetylation. In case of the acetylated capsule of *E. coli* that is synthesized by an ABC-transporter dependent pathway, O-acetylation takes place on the level of the oligosaccharide before export (433, 436). During the synthase dependent pathway required for alginate production of *P. aeruginosa,* O-acetylation takes place in the periplasm while the EPS is exported (52) (see chapter: 1.2.4.2.) Synthesis of di-N-acetylated O-antigen of the *P. aeruginosa*

LPS, on the other hand, requires a di-N-acetylated UDP-mannuronic acid precursor (434). Precursor synthesis usually takes place in the cytosol. Since our data indicated that HfsK is active at the inner membrane, it is more likely that HfsK modifies the lipid-linked oligosaccharide at the membrane, rather than participating in precursor synthesis.

FemX of *W. viridescensis* is the closest homolog of HfsK for which structural information is available. FemX has two GNAT domains in tandem and is required for peptidoglycan crosslinking in gram-positive bacteria and transfers an aminoacyl group from aminoacyl-tRNA to Lipid II (see 1.4.2). The Lipid II binding side is mainly comprised in the N-terminal GNAT domain while the C-terminal domain accommodates the aminoacyl-tRNA. According to a structure-based alignment, FemX and HfsK show less similarity in the N-terminal domain, suggesting that their acyl acceptor might differ. It is possible that HfsK evolved to bind to and acylate lipid anchored holdfast oligosaccharide precursors. Consequently, different orthologs of HfsK may use different lipid-linked oligosaccharides as acyl-acceptors depending on the EPS core structure of the respective species. This could explain why HfsK orthologs from *O. alexandrii* and *W. maritima* were unable to functionally complement a Δ*hfsK* phenotype as the exact composition of their holdfast EPS might differ from the *C. crescentus* holdfast.

As FemX and HfsK show more similarity in the C-terminal GNAT domain that binds aminoacyl-tRNA, it is feasible that aminoacyl-tRNA is also the acyl-donor of HfsK. The highly conserved lysine of the Fem family that is required for stabilizing the tetrahedral intermediate of the aminoacylation reaction (379) (Fig. 9C) is also conserved in HfsK (K300), its orthologs, and paralogs. However, without *in vitro* data about the enzymatic function of HfsK it cannot be exclude that HfsK uses another acyl-donor like the classical acetyl-CoA or something similar to myristoyl-CoA which is the substrate of another tandem GNAT protein (see chapter: 1.4).

3.1.2 Acylation of EPS – it can make the difference

Acylation of EPS has been observed, but only in few cases the role of this modification has been investigated. *B. cepacia* for example, synthesizes an acetylated EPS and the acetyl groups were shown to protect against reactive oxygen species (63). *V. cholerae* encodes two acetyltransferases in its EPS *vsp* gene cluster but only deletion of one, *vpsG*, showed a phenotype. A strain lacking VpsG produced less EPS, formed les

biofilm and grew to more smooth colonies (437). A *P. fluorescens* strain deficient in cellulose acetylation forms thinner and less robust biofilms on the liquid-air interface and is not able to retain cells in the matrix (430). The best-described system, however, is alginate of *P. aeruginosa* (see chapter: 1.2.4.2). Acetylation and epimerization were shown to be interdependent and strongly affect the molecular weight of the final EPS product and viscosity (53). Mutants deficient in acetylation only formed thin and less structured biofilms which could be partially attributed to a reduced viscosity of the non-acetylated EPS (53, 432).

Viscosity is an inherent property of EPS. Depending on the interaction forces within individual molecules, EPS can behave like a viscoelastic fluid, which deforms upon a sustained stress or like a viscoelastic solid that does not deform under these circumstances (55) (see chapter: 1.1.2). Under shear stress, a wild-type holdfast does not deform and keeps the cells attached to the surface. In an *hfsK* mutant one can observe such a deformation indicating that interactions within the holdfast have weakened. As discussed above, HfsK possibly adds an acyl group to the holdfast EPS material. Acetyl groups were suggested to form hydrophobic pockets that increase dispersion forces (57). In line with this, acetylated cepacian, the EPS of *B. cepacia*, is slightly less viscous than in its deacetylated form and forms dimeric polymer structures while deacetylated polymers remain monomeric (58). Yet dispersion forces are still very transient and thus do not explain the tremendous increase of viscosity (i.e. decreased cohesion) of the *hfsK* mutant holdfast. On the other hand, it is more feasible that HfsK transfers an aminoacyl group. Depending on its nature this group could participate in stronger electrostatic interactions or, in analogy to the peptide bridges in peptidoglycan, even engage in a covalent linkage either within the EPS polymer or between the polymer and the anchor proteins (378, 438) (see chapter: 1.4.2).

As described in chapter 1.1.2, underwater adhesion is a challenging process and EPS adhesins need certain prerequisites, mainly in form of polymer modification, in order to fulfill this task. Again, depending on the nature of the acyl reaction catalyzed by HfsK, the protein might also affect water solubility or the surface adhesion force of the holdfast directly. However, considering the massive amounts of adherent but shed holdfast material on glass observed for Δ*hfsK* cells, the latter is not likely. The reduced adhesive force measured for Δ*hfsK* in comparison to wild type cells is probably a consequence of reduced interaction forces within the holdfast structure or between

holdfast and anchor. Likewise, HfsK overexpression may increase these interaction forces. Li and colleagues proposed that the holdfast first spreads like a viscous fluid to form a surface adherent disc and then cures to a more rigid structure (315) (see chapter: 1.3.3.1). Increased interaction forces might change the speed of this curing reaction, which could impair surface contact of the holdfast disc. This would explain the reduced surface adhesion of the HfsK overexpressing strain.

3.1.3 The holdfast anchor model

While the proteins needed to anchor the holdfast on the cell envelope, HfaA,B,D, are known for many years (328, 329) the exact mechanism of how the holdfast polymer is anchored is still not clear today.

It is thought that HfaB is the outer membrane export pore for HfaA and HfaD that are predicted to constitute an amyloid-like anchor held in the outer membrane (see chapter: 1.3.3.2). This idea can be combined with the hypothesis that HfsK catalyzes a modification of the holdfast EPS that is needed for crosslinking of the saccharide polymers with the anchor (see chapter above). Such multiple anchor-to-EPS crosslinks could confer a stable interaction network needed to make the holdfast non-deformable and strong and to anchor it firmly in the cell envelope. HfaA and HfaD require each other to polymerize (331). Therefore, as observed in the flow channel, deletion of either should have the same phenotype as an *hfaAD* double mutant. Thus, the stability conferring interaction network should not be created in neither an *hfaA*, *hfaD* nor an *hfsK* mutant.

As HfaA and HfaD seem not to be exported in a Δ*hfaB* mutant (331) it is to be expected that a Δ*hfaB* mutant additionally also lacks HfaA and HfaD on the envelope. But as already previously observed, the Δ*hfaA*, Δ*hfaD* or Δ*hfaAD* double mutant did not phenocopy a Δ*hfaB* mutant. While deletion of *hfaA* and *hfaD* resulted in the shedding of a holdfast, which is deformed by flow, deletion of *hfaB* resulted in the shedding of a globular and non-deformed holdfast. However, when observing shed holdfasts of Δ*hfsK* and Δ*hfaB* mutants on glass slides after cultures were grown with orbital shaking (Manuscript Figure 2B), the strains were not distinguishable and neither formed filamentous holdfasts.

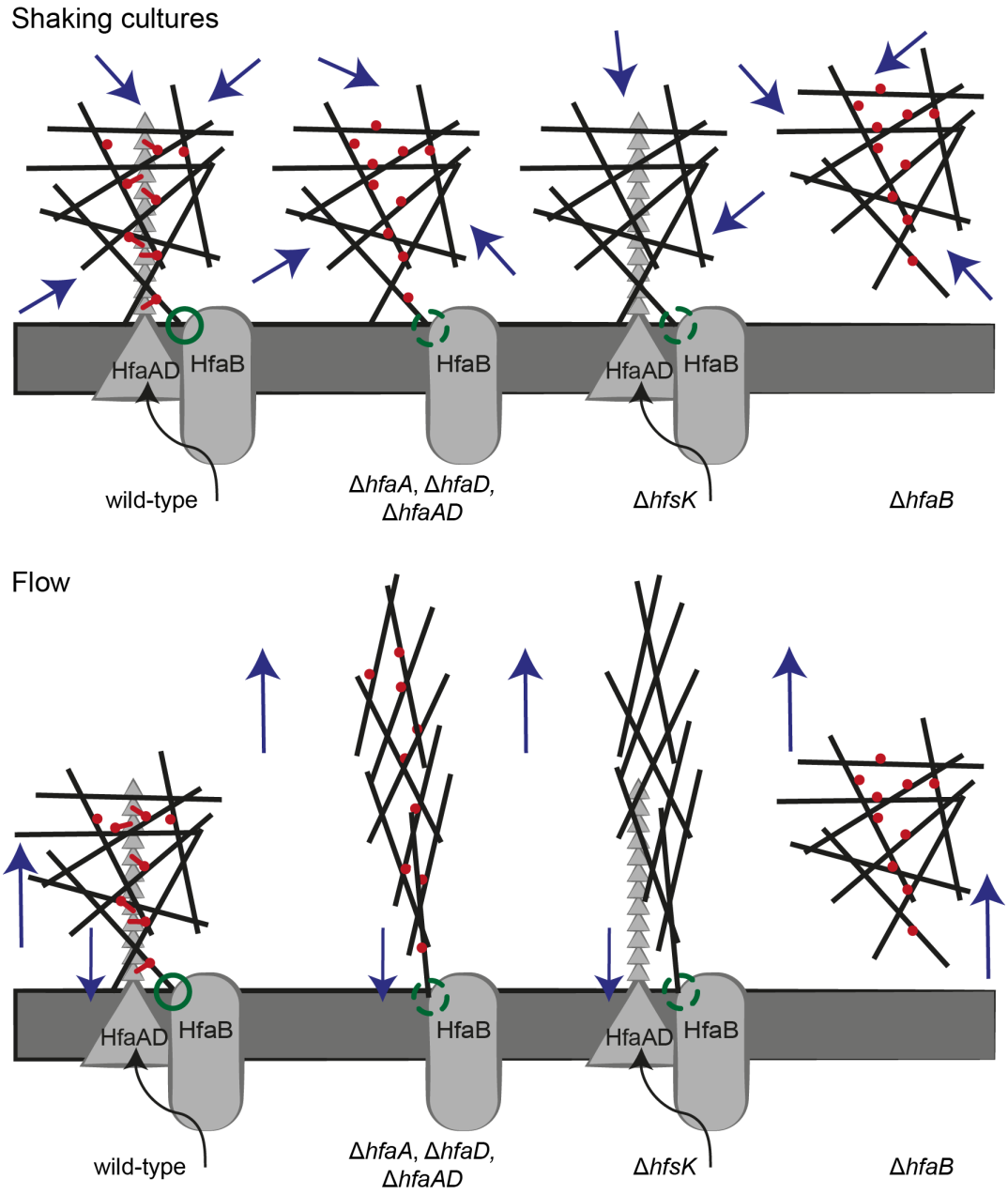

Fig. 19: The holdfast anchor model

The holdfast EPS is held together by weak entanglement interaction forces between the saccharide polymers. Additionally, crosslinks (red lines) between an HfsK catalyzed EPS modification (red dots) and the holdfast anchor consisting of HfaAD additionally anchor and stabilize the structure and make it non-deformable. The holdfast is also connected to the cell by an HfaAD-independent HfaB mediated mechanism (green circle, dashed when prone to break). In shaking cultures (upper panel) none of the mutant holdfasts deform, as the undirected forces (blue arrows) experienced are short-lived and cannot disrupt the weak EPS interactions. Yet, under flow conditions (lower panel) the forces are unidirectional and act over longer time-scales. In the presence of HfaB cells pull on the holdfast structure. Thus, saccharide polymers are sheared and the holdfast is deformed when the HfaAD-HfsK mediated interaction network is not established but a residual connection between the cell envelope and the saccharide polymers is maintained via HfaB.

A possible explanation could be that HfaB is involved in an additional weak but HfaAD and HfsK independent anchor mechanism. Besides, as described for other EPS systems, the holdfast saccharide polymers are probably still held together via many weak and rather transient entanglement interactions and can only be sheared (i.e. behave like a viscoelastic fluid) when subject to a mechanical stress that lasts longer as the time constant of these interactions (see chapter: 1.1.2). Thus, in strains that lack either *hfaA, hfaD, or hfsK* the holdfast would still be connected to the cell via HfaB, while the interaction network conferring stability and strong anchoring is missing. When cells are grown under shaking conditions, short-lived forces from different angles act on the weak holdfast, which under these conditions is held together by the transient interactions between the saccharide polymers and does not deform. Yet it is eventually disconnected from the cell. When cells are grown in flow, directed long lasting forces act on the weak holdfast and additionally the cells pull on the holdfast. The weak interactions between saccharide polymers are sheared into one direction and form an elongated holdfast filament that is just connected at one end to the cell via HfaB and this connection would also rupture after some time. An *hfaB* mutant, on the other hand, would lack both the stability conferring HfaAD-HfsK based interaction network and the additional anchor. The holdfasts of these cells would be immediately disconnected from the cell. In a flow channel, flow velocity decreases towards the channel walls (439). Therefore, directly shed holdfasts of Δ*hfaB* mutants would probably experience far less mechanical stress, as there are not connected to the bulkier cells that project more into areas with higher flow velocity. This would explain why holdfasts from *hfaB* mutants do not form filaments, not even in conditions with a continuous flow.

3.1.4 Function of CC2278 and CC1244

While HfsK is functionally connected with holdfast anchoring and has a strong implication in holdfast cohesion, its paralogs CC2278 and CC1244 seem to have only minor influence on the adhesin. Yet, mutants lacking one of these proteins showed a holdfast and/or attachment related phenotype. E.g. holdfasts of a Δ*cc2278* strain were generally smaller but not shed, which might be explained by a defect in EPS export due to an altered acetylation state of the polymer as observed for PGA of *E. coli* strains that lack the periplasmic deacetylase (239). A Δ*cc1244* mutation, on the other hand, very specifically abolished adhesion on glass in a Δ*cc2278* background. Although the

holdfast of the Δ*cc1244* Δ*cc2278* double mutant has not yet been investigated in detail, the finding that it shows similar adherence to polystyrene as a Δ*cc2278* single mutant, indicated that this strain does form a holdfast. Both, gas plasma treated polystyrene and glass are negatively charged at neutral pH, but the negative charge of glass decreases at lower pH which also has an effect on holdfast adhesion (310, 440, 441). Fresh PYE has a pH slightly below 6 and, as a consequence, the negative charge on glass is probably lower compared to polystyrene in the course of the glass-binding assay. Therefore, it is possible that the holdfast adhesive properties are changed in the Δ*cc1244* Δ*cc2278* mutant in such a way that mainly its adhesion on neutral surfaces is affected.

3.1.5 GNAT proteins – ignored players in EPS synthesis

HfsK and its homologs are presented here as a so far uncharacterized family that can take part in EPS synthesis. However, involvement of GNAT proteins in EPS synthesis is not a new, yet a largely ignored detail. In 1995, Matthysse and colleagues described the gene cluster required for cellulose synthesis in *Agrobacterium tumefaciens* (442, 443). They found that a two-gene operon consisting of CelD and CelE is required for early steps in cellulose synthesis. However, as they worked with transposon mutants and could not exclude polar effects of the transposon within the *celD* gene onto *celE,* function and requirements for CelD remained elusive (443). Today, we know that CelD is a GNAT family protein that belongs to the same subgroup as HfsK (Pfam: Acetyltransf_6) (149, 444). Also for CelD a structure based HHpred search identifies FemX as the closes homolog with known structure (149, 390, 444). However, CelD has an additional C-terminal TPR repeat, which is absent in HfsK and a sequence homology search using CelD as query with Blast (413) gives no reasonable hit in *C. crescentus*. But sequence similarities among GNAT proteins are very poor and even HfsK orthologs do not reach sequence similarities above 35% outside of the *Caulobacter* clade. Furthermore, holdfast synthesis goes via a Wzx/Wzy-dependent pathway, while cellulose synthesis is a synthase dependent process (see chapter: 1.2.4.1). This makes the differences between CelD and HfsK explicable.

To my knowledge, cellulose modification has not been shown in *A. tumefaciens*. But due to the big variety of additional genes found in various cellulose synthesis clusters, different types of cellulose modification were predicted for several bacteria, including *A. tumefaciens* (149). In case of *Pseudomonas fluorescens* synthesis of

acetylated cellulose has been confirmed and it depends on proteins that are similar to periplasmic O-acetyltransferases employed in alginate synthesis of *P. aeruginosa* (430). Unmodified cellulose is composed of glucose chains that do not provide any amine. There are, however, some rare reports of GNAT proteins capable to perform acetylation on an amine (N-) and on a hydroxide (O- acetylation) (445, 446). It could therefore be possible that CelD acylates the early cellulose polymer on a hydroxide group.

3.1.6 C−di−GMP dependent control of HfsK

We could show that HfsK binds c−di−GMP specifically and that nucleotide binding requires both, residues from the GNAT core and from a C-terminal extension that is not present in FemX. Most HfsK orthologs have such a C-terminal extension containing a conserved arginine rich motive (R/K)xx(R/K)RxxxxR. This is striking, as c−di−GMP binding sites in general contain several arginine residues (114) (see chapter: 1.2.3). The two arginines in the middle of the motive correspond to R352/R353 which were required for full c−di−GMP binding of HfsK. On the other hand, R112, which locates to the GNAT core structure, is only conserved in a proteobacteria-specific subgroup of HfsK homologs and it is possible that c-di-GMP binding is specific to this particular subgroup. Considering the importance of the C-terminal extension for HfsK localization, the primary role of its conserved arginine residues might be to mediate interaction with a membrane partner, while c−di−GMP binding to this site may have evolved later in a subgroup to specifically interfere with HfsK membrane localization.

But how and why does c−di−GMP control HfsK? Although the functional consequences of HfsK dispersal to the cytosol are not entirely clear, several pieces of evidence suggested that this step inactivates the protein. (I) A truncated version of HfsK is fully dispersed in the cytosol and inactive. Moving this mutant back to the membrane by replacing the C-terminus with a transmembrane anchor did not restore its activity. This could either indicate that loss of function is a simple consequence of the truncation, which might impair activity or stability/folding, or that the C-terminus mediated localization is required for activity. The C-terminus could, for example, engage in a functionally important interaction with a membrane partner. (II) Full length protein variants that were forced to remain in the membrane either due to an added membrane anchor or as a result of mutating one of the critical Arg residues for

c-di-GMP binding (R112), retained full activity *in vivo*. This led us to conclude that HfsK adopts its active conformation at the membrane while its cytosolic form is inactive. Arg mutations in the C-terminus, although permanently membrane associated, were, however, not active. This would be again in line with an important functional role of the C-terminus beyond simple localization (III). When holdfast synthesis is rescued in the cdG^0 strain by overexpression of the glycosyltransferase HfsJ, the emerging holdfast is not shed and HfsK remains fully membrane associated. This strongly argued that under these conditions (lack of c–di–GMP) HfsK is in the active, membrane associated from. (IV) Contrarily to this, when c–di–GMP levels were increased artificially above wild-type levels, HfsK is fully dispersed and holdfasts phenocopies the Δ*hfsK* mutant strain.

Which cyclase is responsible to turn off HfsK activity remains to be shown. It is possible that this function is carried out by a specific member of this enzyme family in *C. crescentus*, similar to related processes in other bacteria (119–121, 447). For example in *P. fluorescens* a physical interaction of LapD with its DGC was required for maximal signal transduction (447). This could also explain why in this c–di–GMP high background the holdfast defects were still not as severe as in a Δ*hfsK* mutant.

Studies in *C. crescentus* indicated that the general paradigm of low c–di–GMP levels promoting motility and high c–di–GMP levels stimulating adhesion and biofilm formation maybe oversimplified. For example, as described in chapter: 1.3.2, flagellar function requires an optimal window of intracellular c–di–GMP and either too low or too high levels of c–di–GMP abolish its biogenesis and function. Likewise, pili function and surface colonization have a c–di–GMP optimum (118). By having cell cycle controlled oscillating c–di–GMP levels, this optimal range is exploited by *C. crescentus* to time function of these processes, e.g. flagellum synthesis in predivisional cells requires c–di–GMP while in swarmer cells c–di–GMP levels have to be kept low in order to allow flagellar rotation. In contrast, in an experiment were c–di–GMP levels were gradually increased, holdfast production plateaued as measured by WGA staining intensities and did not decrease even at very high c–di–GMP levels (118). This indicated that c–di–GMP has a simple role in stimulating holdfast production. However, as suggested by the inactivation of HfsK by c–di–GMP, holdfast functionality might require an optimal c–di–GMP concentration window. It is possible that *C. crescentus* makes use of oscillating c–di–GMP levels during the cell cycle to activate

overall biogenesis of the EPS polymer as c–di–GMP levels begin to rise, followed by the deactivation of HfsK at peak levels of c–di–GMP. Constant high c–di–GMP levels, as simulated with the rcdG^0 p*dgcZ* strain, might thus disrupt the proper coordination of successive steps in holdfast biogenesis, resulting in non-cohesive or poorly anchored EPS. The idea that the timing of HfsK activity is important is supported by the finding that *hfsK* overexpression from a high-copy plasmid leads to a strong growth defect. It is possible that the activity of HfsK at the wrong time and/or place interferes with important cellular processes like peptidoglycan synthesis. As a consequence, also cells expressing c–di–GMP blind HfsK variants, which do not delocalize to the cytosol, should have growth defects. This, however, was not observed for the R112A mutant although it was still active in vivo. Yet, this variant seems to have retained some c–di–GMP binding capacity, which might be enough to prevent it from being toxic. Alternatively, toxicity in the overexpression strain could arise not from accumulated membrane associated but from accumulated cytosolic HfsK. The latter was not detected in the R112A mutant.

Inactivation of HfsK by c–di–GMP might have yet another purpose. Although we have no knowledge about c–di–GMP levels in *C. crescentus* cells in a growing biofilm, they might be high enough to deactivate HfsK completely during the course of holdfast synthesis. Keeping HfsK turned off in such an environment may contribute to the formation of complex 3D cellular structures. *C. crescentus* biofilms grown in microfluidic devices show WGA staining all around the cells (428), indicating that at this stage, either another non-polar N-acetylglucosamine-containing EPS is produced or that the holdfast material has lost its topological specificity and has altered into a more viscous cell embedding matrix. Besides capsule and holdfast, there seems to be no other EPS synthesis cluster in *C. crescentus*. Specific inactivation of HfsK might therefore be the means to convert the polar holdfast adhesin into a matrix EPS, possibly explaining why this protein is regulated by c–di–GMP in a negative manner.

A Δ*hfsK* mutant holdfast was sheared when subject to flow. Shearing of entire biofilms in response to a directed stress has been described for several environmental isolates, for *P. aeruginosa* and for *S. aureus.* It has been suggested that this viscoelastic behavior decreases the strain experienced by the biofilm and thus prevents structural failure (448, 449). Additionally, loose biofilm flocs of *P. fluorescens* shear to elongated streamers within seconds when they collide with a surface (450). But bacteria can also adapt to the shear stress strength and change biofilm cohesion in order to have

maximal stability (451). Thus, by modulating activity of HfsK via c–di–GMP, *C. crescentus* could influence the viscoelasticity of its biofilm matrix and adapt to different shear stress regimes found e.g. in ponds or rivers.

3.1.7 Holdfast synthesis and surface adhesion control pathways - a highly connected c–di–GMP network

Several pathways were shown to integrate c–di–GMP signaling at different levels. For example in *E. coli* maximal cellulose synthesis requires two post-transcriptional c–di–GMP effectors (184, 217) (see chapter: 1.2.4.1) and flagellum function in *C. crescentus* is regulated both positively and negatively by c–di–GMP (185, 309) (see above and chapter: 1.3.2.2). Synthesis of the EPS Pel of *P. aeruginosa* is controlled by c–di–GMP on the transcriptional level via FleQ and on the post-translational level via PelD (180, 199, 229) (see chapter: 1.2.4.3). Also in *C. crescentus* several c–di–GMP dependent pathways have emerged that either translationally or post-translationally converge into holdfast synthesis and are reviewed and discussed in the following chapter.

All *hfs* genes have a similar expression pattern, which is mainly governed by CtrA (57, 296; S. Abel, unpublished data). As described in 1.3.2.1 CtrA stability and activity is regulated by at least two c–di–GMP effector proteins. Expression of *hfiA*, was shown to be additionally repressed by StaR that is also controlled by a c–di–GMP dependent pathway (C. von Arx, personal communication). Yet, interestingly there seems to be over all only little influence of c–di–GMP on *hfs* gene expression. Protein levels of HfsK, for example, were only marginally changed in an rcdG^0 strain in comparison to the wild type strain. Additionally, the findings that holdfast production can be rescued in the cdG^0 strain by overexpression of *hfsJ* without changing expression of the main *hfs*-operons is an indirect evidence that even in a strain without c–di–GMP the holdfast synthesis machinery is assembled. This is in contrast to Pel of *P. aeruginosa*. Expression of *pel* is highly increased in strains with elevated c–di–GMP levels in comparison to the wild type strain (199) or in biofilms in comparison to planktonic cells, which also translates into the measured protein levels (74). We know, that the holdfast synthesis machinery is already produced before cell division (317, 336). Consequently, it seems that the holdfast machinery is constitutively present in the cells and ready to react quickly. This illustrates that for *C. crescentus* surface

colonization is important and in nature it could be even fundamental for its existence. The question for this bacterium seems not to be whether it should adhere to a surface but rather whether the conditions are favorable enough to do so.

The decision, whether conditions are favorable for colonization appears to be largely influence by c–di–GMP on a post-translational level. Although there is evidence that under lab conditions the holdfast machinery is synthesized even in absence of c–di–GMP, the nucleotide is strictly required for holdfast formation (118). Several experimental observations have recently identified the glycosyltransferase HfsJ (see chapter: 1.3.3.2) as a c–di–GMP binding, rate-limiting enzyme in holdfast precursor biogenesis (49; J. Nesper & I. Hug, personal communication). In this work it was shown that overexpression of HfsJ can rescue holdfast formation in the cdG^0 strain, arguing that this protein may represent the enzymatic step that is tightly controlled by c–di–GMP. These results strongly argued that HfsJ constitutes the switch to initiate holdfast synthesis when c–di–GMP levels rise in the cell, either as a result of development during SW-to-ST transition, or as a consequence of cells experiencing surface contact. The finding that HfsJ is the central regulatory player in holdfast formation was underscored by the observation that its activity is also restrained by HfiA, a small protein that responds to the cells' nutritional status (317) (see chapter: 1.3.3.3). Interestingly, this nutritional checkpoint includes yet another c–di–GMP binding protein, located upstream of HfiA, that integrates c–di–GMP levels with information of the general stress response pathway and ppGpp levels (V. Shyp, personal communication). Furthermore, also CC1244 was found in a CCMS screen for specific c–di–GMP binding proteins. Thus, also this protein might present another branch through which c–di–GMP could control holdfast formation. This exemplifies the c–di–GMP signaling complexity that integrates different environmental and probably internal cues to regulate holdfast production and thus surface colonization. It is likely that more pathways exist to integrate additional signals into this important cellular transition.

Although holdfast biogenesis is key for permanent attachment of *C. crescentus*, it is not sufficient for successful surface colonization (42, 118, 306, 335). This is again exemplified by the stains used in this study that have no or strongly increased c–di–GMP levels. A cdG^0 strain that synthesizes holdfast still failed to colonize surfaces and also the shed holdfasts of a strain massively overproducing DgcZ were not deposited on glass. The reason for this is most probably that both, a cdG^0 strain

and a strain with enhanced c–di–GMP levels fail to assemble a functional flagellum and functional pili (118). The flagellar motor is involved in the surface sensing process that translates into rapid holdfast biogenesis (I. Hug, personal communication). In general, an underwater adhesin needs to dispatch H_2O molecules in order to firmly interact with the surface and to adhere (77) (see chapter: 1.1.2). Furthermore, freshly produced holdfast seems to be able to quickly spread on the surface before curing and forming an adhesive disc onto which more holdfast material is added (315) (see chapter: 1.3.3.1). Both processes thus require a close or even enforced contact to the surface in order to be effective, which would explain the importance of pili for adhesion as they can pull the cell to the substratum. It is thus possible that in addition to the multi-layered c–di–GMP-mediated control of holdfast formation, the overall process of "surface adhesion" integrates even more c–di–GMP dependent signals and pathways to optimize assembly and function of additional cellular organelles that are required for this lifestyle change.

3.2 Outlook

This work has been the first step to unravel the function and control of the novel c–di–GMP effector HfsK. Nevertheless, there are still several aspects about this protein which are not fully understood.

First of all, the enzymatic function of HfsK is unclear and it is not even certain that HfsK is enzymatically active. There are two imminent questions when assuming that HfsK is an active acyltransferase: What substrate does it acylate and what acyl donor does it use? As a first step, it would be interesting to see whether the holdfast EPS is changed in a Δ*hfsK* mutant in comparison to Wild-type. This is challenging to test, as the amounts of holdfast produced are minuscule and due to its adhesive properties the material is difficult to handle. We initiated a subproject, where lipid-linked holdfast oligosaccharide intermediates were isolated. Preliminary data indicate that isolation does work (data not shown). However, also here it remains to be seen whether the amount of isolated material would be enough for detailed analysis with mass spectroscopy (452, 453) or even NMR (244). In contrast to investigating holdfast composition, substrate binding of purified HfsK could be screened. Such a screen has been performed with several uncharacterized GNAT proteins using a library consisting of 95 different compounds including antibiotics, polyamines, amino acids, nucleosides, and other metabolites (454). Best candidates for HfsK to start with would be different mono-/ di and oligosaccharides that could serve as acyl-acceptors and different acyl-tRNAs that could be used as acyl-donors.

Also information about the c–di–GMP binding mode is scarce. Attempts to identify residues involved in c–di–GMP binding using the hydrogen-deuterium exchange method failed for unknown reasons (G. Bange, personal communication). Crystallization of HfsK in presence and absence of c–di–GMP could not only help to define the ligand binding site, but could also give new insights into the mechanics of protein regulation. It might help to understand the role of HfsK's C-terminus and could solve the question, whether the C-terminus has a direct regulatory role or whether it is mainly involved in protein localization. In relation to this, it would be interesting to see whether the C-terminus is sufficient to localize proteins. A simple fusion of a fluorophore to the C-terminus of HfsK could answer this question. Additionally, it is not known how HfsK is retained at the membrane. It could interact with another protein or with the membrane lipids directly. It was extensively tried to find HfsK

interaction partners by co-immunoprecipitation coupled to mass spectroscopy. But no possible interaction partner could be enriched even when c–di–GMP levels were adjusted in order to push the protein into its membrane bound or cytosolic form (data not shown). However, instability of the protein upon lysis could have interfered with the procedure. If a fluorophore fused to the C-terminus of HfsK does localize to the membrane, it could be used for interaction studies as an alternative to the native protein. Alternatively, considering the possibility that HfsK might interact with the membrane directly, it might be interesting to isolate *C. crescentus* membranes (455), treat them with proteases and then test, whether HfsK could bind to these clean membranes.

Another intriguing question is why HfsK is controlled by c–di–GMP. The findings that overexpression of HfsK leads to strongly reduced growth could be exploited in a suppressor screen. This could not only give information about the cause of this growth defect. As suppression of the growth defect might include also other proteins involved in holdfast synthesis, this could also help to understand the role of HfsK in this pathway.

Alternatively, as discussed above, one possibility is that inactivation of HfsK plays a major role in biofilms. To assess this, a tight and inducible *hfsK* system in a Δ*hfsK* mutant could be used to study protein function in growing biofilms. In a microfluidics system this could be combined with changes in flow rate to assess the system in dependence of shear stress. In parallel, having established the basics of c–di–GMP control during *C. crescentus* cell cycle, the next logical step would be to investigate the role of c–di–GMP in biofilms by using inducible systems that are already used in planktonic cells (118).

Furthermore, the putative connection of HfsK with the holdfast anchoring mechanisms is a very interesting finding. Elucidating the exact mechanism of holdfast anchoring would be another step to unravel the enigma of the holdfast's remarkable adhesion strength. Analyzing the exact holdfast phenotype of strains with different combinations of *hfaA*, *B*, *C*, *D* and *hfsK* deletions could already help to understand the connection of these proteins.

Last but not least, many of the approaches suggested above could also be applied for CC2278 and CC1244. Their exact function and regulation certainly differ from HfsK as they also show other deletion phenotypes. However, in certain ways, e.g. general nature of the substrate, they might be also very similar and insights into one of the paralogs could possibly help to understand the others as well.

Bibliography

1. **Elasri MO**, **Miller RV**. 1999. Study of the response of a biofilm bacterial community to UV radiation. Appl Environ Microbiol **65**:2025–31.
2. **Dib J**, **Motok J**, **Zenoff VF**, **Ordoñez O**, **Farías ME**. 2008. Occurrence of Resistance to Antibiotics, UV-B, and Arsenic in Bacteria Isolated from Extreme Environments in High-Altitude (Above 4400 m) Andean Wetlands. Curr Microbiol **56**:510–517.
3. **Meyer-Dombard DR**, **Swingley W**, **Raymond J**, **Havig J**, **Shock EL**, **Summons RE**. 2011. Hydrothermal ecotones and streamer biofilm communities in the Lower Geyser Basin, Yellowstone National Park. Environ Microbiol **13**:2216–2231.
4. **Harrison JJ**, **Ceri H**, **Turner RJ**. 2007. Multimetal resistance and tolerance in microbial biofilms. Nat Rev Microbiol **5**:928–938.
5. **Gauthier MJ**, **Lafay B**, **Christen R**, **Fernandez L**, **Acquaviva M**, **Bonin P**, **Bertrand J-C**. 1992. *Marinobacter hydrocarbonoclasticus* gen. nov., sp. nov., a New, Extremely Halotolerant, Hydrocarbon-Degrading Marine Bacterium. Int J Syst Bacteriol **42**:568–576.
6. **Hall-Stoodley L**, **Costerton JW**, **Stoodley P**. 2004. Bacterial biofilms: from the natural environment to infectious diseases. Nat Rev Microbiol **2**:95–108.
7. **Nadell CD**, **Xavier JB**, **Foster KR**. 2009. The sociobiology of biofilms. FEMS Microbiol Rev **33**:206–224.
8. **Bjarnsholt T**. 2013. The role of bacterial biofilms in chronic infections. APMIS **121**:1–58.
9. **Flemming H-C**, **Wingender J**. 2010. The biofilm matrix. Nat Rev Microbiol **8**:623–33.
10. **Flemming H-C**. 2016. EPS—Then and Now. Microorganisms **4**:41.
11. **Liang Y**, **Gao H**, **Chen J**, **Dong Y**, **Wu L**, **He Z**, **Liu X**, **Qiu G**, **Zhou J**. 2010. Pellicle formation in *Shewanella oneidensis*. BMC Microbiol **10**:291.
12. **Stoodley P**, **Lewandowski Z**, **Boyle JD**, **Lappin-Scott HM**. 1998. Oscillation characteristics of biofilm streamers in turbulent flowing water as related to drag and pressure drop. Biotechnol Bioeng **57**:536–44.
13. **Costerton JW**, **Cheng KJ**, **Geesey GG**, **Ladd TI**, **Nickel JC**, **Dasgupta M**, **Marrie TJ**. 1987. Bacterial biofilms in nature and disease. Annu Rev Microbiol **41**:435–64.
14. **Zobell CE**. 1943. The Effect of Solid Surfaces upon Bacterial Activity. J Bacteriol **46**:39–56.
15. **Costerton JW**. 1999. Bacterial Biofilms: A Common Cause of Persistent Infections. Science **284**:1318–1322.
16. **Petrova OE**, **Sauer K**. 2012. Sticky situations: key components that control bacterial surface attachment. J Bacteriol **194**:2413–25.
17. **Wolska KI**, **Grudniak AM**, **Rudnicka Z**, **Markowska K**. 2016. Genetic control of bacterial biofilms. J Appl Genet **57**:225–238.
18. **Flemming H-C**. 2011. Microbial Biofouling: Unsolved Problems, Insufficient Approaches, and Possible Solutions, p. 81–109. *In* Microbiology.
19. **Hwang G**, **Kang S**, **El-Din MG**, **Liu Y**. 2012. Impact of conditioning films on the initial adhesion of *Burkholderia cepacia*. Colloids Surfaces B Biointerfaces **91**:181–188.
20. **O'Toole G**, **Kaplan HB**, **Kolter R**. 2000. Biofilm Formation as Microbial Development. Annu Rev Microbiol **54**:49–79.
21. **Goulter RM**, **Gentle IR**, **Dykes GA**. 2009. Issues in determining factors influencing bacterial attachment: a review using the attachment of *Escherichia coli* to abiotic surfaces as an example. Lett Appl Microbiol **49**:1–7.
22. **Lu S**, **Giuliani M**, **Harvey H**, **Burrows LL**, **Wickham RA**, **Dutcher JR**. 2015. Nanoscale Pulling of Type IV Pili Reveals Their Flexibility and Adhesion to Surfaces over Extended Lengths of the Pili. Biophys J **108**:2865–2875.
23. **Persat A**, **Stone HA**, **Gitai Z**. 2014. The curved shape of *Caulobacter crescentus* enhances surface colonization in flow. Nat Commun **5**:3824.
24. **Persat A**, **Inclan YF**, **Engel JN**, **Stone HA**, **Gitai Z**. 2015. Type IV pili mechanochemically regulate virulence factors in *Pseudomonas aeruginosa*. Proc Natl

Acad Sci **112**:7563–7568.
25. **Haiko J**, **Westerlund-Wikström B**. 2013. The Role of the Bacterial Flagellum in Adhesion and Virulence. Biology **2**:1242–1267.
26. **Friedlander RS**, **Vlamakis H**, **Kim P**, **Khan M**, **Kolter R**, **Aizenberg J**. 2013. Bacterial flagella explore microscale hummocks and hollows to increase adhesion. Proc Natl Acad Sci **110**:5624–5629.
27. **Goldman AJ**, **Cox RG**, **Brenner H**. 1967. Slow viscous motion of a sphere parallel to a plane wall- I Motion through a quiescent fluid. Chem Eng Sci **22**:637–651.
28. **Persat A**, **Nadell CD**, **Kim MK**, **Ingremeau F**, **Siryaporn A**, **Drescher K**, **Wingreen NS**, **Bassler BL**, **Gitai Z**, **Stone HA**. 2015. The Mechanical World of Bacteria. Cell **161**:988–997.
29. **Belas R**. 2014. Biofilms, flagella, and mechanosensing of surfaces by bacteria. Trends Microbiol **22**:517–527.
30. **Stoodley P**, **Sauer K**, **Davies DG**, **Costerton JW**. 2002. Biofilms as complex differentiated communities. Annu Rev Microbiol **56**:187–209.
31. **Römling U**, **Galperin MY**, **Gomelsky M**. 2013. Cyclic di-GMP: the first 25 years of a universal bacterial second messenger. Microbiol Mol Biol Rev **77**:1–52.
32. **O'Toole GA**, **Wong GC**. 2016. Sensational biofilms: surface sensing in bacteria. Curr Opin Microbiol **30**:139–146.
33. **Tseng BS**, **Majerczyk CD**, **Passos da Silva D**, **Chandler JR**, **Greenberg EP**, **Parsek MR**. 2016. Quorum Sensing Influences *Burkholderia thailandensis* Biofilm Development and Matrix Production. J Bacteriol **198**:2643–2650.
34. **Irie Y**, **Borlee BR**, **O'Connor JR**, **Hill PJ**, **Harwood CS**, **Wozniak DJ**, **Parsek MR**. 2012. Self-produced exopolysaccharide is a signal that stimulates biofilm formation in *Pseudomonas aeruginosa*. Proc Natl Acad Sci **109**:20632–20636.
35. **Lynch DJ**, **Fountain TL**, **Mazurkiewicz JE**, **Banas JA**. 2007. Glucan-binding proteins are essential for shaping *Streptococcus mutans* biofilm architecture. FEMS Microbiol Lett **268**:158–165.
36. **Romero D**, **Aguilar C**, **Losick R**, **Kolter R**. 2010. Amyloid fibers provide structural integrity to *Bacillus subtilis* biofilms. Proc Natl Acad Sci **107**:2230–2234.
37. **Whitchurch CB**. 2002. Extracellular DNA Required for Bacterial Biofilm Formation. Science **295**:1487–1487.
38. **Watanabe M**, **Sasaki K**, **Nakashimada Y**, **Kakizono T**, **Noparatnaraporn N**, **Nishio N**. 1998. Growth and flocculation of a marine photosynthetic bacterium *Rhodovulum* sp. Appl Microbiol Biotechnol **50**:682–691.
39. **Wang S**, **Liu X**, **Liu H**, **Zhang L**, **Guo Y**, **Yu S**, **Wozniak DJ**, **Ma LZ**. 2015. The exopolysaccharide Psl-eDNA interaction enables the formation of a biofilm skeleton in *Pseudomonas aeruginosa*. Environ Microbiol Rep **7**:330–340.
40. **Allesen-Holm M**, **Barken KB**, **Yang L**, **Klausen M**, **Webb JS**, **Kjelleberg S**, **Molin S**, **Givskov M**, **Tolker-Nielsen T**. 2006. A characterization of DNA release in *Pseudomonas aeruginosa* cultures and biofilms. Mol Microbiol **59**:1114–1128.
41. **Serra DO**, **Klauck G**, **Hengge R**. 2015. Vertical stratification of matrix production is essential for physical integrity and architecture of macrocolony biofilms of *Escherichia coli*. Environ Microbiol **17**:5073–5088.
42. **Entcheva-Dimitrov P**, **Spormann AM**. 2004. Dynamics and control of biofilms of the oligotrophic bacterium *Caulobacter crescentus*. J Bacteriol **186**:8254–66.
43. **Chiang P**, **Burrows LL**. 2003. Biofilm formation by hyperpiliated mutants of *Pseudomonas aeruginosa*. J Bacteriol **185**:2374–2378.
44. **Klausen M**, **Aaes-Jørgensen A**, **Molin S**, **Tolker-Nielsen T**. 2003. Involvement of bacterial migration in the development of complex multicellular structures in *Pseudomonas aeruginosa* biofilms. Mol Microbiol **50**:61–68.
45. **Serra DO**, **Richter AM**, **Hengge R**. 2013. Cellulose as an Architectural Element in Spatially Structured *Escherichia coli* Biofilms. J Bacteriol **195**:5540–5554.
46. **Wilking JN**, **Zaburdaev V**, **De Volder M**, **Losick R**, **Brenner MP**, **Weitz DA**. 2013. Liquid transport facilitated by channels in *Bacillus subtilis* biofilms. Proc Natl Acad Sci U S A **110**:848–52.

47. **Asally M**, **Kittisopikul M**, **Rue P**, **Du Y**, **Hu Z**, **Cagatay T**, **Robinson AB**, **Lu H**, **Garcia-Ojalvo J**, **Suel GM**. 2012. Localized cell death focuses mechanical forces during 3D patterning in a biofilm. Proc Natl Acad Sci **109**:18891–18896.
48. **Houry A**, **Gohar M**, **Deschamps J**, **Tischenko E**, **Aymerich S**, **Gruss A**, **Briandet R**. 2012. Bacterial swimmers that infiltrate and take over the biofilm matrix. Proc Natl Acad Sci U S A **109**:13088–93.
49. **Nwodo UU**, **Green E**, **Okoh AI**. 2012. Bacterial exopolysaccharides: functionality and prospects. Int J Mol Sci **13**:14002–14015.
50. **Schmid J**, **Sieber V**, **Rehm B**. 2015. Bacterial exopolysaccharides: biosynthesis pathways and engineering strategies. Front Microbiol **6**:496.
51. **Whitney JC**, **Howell PL**. 2013. Synthase-dependent exopolysaccharide secretion in Gram-negative bacteria. Trends Microbiol **21**:63–72.
52. **Hay ID**, **Ur Rehman Z**, **Moradali MF**, **Wang Y**, **Rehm BHA**. 2013. Microbial alginate production, modification and its applications. Microb Biotechnol **6**:637–50.
53. **Fata Moradali M**, **Donati I**, **Sims IM**, **Ghods S**, **Rehm BHA**. 2015. Alginate Polymerization and Modification Are Linked in *Pseudomonas aeruginosa*. MBio **6**:e00453-15.
54. **Cuthbertson L**, **Kos V**, **Whitfield C**. 2010. ABC Transporters Involved in Export of Cell Surface Glycoconjugates. Microbiol Mol Biol Rev **74**:341–362.
55. **Körstgens V**, **Flemming H-C**, **Wingender J**, **Borchard W**. 2001. Uniaxial compression measurement device for investigation of the mechanical stability of biofilms. J Microbiol Methods **46**:9–17.
56. **Wloka M**, **Rehage H**, **Flemming H-C**, **Wingender J**. 2005. Structure and rheological behaviour of the extracellular polymeric substance network of mucoid *Pseudomonas aeruginosa* biofilms. Biofilms **2**:275.
57. **Mayer C**, **Moritz R**, **Kirschner C**, **Borchard W**, **Maibaum R**, **Wingender J**, **Flemming H-C**. 1999. The role of intermolecular interactions: studies on model systems for bacterial biofilms. Int J Biol Macromol **26**:3–16.
58. **Herasimenka Y**, **Cescutti P**, **Sampaio Noguera CE**, **Ruggiero JR**, **Urbani R**, **Impallomeni G**, **Zanetti F**, **Campidelli S**, **Prato M**, **Rizzo R**. 2008. Macromolecular properties of cepacian in water and in dimethylsulfoxide. Carbohydr Res **343**:81–89.
59. **Whitfield GB**, **Marmont LS**, **Howell PL**. 2015. Enzymatic modifications of exopolysaccharides enhance bacterial persistence. Front Microbiol **6**:1–21.
60. **Huang L**, **Takahashi R**, **Kobayashi S**, **Kawase T**, **Nishinari K**. 2002. Gelation behavior of native and acetylated konjac glucomannan. Biomacromolecules **3**:1296–1303.
61. **Menchicchi B**, **Fuenzalida JP**, **Hensel A**, **Swamy MJ**, **David L**, **Rochas C**, **Goycoolea FM**. 2015. Biophysical Analysis of the Molecular Interactions between Polysaccharides and Mucin. Biomacromolecules **16**:924–935.
62. **Casillo A**, **Parrilli E**, **Sannino F**, **Mitchell DE**, **Gibson MI**, **Marino G**, **Lanzetta R**, **Parrilli M**, **Cosconati S**, **Novellino E**, **Randazzo A**, **Tutino ML**, **Corsaro MM**. 2017. Structure-activity relationship of the exopolysaccharide from a psychrophilic bacterium: a strategy for cryoprotection. Carbohydr Polym **156**:364–371.
63. **Cuzzi B**, **Cescutti P**, **Furlanis L**, **Lagatolla C**, **Sturiale L**, **Garozzo D**, **Rizzo R**. 2012. Investigation of bacterial resistance to the immune system response: Cepacian depolymerisation by reactive oxygen species. Innate Immun **18**:661–671.
64. **Zhang G**, **Meredith TC**, **Kahne D**. 2013. On the essentiality of lipopolysaccharide to Gram-negative bacteria. Curr Opin Microbiol **16**:779–785.
65. **Fumeaux C**, **Radhakrishnan SK**, **Ardissone S**, **Théraulaz L**, **Frandi A**, **Martins D**, **Nesper J**, **Abel S**, **Jenal U**, **Viollier PH**. 2014. Cell cycle transition from S-phase to G1 in *Caulobacter* is mediated by ancestral virulence regulators. Nat Commun **5**:4081.
66. **Toh E**, **Kurtz HD**, **Brun YV**. 2008. Characterization of the *Caulobacter crescentus* holdfast polysaccharide biosynthesis pathway reveals significant redundancy in the initiating glycosyltransferase and polymerase steps. J Bacteriol **190**:7219–31.
67. **Agladze K**, **Wang X**, **Romeo T**. 2005. Spatial Periodicity of *Escherichia coli* K-12 Biofilm Microstructure Initiates during a Reversible, Polar Attachment Phase of Development and Requires the Polysaccharide Adhesin PGA. J Bacteriol **187**:8237–8246.

68. **Danese PN**, **Pratt LA**, **Kolter R**. 2000. Exopolysaccharide Production Is Required for Development of *Escherichia coli* K-12 Biofilm Architecture. J Bacteriol **182**:3593–3596.
69. **Davies DG**, **Geesey GG**. 1995. Regulation of the alginate biosynthesis gene *algC* in *Pseudomonas aeruginosa* during biofilm development in continuous culture. Appl Environ Microbiol **61**:860–7.
70. **Hentzer M**, **Teitzel GM**, **Balzer GJ**, **Heydorn A**, **Molin S**, **Givskov M**, **Parsek MR**. 2001. Alginate overproduction affects *Pseudomonas aeruginosa* biofilm structure and function. J Bacteriol **183**:5395–401.
71. **Wozniak DJ**, **Wyckoff TJO**, **Starkey M**, **Keyser R**, **Azadi P**, **O'Toole GA**, **Parsek MR**. 2003. Alginate is not a significant component of the extracellular polysaccharide matrix of PA14 and PAO1 *Pseudomonas aeruginosa* biofilms. Proc Natl Acad Sci **100**:7907–7912.
72. **Ma L**, **Conover M**, **Lu H**, **Parsek MR**, **Bayles K**, **Wozniak DJ**. 2009. Assembly and Development of the *Pseudomonas aeruginosa* Biofilm Matrix. PLoS Pathog **5**:e1000354.
73. **Jennings LK**, **Storek KM**, **Ledvina HE**, **Coulon C**, **Marmont LS**, **Sadovskaya I**, **Secor PR**, **Tseng BS**, **Scian M**, **Filloux A**, **Wozniak DJ**, **Howell PL**, **Parsek MR**. 2015. Pel is a cationic exopolysaccharide that cross-links extracellular DNA in the *Pseudomonas aeruginosa* biofilm matrix. Proc Natl Acad Sci U S A **112**:11353–8.
74. **Colvin KM**, **Gordon VD**, **Murakami K**, **Borlee BR**, **Wozniak DJ**, **Wong GCL**, **Parsek MR**. 2011. The Pel Polysaccharide Can Serve a Structural and Protective Role in the Biofilm Matrix of *Pseudomonas aeruginosa*. PLoS Pathog **7**:e1001264.
75. **Haag AP**. 2006. Mechanical Properties of Bacterial Exopolymeric Adhesives and their Commercial Development. Biol Adhes 1–19.
76. **Lazaridou A**, **Biliaderis CG**, **Kontogiorgos V**. 2003. Molecular weight effects on solution rheology of pullulan and mechanical properties of its films. Carbohydr Polym **52**:151–166.
77. **Nyarko A**, **Barton H**, **Dhinojwala A**. 2016. Scaling down for a broader understanding of underwater adhesives – a case for the *Caulobacter crescentus* holdfast. Soft Matter **12**:9132–9141.
78. **Zhou G**, **Yuan J**, **Gao H**. 2015. Regulation of biofilm formation by BpfA, BpfD, and BpfG in *Shewanella oneidensis*. Front Microbiol **6**:790.
79. **Gjermansen M**, **Ragas P**, **Sternberg C**, **Molin S**, **Tolker-Nielsen T**. 2005. Characterization of starvation-induced dispersion in *Pseudomonas putida* biofilms. Environ Microbiol **7**:894–904.
80. **Ivanov IE**, **Boyd CD**, **Newell PD**, **Schwartz ME**, **Turnbull L**, **Johnson MS**, **Whitchurch CB**, **O'Toole GA**, **Camesano TA**. 2012. Atomic force and super-resolution microscopy support a role for LapA as a cell-surface biofilm adhesin of *Pseudomonas fluorescens*. Res Microbiol **163**:685–691.
81. **Ambrosis N**, **Boyd CD**, **O´Toole GA**, **Fernández J**, **Sisti F**. 2016. Homologs of the LapD-LapG c-di-GMP Effector System Control Biofilm Formation by *Bordetella bronchiseptica*. PLoS One **11**:e0158752.
82. **El-Kirat-Chatel S**, **Beaussart A**, **Boyd CD**, **O'Toole GA**, **Dufrêne YF**. 2014. Single-Cell and Single-Molecule Analysis Deciphers the Localization, Adhesion, and Mechanics of the Biofilm Adhesin LapA. ACS Chem Biol **9**:485–494.
83. **Newell PD**, **Monds RD**, **O'Toole GA**. 2009. LapD is a bis-(3',5')-cyclic dimeric GMP-binding protein that regulates surface attachment by *Pseudomonas fluorescens* Pf0-1. Proc Natl Acad Sci U S A **106**:3461–6.
84. **Newell PD**, **Yoshioka S**, **Hvorecny KL**, **Monds RD**, **O'Toole GA**. 2011. Systematic analysis of diguanylate cyclases that promote biofilm formation by *Pseudomonas fluorescens* Pf0-1. J Bacteriol **193**:4685–98.
85. **Newell PD**, **Boyd CD**, **Sondermann H**, **O'Toole GA**. 2011. A c-di-GMP Effector System Controls Cell Adhesion by Inside-Out Signaling and Surface Protein Cleavage. PLoS Biol **9**:e1000587.
86. **Huggett MJ**, **Williamson JE**, **de Nys R**, **Kjelleberg S**, **Steinberg PD**. 2006. Larval settlement of the common Australian sea urchin *Heliocidaris erythrogramma* in response to bacteria from the surface of coralline algae. Oecologia **149**:604–619.

87. **Callow JA**, **Callow ME**. 2011. Trends in the development of environmentally friendly fouling-resistant marine coatings. Nat Commun **2**:244.
88. **Schultz MP**, **Bendick JA**, **Holm ER**, **Hertel WM**. 2011. Economic impact of biofouling on a naval surface ship. Biofouling **27**:87–98.
89. **Fitridge I**, **Dempster T**, **Guenther J**, **de Nys R**. 2012. The impact and control of biofouling in marine aquaculture: a review. Biofouling **28**:649–69.
90. **Flemming H-C**. 2002. Biofouling in water systems – cases, causes and countermeasures. Appl Microbiol Biotechnol **59**:629–640.
91. **Balcázar JL**, **Subirats J**, **Borrego CM**. 2015. The role of biofilms as environmental reservoirs of antibiotic resistance. Front Microbiol **6**:1–9.
92. **Rani SA**, **Pitts B**, **Beyenal H**, **Veluchamy RA**, **Lewandowski Z**, **Davison WM**, **Buckingham-Meyer K**, **Stewart PS**. 2007. Spatial Patterns of DNA Replication, Protein Synthesis, and Oxygen Concentration within Bacterial Biofilms Reveal Diverse Physiological States. J Bacteriol **189**:4223–4233.
93. **Williamson KS**, **Richards LA**, **Perez-Osorio AC**, **Pitts B**, **McInnerney K**, **Stewart PS**, **Franklin MJ**. 2012. Heterogeneity in *Pseudomonas aeruginosa* Biofilms Includes Expression of Ribosome Hibernation Factors in the Antibiotic-Tolerant Subpopulation and Hypoxia-Induced Stress Response in the Metabolically Active Population. J Bacteriol **194**:2062–2073.
94. **Rybtke M**, **Hultqvist LD**, **Givskov M**, **Tolker-Nielsen T**. 2015. *Pseudomonas aeruginosa* Biofilm Infections: Community Structure, Antimicrobial Tolerance and Immune Response. J Mol Biol **427**:3628–3645.
95. **Veerachamy S**, **Yarlagadda T**, **Manivasagam G**, **Yarlagadda PK**. 2014. Bacterial adherence and biofilm formation on medical implants: a review. Proc Inst Mech Eng Part H J Eng Med **228**:1083–1099.
96. **Wu H**, **Moser C**, **Wang H-Z**, **Høiby N**, **Song Z-J**. 2014. Strategies for combating bacterial biofilm infections. Int J Oral Sci **7**:1–7.
97. **Bjarnsholt T**. 2005. Garlic blocks quorum sensing and promotes rapid clearing of pulmonary *Pseudomonas aeruginosa* infections. Microbiology **151**:3873–3880.
98. **Song Z**, **Kong KF**, **Wu H**, **Maricic N**, **Ramalingam B**, **Priestap H**, **Schneper L**, **Quirke JME**, **Høiby N**, **Mathee K**. 2010. Panax ginseng has anti-infective activity against opportunistic pathogen *Pseudomonas aeruginosa* by inhibiting quorum sensing, a bacterial communication process critical for establishing infection. Phytomedicine **17**:1040–1046.
99. **Hoffmann N**, **Lee B**, **Hentzer M**, **Rasmussen TB**, **Song Z**, **Johansen HK**, **Givskov M**, **Hoiby N**. 2007. Azithromycin Blocks Quorum Sensing and Alginate Polymer Formation and Increases the Sensitivity to Serum and Stationary-Growth-Phase Killing of *Pseudomonas aeruginosa* and Attenuates Chronic *P. aeruginosa* Lung Infection in Cftr-/-. Antimicrob Agents Chemother **51**:3677–3687.
100. **Wu H**, **Song Z**, **Hentzer M**, **Andersen JB**, **Molin S**, **Givskov M**, **Høiby N**. 2004. Synthetic furanones inhibit quorum-sensing and enhance bacterial clearance in *Pseudomonas aeruginosa* lung infection in mice. J Antimicrob Chemother **53**:1054–61.
101. **Sambanthamoorthy K**, **Luo C**, **Pattabiraman N**, **Feng X**, **Koestler B**, **Waters CM**, **Palys TJ**. 2014. Identification of small molecules inhibiting diguanylate cyclases to control bacterial biofilm development. Biofouling **30**:17–28.
102. **Lieberman OJ**, **Orr MW**, **Wang Y**, **Lee VT**. 2014. High-Throughput Screening Using the Differential Radial Capillary Action of Ligand Assay Identifies Ebselen As an Inhibitor of Diguanylate Cyclases. ACS Chem Biol **9**:183–192.
103. **Tramper-Stranders GA**, **Wolfs TF**, **Fleer A**, **Kimpen JL**, **van der Ent CK**. 2007. Maintenance azithromycin treatment in pediatric patients with cystic fibrosis: long-term outcomes related to macrolide resistance and pulmonary function. Pediatr Infect Dis J **26**:8–12.
104. **Meyer JL**. 1994. The microbial loop in flowing waters. Microb Ecol **28**:195–199.
105. **Engel AS**, **Porter ML**, **Stern LA**, **Quinlan S**, **Bennett PC**. 2004. Bacterial diversity and ecosystem function of filamentous microbial mats from aphotic (cave) sulfidic springs dominated by chemolithoautotrophic "*Epsilonproteobacteria*." FEMS Microbiol Ecol

51:31–53.
106. **Malik MA**, **Khan KS**, **Marschner P**. 2013. Microbial biomass , nutrient availability and nutrient uptake by wheat in two soils with organic amendments. J Soil Sci plant Nutr **13**:955–966.
107. **Shahot KM**, **Ekhmaj IA**. 2012. Evaluation Biofilm Sewage Treatment Plant. World Acad Sci Eng Technol **6**:268–271.
108. **Sehar S**, **Naz I**. 2016. Role of the Biofilms in Wastewater TreatmentMicrobial Biofilms - Importance and Applications. InTech.
109. **Abbasi U**, **Jin W**, **Pervez A**, **Bhatti ZA**, **Tariq M**, **Shaheen S**, **Iqbal A**, **Mahmood Q**. 2016. Anaerobic microbial fuel cell treating combined industrial wastewater: correlation of electricity generation with pollutants. Bioresour Technol **200**:1–7.
110. **Johnston CS**, **Gaas CA**. 2006. Vinegar: medicinal uses and antiglycemic effect. MedGenMed **8**:61.
111. **Qureshi N**, **Annous BA**, **Ezeji TC**, **Karcher P**, **Maddox IS**. 2005. Biofilm reactors for industrial bioconversion processes: employing potential of enhanced reaction rates. Microb Cell Fact **4**:24.
112. **Wang ZW**, **Chen S**. 2009. Potential of biofilm-based biofuel production. Appl Microbiol Biotechnol **83**:1–18.
113. **Galperin MY**, **Nikolskaya AN**, **Koonin EV**. 2001. Novel domains of the prokaryotic two-component signal transduction systems. FEMS Microbiol Lett **203**:11–21.
114. **Chou S-HSH**, **Galperin MYY**. 2016. Diversity of Cyclic Di-GMP-Binding Proteins and Mechanisms. J Bacteriol **198**:32–46.
115. **Burdette DL**, **Monroe KM**, **Sotelo-Troha K**, **Iwig JS**, **Eckert B**, **Hyodo M**, **Hayakawa Y**, **Vance RE**. 2011. STING is a direct innate immune sensor of cyclic di-GMP. Nature **478**:515–8.
116. **Wu J**, **Sun L**, **Chen X**, **Du F**, **Shi H**, **Chen C**, **Chen ZJ**. 2013. Cyclic GMP-AMP is an endogenous second messenger in innate immune signaling by cytosolic DNA. Science **339**:826–30.
117. **Sondermann H**, **Shikuma NJ**, **Yildiz FH**. 2012. You've come a long way: c-di-GMP signaling. Curr Opin Microbiol **15**:140–6.
118. **Abel S**, **Bucher T**, **Nicollier M**, **Hug I**, **Kaever V**, **Abel Zur Wiesch P**, **Jenal U**. 2013. Bi-modal distribution of the second messenger c-di-GMP controls cell fate and asymmetry during the *Caulobacter* cell cycle. PLoS Genet **9**:e1003744.
119. **Hobley L**, **Fung RKY**, **Lambert C**, **Harris MATS**, **Dabhi JM**, **King SS**, **Basford SM**, **Uchida K**, **Till R**, **Ahmad R**, **Aizawa SI**, **Gomelsky M**, **Sockett RE**. 2012. Discrete cyclic di-GMP-dependent control of bacterial predation versus axenic growth in *Bdellovibrio bacteriovorus*. PLoS Pathog **8**.
120. **Zhu B**, **Liu C**, **Liu S**, **Cong H**, **Chen Y**, **Gu L**, **Ma LZ**. 2016. Membrane association of SadC enhances its diguanylate cyclase activity to control exopolysaccharides synthesis and biofilm formation in *Pseudomonas aeruginosa*. Environ Microbiol **18**:3440–3452.
121. **Tagliabue L**, **Antoniani D**, **Maciag A**, **Bocci P**, **Raffaelli N**, **Landini P**. 2010. The diguanylate cyclase YddV controls production of the exopolysaccharide poly-N-acetylglucosamine (PNAG) through regulation of the PNAG biosynthetic *pgaABCD* operon. Microbiology **156**:2901–2911.
122. **Chan C**, **Paul R**, **Samoray D**, **Amiot NC**, **Giese B**, **Jenal U**, **Schirmer T**. 2004. Structural basis of activity and allosteric control of diguanylate cyclase. Proc Natl Acad Sci U S A **101**:17084–9.
123. **Zähringer F**, **Massa C**, **Schirmer T**. 2011. Efficient enzymatic production of the bacterial second messenger c-di-GMP by the diguanylate cyclase YdeH from *E. coli*. Appl Biochem Biotechnol **163**:71–9.
124. **Christen B**, **Christen M**, **Paul R**, **Schmid F**, **Folcher M**, **Jenoe P**, **Meuwly M**, **Jenal U**. 2006. Allosteric control of cyclic di-GMP signaling. J Biol Chem **281**:32015–24.
125. **Christen M**, **Christen B**, **Folcher M**, **Schauerte A**, **Jenal U**. 2005. Identification and characterization of a cyclic di-GMP-specific phosphodiesterase and its allosteric control by GTP. J Biol Chem **280**:30829–37.
126. **Deepthi A**, **Liew CW**, **Liang Z-X**, **Swaminathan K**, **Lescar J**. 2014. Structure of a

Diguanylate Cyclase from *Thermotoga maritima*: insights into Activation, Feedback Inhibition and Thermostability. PLoS One **9**:e110912.

127. **Wassmann P**, **Chan C**, **Paul R**, **Beck A**, **Heerklotz H**, **Jenal U**, **Schirmer T**. 2007. Structure of BeF3-modified response regulator PleD: implications for diguanylate cyclase activation, catalysis, and feedback inhibition. Structure **15**:915–27.
128. **Huangyutitham V**, **Guvener ZT**, **Harwood CS**. 2013. Subcellular Clustering of the Phosphorylated WspR Response Regulator Protein Stimulates Its Diguanylate Cyclase Activity. MBio **4**:e00242-13.
129. **De N**, **Navarro MVAS**, **Raghavan RV.**, **Sondermann H**. 2009. Determinants for the Activation and Autoinhibition of the Diguanylate Cyclase Response Regulator WspR. J Mol Biol **393**:619–633.
130. **Schmidt AJ**, **Ryjenkov DA**, **Gomelsky M**. 2005. The ubiquitous protein domain EAL is a cyclic diguanylate-specific phosphodiesterase: enzymatically active and inactive EAL domains. J Bacteriol **187**:4774–81.
131. **Tamayo R**, **Tischler AD**, **Camilli A**. 2005. The EAL domain protein VieA is a cyclic diguanylate phosphodiesterase. J Biol Chem **280**:33324–30.
132. **Ryan RP**, **Fouhy Y**, **Lucey JF**, **Crossman LC**, **Spiro S**, **He Y-W**, **Zhang L-H**, **Heeb S**, **Cámara M**, **Williams P**, **Dow JM**. 2006. Cell-cell signaling in *Xanthomonas campestris* involves an HD-GYP domain protein that functions in cyclic di-GMP turnover. Proc Natl Acad Sci U S A **103**:6712–7.
133. **Stelitano V**, **Giardina G**, **Paiardini A**, **Castiglione N**, **Cutruzzolà F**, **Rinaldo S**. 2013. C-di-GMP Hydrolysis by *Pseudomonas aeruginosa* HD-GYP Phosphodiesterases: Analysis of the Reaction Mechanism and Novel Roles for pGpG. PLoS One **8**:e74920.
134. **Stelitano V**, **Brandt A**, **Fernicola S**, **Franceschini S**, **Giardina G**, **Pica A**, **Rinaldo S**, **Sica F**, **Cutruzzolà F**. 2013. Probing the activity of diguanylate cyclases and c-di-GMP phosphodiesterases in real-time by CD spectroscopy. Nucleic Acids Res 1–9.
135. **Orr MW**, **Donaldson GP**, **Severin GB**, **Wang J**, **Sintim HO**, **Waters CM**, **Lee VT**. 2015. Oligoribonuclease is the primary degradative enzyme for pGpG in *Pseudomonas aeruginosa* that is required for cyclic-di-GMP turnover. Proc Natl Acad Sci **112**:E5048–E5057.
136. **Cohen D**, **Mechold U**, **Nevenzal H**, **Yarmiyhu Y**, **Randall TE**, **Bay DC**, **Rich JD**, **Parsek MR**, **Kaever V**, **Harrison JJ**, **Banin E**. 2015. Oligoribonuclease is a central feature of cyclic diguanylate signaling in *Pseudomonas aeruginosa*. Proc Natl Acad Sci **112**:11359–11364.
137. **Barends TRM**, **Hartmann E**, **Griese JJ**, **Beitlich T**, **Kirienko NV**, **Ryjenkov DA**, **Reinstein J**, **Shoeman RL**, **Gomelsky M**, **Schlichting I**. 2009. Structure and mechanism of a bacterial light-regulated cyclic nucleotide phosphodiesterase. Nature **459**:1015–1018.
138. **Rao F**, **Yang Y**, **Qi Y**, **Liang Z-X**. 2008. Catalytic Mechanism of Cyclic Di-GMP-Specific Phosphodiesterase: a Study of the EAL Domain-Containing RocR from *Pseudomonas aeruginosa*. J Bacteriol **190**:3622–3631.
139. **Winkler A**, **Udvarhelyi A**, **Hartmann E**, **Reinstein J**, **Menzel A**, **Shoeman RL**, **Schlichting I**. 2014. Characterization of elements involved in allosteric light regulation of phosphodiesterase activity by comparison of different functional BlrP1 states. J Mol Biol **426**:853–68.
140. **Sundriyal A**, **Massa C**, **Samoray D**, **Zehender F**, **Sharpe T**, **Jenal U**, **Schirmer T**. 2014. Inherent Regulation of EAL Domain-catalyzed Hydrolysis of Second Messenger Cyclic di-GMP. J Biol Chem **289**:6978–6990.
141. **Minasov G**, **Padavattan S**, **Shuvalova L**, **Brunzelle JS**, **Miller DJ**, **Basle A**, **Massa C**, **Collart FR**, **Schirmer T**, **Anderson WF**. 2009. Crystal Structures of YkuI and Its Complex with Second Messenger Cyclic Di-GMP Suggest Catalytic Mechanism of Phosphodiester Bond Cleavage by EAL Domains. J Biol Chem **284**:13174–13184.
142. **Tchigvintsev A**, **Xu X**, **Singer A**, **Chang C**, **Brown G**, **Proudfoot M**, **Cui H**, **Flick R**, **Anderson WF**, **Joachimiak A**, **Galperin MY**, **Savchenko A**, **Yakunin AF**. 2010. Structural Insight into the Mechanism of c-di-GMP Hydrolysis by EAL Domain Phosphodiesterases. J Mol Biol **402**:524–538.

143. **Rao F**, **Qi Y**, **Chong HS**, **Kotaka M**, **Li B**, **Li J**, **Lescar J**, **Tang K**, **Liang Z-X**. 2009. The functional role of a conserved loop in EAL domain-based cyclic di-GMP-specific phosphodiesterase. J Bacteriol **191**:4722–31.
144. **Schirmer T**, **Jenal U**. 2009. Structural and mechanistic determinants of c-di-GMP signalling. Nat Rev Microbiol **7**:724–35.
145. **Rinaldo S**, **Paiardini A**, **Stelitano V**, **Brunotti P**, **Cervoni L**, **Fernicola S**, **Protano C**, **Vitali M**, **Cutruzzolà F**, **Giardina G**. 2015. Structural Basis of Functional Diversification of the HD-GYP Domain Revealed by the *Pseudomonas aeruginosa* PA4781 Protein, Which Displays an Unselective Bimetallic Binding Site. J Bacteriol **197**:1525–1535.
146. **Bellini D**, **Caly DL**, **McCarthy Y**, **Bumann M**, **An S-Q**, **Dow JM**, **Ryan RP**, **Walsh MA**. 2014. Crystal structure of an HD-GYP domain cyclic-di-GMP phosphodiesterase reveals an enzyme with a novel trinuclear catalytic iron centre. Mol Microbiol **91**:26–38.
147. **Miner KD**, **Kurtz DM**. 2016. Active Site Metal Occupancy and Cyclic Di-GMP Phosphodiesterase Activity of *Thermotoga maritima* HD-GYP. Biochemistry **55**:970–979.
148. **Lovering AL**, **Capeness MJ**, **Lambert C**, **Hobley L**, **Sockett RE**. 2011. The Structure of an Unconventional HD-GYP Protein from *Bdellovibrio* Reveals the Roles of Conserved Residues in this Class of Cyclic-di-GMP Phosphodiesterases. MBio **2**:e00163-11.
149. **Römling U**, **Galperin MY**. 2015. Bacterial cellulose biosynthesis: diversity of operons, subunits, products, and functions. Trends Microbiol **23**:545–557.
150. **Seshasayee ASN**, **Fraser GM**, **Luscombe NM**. 2010. Comparative genomics of cyclic-di-GMP signalling in bacteria: post-translational regulation and catalytic activity. Nucleic Acids Res **38**:5970–81.
151. **Koestler BJ**, **Waters CM**. 2013. Exploring Environmental Control of Cyclic di-GMP Signaling in Vibrio cholerae by Using the Ex Vivo Lysate Cyclic di-GMP Assay (TELCA). Appl Environ Microbiol **79**:5233–5241.
152. **Sommerfeldt N**, **Possling A**, **Becker G**, **Pesavento C**, **Tschowri N**, **Hengge R**. 2009. Gene expression patterns and differential input into curli fimbriae regulation of all GGDEF/EAL domain proteins in *Escherichia coli*. Microbiology **155**:1318–1331.
153. **Reinders A**, **Hee C-S**, **Ozaki S**, **Mazur A**, **Boehm A**, **Schirmer T**, **Jenal U**. 2016. Expression and Genetic Activation of Cyclic Di-GMP-Specific Phosphodiesterases in *Escherichia coli*. J Bacteriol **198**:448–462.
154. **Ren GX**, **Fan S**, **Guo XP**, **Chen S**, **Sun YC**. 2016. Differential regulation of c-di-GMP metabolic enzymes by environmental signals modulates biofilm formation in *Yersinia pestis*. Front Microbiol **7**:1–12.
155. **Abel S**, **Chien P**, **Wassmann P**, **Schirmer T**, **Kaever V**, **Laub MT**, **Baker TA**, **Jenal U**. 2011. Regulatory cohesion of cell cycle and cell differentiation through interlinked phosphorylation and second messenger networks. Mol Cell **43**:550–60.
156. **Qi Y**, **Rao F**, **Luo Z**, **Liang Z-X**. 2009. A Flavin Cofactor-Binding PAS Domain Regulates c-di-GMP Synthesis in Ax DGC2 from *Acetobacter xylinum*. Biochemistry **48**:10275–10285.
157. **Lacey MM**, **Partridge JD**, **Green J**. 2010. *Escherichia coli* K-12 YfgF is an anaerobic cyclic di-GMP phosphodiesterase with roles in cell surface remodelling and the oxidative stress response. Microbiology **156**:2873–2886.
158. **Galperin MY**. 2004. Bacterial signal transduction network in a genomic perspective. Environ Microbiol **6**:552–67.
159. **Galperin MY**. 2006. Structural Classification of Bacterial Response Regulators: Diversity of Output Domains and Domain Combinations. J Bacteriol **188**:4169–4182.
160. **Nikolskaya AN**, **Mulkidjanian AY**, **Beech IB**, **Galperin MY**. 2003. MASE1 and MASE2: Two Novel Integral Membrane Sensory Domains. J Mol Microbiol Biotechnol **5**:11–16.
161. **Ho Y-SJ**, **Burden LM**, **Hurley JH**. 2000. Structure of the GAF domain, a ubiquitous signaling motif and a new class of cyclic GMP receptor. EMBO J **19**:5288–5299.
162. **Chang AL**, **Tuckerman JR**, **Gonzalez G**, **Mayer R**, **Weinhouse H**, **Volman G**, **Amikam D**, **Benziman M**, **Gilles-Gonzalez M-A**. 2001. Phosphodiesterase A1, a Regulator of Cellulose Synthesis in *Acetobacter xylinum*, is a Heme-Based Sensor. Biochemistry **40**:3420–3426.

163. **Henry JT**, **Crosson S**. 2011. Ligand-Binding PAS Domains in a Genomic, Cellular, and Structural Context. Annu Rev Microbiol **65**:261–286.
164. **Savakis P**, **De Causmaecker S**, **Angerer V**, **Ruppert U**, **Anders K**, **Essen L-O**, **Wilde A**. 2012. Light-induced alteration of c-di-GMP level controls motility of *Synechocystis* sp. PCC 6803. Mol Microbiol **85**:239–251.
165. **Enomoto G**, **Ni-Ni-Win**, **Narikawa R**, **Ikeuchi M**. 2015. Three cyanobacteriochromes work together to form a light color-sensitive input system for c-di-GMP signaling of cell aggregation. Proc Natl Acad Sci **112**:8082–8087.
166. **Rood KL**, **Clark NE**, **Stoddard PR**, **Garman SC**, **Chien P**. 2012. Adaptor-dependent degradation of a cell-cycle regulator uses a unique substrate architecture. Structure **20**:1223–32.
167. **Tarnawski M**, **Barends TRM**, **Schlichting I**. 2015. Structural analysis of an oxygen-regulated diguanylate cyclase. Acta Crystallogr Sect D Biol Crystallogr **71**:2158–2177.
168. **Wan X**, **Tuckerman JR**, **Saito JA**, **Freitas TAK**, **Newhouse JS**, **Denery JR**, **Galperin MY**, **Gonzalez G**, **Gilles-Gonzalez M-A**, **Alam M**. 2009. Globins Synthesize the Second Messenger Bis-(3′–5′)-Cyclic Diguanosine Monophosphate in Bacteria. J Mol Biol **388**:262–270.
169. **Sawai H**, **Yoshioka S**, **Uchida T**, **Hyodo M**, **Hayakawa Y**, **Ishimori K**, **Aono S**. 2010. Molecular oxygen regulates the enzymatic activity of a heme-containing diguanylate cyclase (HemDGC) for the synthesis of cyclic di-GMP. Biochim Biophys Acta **1804**:166–172.
170. **Burns JL**, **Douglas Deer D**, **Weinert EE**. 2014. Oligomeric state affects oxygen dissociation and diguanylate cyclase activity of globin coupled sensors. Mol BioSyst **10**:2823–2826.
171. **Liu N**, **Xu Y**, **Hossain S**, **Huang N**, **Coursolle D**, **Gralnick JA**, **Boon EM**. 2012. Nitric Oxide Regulation of Cyclic di-GMP Synthesis and Hydrolysis in *Shewanella woodyi*. Biochemistry **51**:2087–2099.
172. **Zschiedrich CP**, **Keidel V**, **Szurmant H**. 2016. Molecular Mechanisms of Two-Component Signal Transduction. J Mol Biol **428**:3752–3775.
173. **Kazmierczak BI**, **Lebron MB**, **Murray TS**. 2006. Analysis of FimX, a phosphodiesterase that governs twitching motility in *Pseudomonas aeruginosa*. Mol Microbiol **60**:1026–43.
174. **An S**, **Wu J**, **Zhang L-H**. 2010. Modulation of *Pseudomonas aeruginosa* Biofilm Dispersal by a Cyclic-Di-GMP Phosphodiesterase with a Putative Hypoxia-Sensing Domain. Appl Environ Microbiol **76**:8160–8173.
175. **Düvel J**, **Bertinetti D**, **Möller S**, **Schwede F**, **Morr M**, **Wissing J**, **Radamm L**, **Zimmermann B**, **Genieser H-G**, **Jänsch L**, **Herberg FW**, **Häussler S**. 2012. A chemical proteomics approach to identify c-di-GMP binding proteins in *Pseudomonas aeruginosa*. J Microbiol Methods **88**:229–36.
176. **Nesper J**, **Reinders A**, **Glatter T**, **Schmidt A**, **Jenal U**. 2012. A novel capture compound for the identification and analysis of cyclic di-GMP binding proteins. J Proteomics **75**:4874–8.
177. **Roelofs KG**, **Wang J**, **Sintim HO**, **Lee VT**. 2011. Differential radial capillary action of ligand assay for high-throughput detection of protein-metabolite interactions. Proc Natl Acad Sci U S A **108**:15528–33.
178. **Düvel J**, **Bense S**, **Möller S**, **Bertinetti D**, **Schwede F**, **Morr M**, **Eckweiler D**, **Genieser H-G**, **Jänsch L**, **Herberg FW**, **Frank R**, **Häussler S**. 2016. Application of Synthetic Peptide Arrays To Uncover Cyclic Di-GMP Binding Motifs. J Bacteriol **198**:138–146.
179. **Laventie B-J**, **Nesper J**, **Ahrné E**, **Glatter T**, **Schmidt A**, **Jenal U**. 2015. Capture Compound Mass Spectrometry - A Powerful Tool to Identify Novel c-di-GMP Effector Proteins. J Vis Exp e51404–e51404.
180. **Lee VT**, **Matewish JM**, **Kessler JL**, **Hyodo M**, **Hayakawa Y**, **Lory S**. 2007. A cyclic-di-GMP receptor required for bacterial exopolysaccharide production. Mol Microbiol **65**:1474–1484.
181. **Yang F**, **Tian F**, **Li X**, **Fan S**, **Chen H**, **Wu M**, **Yang C-H**, **He C**. 2014. The Degenerate EAL-GGDEF Domain Protein Filp Functions as a Cyclic di-GMP Receptor and Specifically Interacts with the PilZ-Domain Protein PXO_02715 to Regulate Virulence in

Xanthomonas oryzae pv. *oryzae*. Mol Plant-Microbe Interact **27**:578–589.

182. **Davis NJ**, **Cohen Y**, **Sanselicio S**, **Fumeaux C**, **Ozaki S**, **Luciano J**, **Guerrero-Ferreira RC**, **Wright ER**, **Jenal U**, **Viollier PH**. 2013. De- and repolarization mechanism of flagellar morphogenesis during a bacterial cell cycle. Genes Dev **27**:2049–62.
183. **Qi Y**, **Chuah MLC**, **Dong X**, **Xie K**, **Luo Z**, **Tang K**, **Liang Z-X**. 2011. Binding of cyclic diguanylate in the non-catalytic EAL domain of FimX induces a long-range conformational change. J Biol Chem **286**:2910–7.
184. **Fang X**, **Ahmad I**, **Blanka A**, **Schottkowski M**, **Cimdins A**, **Galperin MY**, **Römling U**, **Gomelsky M**. 2014. GIL, a new c-di-GMP binding protein domain involved in regulation of cellulose synthesis in enterobacteria. Mol Microbiol.
185. **Christen M**, **Christen B**, **Allan MG**, **Folcher M**, **Jenö P**, **Grzesiek S**, **Jenal U**. 2007. DgrA is a member of a new family of cyclic diguanosine monophosphate receptors and controls flagellar motor function in *Caulobacter crescentus*. Proc Natl Acad Sci U S A **104**:4112–7.
186. **Habazettl J**, **Allan MG**, **Jenal U**, **Grzesiek S**. 2011. Solution structure of the PilZ domain protein PA4608 complex with cyclic di-GMP identifies charge clustering as molecular readout. J Biol Chem **286**:14304–14.
187. **Yang F**, **Tian F**, **Chen H**, **Hutchins W**, **Yang C-H**, **He C**. 2015. The *Xanthomonas oryzae* pv. *oryzae* PilZ Domain Proteins Function Differentially in Cyclic di-GMP Binding and Regulation of Virulence and Motility. Appl Environ Microbiol **81**:4358–4367.
188. **Ryjenkov DA**, **Simm R**, **Römling U**, **Gomelsky M**. 2006. The PilZ Domain Is a Receptor for the Second Messenger c-di-GMP. J Biol Chem **281**:30310–30314.
189. **Morgan JLW**, **McNamara JT**, **Zimmer J**. 2014. Mechanism of activation of bacterial cellulose synthase by cyclic di-GMP. Nat Struct Mol Biol **21**:489–496.
190. **Merighi M**, **Lee VT**, **Hyodo M**, **Hayakawa Y**, **Lory S**. 2007. The second messenger bis-(3'-5')-cyclic-GMP and its PilZ domain-containing receptor Alg44 are required for alginate biosynthesis in *Pseudomonas aeruginosa*. Mol Microbiol **65**:876–95.
191. **Wilksch JJ**, **Yang J**, **Clements A**, **Gabbe JL**, **Short KR**, **Cao H**, **Cavaliere R**, **James CE**, **Whitchurch CB**, **Schembri MA**, **Chuah MLC**, **Liang Z-X**, **Wijburg OL**, **Jenney AW**, **Lithgow T**, **Strugnell RA**. 2011. MrkH, a Novel c-di-GMP-Dependent Transcriptional Activator, Controls *Klebsiella pneumoniae* Biofilm Formation by Regulating Type 3 Fimbriae Expression. PLoS Pathog **7**:e1002204.
192. **Alm RA**, **Bodero AJ**, **Free PD**, **Mattick JS**. 1996. Identification of a novel gene, *pilZ*, essential for type 4 fimbrial biogenesis in *Pseudomonas aeruginosa*. J Bacteriol **178**:46–53.
193. **Li T-N**, **Chin K-H**, **Fung K-M**, **Yang M-T**, **Wang AH-J**, **Chou S-H**. 2011. A Novel Tetrameric PilZ Domain Structure from *Xanthomonads*. PLoS One **6**:e22036.
194. **Wang Y-C**, **Chin K-H**, **Tu Z-L**, **He J**, **Jones CJ**, **Sanchez DZ**, **Yildiz FH**, **Galperin MY**, **Chou S-H**. 2016. Nucleotide binding by the widespread high-affinity cyclic di-GMP receptor MshEN domain. Nat Commun **7**:12481.
195. **Roelofs KG**, **Jones CJ**, **Helman SR**, **Shang X**, **Orr MW**, **Goodson JR**, **Galperin MY**, **Yildiz FH**, **Lee VT**. 2015. Systematic Identification of Cyclic-di-GMP Binding Proteins in *Vibrio cholerae* Reveals a Novel Class of Cyclic-di-GMP-Binding ATPases Associated with Type II Secretion Systems. PLOS Pathog **11**:e1005232.
196. **Tuckerman JR**, **Gonzalez G**, **Gilles-Gonzalez M-A**. 2011. Cyclic di-GMP activation of polynucleotide phosphorylase signal-dependent RNA processing. J Mol Biol **407**:633–9.
197. **Trampari E**, **Stevenson CEM**, **Little RH**, **Wilhelm T**, **Lawson DM**, **Malone JG**. 2015. Bacterial Rotary Export ATPases Are Allosterically Regulated by the Nucleotide Second Messenger Cyclic-di-GMP. J Biol Chem **290**:24470–24483.
198. **Yang J**, **Wilksch JJ**, **Tan JWH**, **Hocking DM**, **Webb CT**, **Lithgow T**, **Robins-Browne RM**, **Strugnell RA**. 2013. Transcriptional Activation of the *mrkA* Promoter of the *Klebsiella pneumoniae* Type 3 Fimbrial Operon by the c-di-GMP-Dependent MrkH Protein. PLoS One **8**:e79038.
199. **Hickman JW**, **Harwood CS**. 2008. Identification of FleQ from *Pseudomonas aeruginosa* as a c-di-GMP-responsive transcription factor. Mol Microbiol **69**:376–89.
200. **Li W**, **He ZG**. 2012. LtmA, a novel cyclic di-GMP-responsive activator, broadly regulates

the expression of lipid transport and metabolism genes in *Mycobacterium smegmatis*. Nucleic Acids Res **40**:11292–11307.

201. **Russell MH**, **Bible AN**, **Fang X**, **Gooding JR**, **Campagna SR**, **Gomelsky M**, **Alexandre G**. 2013. Integration of the second messenger c-di-GMP into the chemotactic signaling pathway. MBio **4**:e00001-13.
202. **Duerig A**, **Abel S**, **Folcher M**, **Nicollier M**, **Schwede T**, **Amiot N**, **Giese B**, **Jenal U**. 2009. Second messenger-mediated spatiotemporal control of protein degradation regulates bacterial cell cycle progression. Genes Dev **23**:93–104.
203. **Xu L**, **Xin L**, **Zeng Y**, **Yam JKH**, **Ding Y**, **Venkataramani P**, **Cheang QW**, **Yang X**, **Tang X**, **Zhang L-H**, **Chiam K-H**, **Yang L**, **Liang Z-X**. 2016. A cyclic di-GMP-binding adaptor protein interacts with a chemotaxis methyltransferase to control flagellar motor switching. Sci Signal **9**:ra102-ra102.
204. **Sudarsan N**, **Lee ER**, **Weinberg Z**, **Moy RH**, **Kim JN**, **Link KH**, **Breaker RR**. 2008. Riboswitches in eubacteria sense the second messenger cyclic di-GMP. Science **321**:411–3.
205. **Smith KD**, **Lipchock SV**, **Ames TD**, **Wang J**, **Breaker RR**, **Strobel SA**. 2009. Structural basis of ligand binding by a c-di-GMP riboswitch. Nat Struct Mol Biol **16**:1218–1223.
206. **Jones CJ**, **Utada A**, **Davis KR**, **Thongsomboon W**, **Zamorano Sanchez D**, **Banakar V**, **Cegelski L**, **Wong GCL**, **Yildiz FH**. 2015. C-di-GMP Regulates Motile to Sessile Transition by Modulating MshA Pili Biogenesis and Near-Surface Motility Behavior in *Vibrio cholerae*. PLOS Pathog **11**:e1005068.
207. **Lori C**, **Ozaki S**, **Steiner S**, **Böhm R**, **Abel S**, **Dubey BN**, **Schirmer T**, **Hiller S**, **Jenal U**. 2015. Cyclic di-GMP acts as a cell cycle oscillator to drive chromosome replication. Nature **523**:236–239.
208. **Navarro MVAS**, **Newell PD**, **Krasteva PV.**, **Chatterjee D**, **Madden DR**, **O'Toole GA**, **Sondermann H**. 2011. Structural Basis for c-di-GMP-Mediated Inside-Out Signaling Controlling Periplasmic Proteolysis. PLoS Biol **9**:e1000588.
209. **Pérez-Mendoza D**, **Sanjuán J**. 2016. Exploiting the commons: cyclic diguanylate regulation of bacterial exopolysaccharide production. Curr Opin Microbiol **30**:36–43.
210. **Ausmees N**, **Jonsson H**, **Höglund S**, **Ljunggren H**, **Lindberg M**. 1999. Structural and putative regulatory genes involved in cellulose synthesis in *Rhizobium leguminosarum* bv. *trifolii*. Microbiology **145**:1253–62.
211. **Castiblanco LF**, **Sundin GW**. 2016. Cellulose production, activated by cyclic di-GMP through BcsA and BcsZ, is a virulence factor and an essential determinant of the three-dimensional architectures of biofilms formed by *Erwinia amylovora* Ea1189. Mol Plant Pathol.
212. **Barak JD**, **Jahn CE**, **Gibson DL**, **Charkowski AO**. 2007. The Role of Cellulose and O-Antigen Capsule in the Colonization of Plants by *Salmonella enterica*. Mol Plant-Microbe Interact **20**:1083–1091.
213. **Ross P**, **Weinhouse H**, **Aloni Y**, **Michaeli D**, **Weinberger-Ohana P**, **Mayer R**, **Braun S**, **de Vroom E**, **van der Marel GA**, **van Boom JH**, **Benziman M**. 1987. Regulation of cellulose synthesis in *Acetobacter xylinum* by cyclic diguanylic acid. Nature **325**:279–281.
214. **Weinhouse H**, **Sapir S**, **Amikam D**, **Shilo Y**, **Volman G**, **Ohana P**, **Benziman M**. 1997. c-di-GMP-binding protein, a new factor regulating cellulose synthesis in *Acetobacter xylinum*. FEBS Lett **416**:207–11.
215. **Omadjela O**, **Narahari A**, **Strumillo J**, **Melida H**, **Mazur O**, **Bulone V**, **Zimmer J**. 2013. BcsA and BcsB form the catalytically active core of bacterial cellulose synthase sufficient for in vitro cellulose synthesis. Proc Natl Acad Sci **110**:17856–17861.
216. **Wong HC**, **Fear AL**, **Calhoon RD**, **Eichinger GH**, **Mayer R**, **Amikam D**, **Benziman M**, **Gelfand DH**, **Meade JH**, **Emerick AW**, **Bruner R**, **Ben-Bassat A**, **Tal R**. 1990. Genetic organization of the cellulose synthase operon in *Acetobacter xylinum*. Proc Natl Acad Sci **87**:8130–8134.
217. **Morgan JLW**, **Strumillo J**, **Zimmer J**. 2012. Crystallographic snapshot of cellulose synthesis and membrane translocation. Nature **493**:181–6.
218. **Amikam D**, **Galperin MY**. 2006. PilZ domain is part of the bacterial c-di-GMP binding

protein. Bioinformatics **22**:3–6.
219. **Solano C**, **Garcia B**, **Latasa C**, **Toledo-Arana A**, **Zorraquino V**, **Valle J**, **Casals J**, **Pedroso E**, **Lasa I**. 2009. Genetic reductionist approach for dissecting individual roles of GGDEF proteins within the c-di-GMP signaling network in *Salmonella*. Proc Natl Acad Sci **106**:7997–8002.
220. **Oglesby LL**, **Jain S**, **Ohman DE**. 2008. Membrane topology and roles of *Pseudomonas aeruginosa* Alg8 and Alg44 in alginate polymerization. Microbiology **154**:1605–15.
221. **Remminghorst U**, **Rehm BHA**. 2006. Alg44, a unique protein required for alginate biosynthesis in *Pseudomonas aeruginosa*. FEBS Lett **580**:3883–3888.
222. **Whitney JC**, **Whitfield GB**, **Marmont LS**, **Yip P**, **Neculai AM**, **Lobsanov YD**, **Robinson H**, **Ohman DE**, **Howell PL**. 2015. Dimeric c-di-GMP is required for post-translational regulation of alginate production in *Pseudomonas aeruginosa*. J Biol Chem **290**:12451–62.
223. **Rehman ZU**, **Wang Y**, **Moradali MF**, **Hay ID**, **Rehm BHA**. 2013. Insights into the Assembly of the Alginate Biosynthesis Machinery in *Pseudomonas aeruginosa*. Appl Environ Microbiol **79**:3264–3272.
224. **Hay ID**, **Remminghorst U**, **Rehm BHA**. 2009. MucR, a novel membrane-associated regulator of alginate biosynthesis in *Pseudomonas aeruginosa*. Appl Environ Microbiol **75**:1110–1120.
225. **Li Y**, **Heine S**, **Entian M**, **Sauer K**, **Frankenberg-Dinkel N**. 2013. NO-Induced Biofilm Dispersion in *Pseudomonas aeruginosa* Is Mediated by an MHYT Domain-Coupled Phosphodiesterase. J Bacteriol **195**:3531–3542.
226. **Baraquet C**, **Murakami K**, **Parsek MR**, **Harwood CS**. 2012. The FleQ protein from *Pseudomonas aeruginosa* functions as both a repressor and an activator to control gene expression from the pel operon promoter in response to c-di-GMP. Nucleic Acids Res **40**:7207–18.
227. **Su T**, **Liu S**, **Wang K**, **Chi K**, **Zhu D**, **Wei T**, **Huang Y**, **Guo L**, **Hu W**, **Xu S**, **Lin Z**, **Gu L**. 2015. The REC domain mediated dimerization is critical for FleQ from *Pseudomonas aeruginosa* to function as a c-di-GMP receptor and flagella gene regulator. J Struct Biol **192**:1–13.
228. **Matsuyama BY**, **Krasteva PV**, **Baraquet C**, **Harwood CS**, **Sondermann H**, **Navarro MVAS**. 2015. Mechanistic insights into c-di-GMP-dependent control of the biofilm regulator FleQ from *Pseudomonas aeruginosa*. Proc Natl Acad Sci U S A **113**:E209-18.
229. **Whitney JC**, **Colvin KM**, **Marmont LS**, **Robinson H**, **Parsek MR**, **Howell PL**. 2012. Structure of the Cytoplasmic Region of PelD, a Degenerate Diguanylate Cyclase Receptor That Regulates Exopolysaccharide Production in *Pseudomonas aeruginosa*. J Biol Chem **287**:23582–23593.
230. **Li Z**, **Chen J-H**, **Hao Y**, **Nair SK**. 2012. Structures of the PelD Cyclic Diguanylate Effector Involved in Pellicle Formation in *Pseudomonas aeruginosa* PAO1. J Biol Chem **287**:30191–30204.
231. **Merritt JH**, **Ha D-G**, **Cowles KN**, **Lu W**, **Morales DK**, **Rabinowitz J**, **Gitai Z**, **O'Toole GA**. 2010. Specific control of *Pseudomonas aeruginosa* surface-associated behaviors by two c-di-GMP diguanylate cyclases. MBio **1**:e00183-10.
232. **Bernier SP**, **Ha D-G**, **Khan W**, **Merritt JH**, **O'Toole GA**. 2011. Modulation of *Pseudomonas aeruginosa* surface-associated group behaviors by individual amino acids through c-di-GMP signaling. Res Microbiol **162**:680–688.
233. **Malone JG**, **Jaeger T**, **Spangler C**, **Ritz D**, **Spang A**, **Arrieumerlou C**, **Kaever V**, **Landmann R**, **Jenal U**. 2010. YfiBNR mediates cyclic di-GMP dependent small colony variant formation and persistence in *Pseudomonas aeruginosa*. PLoS Pathog **6**.
234. **Hickman JW**, **Tifrea DF**, **Harwood CS**. 2005. A chemosensory system that regulates biofilm formation through modulation of cyclic diguanylate levels. Proc Natl Acad Sci U S A **102**:14422–7.
235. **Kuchma SL**, **Brothers KM**, **Merritt JH**, **Liberati NT**, **Ausubel FM**, **O'Toole GA**. 2007. BifA, a cyclic-di-GMP phosphodiesterase, inversely regulates biofilm formation and swarming motility by *Pseudomonas aeruginosa* PA14. J Bacteriol **189**:8165–8178.
236. **Bush MJ**, **Tschowri N**, **Schlimpert S**, **Flärdh K**, **Buttner MJ**. 2015. C-di-GMP signalling

and the regulation of developmental transitions in streptomycetes. Nat Rev Microbiol **13**:749–760.

237. **Wang X**, **Preston JF**, **Romeo T**. 2004. The *pgaABCD* Locus of *Escherichia coli* Promotes the Synthesis of a Polysaccharide Adhesin Required for Biofilm Formation. J Bacteriol **186**:2724–2734.
238. **Mack D**. 1996. The intercellular adhesion involved in biofilm accumulation of *Staphylococcus epidermidis* is a linear [beta]-1,6-linked glycosaminoglycan: purification and structural analysis. J Bacteriol **178**:175–183.
239. **Itoh Y**, **Rice JD**, **Goller C**, **Pannuri A**, **Taylor J**, **Meisner J**, **Beveridge TJ**, **Preston JF**, **Romeo T**. 2008. Roles of *pgaABCD* genes in synthesis, modification, and export of the *Escherichia coli* biofilm adhesin poly-beta-1,6-N-acetyl-D-glucosamine. J Bacteriol **190**:3670–80.
240. **Tuckerman JR**, **Gonzalez G**, **Sousa EHS**, **Wan X**, **Saito JA**, **Alam M**, **Gilles-Gonzalez MA**. 2009. An oxygen-sensing diguanylate cyclase and phosphodiesterase couple for c-di-GMP control. Biochemistry **48**:9764–9774.
241. **Boehm A**, **Steiner S**, **Zaehringer F**, **Casanova A**, **Hamburger F**, **Ritz D**, **Keck W**, **Ackermann M**, **Schirmer T**, **Jenal U**. 2009. Second messenger signalling governs *Escherichia coli* biofilm induction upon ribosomal stress. Mol Microbiol **72**:1500–1516.
242. **Steiner S**, **Lori C**, **Boehm A**, **Jenal U**. 2012. Allosteric activation of exopolysaccharide synthesis through cyclic di-GMP-stimulated protein–protein interaction. EMBO J **32**:354–368.
243. **Liang Z-X**. 2015. The expanding roles of c-di-GMP in the biosynthesis of exopolysaccharides and secondary metabolites. Nat Prod Rep **32**:663–683.
244. **Pérez-Mendoza D**, **Rodríguez-Carvajal MÁ**, **Romero-Jiménez L**, **De Araujo Farias G**, **Lloret J**, **Gallegos MT**, **Sanjuán J**. 2015. Novel mixed-linkage β-glucan activated by c-di-GMP in *Sinorhizobium meliloti*. Proc Natl Acad Sci U S A **112**:E757–E765.
245. **Chen L-H**, **Köseoğlu VK**, **Güvener ZT**, **Myers-Morales T**, **Reed JM**, **D'Orazio SEF**, **Miller KW**, **Gomelsky M**. 2014. Cyclic di-GMP-dependent Signaling Pathways in the Pathogenic Firmicute *Listeria monocytogenes*. PLoS Pathog **10**:e1004301.
246. **Schmidt JM**. 1966. The Development of Cellular Stalks in Bacteria. J Cell Biol **28**:423–436.
247. **Poindexter JS**. 1981. The *Caulobacters*: ubiquitous unusual bacteria. Microbiol Rev **45**:123–179.
248. **Stove Poindexter JL**, **Cohen-Bazire G**. 1964. The fine structure of stalked bacteria belonging to the family Caulobacteraceae. J Cell Biol **23**:587–607.
249. **Tsang PH**, **Li G**, **Brun YV**, **Freund L Ben**, **Tang JX**. 2006. Adhesion of single bacterial cells in the micronewton range. Proc Natl Acad Sci U S A **103**:5764–8.
250. **Wagner JK**, **Setayeshgar S**, **Sharon LA**, **Reilly JP**, **Brun YV**. 2006. A nutrient uptake role for bacterial cell envelope extensions. Proc Natl Acad Sci **103**:11772–11777.
251. **Ireland MME**, **Karty JA**, **Quardokus EM**, **Reilly JP**, **Brun YV.** 2002. Proteomic analysis of the *Caulobacter crescentus* stalk indicates competence for nutrient uptake. Mol Microbiol **45**:1029–1041.
252. **Newton A**. 1972. Role of transcription in the temporal control of development in *Caulobacter crescentus* . Proc Natl Acad Sci U S A **69**:447–51.
253. **Stove JL**, **Stanier RY**. 1962. Cellular Differentiation in Stalked Bacteria. Nature **196**:1189–1192.
254. **Sommer JM**, **Newton A**. 1989. Turning off flagellum rotation requires the pleiotropic gene *pleD*: *pleA*, *pleC*, and *pleD* define two morphogenic pathways in *Caulobacter crescentus*. J Bacteriol **171**:392–401.
255. **Li G**, **Brown PJB**, **Tang JX**, **Xu J**, **Quardokus EM**, **Fuqua C**, **Brun YV**. 2012. Surface contact stimulates the just-in-time deployment of bacterial adhesins. Mol Microbiol **83**:41–51.
256. **Marczynski GT**. 1999. Chromosome methylation and measurement of faithful, once and only once per cell cycle chromosome replication in *Caulobacter crescentus*. J Bacteriol **181**:1984–1993.
257. **Fioravanti A**, **Fumeaux C**, **Mohapatra SS**, **Bompard C**, **Brilli M**, **Frandi A**, **Castric V**,

Villeret V, **Viollier PH**, **Biondi EG**. 2013. DNA Binding of the Cell Cycle Transcriptional Regulator GcrA Depends on N6-Adenosine Methylation in *Caulobacter crescentus* and Other Alphaproteobacteria. PLoS Genet **9**:e1003541.

258. **Panis G**, **Murray SR**, **Viollier PH**. 2015. Versatility of global transcriptional regulators in alpha-Proteobacteria: from essential cell cycle control to ancillary functions. FEMS Microbiol Rev **39**:120–133.
259. **Holtzendorff J**. 2004. Oscillating Global Regulators Control the Genetic Circuit Driving a Bacterial Cell Cycle. Science **304**:983–987.
260. **Quon KC**, **Marczynski GT**, **Shapiro L**. 1996. Cell cycle control by an essential bacterial two-component signal transduction protein. Cell **84**:83–93.
261. **Tan MH**, **Kozdon JB**, **Shen X**, **Shapiro L**, **McAdams HH**. 2010. An essential transcription factor, SciP, enhances robustness of *Caulobacter* cell cycle regulation. Proc Natl Acad Sci U S A **107**:18985–90.
262. **Zweiger G**, **Marczynski G**, **Shapiro L**. 1994. A *Caulobacter* DNA methyltransferase that functions only in the predivisional cell. J Mol Biol.
263. **Gorbatyuk B**, **Marczynski GT**. 2005. Regulated degradation of chromosome replication proteins DnaA and CtrA in *Caulobacter crescentus*. Mol Microbiol **55**:1233–45.
264. **Quon KC**, **Yang B**, **Domian IJ**, **Shapiro L**, **Marczynski GT**. 1998. Negative control of bacterial DNA replication by a cell cycle regulatory protein that binds at the chromosome origin. Proc Natl Acad Sci U S A **95**:120–5.
265. **Siam R**, **Marczynski GT**. 2000. Cell cycle regulator phosphorylation stimulates two distinct modes of binding at a chromosome replication origin. EMBO J **19**:1138–1147.
266. **Collier J**, **Murray SR**, **Shapiro L**. 2006. DnaA couples DNA replication and the expression of two cell cycle master regulators. EMBO J **25**:346–56.
267. **Taylor JA**, **Ouimet MC**, **Wargachuk R**, **Marczynski GT**. 2011. The *Caulobacter crescentus* chromosome replication origin evolved two classes of weak DnaA binding sites. Mol Microbiol **82**:312–326.
268. **Mott ML**, **Berger JM**. 2007. DNA replication initiation: mechanisms and regulation in bacteria. Nat Rev Microbiol **5**:343–354.
269. **Haakonsen DL**, **Yuan AH**, **Laub MT**. 2015. The bacterial cell cycle regulator GcrA is a σ 70 cofactor that drives gene expression from a subset of methylated promoters. Genes Dev **29**:2272–2286.
270. **Domian IJ**, **Quon KC**, **Shapiro L**. 1997. Cell type-specific phosphorylation and proteolysis of a transcriptional regulator controls the G1-to-S transition in a bacterial cell cycle. Cell **90**:415–24.
271. **Laub MT**, **Chen SL**, **Shapiro L**, **McAdams HH**. 2002. Genes directly controlled by CtrA, a master regulator of the *Caulobacter* cell cycle. Proc Natl Acad Sci **99**:4632–4637.
272. **Stephens CM**, **Zweiger G**, **Shapiro L**. 1995. Coordinate cell cycle control of a *Caulobacter* DNA methyltransferase and the flagellar genetic hierarchy. J Bacteriol **177**:1662–1669.
273. **Kozdon JB**, **Melfi MD**, **Luong K**, **Clark TA**, **Boitano M**, **Wang S**, **Zhou B**, **Gonzalez D**, **Collier J**, **Turner SW**, **Korlach J**, **Shapiro L**, **McAdams HH**. 2013. Global methylation state at base-pair resolution of the *Caulobacter* genome throughout the cell cycle. Proc Natl Acad Sci **110**:E4658–E4667.
274. **Gonzalez D**, **Kozdon JB**, **McAdams HH**, **Shapiro L**, **Collier J**. 2014. The functions of DNA methylation by CcrM in *Caulobacter crescentus*: a global approach. Nucleic Acids Res **42**:3720–3735.
275. **Collier J**, **McAdams HH**, **Shapiro L**. 2007. A DNA methylation ratchet governs progression through a bacterial cell cycle. Proc Natl Acad Sci **104**:17111–17116.
276. **Reisenauer A**. 2002. DNA methylation affects the cell cycle transcription of the CtrA global regulator in *Caulobacter*. EMBO J **21**:4969–4977.
277. **Wright R**, **Stephens C**, **Zweiger G**, **Shapiro L**, **Alley MR**. 1996. *Caulobacter* Lon protease has a critical role in cell-cycle control of DNA methylation. Genes Dev **10**:1532–1542.
278. **Murray SM**, **Panis G**, **Fumeaux C**, **Viollier PH**, **Howard M**. 2013. Computational and

Genetic Reduction of a Cell Cycle to Its Simplest, Primordial Components. PLoS Biol **11**.
279. **Gora KG**, **Tsokos CG**, **Chen YE**, **Srinivasan BS**, **Perchuk BS**, **Laub MT**. 2010. A cell-type-specific protein-protein interaction modulates transcriptional activity of a master regulator in *Caulobacter crescentus*. Mol Cell **39**:455–467.
280. **Li J**, **Bu P**, **Chen K-Y**, **Shen X**. 2013. Spatial perturbation with synthetic protein scaffold reveals robustness of asymmetric cell division. J Biomed Sci Eng **6**:134–143.
281. **Tropini C**, **Huang KC**. 2012. Interplay between the Localization and Kinetics of Phosphorylation in Flagellar Pole Development of the Bacterium *Caulobacter crescentus*. PLoS Comput Biol **8**:e1002602.
282. **Quiñones-Valles C**, **Sánchez-Osorio I**, **Martínez-Antonio A**. 2014. Dynamical Modeling of the Cell Cycle and Cell Fate Emergence in *Caulobacter crescentus*. PLoS One **9**:e111116.
283. **Collier J**. 2016. Cell cycle control in Alphaproteobacteria. Curr Opin Microbiol **30**:107–113.
284. **Lasker K**, **Mann TH**, **Shapiro L**. 2016. An intracellular compass spatially coordinates cell cycle modules in *Caulobacter crescentus*. Curr Opin Microbiol **33**:131–139.
285. **Vandecan Y**, **Biondi E**, **Blossey R**. 2016. Core-oscillator model of *Caulobacter crescentus*. Phys Rev E **93**:62413.
286. **Gonzalez D**, **Collier J**. 2015. Genomic Adaptations to the Loss of a Conserved Bacterial DNA Methyltransferase. MBio **6**:e00952-15.
287. **Biondi EG**, **Reisinger SJ**, **Skerker JM**, **Arif M**, **Perchuk BS**, **Ryan KR**, **Laub MT**. 2006. Regulation of the bacterial cell cycle by an integrated genetic circuit. Nature **444**:899–904.
288. **Hecht GB**, **Lane T**, **Ohta N**, **Sommer JM**, **Newton A**. 1995. An essential single domain response regulator required for normal cell division and differentiation in *Caulobacter crescentus*. EMBO J **14**:3915–3924.
289. **Jacobs C**, **Hung D**, **Shapiro L**. 2001. Dynamic localization of a cytoplasmic signal transduction response regulator controls morphogenesis during the *Caulobacter* cell cycle. Proc Natl Acad Sci **98**:4095–4100.
290. **Matroule J-Y**, **Lam H**, **Burnette DT**, **Jacobs-Wagner C**. 2004. Cytokinesis Monitoring during Development: Rapid Pole-to-Pole Shuttling of a Signaling Protein by Localized Kinase and Phosphatase in *Caulobacter*. Cell **118**:579–590.
291. **Ryan KR**, **Huntwork S**, **Shapiro L**. 2004. Recruitment of a cytoplasmic response regulator to the cell pole is linked to its cell cycle-regulated proteolysis. Proc Natl Acad Sci **101**:7415–7420.
292. **Lam H**, **Matroule J-Y**, **Jacobs-Wagner C**. 2003. The Asymmetric Spatial Distribution of Bacterial Signal Transduction Proteins Coordinates Cell Cycle Events. Dev Cell **5**:149–159.
293. **Wheeler RT**, **Shapiro L**. 1999. Differential Localization of Two Histidine Kinases Controlling Bacterial Cell Differentiation. Mol Cell **4**:683–694.
294. **Tsokos CG**, **Perchuk BS**, **Laub MT**. 2011. A Dynamic Complex of Signaling Proteins Uses Polar Localization to Regulate Cell-Fate Asymmetry in *Caulobacter crescentus*. Dev Cell **20**:329–341.
295. **Reisinger SJ**, **Huntwork S**, **Viollier PH**, **Ryan KR**. 2007. DivL Performs Critical Cell Cycle Functions in *Caulobacter crescentus* Independent of Kinase Activity. J Bacteriol **189**:8308–8320.
296. **Paul R**, **Jaeger T**, **Abel S**, **Wiederkehr I**, **Folcher M**, **Biondi EG**, **Laub MT**, **Jenal U**. 2008. Allosteric regulation of histidine kinases by their cognate response regulator determines cell fate. Cell **133**:452–61.
297. **Wu J**, **Ohta N**, **Newton A**. 1998. An essential, multicomponent signal transduction pathway required for cell cycle regulation in *Caulobacter*. Proc Natl Acad Sci U S A **95**:1443–1448.
298. **Iniesta AA**, **Shapiro L**. 2008. A bacterial control circuit integrates polar localization and proteolysis of key regulatory proteins with a phospho-signaling cascade. Proc Natl Acad Sci **105**:16602–16607.
299. **Lau J**, **Hernandez-Alicea L**, **Vass RH**, **Chien P**. 2015. A Phosphosignaling Adaptor

Primes the AAA+ Protease ClpXP to Drive Cell Cycle-Regulated Proteolysis. Mol Cell **59**:104–116.

300. **Joshi KK**, **Bergé M**, **Radhakrishnan SK**, **Viollier PH**, **Chien P**. 2015. An Adaptor Hierarchy Regulates Proteolysis during a Bacterial Cell Cycle. Cell **163**:419–431.
301. **Christen M**, **Kulasekara HD**, **Christen B**, **Kulasekara BR**, **Hoffman LR**, **Miller SI**. 2010. Asymmetrical distribution of the second messenger c-di-GMP upon bacterial cell division. Science **328**:1295–7.
302. **Paul R**, **Weiser S**, **Amiot NC**, **Chan C**, **Schirmer T**, **Giese B**, **Jenal U**. 2004. Cell cycle-dependent dynamic localization of a bacterial response regulator with a novel di-guanylate cyclase output domain. Genes Dev **18**:715–27.
303. **Aldridge P**, **Paul R**, **Goymer P**, **Rainey P**, **Jenal U**. 2003. Role of the GGDEF regulator PleD in polar development of *Caulobacter crescentus*. Mol Microbiol **47**:1695–708.
304. **Paul R**, **Abel S**, **Wassmann P**, **Beck A**, **Heerklotz H**, **Jenal U**. 2007. Activation of the diguanylate cyclase PleD by phosphorylation-mediated dimerization. J Biol Chem **282**:29170–7.
305. **Aldridge P**, **Jenal U**. 1999. Cell cycle-dependent degradation of a flagellar motor component requires a novel-type response regulator. Mol Microbiol **32**:379–91.
306. **Levi A**, **Jenal U**. 2006. Holdfast formation in motile swarmer cells optimizes surface attachment during *Caulobacter crescentus* development. J Bacteriol **188**:5315–8.
307. **Ardissone S**, **Viollier PH**. 2015. Interplay between flagellation and cell cycle control in *Caulobacter*. Curr Opin Microbiol **28**:83–92.
308. **Huitema E**, **Pritchard S**, **Matteson D**, **Radhakrishnan SK**, **Viollier PH**. 2006. Bacterial birth scar proteins mark future flagellum assembly site. Cell **124**:1025–37.
309. **Davis NJ**, **Viollier PH**. 2011. Probing flagellar promoter occupancy in wild-type and mutant *Caulobacter crescentus* by chromatin immunoprecipitation. FEMS Microbiol Lett **319**:146–152.
310. **Berne C**, **Ma X**, **Licata NA**, **Neves BRA**, **Setayeshgar S**, **Brun YV**, **Dragnea B**. 2013. Physiochemical properties of *Caulobacter crescentus* holdfast: a localized bacterial adhesive. J Phys Chem B **117**:10492–503.
311. **Merker RI**, **Smit J**. 1988. Characterization of the adhesive holdfast of marine and freshwater *Caulobacters*. Appl Environ Microbiol **54**:2078–85.
312. **Debray H**, **Decout D**, **Strecker G**, **Spik G**, **Montreul J**. 1981. Specificity of twelve lectins towards oligosaccharides and glycopeptides related to N-glycosylproteins. Eur J Biochem **117**:41–55.
313. **Li G**, **Smith CS**, **Brun YV**, **Tang JX**. 2005. The elastic properties of the *Caulobacter crescentus* adhesive holdfast are dependent on oligomers of N-acetylglucosamine. J Bacteriol **187**:257–65.
314. **Alipour-Assiabi E**, **Li G**, **Powers TR**, **Tang JX**. 2006. Fluctuation analysis of *Caulobacter crescentus* adhesion. Biophys J **90**:2206–12.
315. **Li G**, **Brun YV**, **Tang JX**. 2013. Holdfast spreading and thickening during *Caulobacter crescentus* attachment to surfaces. BMC Microbiol **13**:139.
316. **Hinz AJ**, **Larson DE**, **Smith CS**, **Brun YV**. 2003. The *Caulobacter crescentus* polar organelle development protein PodJ is differentially localized and is required for polar targeting of the PleC development regulator. Mol Microbiol **47**:929–41.
317. **Fiebig A**, **Herrou J**, **Fumeaux C**, **Radhakrishnan SK**, **Viollier PH**, **Crosson S**. 2014. A cell cycle and nutritional checkpoint controlling bacterial surface adhesion. PLoS Genet **10**:e1004101.
318. **Patel KB**, **Toh E**, **Fernandez XB**, **Hanuszkiewicz A**, **Hardy GG**, **Brun YV**, **Bernards MA**, **Valvano MA**. 2012. Functional characterization of UDP-glucose:undecaprenyl-phosphate glucose-1-phosphate transferases of *Escherichia coli* and *Caulobacter crescentus*. J Bacteriol **194**:2646–57.
319. **Ardissone S**, **Fumeaux C**, **Bergé M**, **Beaussart A**, **Théraulaz L**, **Radhakrishnan SK**, **Dufrêne YF**, **Viollier PH**. 2014. Cell cycle constraints on capsulation and bacteriophage susceptibility. Elife **3**:1–30.
320. **Erbel PJA**, **Barr K**, **Gao N**, **Gerwig GJ**, **Rick PD**, **Gardner KH**. 2003. Identification and Biosynthesis of Cyclic Enterobacterial Common Antigen in *Escherichia coli*. J Bacteriol

185:1995–2004.
321. **Zhang Y-H**, **Ginsberg C**, **Yuan Y**, **Walker S**. 2006. Acceptor substrate selectivity and kinetic mechanism of *Bacillus subtilis* TagA. Biochemistry **45**:10895–904.
322. **Wan Z**, **Brown PJB**, **Elliott EN**, **Brun YV**. 2013. The adhesive and cohesive properties of a bacterial polysaccharide adhesin are modulated by a deacetylase. Mol Microbiol **88**:486–500.
323. **Smith CS**, **Hinz A**, **Bodenmiller D**, **Larson DE**, **Brun YV**. 2003. Identification of genes required for synthesis of the adhesive holdfast in *Caulobacter crescentus*. J Bacteriol **185**:1432–42.
324. **Brown PJB**, **Hardy GG**, **Trimble MJ**, **Brun YV**. 2009. Complex regulatory pathways coordinate cell-cycle progression and development in *Caulobacter crescentus*. Adv Microb Physiol **54**:1–101.
325. **Cuthbertson L**, **Mainprize IL**, **Naismith JH**, **Whitfield C**. 2009. Pivotal roles of the outer membrane polysaccharide export and polysaccharide copolymerase protein families in export of extracellular polysaccharides in gram-negative bacteria. Microbiol Mol Biol Rev **73**:155–77.
326. **Javens J**, **Wan Z**, **Hardy GG**, **Brun YV**. 2013. Bypassing the need for subcellular localization of a polysaccharide export-anchor complex by overexpressing its protein subunits. Mol Microbiol.
327. **Dong C**, **Beis K**, **Nesper J**, **Brunkan-LaMontagne AL**, **Clarke BR**, **Whitfield C**, **Naismith JH**. 2006. Wza the translocon for *E. coli* capsular polysaccharides defines a new class of membrane protein. Nature **444**:226–229.
328. **Mitchell D**, **Smit J**. 1990. Identification of genes affecting production of the adhesion organelle of *Caulobacter crescentus* CB2. J Bacteriol **172**:5425–31.
329. **Kurtz HD**, **Smith J**. 1992. Analysis of a *Caulobacter crescentus* gene cluster involved in attachment of the holdfast to the cell. J Bacteriol **174**:687–94.
330. **Cole JL**, **Hardy GG**, **Bodenmiller D**, **Toh E**, **Hinz A**, **Brun YV.** 2003. The HfaB and HfaD adhesion proteins of *Caulobacter crescentus* are localized in the stalk. Mol Microbiol **49**:1671–83.
331. **Hardy GG**, **Allen RC**, **Toh E**, **Long M**, **Brown PJB**, **Cole-Tobian JL**, **Brun YV**. 2010. A localized multimeric anchor attaches the *Caulobacter* holdfast to the cell pole. Mol Microbiol **76**:409–27.
332. **Van Gerven N**, **Klein RD**, **Hultgren SJ**, **Remaut H**. 2015. Bacterial Amyloid Formation: Structural Insights into Curli Biogensis. Trends Microbiol **23**:693–706.
333. **Umbreit TH**, **Pate JL**. 1978. Characterization of the holdfast region of wild-type cells and holdfast mutants of *Asticcacaulis biprosthecum*. Arch Microbiol **118**:157–168.
334. **Ong CJ**, **Wong ML**, **Smit J**. 1990. Attachment of the adhesive holdfast organelle to the cellular stalk of *Caulobacter crescentus*. J Bacteriol **172**:1448–56.
335. **Bodenmiller D**, **Toh E**, **Brun YV**. 2004. Development of surface adhesion in *Caulobacter crescentus*. J Bacteriol **186**:1438–47.
336. **Janakiraman RS**, **Brun YV**. 1999. Cell cycle control of a holdfast attachment gene in *Caulobacter crescentus*. J Bacteriol **181**:1118–25.
337. **Purcell EB**, **Siegal-Gaskins D**, **Rawling DC**, **Fiebig A**, **Crosson S**. 2007. A photosensory two-component system regulates bacterial cell attachment. Proc Natl Acad Sci U S A **104**:18241–6.
338. **Eaton DS**, **Crosson S**, **Fiebig A**. 2016. Proper Control of *Caulobacter crescentus* Cell Surface Adhesion Requires the General Protein Chaperone DnaK. J Bacteriol **198**:2631–2642.
339. **Whiteley M**, **Bangera MG**, **Bumgarner RE**, **Parsek MR**, **Teitzel GM**, **Lory S**, **Greenberg EP**. 2001. Gene expression in *Pseudomonas aeruginosa* biofilms. Nature **413**:860–864.
340. **Ram RJ**, **VerBerkmoes NC**, **Thelen MP**, **Tyson GW**, **Baker BJ**, **Blake RC**, **Shah M**, **Hettich RL**, **Banfield JF**. 2005. Community proteomics of a natural microbial biofilm. Science **308**:1915–1920.
341. **van der Veen S**, **Abee T**. 2010. HrcA and DnaK are important for static and continuous-flow biofilm formation and disinfectant resistance in *Listeria monocytogenes*.

Microbiology **156**:3782–3790.
342. **Lemos JA**, **Luzardo Y**, **Burne RA**. 2007. Physiologic Effects of Forced Down-Regulation of *dnaK* and *groEL* Expression in *Streptococcus mutans*. J Bacteriol **189**:1582–1588.
343. **Singh VK**, **Syring M**, **Singh A**, **Singhal K**, **Dalecki A**, **Johansson T**. 2012. An insight into the significance of the DnaK heat shock system in *Staphylococcus aureus*. Int J Med Microbiol **302**:242–252.
344. **Arita-Morioka K**, **Yamanaka K**, **Mizunoe Y**, **Ogura T**, **Sugimoto S**. 2015. Novel Strategy for Biofilm Inhibition by Using Small Molecules Targeting Molecular Chaperone DnaK. Antimicrob Agents Chemother **59**:633–641.
345. **De Angelis M**, **Siragusa S**, **Campanella D**, **Di Cagno R**, **Gobbetti M**. 2015. Comparative proteomic analysis of biofilm and planktonic cells of *Lactobacillus plantarum* DB200. Proteomics **15**:2244–2257.
346. **Salah Ud-Din A**, **Tikhomirova A**, **Roujeinikova A**. 2016. Structure and Functional Diversity of GCN5-Related N-Acetyltransferases (GNAT). Int J Mol Sci **17**:1018.
347. **Brownell JE**, **Zhou J**, **Ranalli T**, **Kobayashi R**, **Edmondson DG**, **Roth SY**, **Allis CD**. 1996. Tetrahymena Histone Acetyltransferase A: A Homolog to Yeast Gcn5p Linking Histone Acetylation to Gene Activation. Cell **84**:843–851.
348. **Shen Y**, **Wei W**, **Zhou D-X**. 2015. Histone Acetylation Enzymes Coordinate Metabolism and Gene Expression. Trends Plant Sci **20**:614–621.
349. **Cain JA**, **Solis N**, **Cordwell SJ**. 2013. Beyond gene expression: the impact of protein post-translational modifications in bacteria. J Proteomics.
350. **Spange S**, **Wagner T**, **Heinzel T**, **Krämer OH**. 2009. Acetylation of non-histone proteins modulates cellular signalling at multiple levels. Int J Biochem Cell Biol **41**:185–198.
351. **Tucker AC**, **Escalante-Semerena JC**. 2013. Acetoacetyl-CoA synthetase activity is controlled by a protein acetyltransferase with unique domain organization in *Streptomyces lividans*. Mol Microbiol **87**:152–167.
352. **Llano-Sotelo B**, **Azucena EF**, **Kotra LP**, **Mobashery S**, **Chow CS**. 2002. Aminoglycosides Modified by Resistance Enzymes Display Diminished Binding to the Bacterial Ribosomal Aminoacyl-tRNA Site. Chem Biol **9**:455–463.
353. **He H**, **Ding Y**, **Bartlam M**, **Sun F**, **Le Y**, **Qin X**, **Tang H**, **Zhang R**, **Joachimiak A**, **Liu J**, **Zhao N**, **Rao Z**. 2003. Crystal Structure of Tabtoxin Resistance Protein Complexed with Acetyl Coenzyme A Reveals the Mechanism for β-Lactam Acetylation. J Mol Biol **325**:1019–1030.
354. **Marek ET**, **Dickson RC**. 1987. Cloning and characterization of *Saccharomyces cerevisiae* genes that confer L-methionine sulfoximine and tabtoxin resistance. J Bacteriol **169**:2440–8.
355. **Novikova M**, **Kazakov T**, **Vondenhoff GH**, **Semenova E**, **Rozenski J**, **Metlytskaya A**, **Zukher I**, **Tikhonov A**, **Van Aerschot A**, **Severinov K**. 2010. MccE Provides Resistance to Protein Synthesis Inhibitor Microcin C by Acetylating the Processed Form of the Antibiotic. J Biol Chem **285**:12662–12669.
356. **Agarwal V**, **Metlitskaya A**, **Severinov K**, **Nair SK**. 2011. Structural Basis for Microcin C7 Inactivation by the MccE Acetyltransferase. J Biol Chem **286**:21295–21303.
357. **Montemayor EJ**, **Hoffman DW**. 2008. The Crystal Structure of Spermidine/Spermine N 1 -Acetyltransferase in Complex with Spermine Provides Insights into Substrate Binding and Catalysis. Biochemistry **47**:9145–9153.
358. **Pegg AE**. 2008. Spermidine/spermine- N 1 -acetyltransferase: a key metabolic regulator. Am J Physiol - Endocrinol Metab **294**:E995–E1010.
359. **Nasuno R**, **Hirano Y**, **Itoh T**, **Hakoshima T**, **Hibi T**, **Takagi H**. 2013. Structural and functional analysis of the yeast N-acetyltransferase Mpr1 involved in oxidative stress tolerance via proline metabolism. Proc Natl Acad Sci **110**:11821–11826.
360. **Mio T**, **Yamada-Okabe T**, **Arisawa M**, **Yamada-Okabe H**. 1999. *Saccharomyces cerevisiae* GNA1, an essential gene encoding a novel acetyltransferase involved in UDP-N-acetylglucosamine synthesis. J Biol Chem **274**:424–9.
361. **Vetting MW**, **S de Carvalho LP**, **Yu M**, **Hegde SS**, **Magnet S**, **Roderick SL**, **Blanchard JS**. 2005. Structure and functions of the GNAT superfamily of acetyltransferases. Arch

Biochem Biophys **433**:212–26.
362. **Ramos-Morales F**, **Prieto AI**, **Beuzo CR**, **Holden DW**. 2003. Role for *Salmonella enterica* Enterobacterial Common Antigen in Bile Resistance and Virulence **185**:5328–5332.
363. **Vetting MW**, **Errey JC**, **Blanchard JS**. 2008. Rv0802c from *Mycobacterium tuberculosis*: the first structure of a succinyltransferase with the GNAT fold. Acta Crystallogr Sect F Struct Biol Cryst Commun **64**:978–85.
364. **Martin DDO**, **Beauchamp E**, **Berthiaume LG**. 2011. Post-translational myristoylation: fat matters in cellular life and death. Biochimie **93**:18–31.
365. **Bhatnagar RS**, **Fütterer K**, **Farazi TA**, **Korolev S**, **Murray CL**, **Jackson-Machelski E**, **Gokel GW**, **Gordon JI**, **Waksman G**. 1998. Structure of N-myristoyltransferase with bound myristoylCoA and peptide substrate analogs. Nat Struct Biol **5**:1091–7.
366. **Farazi TA**, **Waksman G**, **Gordon JI**. 2001. Structures of *Saccharomyces cerevisiae* N-myristoyltransferase with bound myristoylCoA and peptide provide insights about substrate recognition and catalysis. Biochemistry **40**:6335–43.
367. **Biarrotte-Sorin S**, **Maillard AP**, **Delettré J**, **Sougakoff W**, **Arthur M**, **Mayer C**. 2004. Crystal structures of *Weissella viridescens* FemX and its complex with UDP-MurNAc-pentapeptide: insights into FemABX family substrates recognition. Structure **12**:257–67.
368. **Plapp R**, **Strominger JL**. 1970. Biosynthesis of the peptidoglycan of bacterial cell walls. 18 Purification and properties of L-alanyl transfer ribonucleic acid-uridine diphosphate-N-acetylmuramyl-pentapeptide transferase from *Lactobacillus viridescens*. J Biol Chem **245**:3675–82.
369. **de Jonge BL**, **Sidow T**, **Chang YS**, **Labischinski H**, **Berger-Bachi B**, **Gage DA**, **Tomasz A**. 1993. Altered muropeptide composition in *Staphylococcus aureus* strains with an inactivated *femA locus*. J Bacteriol **175**:2779–82.
370. **Vetting MW**, **Roderick SL**, **Yu M**, **Blanchard JS**. 2003. Crystal structure of mycothiol synthase (Rv0819) from *Mycobacterium tuberculosis* shows structural homology to the GNAT family of N-acetyltransferases. Protein Sci **12**:1954–9.
371. **Angus-Hill ML**, **Dutnall RN**, **Tafrov ST**, **Sternglanz R**, **Ramakrishnan V**. 1999. Crystal structure of the histone acetyltransferase Hpa2: a tetrameric member of the Gcn5-related N-acetyltransferase superfamily. J Mol Biol **294**:1311–25.
372. **Chen W**, **Biswas T**, **Porter VR**, **Tsodikov OV**, **Garneau-Tsodikova S**. 2011. Unusual regioversatility of acetyltransferase Eis, a cause of drug resistance in XDR-TB. Proc Natl Acad Sci U S A **108**:9804–9808.
373. **Scheibner KA**, **De Angelis J**, **Burley SK**, **Cole PA**. 2002. Investigation of the Roles of Catalytic Residues in Serotonin N-Acetyltransferase. J Biol Chem **277**:18118–18126.
374. **Weston SA**, **Camble R**, **Colls J**, **Rosenbrock G**, **Taylor I**, **Egerton M**, **Tucker AD**, **Tunnicliffe A**, **Mistry A**, **Mancia F**, **de la Fortelle E**, **Irwin J**, **Bricogne G**, **Pauptit RA**. 1998. Crystal structure of the anti-fungal target N-myristoyl transferase. Nat Struct Biol **5**:213–21.
375. **Benson TE**, **Prince DB**, **Mutchler VT**, **Curry KA**, **Ho AM**, **Sarver RW**, **Hagadorn JC**, **Choi GH**, **Garlick RL**. 2002. X-ray crystal structure of *Staphylococcus aureus* FemA. Structure **10**:1107–15.
376. **Iqbal A**, **Arunlanantham H**, **Brown T**, **Chowdhury R**, **Clifton IJ**, **Kershaw NJ**, **Hewitson KS**, **McDonough MA**, **Schofield CJ**. 2010. Crystallographic and mass spectrometric analyses of a tandem GNAT protein from the clavulanic acid biosynthesis pathway. Proteins **78**:1398–407.
377. **Favrot L**, **Blanchard JS**, **Vergnolle O**. 2016. Bacterial GCN5-Related N -Acetyltransferases: From Resistance to Regulation. Biochemistry **55**:989–1002.
378. **Ton-That H**, **Labischinski H**, **Berger-Bächi B**, **Schneewind O**. 1998. Anchor structure of staphylococcal surface proteins. III. Role of the FemA, FemB, and FemX factors in anchoring surface proteins to the bacterial cell wall. J Biol Chem **273**:29143–9.
379. **Fonvielle M**, **Li de La Sierra-Gallay I**, **El-Sagheer AH**, **Lecerf M**, **Patin D**, **Mellal D**, **Mayer C**, **Blanot D**, **Gale N**, **Brown T**, **van Tilbeurgh H**, **Ethève-Quelquejeu M**, **Arthur M**. 2013. The Structure of $FemX_{Wv}$ in Complex with a Peptidyl-RNA Conjugate:

Mechanism of Aminoacyl Transfer from Ala-tRNA^{Ala} to Peptidoglycan Precursors. Angew Chemie Int Ed **52**:7278–7281.

380. **Rohrer S**, **Ehlert K**, **Tschierske M**, **Labischinski H**, **Berger-Bächi B**. 1999. The essential *Staphylococcus aureus* gene *fmhB* is involved in the first step of peptidoglycan pentaglycine interpeptide formation. Proc Natl Acad Sci U S A **96**:9351–6.
381. **Cheverton AM**, **Gollan B**, **Przydacz M**, **Wong CT**, **Mylona A**, **Hare SA**, **Helaine S**. 2016. A *Salmonella* Toxin Promotes Persister Formation through Acetylation of tRNA. Mol Cell **63**:86–96.
382. **Helaine S**, **Kugelberg E**. 2014. Bacterial persisters: formation, eradication, and experimental systems. Trends Microbiol **22**:417–424.
383. **Sprecher KS**. 2013. Characterization of a Novel c-di-GMP Effector Involved in *Caulobacter crescentus* Surface Adhesion. University of Basel.
384. **Thormann KM**, **Saville RM**, **Shukla S**, **Spormann AM**. 2005. Induction of Rapid Detachment in *Shewanella oneidensis* MR-1 Biofilms. J Bacteriol **187**:1014–1021.
385. **Sauer K**, **Cullen MC**, **Rickard AH**, **Zeef LAH**, **Davies DG**, **Gilbert P**. 2004. Characterization of Nutrient-Induced Dispersion in *Pseudomonas aeruginosa* PAO1 Biofilm. J Bacteriol **186**:7312–7326.
386. **Jenal U**, **Reinders A**, **Lori C**. 2017. Cyclic di-GMP: second messenger extraordinaire. Nat Rev Microbiol.
387. **Boehm A**, **Kaiser M**, **Li H**, **Spangler C**, **Kasper CA**, **Ackermann M**, **Kaever V**, **Sourjik V**, **Roth V**, **Jenal U**. 2010. Second messenger-mediated adjustment of bacterial swimming velocity. Cell **141**:107–16.
388. **Monds RD**, **Newell PD**, **Gross RH**, **O'Toole GA**. 2007. Phosphate-dependent modulation of c-di-GMP levels regulates *Pseudomonas fluorescens* Pf0-1 biofilm formation by controlling secretion of the adhesin LapA. Mol Microbiol **63**:656–79.
389. **Morgan JLW**, **McNamara JT**, **Fischer M**, **Rich J**, **Chen H-M**, **Withers SG**, **Zimmer J**. 2016. Observing cellulose biosynthesis and membrane translocation in crystallo. Nature **531**:329–334.
390. **Söding J**, **Biegert A**, **Lupas AN**. 2005. The HHpred interactive server for protein homology detection and structure prediction. Nucleic Acids Res **33**:W244-8.
391. **Abraham WR**, **Strömpl C**, **Vancanneyt M**, **Bennasar A**, **Swings J**, **Lünsdorf H**, **Smit J**, **Moore ERB**. 2004. *Woodsholea maritima* gen. nov., sp. nov., a marine bacterium with a low diversity of polar lipids. Int J Syst Evol Microbiol **54**:1227–1234.
392. **Potthoff E**, **Ossola D**, **Zambelli T**, **Vorholt JA**. 2015. Bacterial adhesion force quantification by fluidic force microscopy. Nanoscale **7**:4070–4079.
393. **Guillaume-Gentil O**, **Potthoff E**, **Ossola D**, **Franz CM**, **Zambelli T**, **Vorholt JA**. 2014. Force-controlled manipulation of single cells: from AFM to FluidFM. Trends Biotechnol **32**:381–388.
394. **Ozaki S**, **Schalch-Moser A**, **Zumthor L**, **Manfredi P**, **Ebbensgaard A**, **Schirmer T**, **Jenal U**. 2014. Activation and polar sequestration of PopA, a c-di-GMP effector protein involved in *Caulobacter crescentus* cell cycle control. Mol Microbiol **94**:580–594.
395. **Fang G**, **Passalacqua KD**, **Hocking J**, **Llopis P**, **Gerstein M**, **Bergman NH**, **Jacobs-Wagner C**. 2013. Transcriptomic and phylogenetic analysis of a bacterial cell cycle reveals strong associations between gene co-expression and evolution. BMC Genomics **14**:450.
396. **Yu NY**, **Wagner JR**, **Laird MR**, **Melli G**, **Rey S**, **Lo R**, **Dao P**, **Sahinalp SC**, **Ester M**, **Foster LJ**, **Brinkman FSL**. 2010. PSORTb 3.0: improved protein subcellular localization prediction with refined localization subcategories and predictive capabilities for all prokaryotes. Bioinformatics **26**:1608–1615.
397. **Speers AE**, **Wu CC**. 2007. Proteomics of Integral Membrane Proteins-Theory and Application. Chem Rev **107**:3687–3714.
398. **Jenal U**, **Malone J**. 2006. Mechanisms of cyclic-di-GMP signaling in bacteria. Annu Rev Genet **40**:385–407.
399. **Hegde SS**, **Shrader TE**. 2001. FemABX family members are novel nonribosomal peptidyltransferases and important pathogen-specific drug targets. J Biol Chem **276**:6998–7003.

400. **Craney A**, **Tahlan K**, **Andrews D**, **Nodwell J**. 2011. Bacterial transmembrane proteins that lack N-terminal signal sequences. PLoS One **6**.
401. **Jenal U**, **Shapiro L**. 1996. Cell cycle-controlled proteolysis of a flagellar motor protein that is asymmetrically distributed in the *Caulobacter* predivisional cell. EMBO J **15**:2393–406.
402. **Gustafsson MG**. 2000. Surpassing the lateral resolution limit by a factor of two using structured illumination microscopy. J Microsc **198**:82–7.
403. **Schermelleh L**, **Carlton PM**, **Haase S**, **Shao L**, **Winoto L**, **Kner P**, **Burke B**, **Cardoso MC**, **Agard DA**, **Gustafsson MGL**, **Leonhardt H**, **Sedat JW**. 2008. Subdiffraction multicolor imaging of the nuclear periphery with 3D structured illumination microscopy. Science **320**:1332–6.
404. **Schindelin J**, **Arganda-Carreras I**, **Frise E**, **Kaynig V**, **Longair M**, **Pietzsch T**, **Preibisch S**, **Rueden C**, **Saalfeld S**, **Schmid B**, **Tinevez J-Y**, **White DJ**, **Hartenstein V**, **Eliceiri K**, **Tomancak P**, **Cardona A**. 2012. Fiji: an open-source platform for biological-image analysis. Nat Methods **9**:676–682.
405. **Paintdakhi A**, **Parry B**, **Campos M**, **Irnov I**, **Elf J**, **Surovtsev I**, **Jacobs-Wagner C**. 2015. Oufti: an integrated software package for high-accuracy, high-throughput quantitative microscopy analysis. Mol Microbiol 1–11.
406. **Deshpande S**, **Pfohl T**. 2012. Hierarchical self-assembly of actin in micro-confinements using microfluidics. Biomicrofluidics **6**:34120.
407. **Schneider CA**, **Rasband WS**, **Eliceiri KW**. 2012. NIH Image to ImageJ: 25 years of image analysis. Nat Methods **9**:671–5.
408. **Grüter RR**, **Vörös J**, **Zambelli T**. 2013. FluidFM as a lithography tool in liquid: spatially controlled deposition of fluorescent nanoparticles. Nanoscale **5**:1097–1104.
409. **Potthoff E**, **Guillaume-Gentil O**, **Ossola D**, **Polesel-Maris J**, **LeibundGut-Landmann S**, **Zambelli T**, **Vorholt JA**. 2012. Rapid and serial quantification of adhesion forces of yeast and Mammalian cells. PLoS One **7**:e52712.
410. **Huang N-P**, **Michel R**, **Voros J**, **Textor M**, **Hofer R**, **Rossi A**, **Elbert DL**, **Hubbell JA**, **Spencer ND**. 2001. Poly(l-lysine)-g-poly(ethylene glycol) Layers on Metal Oxide Surfaces: Surface-Analytical Characterization and Resistance to Serum and Fibrinogen Adsorption. Langmuir **17**:489–498.
411. **Sader JE**, **Chon JWM**, **Mulvaney P**. 1999. Calibration of rectangular atomic force microscope cantilevers. Rev Sci Instrum **70**:3967–3969.
412. **Spangler C**, **Böhm A**, **Jenal U**, **Seifert R**, **Kaever V**. 2010. A liquid chromatography-coupled tandem mass spectrometry method for quantitation of cyclic di-guanosine monophosphate. J Microbiol Methods **81**:226–231.
413. **Johnson M**, **Zaretskaya I**, **Raytselis Y**, **Merezhuk Y**, **McGinnis S**, **Madden TL**. 2008. NCBI BLAST: a better web interface. Nucleic Acids Res **36**:W5-9.
414. **Alva V**, **Nam S-Z**, **Söding J**, **Lupas AN**. 2016. The MPI bioinformatics toolkit as an integrative platform for advanced protein sequence and structure analysis. Nucleic Acids Res **44**:W410–W415.
415. **Hildebrand A**, **Remmert M**, **Biegert A**, **Söding J**. 2009. Fast and accurate automatic structure prediction with HHpred. Proteins Struct Funct Bioinforma **77**:128–132.
416. **Edgar RC**. 2004. MUSCLE: multiple sequence alignment with high accuracy and high throughput. Nucleic Acids Res **32**:1792–7.
417. **Ely B**. 1991. Genetics of *Caulobacter crescentus*, p. 372–384. *In* Methods in Enzymology.
418. **Thanbichler M**, **Iniesta AA**, **Shapiro L**. 2007. A comprehensive set of plasmids for vanillate- and xylose-inducible gene expression in *Caulobacter crescentus*. Nucleic Acids Res **35**:e137.
419. **Khan SR**, **Gaines J**, **Roop RM**, **Farrand SK**. 2008. Broad-Host-Range Expression Vectors with Tightly Regulated Promoters and Their Use To Examine the Influence of TraR and TraM Expression on Ti Plasmid Quorum Sensing. Appl Environ Microbiol **74**:5053–5062.
420. **Hanahan D**. 1983. Studies on transformation of *Escherichia coli* with plasmids. J Mol Biol **166**:557–80.
421. **Simon R**, **Priefer U**, **Pühler A**. 1983. A broad host range mobilizationsystem for in vivo

genetic engineering: transposon mutagenesis in gram negative bacteria. Bio/Technology **1**:784–791.

422. **Evinger M**, **Agabian N**. 1977. Envelope-associated nucleoid from *Caulobacter crescentus* stalked and swarmer cells. J Bacteriol **132**:294–301.
423. **Schmidt JM**, **Stanier RY**. 1965. Isolation and Characterization of Bacteriophages Active against Stalked Bacteria. J Gen Microbiol **39**:95–107.
424. **Ely B**, **Johnson RC**. 1977. Generalized transduction in *Caulobacter crescentus*. Genetics **87**:391–399.
425. **Kim H-K**, **Kaang B-K**. 1998. Truncated green fluorescent protein mutants and their expression in Aplysia neurons. Brain Res Bull **47**:35–41.
426. **Drozdetskiy A**, **Cole C**, **Procter J**, **Barton GJ**. 2015. JPred4: a protein secondary structure prediction server. Nucleic Acids Res **43**:W389-94.
427. **Pei J**, **Kim B-H**, **Grishin N V.** 2008. PROMALS3D: a tool for multiple protein sequence and structure alignments. Nucleic Acids Res **36**:2295–2300.
428. **Levi A**. 2007. Genetic dissection of *Caulobacter crescentus* surface colonization. University of Basel.
429. **Kovach ME**, **Elzer PH**, **Hill DS**, **Robertson GT**, **Farris MA**, **Roop RM**, **Peterson KM**. 1995. Four new derivatives of the broad-host-range cloning vector pBBR1MCS, carrying different antibiotic-resistance cassettes. Gene **166**:175–6.
430. **Spiers AJ**, **Bohannon J**, **Gehrig SM**, **Rainey PB**. 2003. Biofilm formation at the air-liquid interface by the *Pseudomonas fluorescens* SBW25 wrinkly spreader requires an acetylated form of cellulose. Mol Microbiol **50**:15–27.
431. **Berry DS**, **Lynn F**, **Lee C-H**, **Frasch CE**, **Bash MC**. 2002. Effect of O acetylation of *Neisseria meningitidis* serogroup A capsular polysaccharide on development of functional immune responses. Infect Immun **70**:3707–13.
432. **Tielen P**, **Strathmann M**, **Jaeger KE**, **Flemming HC**, **Wingender J**. 2005. Alginate acetylation influences initial surface colonization by mucoid *Pseudomonas aeruginosa*. Microbiol Res **160**:165–176.
433. **Whitfield C**. 2006. Biosynthesis and assembly of capsular polysaccharides in *Escherichia coli*. Annu Rev Biochem **75**:39–68.
434. **Wenzel CQ**, **Daniels C**, **Keates RAB**, **Brewer D**, **Lam JS**. 2005. Evidence that WbpD is an N-acetyltransferase belonging to the hexapeptide acyltransferase superfamily and an important protein for O-antigen biosynthesis in *Pseudomonas aeruginosa* PAO1. Mol Microbiol **57**:1288–303.
435. **Glucksmann MA**, **Reuber TL**, **Walker GC**. 1993. Genes needed for the modification, polymerization, export, and processing of succinoglycan by *Rhizobium meliloti*: a model for succinoglycan biosynthesis. J Bacteriol **175**:7045–55.
436. **Deszo EL**, **Steenbergen SM**, **Freedberg DI**, **Vimr ER**. 2005. *Escherichia coli* K1 polysialic acid O-acetyltransferase gene, *neuO*, and the mechanism of capsule form variation involving a mobile contingency locus. Proc Natl Acad Sci **102**:5564–5569.
437. **Fong JCN**, **Syed KA**, **Klose KE**, **Yildiz FH**. 2010. Role of *Vibrio* polysaccharide (*vps*) genes in VPS production, biofilm formation and Vibrio cholerae pathogenesis. Microbiology **156**:2757–2769.
438. **Vollmer W**, **Blanot D**, **de Pedro MA**. 2008. Peptidoglycan structure and architecture. FEMS Microbiol Rev **32**:149–67.
439. **Shinohara K**, **Sugii Y**, **Aota A**, **Hibara A**, **Tokeshi M**, **Kitamori T**, **Okamoto K**. 2004. High-speed micro-PIV measurements of transient flow in microfluidic devices. Meas Sci Technol **15**:1965–1970.
440. **Ryan JA**. 2008. Evolution of Cell Culture Surfaces. BioFiles **3**:21–24.
441. **Behrens SH**, **Grier DG**. 2001. The charge of glass and silica surfaces. J Chem Phys **115**:6716–6721.
442. **Matthysse AG**, **Thomas DL**, **White AR**, **White S**, **Lightfoot R**, **Thomas DL**, **White AR**, **White S**, **Lightfoot R**. 1995. Genes required for cellulose synthesis in *Agrobacterium tumefaciens*. J Bacteriol **177**:1069–75.
443. **Matthysse AG**, **Thomas DL**, **White AR**. 1995. Mechanism of cellulose synthesis in *Agrobacterium tumefaciens*. J Bacteriol **177**:1076–81.

444. **Finn RD**, **Coggill P**, **Eberhardt RY**, **Eddy SR**, **Mistry J**, **Mitchell AL**, **Potter SC**, **Punta M**, **Qureshi M**, **Sangrador-Vegas A**, **Salazar GA**, **Tate J**, **Bateman A**. 2016. The Pfam protein families database: towards a more sustainable future. Nucleic Acids Res **44**:D279–D285.
445. **Majorek KA**, **Kuhn ML**, **Chruszcz M**, **Anderson WF**, **Minor W**. 2013. Structural, functional and inhibition studies of a GNAT superfamily protein PA4794: a new C-terminal lysine protein acetyltransferase from Pseudomonas aeruginosa. J Biol Chem 0–27.
446. **Hegde SS**, **Javid-Majd F**, **Blanchard JS**. 2001. Overexpression and Mechanistic Analysis of Chromosomally Encoded Aminoglycoside 2'-N-Acetyltransferase (AAC(2')-Ic) from *Mycobacterium tuberculosis*. J Biol Chem **276**:45876–45881.
447. **Dahlstrom KM**, **Giglio KM**, **Collins AJ**, **Sondermann H**, **O'Toole GA**. 2015. Contribution of Physical Interactions to Signaling Specificity between a Diguanylate Cyclase and Its Effector. MBio **6**:e01978-15.
448. **Klapper I**, **Rupp CJ**, **Cargo R**, **Purvedorj B**, **Stoodley P**. 2002. Viscoelastic fluid description of bacterial biofilm material properties. Biotechnol Bioeng **80**:289–296.
449. **Shaw T**, **Winston M**, **Rupp CJ**, **Klapper I**, **Stoodley P**. 2004. Commonality of elastic relaxation times in biofilms. Phys Rev Lett **93**:1–4.
450. **Hassanpourfard M**, **Nikakhtari Z**, **Ghosh R**, **Das S**, **Thundat T**, **Liu Y**, **Kumar A**. 2015. Bacterial floc mediated rapid streamer formation in creeping flows. Sci Rep.
451. **Stoodley P**, **Jacobsen A**, **Dunsmore BC**, **Purevdorj B**, **Wilson S**, **Lappin-Scott HM**, **Costerton JW**. 2001. The influence of fluid shear and AICI3 on the material properties of *Pseudomonas aeruginosa* PAO1 and *Desulfovibrio* sp. EX265 biofilms. Water Sci Technol **43**:113–20.
452. **Leijdekkers AGM**, **Huang J-H**, **Bakx EJ**, **Gruppen H**, **Schols HA**. 2015. Identification of novel isomeric pectic oligosaccharides using hydrophilic interaction chromatography coupled to traveling-wave ion mobility mass spectrometry. Carbohydr Res **404**:1–8.
453. **Hofmann J**, **Hahm HS**, **Seeberger PH**, **Pagel K**. 2015. Identification of carbohydrate anomers using ion mobility–mass spectrometry. Nature **526**:241–244.
454. **Kuhn ML**, **Majorek KA**, **Minor W**, **Anderson WF**. 2013. Broad-substrate screen as a tool to identify substrates for bacterial Gcn5-related N-acetyltransferases with unknown substrate specificity. Protein Sci **22**:222–30.
455. **Poole RK**. The Isolation of Membranes from Bacteria, p. 109–122. *In* Biomembrane Protocols. Humana Press, New Jersey.

Acknowledgements

For the last few years this research project was an important part of my life and with it, I grew on both professional and personal level. On my journey, many people accompanied and supported me. Here, I would like to express my highest gratitude to them.

First of all, I would like to thank my supervisor Prof. Dr. Urs Jenal, for supporting me during my master and my PhD. He gave me a lot of freedom within my project and the possibility to develop my own ideas. His scientific enthusiasm was contagious at times and his ability to make complex processes look easy and comprehensible was admirable and helped me to unwind the entanglement of my findings.

Furthermore, I would like to thank my PhD committee, Prof. Dr. Julia Vorholt and Prof. Dr. Marek Basler for extended brainstorming and guidance throughout my PhD.

Highly appreciated is the input of my external collaborators Ali and Eva. Ali contributed to this work by taming HfsK for ITC measurements and Eva provided insights into holdfast adhesion from a completely different angle using the pioneering technology FluidAFM.

Very importantly, I like to acknowledge all current and former members of the Jenal group for a great working atmosphere and the many stimulating scientific and non-scientific conversations. I was privileged to work in such an amazing team. Especially, I want to mention Christoph who was a patient listener, Isa who contributed substantially to this work with the microfluidics assays and was my first contact for scientific advice, Matteo who programmed the software WHISIT that saved me a lot of time, Christian and Benoît who helped me a lot with biochemical assays, Fabs who used her magic whenever my clonings got stuck, Chee-Seng who supported my first steps in structural modelling, Antje who kept seeing the positive side, Shogo who was a vast source of knowledge and Ursi and Irina who were most enjoyable roommates.

Jutta had the courage to take me as a master student and taught me all the basics of scientific work. She initiated my project, yet she did not have the opportunity to see the end of it. I thank her for her time, help and patience and will keep her in good memory.

I am also grateful for the professional support of the Biozentrum core facilities, especially Alexia and Kai who were taking the super-resolution images with me, and Timo who gave me advice concerning co-immunoprecipitation experiments.

Additionally, I highly appreciated the entire administrative and technical support (sometimes even on very short notice) provided by Marina, Patric, Michaela, Claudia, Anne-Cecile, Verena, Guisi, Cristela and Gerardine, who enabled me to focus on my scientific work.

Endless thanks go to my partner Mathias who was my fountain of strength and joy, and always helps me to order my thoughts on both scientific and personal matters and make the right decisions. My sincere thanks are also given to my parents Franz and Jeannette and my brothers Dominic and Oliver. My family is supporting me at all times and is my safe haven I always can rely on.

Finally, a want to thank all people that have carefully read this thesis and provided me with valuable feedback: Alberto, Christian, Christoph, Isa, Matteo, Benoît, Mathias and Urs.